Development and Characterisation of Nanoparticle Filled Polytetrafluoroethylene for Tribological Applications

Levente Ferenc Tóth

Doctoral dissertation submitted to obtain the academic degrees of
Doctor of Electromechanical Engineering (UGent) and PhD in Mechanical Engineering (BME)

Supervisors

Prof. Patrick De Baets, PhD* - Jacob Sukumaran, PhD* - Prof. Gábor Szebényi, PhD**

* Department of Electromechanical, Systems and Metal Engineering
Faculty of Engineering and Architecture, Ghent University

** Department of Polymer Engineering
Faculty of Mechanical Engineering, Budapest University of Technology and Economics, Hungary

September 2021

GHENT UNIVERSITY

MŰEGYETEM 1782

Development and Characterisation of Nanoparticle Filled Polytetrafluoroethylene for Tribological Applications

Levente Ferenc Tóth

Doctoral dissertation submitted to obtain the academic degrees of
Doctor of Electromechanical Engineering (UGent) and PhD in Mechanical Engineering (BME)

Supervisors

Prof. Patrick De Baets, PhD* - Jacob Sukumaran, PhD* - Prof. Gábor Szebényi, PhD**

* Department of Electromechanical, Systems and Metal Engineering
Faculty of Engineering and Architecture, Ghent University

** Department of Polymer Engineering
Faculty of Mechanical Engineering, Budapest University of Technology and Economics, Hungary

September 2021

GHENT UNIVERSITY

MŰEGYETEM 1782

ISBN 978-94-6355-516-6
NUR 971, 978
Wettelijk depot: D/2021/10.500/64

Members of the Examination Board

Chairs

Prof. Filip De Turck, PhD, Ghent University
Prof. Péter János Szabó, PhD, Budapest University of Technology and Economics, Hungary

Other members entitled to vote

Prof. Károly Belina, PhD, John von Neumann University, Hungary
Prof. Ludwig Cardon, PhD, Ghent University
Prof. Dieter Fauconnier, PhD, Ghent University
Prof. Sergei Glavatskih, PhD, Ghent University
Prof. Gábor Kalácska, PhD, Szent István University, Hungary
Prof. Mitjan Kalin, PhD, University of Ljubljana, Slovenia

Supervisors

Prof. Patrick De Baets, PhD, Ghent University
Jacob Sukumaran, PhD, Ghent University
Prof. Gábor Szebényi, PhD, Budapest University of Technology and Economics, Hungary

English title:

Development and Characterisation of Nanoparticle Filled Polytetrafluoroethylene for Tribological Applications

Dutch title:

Ontwikkeling en karakterisering van met nanopartikels gevulde polytetrafluorethyleen voor tribologische toepassingen

Hungarian title:

Nanorészecske töltésű politetrafluoretilén fejlesztése és vizsgálata tribológiai alkalmazásokhoz

This PhD research was performed under a cooperation agreement for the joint supervision of this doctoral thesis between Ghent University (UGent, Belgium) and Budapest University of Technology and Economics (BME, Hungary), signed on 03 October 2016 and prolonged on 01 October 2020.

"The more complex the world becomes
the more difficult it is to complete something
without the cooperation with others"

Alexander Fleming

ACKNOWLEDGEMENT

First, I would like to express my deepest gratitude to my promoters Prof. Dr. Patrick De Baets (UGent) and Dr. Gábor Szebényi (BME) for their support, persistent help and guidance. I am also very thankful to my co-supervisor Dr. Jacob Sukumaran (UGent) for his support and supervising in my research works and doctoral thesis. I would like to express my gratitude to Prof. Dr. József Karger-Kocsis† (BME) for his guidance, support, valuable advices and encouragement.

I am very thankful to Prof. Dr. Patrick De Baets (UGent), Dr. Gábor Szebényi (BME), Prof. Dr. Tibor Czigány (BME), Prof. Dr. Gábor Kalácska (Szent István University), Dr. Tamás Bárány (BME), Dr. Ádám Kovács (BME), Erzsébet Szakács (BME) and Dr. Csaba Hős (BME) for their help to establish this collaboration between UGent and BME.

I appreciate the support of Prof. Dr. Tibor Czvikovszky (BME), Prof. Dr. Tibor Czigány (BME), Prof. Dr. László Mihály Vas (BME), Dr. Meiszel László (BME) and Prof. Dr. Dieter Fauconnier (UGent) who shared their knowledge in the field of polymers and tribology.

I also would like to thank all of the other members of Soete Laboratory (Department of Electromechanical, Systems and Metal Engineering, UGent) especially Dr. Wouter Ost, Ir. Jonathan Vancoillie, Ir. Ádám Kalácska, Dr. Kannaki Pondicherry and Dr. Saosometh Chhith for their valuable discussions, help and useful suggestions. I also would like to thank the all of the other members of Department of Polymer Engineering (BME) especially Dr. Andrea Toldy, Dr. Tamás Bárány, Dr. Gergely Czél, Dr. Péter Tamás-Bényei, Ir. Balázs Pinke, Dr. Kolos Molnár, Dr. Tamás Tábi, Dr. József Gábor Kovács, Dr. András Suplicz, Dr. Péter Bakonyi, Dr. Zoltán Kiss, Dr. Zoltán Tamás Mezey, Ir. Tamás Temesi, Ir. Márk Hatala, Ir. Katalin Litauszki, Ir. Ákos Pomázi and Ir. Ágnes Ureczki for their valuable help and constructive advices. Also, I would like to thank Dr. Beáta Szolnoki, Ir. Decsov Kata Enikő and Ir. Tamás Igricz from Department of Organic Chemistry and Technology (BME), Ir. Tegze Borbála from Department of Physical Chemistry and Materials Science (BME), Prof. Dr. Imre Norbert Orbulov and Ir. Attila Szlancsik from Department of Materials Science and Engineering (BME), Prof. Dr. Zoltán Gácsi and Ir. Tamás Bubonyi from Institute of Physical Metallurgy, Metal Forming and Nanotechnology (University of Miskolc) and Dr. János Madarász from Department of Inorganic and Analytical Chemistry (BME) for their valuable help and constructive advices.

I acknowledges the financial support received through ÚNKP-18-3-I-BME-176 New National Excellence Program of the Ministry of Human Capacities. Also, I would like to thank Zsuzsanna Brindza from 3M Company and Azelis for the material support and Dr. Louis Van Rooyen from Faculty of Engineering and the Built Environment (Tshwane University of Technology) for the material support and useful suggestions.

I received generous administrative support from Georgette D'hondt, Muriel Vervaeke, Péterné Abonyi, Erzsébet Varkoly, Szilvia Ollári, Szilvia Szalók Jánosné and Anna Pálovics. I received excellent technical support from István Horváth, Ferenc de Rivo, Bertalan Papp, Szabolcs Pántya, Dávid Bartók, György Bartók, Attila Balaskó, Sam Demeester, Johan Van Den Bossche, Hans Van Severen, Lieven Van West, Tonino Vandecasteele and Michel De Wale.

I owe a deep gratitude to my family and friends for their support, advices and for the kind and nice atmosphere which they gave me. I would like to thank Anna Diána Adorjáni for her support during these years. I would like to express my gratitude to my grandmother Erika Rajos Gyuláné Földes for her support. The final and the biggest gratitude is to my parents Erika Mária Tóthné Rajos and Ferenc Tóth for their endless support and encouragement in my whole life. Without their help I could not achieve these results.

TABLE OF CONTENTS

SYMBOLS AND UNITS

Latin symbols:

A	(m^2)	Surface area of the sample
A_s	(mm^2)	Surface area of the sample cross-section
CoF	(-)	Coefficient of friction
d_s	(m)	Sliding distance
D	(mm)	Diameter of the polymer pin sample
D_{in}	(mm)	Initial diameter of the tested samples
D_{wt}	(mm)	Diameter of the wear track centreline
E'	(MPa)	Storage Young's modulus
E''	(MPa)	Loss Young's modulus
F_N	(N)	Normal force
Fr	(N)	Friction force
F_{shear}	(N)	Shear force
$F_{x\%}$	(N)	Acting normal force at $x\%$ compressive deformation
G'	(MPa)	Storage shear modulus
G''	(MPa)	Loss shear modulus
k	(mm^3/Nm)	Specific wear rate
M	(Nm)	Torque
$m_{d,mass\ loss}$	(g)	Measured mass loss after the wear test
M_n	(g/mol)	Molecular weight
m_r	(%)	Residual mass
$m_{s,air}$	(g)	Measured sample mass in air
$m_{s,et}$	(g)	Measured sample mass in ethanol
P	(W)	Heating power
p	(MPa)	Contact pressure
r	(mm)	Radius of wear track centreline
$t_{c,creep}$	(µm)	Change of thickness caused by creep
$t_{c,thermal}$	(µm)	Change of thickness caused by the thermal expansion
$t_{c,total}$	(µm)	Total change of thickness
$t_{c,wear}$	(µm)	Change of thickness caused by the wear (wear depth)
T_{et}	(°C)	Measured temperature in ethanol
T_g	(°C)	Glass transition temperature
T_{g1}	(°C)	Glass transition temperature of the applied homopolymer

T_{g2}	(°C)	Glass transition temperature of the applied homopolymer
t_s	(mm)	Sample thickness
t_{test}	(s)	Test time
v_s	(m/s)	Sliding speed
$V_{d,mass\ loss}$	(mm^3)	Calculated volume loss after the wear test
V_s	(cm^3)	Evaluated sample volume
w	(mm)	Width of the specimen
w_1	(-)	Weight fraction of the incorporated monomer
w_2	(-)	Weight fraction of the incorporated monomer
$W_{d,mass\ loss}$	(mm)	Wear depth based on the measured mass loss
X	(%)	Degree of crystallinity

Greek symbols:

α	(-)	Mass fraction of the fillers
γ_{xy}	(-)	Shear strain
ΔH_C	(cal/g)	Enthalpy of crystallisation
ΔH_{CC}	(J/g)	Enthalpy of cold-crystallisation
ΔH_f	(J/g)	Enthalpy of fusion for 100% crystalline PTFE
ΔH_m	(J/g)	Enthalpy of fusion
Δm	(g)	Measured mass loss
ΔT_m	(K)	Temperature difference
ε_1	(-)	Measured shear strain
ε_2	(-)	Measured shear strain
θ_1	(°)	Angle between the horizontal axis and the axes of ε_1
θ_2	(°)	Angle between the horizontal axis and the axes of ε_2
λ	(W/mK)	Thermal conductivity
ρ	(g/mm^3)	Density of the pin sample
ρ_{et}	(g/cm^3)	Density of ethanol
ρ_s	(g/cm^3)	Density of the sample
$\sigma_{x\%}$	(MPa)	Compressive stress calculated at $x\%$ compressive deformation
$\tau_{1,2}$	(MPa)	Shear stress
ω	(rpm)	Rotational speed
$tan\delta$	(-)	Loss factor

Acronyms

AISI D2	Cold-working tool steel, high chromium content (X153CrMoV12)
Al_2O_3	Aluminium-oxide, alumina
AlCr	Aluminium-chromium
AlO(OH)	Aluminium hydroxide oxide / boehmite alumina (Disperal Dispal 80)
APK	Aliphatic polyketone
ATR	Attenuated total reflection
BA80	Boehmite alumina / aluminium hydroxide oxide (Disperal Dispal 80)
BN	Boron nitride
C	Carbon, chemical element
CCD	Charge-coupled device
COOH	Carboxyl functional group
Cr	Chromium, chemical element
Cu_2O	Copper(I) oxide
DMA	Dynamic mechanical analysis
DIC	Digital image correlation
DSC	Differential scanning calorimetry
DTA	Differential thermal analysis
DTGS	Deuterated triglycine sulfate
EDS	Energy dispersive X-ray spectroscopy
EoS	Equation of state
Fe	Iron (*ferrum*), chemical element
Fe_2O_3	Iron(III) oxide
Fe_3O_4	Iron(II,III) oxide
FTIR	Fourier-transform infrared spectroscopy
H_2O	Water (vapor)
HDPE	High density polyethylene
LDPE	Low density polyethylene
Mn	Manganese, chemical element
Mo	Molybdenum, chemical element
MoS_2	Molybdenum disulphide
N_2	Diatomic nitrogen gas
Ni	Nickel, chemical element
OF graphene	Oxyfluorinated graphene
OH	Hydroxyl functional group
O_2	Diatomic oxygen gas

P	Phosphorus, chemical element
PA	Polyamide
PA 6	Polyamide 6
PA 66	Polyamide 66
Pb_3O_4	Lead tetroxide
PbO	Lead monoxide
PEEK	Polyether ether ketone
PES	Polyether sulfone
PET	Poly(ethylene) terephthalate
PMMA	Polymethyl methacrylate
POM	Polyoxymethylene
PP	Polypropylene
PPS	Polyphenylene sulphide
PTFE	Polytetrafluoroethylene
RH%	Relative humidity
S	Sulphur, chemical element
SEM	Scanning electron microscopy
SFE	Surface free energy
Si	Silicon, chemical element
TGA	Thermogravimetric analysis
UHMWPE	Ultrahigh molecular weight polyethylene
vol%	Volume percent
wt%	Weight percent
XPS	X-ray photoelectron spectroscopy

α-$Al(OH)_3$	Aluminium trihydroxide (bayerite)
α-AlO(OH)	Aluminium monohydroxide (diaspore)
γ-$Al(OH)_3$	Aluminium trihydroxide (gibbsite)
γ-AlO(OH)	Aluminium monohydroxide (boehmite)

SUMMARY

Nanoparticle filled thermoplastics are widely investigated materials due to their beneficial features. The nanoparticles can enhance the mechanical, thermal properties and flame retardancy of the thermoplastics and they can achieve a significant improvement of wear resistance as well. Focusing on polytetrafluoroethylene (PTFE), this thermoplastic has high thermal stability, excellent chemical resistance, low coefficient of friction and good self-lubricating property compared to other semi-crystalline thermoplastics. Well-known limitations of PTFE are the relatively low mechanical properties and the low wear resistance, which can be improved with the use of fillers such as fibers and micro- or nanoparticles. The need for enhanced wear resistance comes from those application areas where PTFE is applied as a matrix material. Sliding bearings can be an example, where the surpassing of the wear performance of neat PTFE is required. Graphene and alumina (Al_2O_3) nanofillers can improve the wear resistance of PTFE by 2 to 3 orders of magnitude.

According to the present understanding, the long PTFE chains undergo mechanical chain scission during wear, whereby under the action of air (oxygen) and humidity terminal carboxyl groups (COOH) form on the PTFE chain fragments (*in situ* “carboxyl functionalization”). The terminal carboxyl groups, formed on the PTFE chain during wear, can react with the atoms of metal counterfaces and with the functional groups of the applied fillers. Some of the applied fillers were chosen, considering a working hypothesis. This hypothesis is that nanofillers which have a large number of functional groups can be beneficial in sliding wear applications. The functional groups of the nanofillers can participate in complex formation with the *in situ* formed “functionalized” PTFE carboxyl groups, forming a more durable and adequate transfer layer. This transfer layer formation can be further supported by the potential complex formation between the functional groups of the fillers and the steel counterface. According to this hypothesis, the aluminium oxide hydroxide (boehmite alumina) and hydrotalcite are promising fillers as they contain relevant functional groups.

Besides the above mentioned relevant mechanism, the wear resistance is affected by the physical, thermal, mechanical and morphological properties of the materials of interest. In literature, a comprehensive investigation of the tribological characterisation of nanoparticle filled PTFE can be found, but a detailed material characterisation is hardly available, and as a result, we lack a thorough understanding of this material.

The aim of this research work was to design and develop nano-particle filled PTFE materials with ultra-low wear rate. The friction and wear decreasing effect of the fillers, the physical and chemical underlying knowledge and the mechanism of transfer layer formation were analysed to build up fundamental insight and understanding.

The proposed fillers are graphene, aluminium oxide, boehmite alumina and hydrotalcite. As the use of graphene and alumina among the tested fillers the most efficiently decreased the wear rate of mono-filled PTFE, the hybridisation of these fillers was also investigated. The applied production technique was a room temperature pressing – free sintering method. PTFE and filler powders were blended by intensive dry mechanical stirring, which is a less hazardous and more environment-friendly alternative to solvent blending method. The material characterisation includes the determination of density, thermal conductivity, hardness, compressive, shear and tensile properties and the filler particle distribution.
The tribological characterisation was carried out to measure and analyse the friction and wear properties and the transfer layer formation. The wear tests were carried out with a pin-on-discs configuration against 42CrMo4 steel disc counterfaces (3 MPa contact pressure, 0.1 m/s sliding speed, 1000 m sliding distance and dry contact at room temperature). A parametrical study of the best performing mono- and hybrid-filled PTFE, related to the influence of contact pressure, sliding speed and pv values was also carried out. The applied parameters and conditions: 1/3/5/7 MPa contact pressure, 0.5/1/1.5/2/3 m/s sliding speed, 3000 m stipulated sliding distance and dry contact at room temperature.

Boehmite alumina can be used as a filler of PTFE, regarding the low decomposition of boehmite alumina during the sintering process, and the mechanical and thermal properties of these composites. The results of thermogravimetric analysis (TGA) and Fourier-transform infrared spectroscopy (FTIR) validated that ~60-75% of the hydroxyl functional groups of boehmite alumina are still persisting in the developed composites after the applied free-sintering process with 2 and 10 hours heat dwelling time at 370°C maximal temperature. In this way, these hydroxyl functional groups can participate in the friction and wear processes between the PTFE/boehmite composites and the counterfaces.
Al_2O_3 filled PTFE had approximately two orders of magnitude decrease in the wear rate, which was caused by the filler accumulation during the wear process, the smaller wear debris and the formed iron-oxide layer on the worn surface of polymer samples. The formed iron-oxide layer from the steel counterfaces on the polymer samples further increased the durability of the transfer layer, increasing the wear resistance. PTFE became thermally unstable during the sintering process due to the added Al_2O_3 filler. In this way, the sintering process of Al_2O_3 filled PTFE is not suggested with 8 wt% or higher filler content or with heat dwelling time longer than 2-3 hours.
Regarding all of the used fillers, the influence of the modified mechanical and thermal properties (thermal conductivity, hardness and compressive/shear/tensile properties) on the wear rate has only a secondary role: their measure and their tendency can not decrease the wear rate with orders of magnitude. These statements were confirmed by testing PTFE

samples with 1/4/8/16 wt% boehmite, 0.25/1/4/8/16 wt% graphene, 1/4 wt% alumina and 1/4 wt% hydrotalcite filler content.

Focusing on the wear debris of all filled and unfilled PTFE tested against steel counterfaces in dry contact, the degree of crystallinity increased by ~20-40% compared to the unworn polymers. The main reason for this phenomenon was the mechanical chain scission of the PTFE molecular chains during the wear tests, which reduced the molecular weight by 1-2 orders of magnitude. In this way, these shorter molecular chains could more efficiently reach an aligned arrangement. The fillers further increased the mechanical chain scission of PTFE molecular chains compared to the unfilled (neat) PTFE.

The alumina and boehmite alumina content of the worn filled PTFE contact surfaces increased between ~100 and ~300% after the wear tests. In contrast, the filler content of the polymer wear debris was lower than the filler content of the unworn sample surfaces. The reason is that the softer PTFE particles can be torn easier from the contact surface than the hard filler particles, and thus increasing the PTFE content of the wear debris. Most of the torn unbroken and broken filler particles pressed and stuck again into the softer PTFE during the wear process, increasing the filler content of the worn surface. In this way, during the wear process, after the running-in period, the wear mechanism is related to a worn surface with a higher filler content compared to the original unworn sample.

The developed filled PTFE can be the base material of sliding bearings, guideways and linear slides, as some examples. None of the fillers damaged significantly the surface of the steel counterfaces during the wear process. PTFE with 4 wt% alumina content (PTFE/Al_2O_3-4) reached the lowest wear rate with $2.9 \cdot 10^{-6}$ mm^3/Nm, but low thermal stability was registered during the sintering process. In this way, the potential heat dwelling time during the sintering process is restricted, which is not beneficial in samples with a larger volume, where the necessary sintering time can be even longer than one day. All hybrid samples reached a low wear rate, PTFE with 0.25 wt% graphene and 4 wt% alumina content (PTFE/G/A-0.25/4), PTFE with 2 wt% graphene and 2 wt% alumina content (PTFE/G/A-2/2) and PTFE with 4 wt% graphene and 4 wt% alumina content (PTFE/G/A-4/4) had $1.2 \cdot 10^{-5}$, $2.8 \cdot 10^{-5}$ and $4.3 \cdot 10^{-6}$ mm^3/Nm wear rate, respectively.

PTFE/Al_2O_3-4 and PTFE/G/A-4/4 can be used in a remarkably wider application range, but their thermal stability was significantly lower during the sintering process compared to PTFE with 4 wt% graphene content (PTFE/Graphene-4) and PTFE with 8 wt% graphene (PTFE/Graphene-8) materials. PTFE/G/A-4/4 had the widest application range and the lowest thermal stability.

SAMENVATTING

(Dutch summary)

Met nanodeeltjes gevulde thermoplasten zijn veel onderzochte materialen vanwege hun gunstige eigenschappen. De nanodeeltjes kunnen de mechanische, thermische eigenschappen en vlamvertraging van de thermoplasten verbeteren en ze kunnen ook een aanzienlijke verbetering van de slijtvastheid opleveren. Polytetrafluorethyleen (PTFE) is een thermoplast met een hoge thermische stabiliteit, een uitstekende chemische bestendigheid, een lage wrijvingscoëfficiënt en goede zelfsmerende eigenschappen in vergelijking met andere semi-kristallijne thermoplasten. Bekende beperkingen van PTFE zijn wel de relatief lage mechanische eigenschappen en de lage slijtvastheid, die beiden verbeterd kunnen worden door het gebruik van vulstoffen zoals vezels en micro- of nanodeeltjes. In die toepassingen waar PTFE gebruikt wordt als matrix voor een kunststofcomposiet, is er een absolute nood aan een verbeterde slijtvastheid. Bij gebruik van PTFE-gebaseerde composieten voor glijlagers is een aanzienlijke betere slijtageweerstand dan die van zuiver PTFE gewenst. Nanovullers zoals grafeen en aluminiumoxide (Al_2O_3) kunnen de slijtvastheid van PTFE met 2 tot 3 grootteordes verbeteren.

Volgens de huidige opvatting ondergaan de lange PTFE-ketens mechanische splitsing tijdens het slijtageproces, waarbij onder invloed van lucht (zuurstof) en vochtigheid carboxylgroepen (COOH) worden gevormd op de uiteinden van de PTFE-ketenfragmenten (in situ carboxylfunctionalisatie). De carboxylgroepen kunnen op hun beurt reageren met de atomen van de metalen tegenvlakken en met de functionele groepen van de ingebrachte vulstoffen. Op basis van de werkhypothese dat nanovullers met een groot aantal functionele groepen gunstig kunnen zijn bij slijtage-toepassingen in glijcondities, is gekozen voor een aantal specifieke vulstoffen. De functionele groepen van de nanovullers kunnen complexen vormen met de in situ gevormde gefunctionaliseerde PTFE-carboxylgroepen, waardoor tijdens het glijden een duurzamere en adequatere transfertlaag op het stalen tegenloopvlak wordt gevormd. De transfertlaagvorming kan verder worden versterkt door de mogelijke complexvorming tussen de functionele groepen van de vulstoffen en het stalen tegenloopvlak. Krachtens deze hypothese zijn het aluminiumoxidehydroxide (boehmiet-aluminiumoxide) en hydrotalciet veelbelovende vulstoffen, omdat ze voor het beschreven proces relevante functionele groepen bevatten.

Naast het hierboven beschreven mechanisme wordt de slijtvastheid beïnvloed door de fysische, thermische, mechanische en morfologische eigenschappen van de beschouwde materialen. In de literatuur vindt men uitgebreid onderzoek naar de tribologische

karakterisering van met nanodeeltjes gevuld PTFE, maar een gedetailleerde materiaalkarakterisering is nauwelijks beschikbaar.
Het doel van het onderhavig onderzoek is dan ook het ontwerpen en ontwikkelen van met nanodeeltjes gevulde PTFE-composieten met een ultralage slijtage. Het wrijvings- en slijtagemilderend effect van de additieven, de fysische en chemische onderliggende mechanismen en het mechanisme van transfertlaagvorming werden geanalyseerd ten einde fundamenteel inzicht te verwerven.
De voorgestelde vulmiddelen zijn grafeen, aluminiumoxide, boehmiet-aluminiumoxide en hydrotalciet. Omdat grafeen en aluminiumoxide de slijtagesnelheid van (monogevuld) PTFE het meest efficiënt verminderde, werd ook de hybridisatie van deze vulstoffen onderzocht. De testmonsters werden geproduceerd door het bij kamertemperatuur persen en drukvrij sinteren. De PTFE en de vulmiddelen worden voorafgaandelijk intensief gemengd door droog mechanisch roeren, wat minder gevaarlijk is en milieuvriendelijker dan mengmethodes met oplosmiddelen. Van de testmonsters worden de volgende eigenschappen gemeten: dichtheid, thermische geleidbaarheid, hardheid, compressie-, afschuif- en trekeigenschappen.
Een tribologische karakterisering werd uitgevoerd om de wrijving en slijtage-eigenschappen en de transferlaagvorming van de PTFE-composieten te meten en te analyseren. De slijtagetesten werden uitgevoerd met een pin-on-disc-configuratie (PTFE pin tegen 42CrMo4-staal schijf, contactdruk 3 MPa, glijsnelheid 0,1 m/s glijsnelheid, glijafstand 1000 m, droog contact bij kamertemperatuur). Voor de best presterende mono- en hybride gevulde PTFE werd vervolgens een parametrische studie (contactdruk, glijsnelheid) uitgevoerd naar de best presterende mono- en hybride gevulde PTFE. De volgende parameterwaarden werden toegepast: 1 / 3 / 5 / 7 MPa contactdruk; 0,5 / 1 / 1,5 / 2 / 3 m/s glijsnelheid; 3000 m voorgeschreven glijafstand, en dit alles bij droog contact en kamertemperatuur.

Boehmiet-aluminiumoxide kan worden gebruikt als vulstof van PTFE, gezien de lage decompositie van boehmiet-aluminiumoxide tijdens het sinterproces en de goed mechanische en thermische eigenschappen van deze composieten. De resultaten van thermogravimetrische analyse (TGA) en Fourier-transform infraroodspectroscopie (FTIR) tonen aan dat ongeveer 60-75% van de hydroxylfunctionele groepen van boehmiet-aluminiumoxide nog steeds aanwezig zijn in de gevormde composieten na het vrije sinterproces met 2 en 10 uren warmteverblijftijd bij een temperatuur van 370 °C. Derhalve kunnen deze hydroxylfunctionele groepen nog deelnemen aan de wrijvings- en slijtageprocessen tussen de PTFE / boehmiet-composieten en de stalen tegenvlakken.
PTFE gevuld met Al_2O_3 heeft een slijtagesnelheid die 2 grootteordes lager is dan voor zuiver PTFE. Dat wordt verwezenlijkt door een opeenhoping van het vulmiddel tijdens het slijtageproces, door de vorming van kleinere slijtagedeeltjes en door de afzetting van een

ijzeroxidelaag in het slijtagespoor op het polymeermonster. Deze ijzeroxidelaag is behoorlijk slijtagebestendig en verhoogt aldus de slijtageweerstand van het polymeer. Aan de andere kant stelt men echter ook vast dat de toevoeging van Al_2O_3 het PTFE thermisch instabiel maakt tijdens het sinterproces. Om die reden wordt aanbevolen om de concentratie van Al_2O_3 in PTFE onder de 8 gew.% te houden voor een sinterproces met een warmteverblijftijd van meer dan 2 à 3 uur.

Voor alle gebruikte vulstoffen geldt dat de gewijzigde mechanische en thermische eigenschappen (warmtegeleidingsvermogen, hardheid en compressie- / trekeigenschappen) op de slijtagesnelheid slechts een ondergeschikte rol spelen: ze kunnen de slijtagesnelheid niet significant verminderen. Dit wordt ook bevestigd door de testen van PTFE-monsters met 1 / 4 / 8 / 16 gew% boehmiet; 0,25 / 1 / 4 / 8 / 16 gew% grafeen, 1 / 4 gew% aluminiumoxide en 1/4 gew% hydrotalciet vulstofgehalte.

De kristalliniteit van het slijtagedebris van alle gevulde en ongevulde PTFE, die in droog contact getest zijn tegen stalen tegenvlakken, is met ongeveer 20 à 40% gestegen in vergelijking met de polymeren vóór slijtage. De belangrijkste reden hiervoor is de mechanische splitsing van de PTFE-moleculaire ketens tijdens de slijtagetesten, waardoor het moleculair gewicht met 1-2 grootteordes vermindert. De aldus gevormde kortere moleculaire ketens kunnen gemakkelijker tot een uitgelijnde opstelling komen. De vulstoffen verhogen de mechanische ketensplitsing van PTFE in vergelijking met de zuivere, ongevulde PTFE.

De aluminiumoxide- en boehmiet-aluminiumoxide-concentratie van de aan slijtage onderworpen gevulde PTFE-contactoppervlakken neemt toe met ongeveer 100 en 300% ten gevolge van het slijtageproces. Daarentegen bevat de slijtagedebris van het polymeer minder vulmiddelen dan de originele PTFE-oppervlakken. De reden hiervan is dat de zachtere PTFE-deeltjes gemakkelijker van het contactoppervlak kunnen worden gescheurd dan de harde vulstofdeeltjes, en zo de PTFE-concentratie in de slijtagdebris verhogen. De meeste afgescheurde (ongebroken of gebroken) deeltjes van het vulmateriaal worden opnieuw in de zachtere PTFE gedrukt tijdens het slijtageproces, wat dus de concentratie aan vullermateriaal in het afgesleten polymeeroppervlak verhoogt. Aldus evolueert het slijtageproces na de running-in periode naar een slijtageproces van een polymeer met hogere vulmiddelconcentratie vergeleken bij het originele polymeermonster.

De PTFE-composiet die in dit werk is ontwikkeld, kan dienen als basismateriaal voor bijvoorbeeld glijlagers, geleiders en lineaire glijbanen. Er is vastgesteld dat geen van de toegepaste vulstoffen het stalen tegenoppervlak noemenswaardig beschadigt tijdens het slijtageproces. PTFE met 4 gew% aluminiumoxide (PTFE/Al_2O_3 4) bereikt met $2{,}9 \cdot 10^{-6}$ mm^3/Nm de laagste slijtagesnelheid, maar tijdens het sinterproces werd wel een relatief lage thermische stabiliteit geregistreerd. Derhalve is de thermische verblijftijd tijdens het sinterproces beperkt, wat vooral ongunstig is voor monsters met een groter volume, omdat

de benodigde sintertijd lang – zelfs langer dan een dag – kan zijn. Alle hybride monsters bereiken een lage slijtagesnelheid, PTFE met 0,25 gew% grafeen en 4 gew% aluminiumoxide (PTFE/G/A-0,25/4), PTFE met 2 gew% grafeen en 2 gew% aluminiumoxide (PTFE/G/A 2/2) en PTFE met 4 gew% grafeen en 4 gew% aluminiumoxide (PTFE/G/A-4/4) hebben een slijtagesnelheid van respectievelijk $1{,}2 \cdot 10^5$; $2{,}8\ 10^5$ en $4{,}3\ 10^6$ mm^3/Nm.

PTFE/Al2O3 4 en PTFE/G/A-4/4 kunnen in een opmerkelijk breder toepassingsgebied worden gebruikt, maar hun thermische stabiliteit is aanzienlijk in vergelijking met PTFE met 4 gew% grafeen (PTFE/Graphene-4) en PTFE met 8 gew% grafeen (PTFE/Graphene-8). PTFE/G/A-4/4 vertoont het breedste toepassingsgebied en de laagste thermische stabiliteit.

ÖSSZEFOGLALÁS

(Hungarian summary)

A nanorészecske erősítésű hőre lágyuló polimerek számos előnyös tulajdonságuknak köszönhetően a széleskörűen elterjedt anyagok közé tartoznak. A nanorészecskék javíthatják a polimerek mechanikai, termikus és éghetőségi jellemzőit, valamint ezeken kívül nagymértékben képesek növelni a kompozitok kopási ellenállóképességét is. A politetrafluoretilén (PTFE) egy hőre lágyuló polimer, ami nagy termikus stabilitással, kiváló kémiai ellenállóképességgel, kis súrlódási tényezővel és jó önkenő képességgel rendelkezik a többi részben kristályos polimerhez képest. Viszont a PTFE jól ismert hátrányai közé tartoznak az alacsony mechanikai jellemzők és a kis kopási ellenállóképesség. Ezek a tulajdonságok erősítőanyagok, mint például szálak, mikro- és nanorészecskék hozzáadásával növelhetők. A fokozott kopási ellenállóképesség azokon az alkalmazási területeken kiemelt jelentőségű, ahol a PTFE mátrixanyagként funkcionál. Erre egy példa a siklócsapágy, amelynél alapvető elvárás a töltetlen PTFE kopási teljesítményének felülmúlása. A grafén és az alumínium-oxid (Al_2O_3) nanorészecskék a PTFE kopási ellenállóképességét 2-3 nagyságrenddel is képesek növelni.

Jelenlegi tudásunk szerint, a kopási folyamatok során, a hosszú PTFE láncok mechanikus lánctöredeződésen mennek keresztül. Ennek folyamán a létrejött PTFE láncvégeken (*in situ* karboxil funkcionalizálás) a levegő oxigén- és páratartalmának közreműködésével karboxil funkciós csoportok (COOH) alakulhatnak ki. Ezek a funkciós csoportok reakcióba léphetnek a fém ellendarab atomjaival és adott esetben az adalékanyagok funkciós csoportjaival. Jelen kutatómunkám folyamán, néhány adalékanyagot az említett hipotézis alapján választottam ki. Eszerint, azok a nanorészecskék, amelyek nagyszámú funkciós csoporttal rendelkeznek előnyösek lehetnek a kopási folyamatokban. Ugyanis bizonyos nanorészecskék funkciós csoportjai komplexet képeznek az *in situ* létrejött PTFE karboxil csoportokkal, egy tartósabb átmeneti réteget létrehozva. Az adalékanyagok funkciós csoportjai és az acél ellendarab között esetlegesen kialakuló komplexek tovább fokozhatják az átmeneti réteg képződését. Ezen hipotézis alapján, a böhmit (alumínium-oxid-hidroxid - AlO(OH)), valamint a hidrotalcit ígéretes adalékanyagoknak tekinthetők, mivel nagyszámú funkciós csoportot tartalmaznak.

Mindazonáltal, a fentebb említett releváns mechanizmus mellett, a kopási ellenállást a felhasznált anyagok fizikai, termikus, mechanikai és morfológiai tulajdonságai is befolyásolják. A szakirodalomban a nanorészecske erősítésű PTFE kompozitok tribológiai jellemzőinek széleskörű vizsgálata megtalálható, de az ezeket befolyásoló anyagjellemzők minden részletre kiterjedő áttekintése és teljeskörű megértése még csak hiányosan elérhető.

Kutatómunkám célja nagy kopási ellenállóképességű nanorészecske erősítésű PTFE kompozitok fejlesztése és vizsgálata. Ez magába foglalja az adalékanyagok súrlódás és kopáscsökkentő hatásának, fizikai és kémiai hátterüknek, illetve az átmeneti réteg képződés mechanizmusának vizsgálatát és megértését is.

Adalékanyagként grafént, alumínium-oxidot, böhmitet és hidrotalcitot alkalmaztam. A felhasznált adalékanyagok közül a grafén és az alumínium-oxid csökkentette a PTFE kopását a legnagyobb mértékben, ezért ezeket a töltőanyagokat, mint hibrid adalékanyagokat is vizsgáltam. Szobahőmérsékletű préselést követő terhelés nélküli szintereléssel gyártottam le a mintadarabokat. A PTFE alapanyagot és az adalékokat por formájában intenzív száraz mechanikai keveréssel elegyítettem. Ez az eljárás az oldószeres keveréssel összehasonlítva egy egészség- és környezetkímélőbb módszernek tekinthető. Az anyagjellemzők vizsgálata magába foglalja a sűrűség, hővezetés, keménység, nyomó-, nyíró- és húzótulajdonságok felderítését.

A tribológiai vizsgálataimmal a súrlódási és kopási jellemzőkre, valamint az átmeneti réteg képződésre fókuszáltam. A kopási vizsgálatokat pin-on-disc konfigurációval végeztem el 42CrMo4 acél ellentárcsa alkalmazásával (3 MPa nyomás, 0.1 m/s koptatási sebesség, 1000 m koptatási út, száraz súrlódás szobahőmérsékleten). Ezen körülmények között a legjobban teljesítő PTFE kompozitoknál a koptatási nyomás és sebesség hatását is vizsgáltam. Az alkalmazott beállítások a következők voltak: 1/3/5/7 MPa nyomás, 0.5/1/1.5/2/3 m/s koptatási sebesség, 3000 m koptatási út és száraz súrlódás szobahőmérsékleten.

A böhmit felhasználható a PTFE adalékanyagaként, a böhmit szintereléskor lejátszódó bomlási folyamatai, és a kompozit mechanikai és termikus anyagjellemzői alapján. Termogravimetriai analízissel (TGA) és Fourier-transzformációs infravörös spektroszkópiával (FTIR) igazoltam, hogy a böhmit adalékanyag hidroxil funkciós csoportjainak ~60-75%-a továbbra is jelen van a szinterelt kompozitban, a maximális 370°C hőmérsékleten, 2 óra, illetve 10 óra hőntartás mellett végzett, terhelés nélküli szinterelési ciklus befejeztével. Így ezek a hidroxil-csoportok részt tudnak venni a PTFE/böhmit kompozit egy külső ellenfelületen történő súrlódási és kopási folyamatában.

Az alumínium-oxiddal töltött PTFE minták kopási sebességének körülbelül két nagyságrendbeli csökkenése mögött a kopás közbeni adalékanyag-feldúsulás, a kisebb méretű kopadékok kialakulása és a polimer minta kopási felületén lerakódott vas-oxid réteg áll. Az acél ellendarabból származó, a polimer felületén lerakódott vas-oxid réteg az átmeneti réteg kopással szembeni ellenállóságának további növelését segítette elő. A PTFE alapanyag, az alumínium-oxid (Al_2O_3) hatására termikusan instabillá válik a szinterelés folyamata közben. Ebből következően az Al_2O_3 adalékanyag 8 m/m%-os vagy annál nagyobb koncentrációban,

és 2-3 óránál hosszabb hőntartási idő alkalmazásával nem javasolt PTFE alapanyaggal szinterelés útján történő feldolgozásra.

A további adalékanyagokat is vizsgálva, bizonyítottam, hogy a mechanikai és termikus jellemzők (hővezetési tényező, keménység, nyomó/nyíró/húzó mechanikai tulajdonságok) változásának hatása a kopási értékekre csak másodlagos, mértékük és tendenciájuk nem indokolja a kopási sebesség több nagyságrendbeli csökkenését. Állításaimat 1/4/8/16 m/m% böhmit, 0,25/1/4/8/16 m/m% grafén, 1/4 m/m% Al_2O_3 és 1/4 m/m% hidrotalcit töltésű mintáknál igazoltam.

Megállapítottam, hogy egy acél ellendarabon történő száraz súrlódásnál, a PTFE kompozitok kopadék szemcséinek a kristályossága minden egyes vizsgált minta esetében ~20-40%-kal nagyobb a nem koptatott anyagokéhoz képest. Ennek fő oka, hogy a PTFE molekulaláncok koptatás közben lejátszódó tördelődéséből adódóan, a kopadék 1-2 nagyságrenddel kisebb átlagos molekulatömeggel rendelkezik, így a PTFE rövidebb molekulaláncai egyszerűbben rendeződnek kristályos szerkezetbe. A töltetlen PTFE anyaghoz viszonyítva az adalékanyagok jelenléte nagyobb fokú PTFE molekulalánc tördelődést okozott.

A PTFE kompozitok koptatott felületén az alumínium-oxid és a böhmit adalékanyag a koptatás következményeként az eredeti, nem koptatott felülethez képest ~100-300%-kal feldúsul. Ezzel szemben a kopadék adalékanyag-tartalma kisebb, mint a koptatás előtt mért adalékanyag-tartalom a minták felületén. Ennek oka, hogy az adalékanyagnál jelentősen kisebb keménységű PTFE részecskék könnyebben leszakadnak a koptatott felületről, mint a töltőanyag, növelve ezzel a kopadék PTFE tartalmát. A leszakadt töltőanyag-részecskék, illetve törmelékek nagy része a koptatás folyamán benyomódik és újból beágyazódik a puha PTFE alapanyagba, növelve ezzel az adalékanyag koncentrációját a felületen. Ennek következménye, hogy a koptatás folyamán, a bekopási szakasz után, a kopási mechanizmus már az eredeti mintához képest egy nagyobb adalékanyagtartalmú koptatási felületen játszódik le.

A vizsgált PTFE kompozitok többek között siklócsapágyaknak, vezetékeknek és lineáris csúszkáknak lehetnek alapanyagai. A koptatási folyamatok során, egyik adalékanyag sem okozott kimutatható felületi sérülést az acél ellendarabokon. A vizsgált PTFE minták 4 m/m% Al_2O_3 adalékanyagtartalommal (PTFE/Al_2O_3-4) érték el a legkisebb kopási sebességet, $2.9 \cdot 10^{-6}$ mm^3/Nm értékkel, viszont a szinterelés közben kis termikus stabilitás volt megfigyelhető. Ebből kifolyólag, a szinterelés közbeni potenciális hőntartási idő korlátozott, ami hátrányos nagyobb térfogatú minták esetében, amelyeknél az alkalmazott szinterelési idő az egy napot is meghaladhatja. Az összes vizsgált hibrid-töltésű PTFE kis kopási sebességet ért el, PTFE 0.25 m/m% grafén és 4 m/m% alumínium-oxid tartalommal (PTFE/G/A-0.25/4), PTFE 2 m/m% grafén és 2 m/m% alumínium-oxid tartalommal (PTFE/G/A-2/2) és PTFE

4 m/m% grafén és 4 m/m% alumínium-oxid tartalommal (PTFE/G/A-4/4) $1.2 \cdot 10^{-5}$, $2.8 \cdot 10^{-5}$ és $4.3 \cdot 10^{-6}$ mm^3/Nm kopási sebességgel rendelkezett.

A PTFE/Al_2O_3-4 és PTFE/G/A-4/4 kompozitok szélesebb alkalmazási tartománnyal, de kisebb szinterelés közbeni hőstabilitással rendelkeznek, mint a 4 m/m% és 8 m/m% grafén tartalmú PTFE minták. PTFE/G/A-4/4 hibrid-töltésű PTFE kompozit mutatta a legszélesebb alkalmazási tartományt, egyben a legkisebb szinterelés közbeni hőstabilitást is.

CHAPTER 1

INTRODUCTION AND GENERAL AIM

This chapter introduces the background, the problem definition and the motivation of this research work. Besides these sections, this chapter discusses the research hypothesis, the research questions, the main purpose and the outline of this thesis book as well.

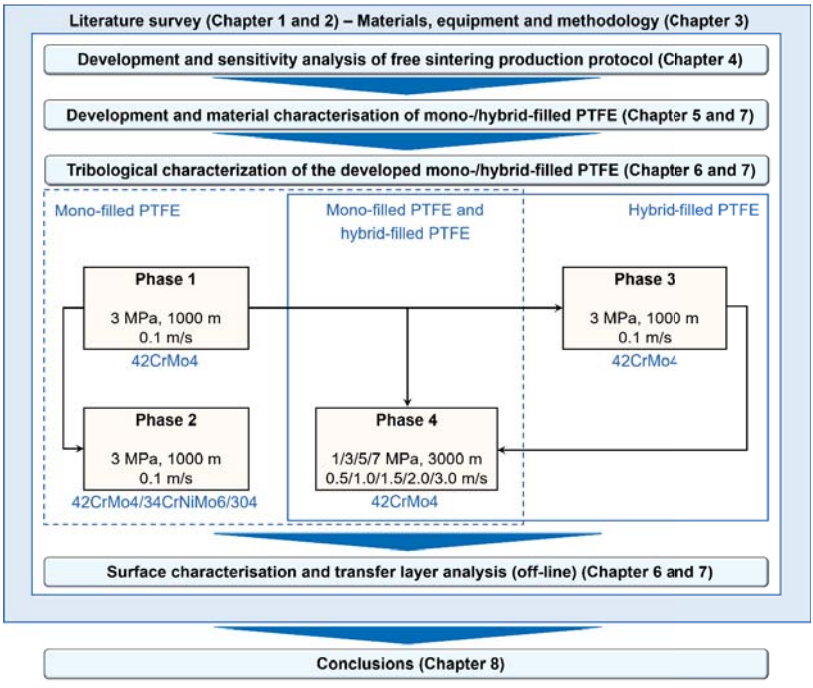

1.1. Background

Tribology is the science of friction, wear and lubrication; it originates from a Greek word, from *tribos*, which means rubbing [1]. Due to the relative motion of interacting surfaces, several machine components are influenced by friction and wear, which decrease the lifetime of these components and increase their operation and maintenance costs. Therefore well-designed tribo-materials and tribo-components have substantial economic and ecological importance. For the development of tribo-materials the designers have to consider an important aspect. Friction and wear are not simple material properties; they are system properties, as many factors influence their values. These factors can be the contact type and geometry, the sliding/rolling speed, the contact pressure, the counterface material, the surface roughness and pattern, the atmosphere, the environmental temperature and the relative humidity.

The word polymer is derived from Greek words as poly (many) and meres (parts). Synthetic polymers are produced via polymerisation of monomers making a long chain molecule with a large number of repeating units and having primary covalent bonds in between. Polymers are beneficial in those applications where vibration absorption, impact and shock load withstanding are needed, or in other words, where customers require high internal damping capacity. Focusing on tribological applications, polymers can also be used in a dirty and dusty environment, and a further advantage is that most of them have quiet running. Polymers have some other beneficial features as well, such as low density, anti-corrosive nature and chemical resistivity [2-5]. Polymers can be classified into two main groups based on their thermal processing behaviour such as thermoplastics and thermosets/crosslinked elastomers. Thermoplastics have secondary bonds between the macromolecules, in this way, these materials have the ability to re-melt after they have solidified. Thermosets and crosslinked elastomers have primary bonds between the molecular chains (covalent bonds). They solidify (cure) via chemical reaction; therefore they cannot be re-melted after solidification. Thermoplastics based on their structure are divided into amorphous and semi-crystalline thermoplastics. In amorphous thermoplastics, the molecules solidify in a random arrangement, while in semi-crystalline ones there are crystalline domains with three-dimensional order. In these materials, both crystalline and amorphous structures can be found (Figure 1.1) [6].

Besides the neat form of these materials, it is also possible to develop polymer composites. These composites involve two or more constituent materials (matrix and fillers) to achieve better performance. The matrix is the base material, while the fillers are usually particles and fibres. The fillers' role is to improve some of the properties of the neat polymer, for example, to enhance the mechanical, the physical, the thermal and/or the tribological features. If the applied fillers are proposed to increase mechanical or tribological properties, the fillers are also referred to as reinforcement materials or tribo-fillers, respectively.

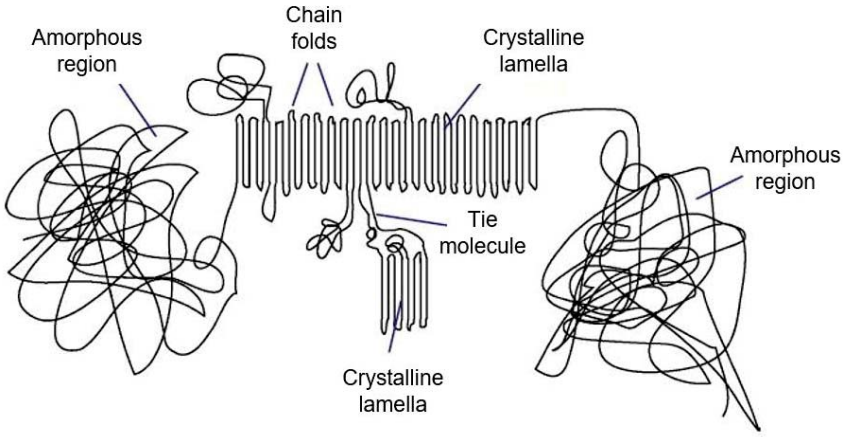

Figure 1.1. Illustration of semi-crystalline thermoplastics [6].

Both semi-crystalline thermoplastics and thermosets are used in tribological applications as bearings, bushings, seals or gears. Traditionally thermosets are beneficial at higher loads, and thermoplastics at higher speeds but new research and developments were continuously expanding their limits. Additional advantages of thermosets are the good creep resistance and high dimensional stability. They can withstand heavy loads and they are proper materials in heavy-duty applications [7]. Thermosets in tribo-systems are only secondary materials due to their high surface energy and low deformation capability. Another challenge with thermosets is the lack of self-lubrication, the inability to form an adequate (uniform and durable) transfer layer because of thermal degradation. In self-lubrication, the transfer layer is formed by the deposits from the applied polymer samples, they are locked in the asperities of the steel counterfaces. During the transfer layer formation, the amount of the deposits increases in the asperities (running-in period), filling the surface roughness valleys and in ideal case forming a thin layer (~few μm) on the steel counter surface (steady-state condition). This phenomenon results in polymer – partly polymer contact instead of the original polymer-metal contact. Functional fillers such as polytetrafluoroethylene (PTFE), molybdenum disulphide (MoS_2) and graphite can support the transfer layer formation to make it more uniform and durable. In recent years, new research has introduced these solid lubricants as an integral part of polymer composites [8, 9]. It is important to understand the relation between the formed transfer layer and the observed tribological characteristics. With this knowledge we can achieve a better material design for tribo-composites. The main reasons for the use of semi-crystalline thermoplastics are the self-lubrication nature and the uniform transfer layer formation, both of them originating from their melting behaviour. The ability to form an adequate uniform transfer layer is the key factor in optimising friction and wear characteristics. As a protective agent, this transfer layer

has a positive influence on the friction and wear characteristics of the materials. In the polymer-metal pair, the transfer layer fills the depressions of the metal counterface, decreases its surface roughness, and alters the polymer-metal contact to polymer-polymer contact. In this way, the abrasive wear can be reduced or fully eliminated. The quality, uniformity and durability of this transfer layer have a serious influence on reducing friction and wear properties [10-13].
Besides the brief discussion of the self-lubrication and transfer layer formation, it is also important to mention the third-body concept, which further explains these phenomena. This approach introduces the dominant role of the wear particles in dry condition and sliding motion. The solid third-body concept was formulated and introduced by Maurice Godet and further developed by Yves Berthier. The so-called third-body include all of the interfacial particles and elements between the contact surfaces, these elements separate the interacting surfaces (first-bodies). The third-body approach's three main steps are the following: wear debris detachment by e.g. adhesion or abrasion, debris circulation, and debris ejection. During the debris circulation, the wear particles are trapped between the contact surfaces reducing their interaction. At this stage, wear debris accumulation can be observed. During the last step, the wear debris is ejected, increasing the interaction between the contact surfaces, and the cycle starts again with the first step. The wear rate of a material is influenced by the balance between the detachment and the elimination of these wear debris. In other words, the wear particles can be even recycled and lost from the contact giving a dynamic balance for the wear rate. The detached wear particles trapped between the contact surfaces can even participate in load-carrying during the wear process, in this way, similarly to fluid third-bodies, the solid third-bodies also have load-carrying properties [14-16].
Regarding the friction of polymers, two main components have to be considered, such as deformation and adhesion. The deformation component comes from the resistance of the polymer to the interpenetrating of the asperities of the steel counter surface. The adhesion component originates from the adhesive junctions between the real contacting surfaces and it is related to the relative surface energy of the interactive surfaces. It is supposed that the adhesion is the dominant component of solid friction [17, 18]. The surface energy of the interactive surfaces can be calculated measuring their wettability by e.g. sessile drop test.
PTFE is a widely used material in tribology, as it has good chemical resistance, broad service temperature range, low coefficient of friction and self-lubrication nature. In industry, PTFE composites are widely used as rolling / sliding bearings, seals, guideways and linear slides if the requested mechanical load is very low. This material is also considered in case of specific requirements (e.g. strong need for chemical resistance and/or high thermal stability).

1.2. Problem definition and motivation of the research

A remarkable challenge with PTFE is the relatively high wear rate which is a relevant drawback compared to other thermoplastics. PTFE was chosen as a matrix material in this research work as the aim is to significantly improve its wear resistance, making it a real competitor of some other semi-crystalline thermoplastics in the aspect of the wear behaviour. The wear rate of PTFE can be reduced by the addition of appropriate fillers [19-25]. These fillers can reduce the wear rate due to the formation of an adequate transfer layer, and as such, reduce the maintenance costs and increase the lifetime of the product. Graphene can be an appropriate filler to decrease the coefficient of friction due to its layered structure and to increase the wear resistance by one-two orders of magnitude [21, 23]. Figure 1.2 shows the resulting friction as a function of the graphene filler content.

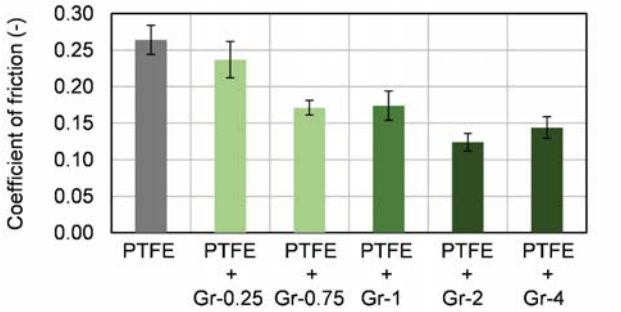

Figure 1.2. Coefficient of friction as a function of graphene filler content in PTFE matrix. The production method was room temperature pressing – free sintering method (plate-on-ring test, dry condition, 1 m/s sliding speed, 1 MPa contact pressure, steel counterface, air atmosphere) [23].

It is supposed that we can further decrease the wear rate of PTFE [23] when the graphene also contains functional groups such as hydroxyl, carboxyl and epoxy (Figure 1.3). Makowiec *et al.* demonstrated this effect in PTFE/functionalized carbon nanotube composites [23]. For understanding the introduced phenomenon, it is imperative to study the physical and chemical background of the filler/PTFE/counterface adhesion, starting with the tribo-chemical reactions in case of unfilled PTFE.

According to the present understanding, the long PTFE chains undergo mechanical chain scission during wear (Figure 1.4), whereby under the action of air (oxygen) and humidity terminal carboxyl groups (COOH) form on the PTFE chain fragments (*in situ* “carboxyl functionalization”) [23, 24, 26, 27]. This hypothesis was confirmed by XPS (X-ray photoelectron spectroscopy), which showed new peaks due to the new chemical bonds after wear test compared to the unworn material [20].

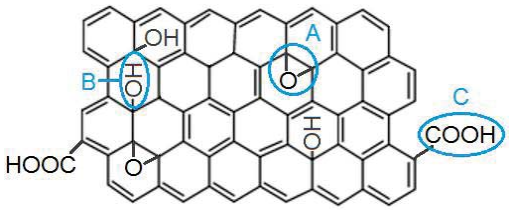

Figure 1.3. Functional groups of functionalized graphene; epoxy (A); hydroxyl (B) and carboxyl (C).

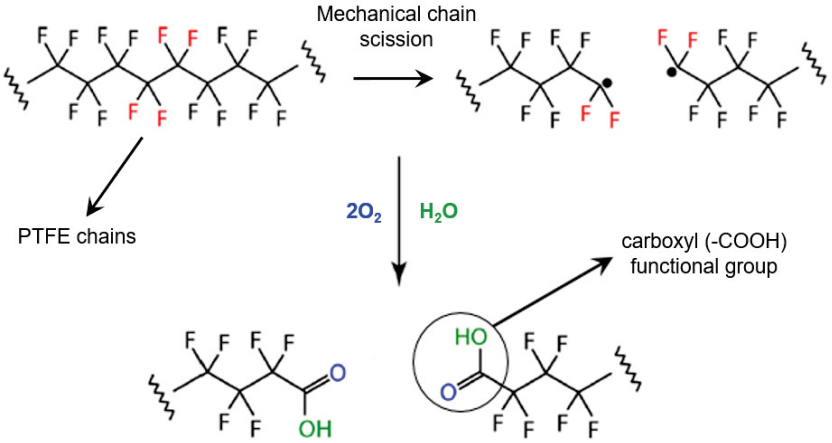

Figure 1.4. Mechanical chain scission and *in situ* carboxyl functionalization of PTFE chains in wear process [24].

The terminal carboxyl groups, formed on the PTFE chain during wear, can react with the atoms of metal counterfaces and with the functional groups of the applied fillers [20, 23-25]. Alumina (Al_2O_3) is another example to show the importance of tribo-chemical reaction in PTFE composites during wear [20, 23]. When the filler is alumina (Al_2O_3), the carboxyl groups of PTFE react with the atoms of alumina particles [20, 24]. The optimal content of fillers and the effect of the environment - such as relative humidity, temperature, counterface material and atmosphere - are still open questions.

1.3. Research hypothesis and research questions

Some of the applied fillers were chosen, considering a working hypothesis. This hypothesis is that nanofillers which have a large number of functional groups can be beneficial in sliding wear applications. The functional groups of the nanofillers can participate in complex formation with the *in situ* formed “functionalized” PTFE carboxyl groups, forming a more durable and adequate transfer layer. This transfer layer formation can be further supported by the potential

complex formation between the functional groups of the fillers and the steel counterface. According to this hypothesis, the aluminium oxide hydroxide (boehmite alumina) and hydrotalcite are promising fillers as they involve relevant functional groups.

Based on the introduced sections, the research questions are the following:

1 The first research question is whether the proposed fillers (graphene, alumina, boehmite alumina and hydrotalcite) are appropriate materials to incorporate into PTFE. The following factors are considered to answer this question:
    - sensitivity (thermal stability) analysis of the neat fillers and the filled PTFE materials during the sintering production of PTFE at 370°C;
    - influence of the fillers on the physical, mechanical and thermal properties of the materials.
2 The second research question is whether the increased number of chelates/complexes and *in situ* "grafting" of aluminium oxide hydroxide (boehmite alumina) and hydrotalcite with PTFE can improve the transfer layer formation and thereby increase the wear resistance of PTFE.
3 Third research question: what is the background of the wear-induced crystallisation of the tested materials? The following factors are considered to answer this question:
    - thermal history of the wear-tested samples;
    - mechanical history of the wear-tested samples;
    - mechanical chain scission during the wear process.
4 Fourth research question: What is the explanation of the ultra-low wear rate of alumina filled PTFE samples? The following factors are considered to answer this question:
    - transfer layer and wear track analysis for both the polymer samples and steel counterfaces;
    - observation of the potential wear mechanism of the polymer samples.
5 Fifth research question: what are the dominant factors of the wear mechanism? The following factors are considered to answer this question:
    - transfer layer formation;
    - mechanical and thermal properties of the tested polymer samples.

1.4. Main purpose

The purpose of this project was to design and develop nano-particle filled PTFE materials with ultra-low wear rate. PTFE provides a maintenance-free product, due to its self-lubricating behaviour, while its low coefficient of friction decreases the operational costs. PTFE is moreover an appropriate material to promote the transfer layer formation between the contact surfaces. PTFE can promote transfer layer formation not only as a base material but also as

an incorporated filler in another polymer matrix [10, 23, 28]. Although the general idea is known, many uncertainties remain about the precise functioning of the transfer layer, and the precise use of adequate fillers to increase more efficiently the wear resistance.
The proposed fillers are graphene, aluminium oxide, aluminium oxide hydroxide (boehmite alumina) and hydrotalcite. The friction and wear decreasing effect of the fillers, the physical and chemical underlying knowledge and the mechanism of transfer layer formation were analysed to build up fundamental insight and understanding.

Three objectives are addressed in this research work:

1) Develop a proper method for the blending and the production of high-quality nanoparticle filled PTFE (homogeneous distribution of nano-fillers in PTFE matrix, mould construction, development of production protocol: applied pressure, sintering time and temperature, heating and cooling thermal profiles).

2) Analyse and compare the developed neat PTFE and PTFE composites in terms of their physical, mechanical, thermal, chemical and tribological behaviour.

3) Fundamental understanding of the wear mechanism and transfer layer formation. Explain how the applied fillers affect the friction and wear mechanism.

1.5. Outline of the thesis

The research outline (Figure 1.5) was divided into six main parts (related to eight chapters) to achieve the introduced goals. These six main parts are the following:

1) Literature survey (Chapter 1 and 2); Materials, equipment and methodology (Chapter 3)
2) Development of free sintering production protocol. Production protocol related sensitivity analysis of the used fillers and the developed composites (Chapter 4)
3) Development and material characterisation of mono-/hybrid-filled PTFE (Chapter 5 and 7)
4) Tribological characterisation of the developed mono-/hybrid-filled PTFE (Chapter 6 and 7)
5) Surface characterisation and transfer layer analysis (off-line) (Chapter 6 and 7)
6) Conclusions (Chapter 8)

The tribological characterisation, surface characterisation and transfer layer analysis (off-line) are divided into four research phases (Phase 1, 2, 3 and 4). Chapter 3.3.6 introduces these research phases in a detailed way.

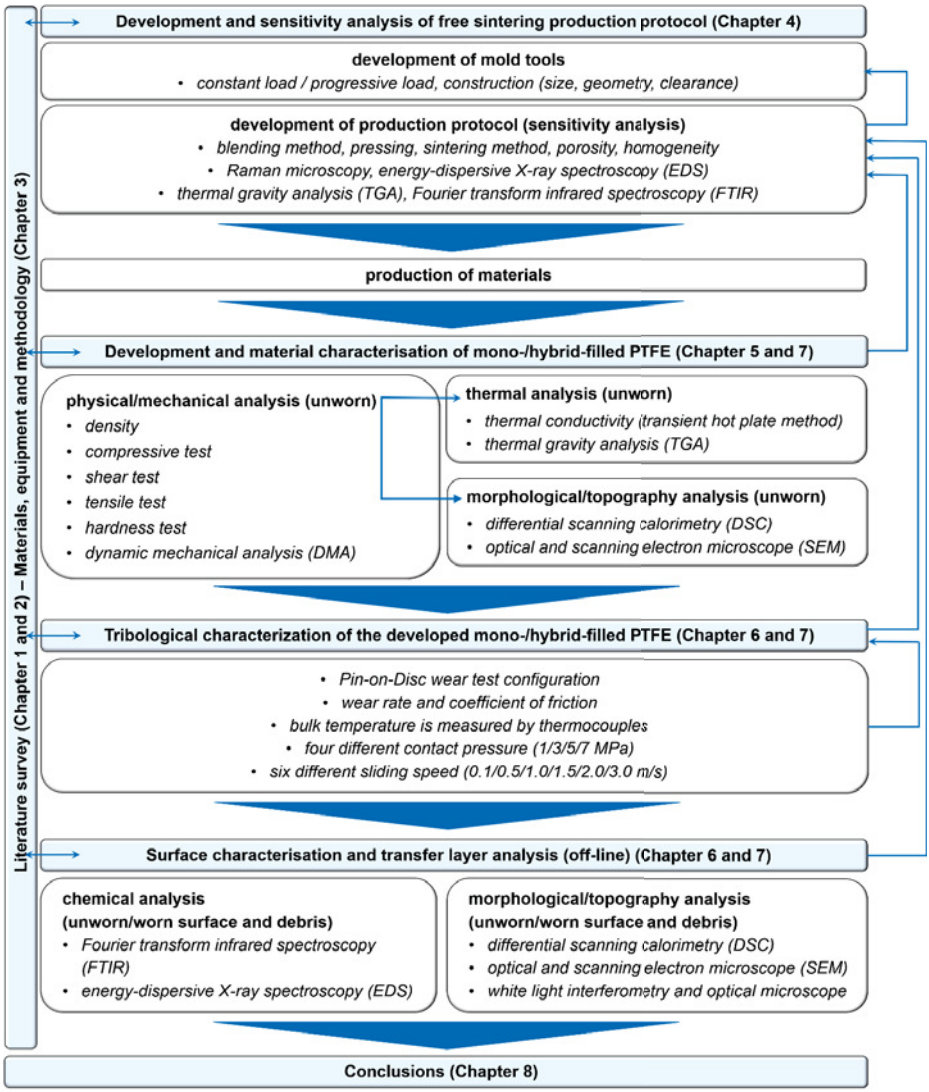

Figure 1.5. Outline of the thesis.

1.6. References

[1] J. Halling: Principles of tribology. Macmillan, London (1975).

[2] B.-B. Jia, T.-S. Li, X.-J. Liu, P.-H. Cong: Tribological behaviors of several polymer–polymer sliding combinations under dry friction and oil-lubricated conditions. Wear 262 (2007) 1353–1359.

[3] K. Mao, W. Li, C.J. Hooke, D. Walton: Friction and wear behaviour of acetal and nylon gears. Wear 267 (2009) 639–645.

[4] J.M. Thorp: Friction of some commercial polymer-based bearing materials against steel. Tribology International (1982) 69–74.

[5] H. Unal, U. Sen, A. Mimaroglu: Dry sliding wear characteristics of some industrial polymers against steel counterface. Tribology International 37 (2004) 727–732.

[6] T.A. Osswald, G. Menges: Material Science of Polymers for Engineers. Hanser Publishers, 3rd edition, Munich (2012).

[7] P.H. Pinchbeck: A review of plastic bearings. Wear 5 (1962) 85–113.

[8] J.T. Shen, M. Top, Y.T. Pei, J.T.M. De Hosson: Wear and friction performance of PTFE filled epoxy composites with a high concentration of SiO2 particles. Wear 322–323 (2015) 171–180.

[9] T. Larsen, T.L. Andersen, B. Thorning, A. Horsewell, M.E. Vigild: Changes in the tribological behavior of an epoxy resin by incorporating CuO nanoparticles and PTFE microparticles. Wear 265 (2008) 203–213.

[10] A.C. Greco, R. Erck, O. Ajayi, G. Fenske: Effect of reinforcement morphology on high-speed sliding friction and wear of PEEK polymers. Wear 271 (2011) 2222–2229.

[11] J.R. Vail, B.A. Krick, K.R. Marchman, W.G. Sawyer: Polytetrafluoroethylene (PTFE) fiber reinforced polyetheretherketone (PEEK) composites. Wear 270 (2011) 737–741.

[12] M. Watanabe, M. Karasawa, K. Matsubara: The frictional properties of nylon. Wear 12 (1968) 185–191.

[13] A. Pogacnik, M. Kalin: Parameters influencing the running-in and long-term tribological behaviour of polyamide (PA) against polyacetal (POM) and steel. Wear 290–291 (2012) 140–148.

[14] M. Godet: The third-body approach: a mechanical view of wear. Wear 100 (1984) 437-452.

[15] Y. Berthier: Maurice Godet's third body. The Third Body Concept: Interpretation of Tribological Phenomena, First edition, Elsevier Science (1996) 21-30.

[16] J. Denape: Third body concept and wear particle behavior in dry friction sliding conditions. Trans Tech Publications, ISBN 978-3-03835-425-3 (2014) 1-12.

[17] S.K. Sinha, B.J. Briscoe: Polymer tribology. Imperial College Press, London, United Kingdom (2009).

[18] E.F. Finkin: Surface energy and the theory of the friction of solids. Applied Physics Letters 30 (1977) 436.

[19] M.E. Makowiec, T.A. Blanchet: Improved wear resistance of nanotube- and other carbon-filled PTFE composites. Wear 374-375 (2017) 77–85.

[20] B.A. Krick, J.J. Ewin, G.S. Blackman, C.P. Junk, W.G. Sawyer: Environmental dependence of ultra-low wear behavior of polytetrafluoroethylene (PTFE) and alumina composites suggests tribochemical mechanisms. Tribology International 51 (2012) 42–46.

[21] S.S. Kandanur, M.A. Rafiee, F. Yavari, M. Schrameyer, Z. Yu, T.A. Blanchet, N. Koratkar: Suppression of wear in graphene polymer composites. Carbon 50 (2012) 3178–3183.

[22] V.N. Aderikha, A.P. Krasnov, V.A. Shapovalov, A.S. Golub: Peculiarities of tribological behaviour of low-filled composites based on polytetrafluoroethylene (PTFE) and molybdenumdisulfide. Wear 320 (2014) 135–142.

[23] E. Padenko, L.J. Van Rooyen, B. Wetzel, J. Karger-Kocsis: “Ultralow” sliding wear polytetrafluoro ethylene nanocomposites with functionalized graphene. Journal of Reinforced Plastics and Composites 35 (2016) 892–901.

[24] K.L. Harris, A.A. Pitenis, W.G. Sawyer, B.A. Krick, G.S. Blackman, D.J. Kasprzak, C.P Junk: PTFE tribology and the role of mechanochemistry in the development of protective surface films. Macromolecules 48 (2015) 3739–3745.

[25] T. Onodera, K. Kawasaki, T. Nakakawaji, Y. Higuchi, N. Ozawa, K. Kurihara, M. Kubo: Effect of tribochemical reaction on transfer-film formation by poly(tetrafluoroethylene). The Journal of Physical Chemistry 118 (2014) 11820–11826.

[26] G. Jintang: Tribochemical effects in formation of polymer transfer film. Wear 245 (2000) 100–106.

[27] Z. Zuo, Y. Yang, X. Qi, W. Su, X. Yang: Analysis of the chemical composition of the PTFE transfer film produced by sliding against Q235 carbon steel. Wear 320 (2014) 87–93.

[28] J. Sukumaran, J. De Pauw, P. D. Neis, L.F. Tóth, P. De Baets: Revisiting polymer tribology for heavy duty application. Wear 376-377 (2017) 1321–1332.

CHAPTER 2

LITERATURE SURVEY

This chapter introduces the principles of tribology, the widely used tribological thermoplastics, the overview of polymer tribology, the different lubrication methods and the tribological behaviour of filled PTFE.

The following review article was published based on this chapter: Tóth Levente Ferenc, Szebényi Gábor, Patrick De Baets: PTFE kopásállóságának növelése részecske adalékanyagokkal – review. Polimerek, 2017, 3, 276-281 (in Hungarian).

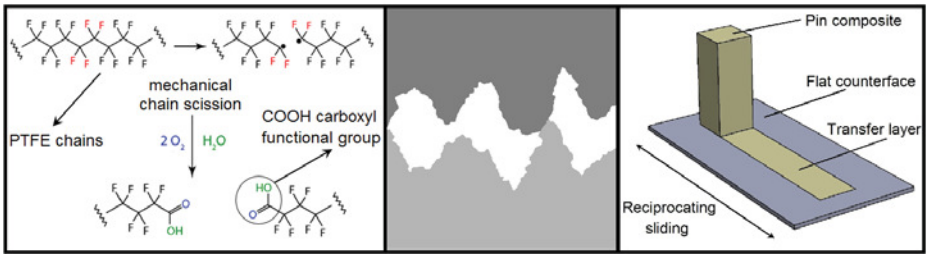

2.1. Introduction

2.1.1. Basics of tribology

According to the relative motion of interactive components, the contact type can be either rolling (e.g. railway lines in an ideal case), sliding (e.g. plain bearings) or sliding-rolling (gears, cams) [1]. This literature overview is focusing on the sliding contact type.

It is well known that in the relative motion of interacting surfaces, the real contact area is different from the nominal contact area. In the real contact area, only some peaks of the interactive surfaces are in contact (Figure 2.1). In this way, the real contact area is influenced by the asperities of the contact surfaces or in other words, by the roughness of the surfaces [1, 2]. The relative motion of interacting surfaces can break or deform the surface peaks, resulting in material loss; this phenomenon is the wear, while the force, resisting the relative motion, is the friction [2, 3]. The friction and wear are not only material properties, but they are also system properties as they depend on the actual tribological system. Many factors can influence the friction and wear properties of the interactive surfaces. There are some influencing parameters which are independent of the material properties; these are for example the contact type, the contact geometry, the counterface material, the sliding/rolling speed, the contact pressure, the surface roughness and pattern, the atmosphere, the ambient temperature and the relative humidity. The friction and wear influencing material properties can be the thermal conductivity, the melting/degradation temperature, the density (porosity), the hardness, the tensile/compressive/shear strength and the modulus of elasticity [1, 2, 4].

Figure 2.1. The asperities of contacting surfaces.

The wear mechanisms can be abrasion, adhesion, erosion, cavitation, corrosion and surface fatigue [5]. In abrasive wear, a rough and hard surface is in contact with a relatively softer surface, resulting in removing some particles from the softer surface [6]. In case of adhesive wear, there is a strong adhesive bond between the interactive surfaces. This strong bond results in plastic deformation and crack formation. The continuous sliding breaks the formed bonds, and as a result, cavities appear on the surfaces [6]. Erosion is a phenomenon where particles' repeated and constant impact is the dominant factor of the wear mechanism. Cavitation is a fatigue phenomenon due to high-impact jets of imploding bubbles. The reduced pressure of the high speed flowing liquid results bubble formation at the solid surface. In this mechanism the formed bubbles collapse and as a consequence some material is removed from the solid surface. In corrosive wear, the material loss originates from (electro-)chemical

reactions at the surface. In oxidative wear, due to the reaction between the metal and the atmospheric oxygen, an oxide layer is formed, which has a remarkable influence on the wear mechanism. In case of surface fatigue, the repeated, alternating (cyclic) stresses in the near-surface region lead to the formation and propagation of cracks under the loaded surface. These cracks have a dominant role in the wear mechanism [7].

2.1.2. A short history of thermoplastics in the viewpoint of tribology

The history of synthetic polymers started in 1907 with the development of Bakelite by Leo Baekeland. From 1938 toothbrushes were commercially available made from the first promising synthetic thermoplastic, Nylon 6 (polyamide 6, PA 6). In the same year, Roy Plunkett, who was an employee of Chemours, invented polytetrafluoroethylene (PTFE) which got the well-known Teflon brand-name [8, 9]. The industrial production of low-density polyethylene (LDPE) started in 1939 due to the development of a reproducible production method by Michael Perrin. Hermann Staudinger discovered the acetal (polyoxymethylene, POM) in the 1920s, but its stable version is commercially available only from 1960 by DuPont. Other well-known tribological thermoplastic, the polyether ether ketone (PEEK), is launched only in the 1980s. Polymer tribology related research started from the 1950s, focusing on rubbers, PTFE and polyamide (PA) [10-14]. In the following decades, semi-crystalline thermoplastics became widely used materials in tribological applications due to their internal damping capacity, low density, chemical and corrosion resistant nature, quiet running, the withstanding of dirty, dusty environment and self-lubrication nature [15-17].

2.1.3. Liquid and solid lubrication for polymers

Liquid and solid lubricants can modify the contact surface properties improving the friction and wear parameters. Some of the semi-crystalline thermoplastics can run in dry condition without liquid or solid lubrication, but for other polymers, lubrication is highly recommended.

2.1.3.1. Liquid lubrication

As it is known, some of the polymers can run dry without any lubrication. Still, the application of lubricants can provide a longer lifetime for the components, especially when the running temperature is high. An important rule is to avoid the same solubility parameters for the lubricant and the polymer, otherwise the lubricant could act as a solvent of the polymer. The used oils must be chemically inert, and they must wet the polymeric surface easily. At this lubrication method, the coefficient of friction is more stable compared to most of the solid lubricants. At high load, the liquid can be squeezed out from the contact surfaces if the speed does not reach a specific minimum value. The liquid lubricant's viscosity and evaporation highly depend on the temperature, and a strong oxidation condition is also unbeneficial for liquid lubricants. Another disadvantage is that in vacuum, the liquid lubricant can evaporate from the

contact surfaces. The construction and design of the tribo-elements are more complex due to the liquid lubrication. Water is generally spoken not an adequate lubricant; however, it can be used as a cooling liquid [18-20].

Novel research focuses on ionic liquids as potential lubricants in tribological applications. These liquids are melted salts, usually consisting of a large organic cation paired with a smaller organic/inorganic anion [21]. The first publication of ionic liquid in a lubrication aspect appeared in 2001 [22]. In general, ionic liquids have high thermal and chemical stability, negligible vapour pressure, broad liquid range, high viscosity and low melting temperature. They can reduce the friction and wear properties as they form absorbed ordered layers on material surfaces. A drawback of the ionic liquids is the relatively high cost compared to conventional liquid lubricants [21, 23, 24].

2.1.3.2. Solid lubricants and coatings

Solid lubricants incorporated into the bulk material or into the coating can be used to decrease the friction forces between the sliding components. The advantages of these materials are the broader temperature range and the higher static load carrying capacity compared to liquid lubricants. The construction of the tribo-system is less complex as no external oil-supply system is required. With solid lubricants, the fluctuations of the coefficient of friction is larger than with liquid ones [19, 20].

Plenty of research focus on the solid lubricants and coatings. As an example in 2013, Dearn *et al*. investigated the performance of different coatings on gears [25]. They used unreinforced PA, reinforced and unreinforced PEEK as bulk material with molybdenum disulphide (MoS_2), graphite, boron nitride (BN) and PTFE coatings. The applied gear pairs were the following: coated-coated, coated-steel and coated-uncoated gears. The observed failure mechanisms were the delamination and abrasive wear of the coatings. PTFE and graphite coatings provided significantly lower friction, temperature and wear for the polymer gears, increasing the power transmission and gear life. PTFE coating achieved the most remarkable enhancement in friction and lifetime. This improvement comes from the 30°C running temperature reduction and from the 90% wear decreasing compared to the uncoated polyamide gears [25].

The incorporation of graphite particles reduced the friction and wear of polyester coatings as well. The lowest friction and wear properties were achieved with 35% filler content [26].

2.1.4. Polytetrafluoroethylene (PTFE) in tribology

Nowadays, PTFE is used in several tribological applications as a matrix material or as a filler (solid lubricant). Some examples are the rolling and plain bearings, the gears, the seals, the membranes and the gaskets. PTFE is well known in medical or food/household applications as well [27-32]. There are examples in the literature where researchers used PTFE in

nanoparticle form. They incorporated PTFE nano-fillers into lubrication oils, reducing the coefficient of friction and wear rate of the contact materials [33-36]. This broad application potential comes from its low coefficient of friction, chemically inert behaviour, self-lubricating nature and high thermal stability compared to other polymers [37-40]. The self-lubricating nature gives the possibility to design tribological systems without external lubrication to make the construction less complex, and to decrease the operational costs. PTFE is a semi-crystalline thermoplastic; the molecular chains include carbon and fluorine atoms with single covalent bonds. The degree of crystallinity depends on the applied processing protocol, and has a significant influence on the tribological performance. Typical degree of crystallinity of PTFE is between 40% and 50% [41-43].

Besides the benefits, there are also some challenges with PTFE. The molecular weight of PTFE is in the range of 10^5 - 10^6 g/mol, which results in extremely high melt viscosity. This value is too high for conventional melt-processing methods such as injection moulding [44]; therefore, high-temperature sintering and ram extrusion are the typical processing method of PTFE. Other challenges are the poor dimensional stability and the high wear rate of neat PTFE. Micro- and nano-fillers can increase the wear resistance with orders of magnitude compared to unfilled PTFE. Widely used and investigated fillers in the PTFE matrix are bronze, graphite, molybdenum-disulphide (MoS_2), copper, glass fibre, alumina (Al_2O_3) or graphene [45-48]. The wear resistance of PTFE can be further improved compared to the commercially available filled PTFE if we develop these materials knowing the tribo-chemical background during the wear process. These tribo-chemical reactions influence the adhesion between the fillers and the PTFE matrix and between the polymer material and the steel counterface. For further wear rate decreasing, we also have to analyse the transfer layer formation, as the quality and durability of the transfer layer remarkably influence the wear rate and the coefficient of friction [49-51].

2.1.5. Friction and wear mechanism of filled and unfilled PTFE

This paragraph discusses the morphological properties of PTFE as it influences the tribological features significantly. The high molecular weight PTFE has banded, lamellar structure. In contrast with most of the semi-crystalline polymers, PTFE has a lack of spherulitic superstructure. Due to the lack of spherulites in a banded structure, less activation energy is needed for the slippage between the crystalline slices during wear compared to the spherulitic structure [52]. This unique morphological structure can be a reason for the observed high wear rate of PTFE compared to other semi-crystalline thermoplastics. According to Tanaka *et al.* [52], this banded structure of PTFE influences more the wear rate than the degree of crystallinity. They also concluded that bands with higher length increased the wear of the PTFE [52, 53].

Kar *et al.* [53] tested PTFE in sliding condition against steel counterface at 1.5/2.5/4 m/s sliding speed. The applied configuration was pin-on-disc with a load of 2750 g. They stated that the sliding surface of PTFE did not reach its melting temperature (327°C) during wear test, at none of the sliding speeds. The melting temperature of the original PTFE and the removed sliding surface of PTFE were investigated by (differential thermal analysis) DTA, and they did not find differences at their melting temperature. They concluded that the high wear rate of PTFE could not originate from reaching the melting temperature. The observed high material loss comes from the continuous removal of thin PTFE films from the steel counterface. This removal is caused by the front edge of the PTFE pin as there is a low adhesion between the formed thin PTFE film and the steel surface. This explanation is in agreement with the introduced morphological structure in the previous paragraph. At higher speeds higher wear rate occurs due to the more intensive material film removal [53]. PTFE has a low coefficient of friction which can come from the formed low shear strength film on its surface. This repetitive and intensive formation and destruction of surface films result in high wear rate [54].

Fillers can enhance the wear resistance, the coefficient of friction and the creep of PTFE. PTFE is a chemically inert material, and in this way PTFE can not make chemical bonds with the applied fillers. The high shear modulus fillers are just encapsulated in the low shear modulus PTFE matrix. Hard particle fillers as a second phase can reduce the wear rate of PTFE as they decrease the sub-surface fracture and minimise the yielding of the material. In this way, the load-carrying capacity of PTFE is increasing [55, 56]. Some fillers can increase the thermal conductivity of PTFE, and due to the increased thermal conductivity, the frictional heating is transferred more effectively from the contact surface of PTFE. As the heat transfer from the contact surface increases, the temperature decreases, resulting in less reduction of temperature-dependent mechanical properties [54, 55].

2.2. Basics of polymer tribology – chronological overview

In 1963 Adams stated that in case of low load and low sliding speed, the friction of a PA hemisphere increases with the increase of sliding speed and load [57]. In 1965, Vinogradov *et al*. published similar results with PP (polypropylene) samples [58]. At constant sliding speed, the higher load increased the coefficient of friction as the real contact area increased between the two interactive surfaces. The higher friction generated higher heat which softened the surface of the PP. Due to the softened surface, the real contact area further increased, which caused a further rise in the coefficient of friction. At a critical value of the load, a thin film of PP melt appeared on the surface of the polymer sample which acted as a lubrication agent due to the lower internal friction of the thin melt layer. As a consequence, above the critical value of the load, the coefficient of friction decreased as the load increased. This critical load

corresponds to the maximum of the curves in Figure 2.2. This behaviour was independent of the applied counterface material (copper, aluminium, steel and cast iron) [58].

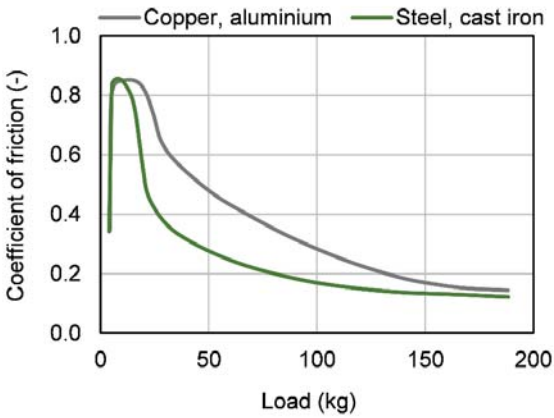

Figure 2.2. Coefficient of friction between metal and PP as a function of the load in dry condition and air atmosphere. The applied sliding speed was 0.146 m/s [58].

In 1968 Watanabe *et al.* published their results related to the friction of PA measured between the end surfaces of two cylindrical steel rings [59]. They confirmed that the coefficient of friction reaches a maximum at a given load. This maximum value of the coefficient of friction and the critical load depend on the roughness of the surfaces, the contacting materials, the ambient temperature and the sliding speed. They did not find any maximum value in case of PA-PTFE pair as the frictional behaviour of PTFE predominated over the PA. They reported that the maximum of the coefficient of friction decreases as the surface roughness decreases. Regarding the lower surface roughness the maximum of the coefficient of friction is reached at a higher load [59].

In 1982 K. Tanaka investigated the wear of high-density polyethylene (HDPE), low-density polyethylene (LDPE), PA 6 and PTFE using a pin-on-disc tribo-tester [60]. The cylindrical polymer specimens were tested against mild steel discs with 10-50 N load, 0.1 m/s sliding speed at room temperature. PTFE had the most significant wear depth (1400 μm) while HDPE had the lowest (40 μm) after 10^4 cycles. All of the polymers, except PTFE, had lower wear rate after an initial transient wear stage (~2000 cycles) with a higher wear rate. At the first 100 cycles, the wear rate was remarkably high, but after this distance, the wear rate decreased with the increasing number of disk revolutions. After ~2000 revolutions the wear rate stabilised to a lower and constant value. PTFE had only a short initial transient wear stage, and the wear depth increased linearly with the number of cycles. This behaviour was observed at both 10 N and 50 N contact load [60].

In 1987 Voss *et al.* published the wear behaviour of glass and carbon fibre reinforced PEEK composites against 100Cr6 steel counterfaces in pin-on-ring configuration [61]. The initial surface roughness (Ra) of the steel counterfaces was ~0.06 μm; the sliding speeds were 0.6, 1.5 and 3.0 m/s. At low speed, glass fibre reinforced PEEK had lower wear rate than the reference neat PEEK. The carbon fibre reinforced PEEK composites reached lower wear rate compared to the glass fibre reinforced ones. Figure 2.3 introduces the wear rate of short glass fibre reinforced PEEK, polyamide 66 (PA 66) and polyethersulfone (PES) as a function of the filler content. PEEK and PA 66 achieved a significantly lower wear rate compared to PES [61].

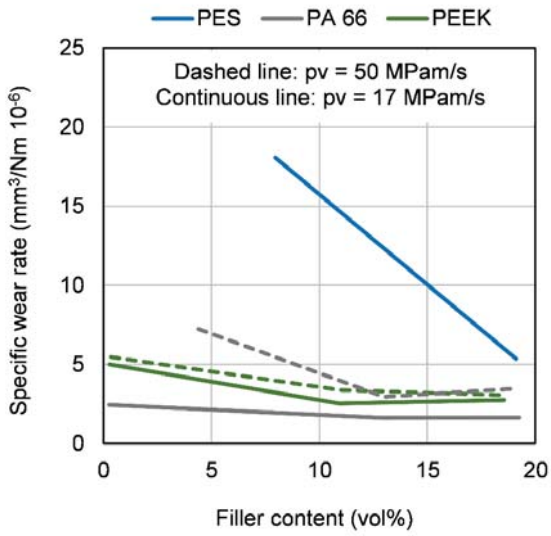

Figure 2.3. Specific wear rates of short glass fibre reinforced PA 66, PEEK and PES as a function of the filler content (vol%) [61].

In 1996 Hooke *et al.* investigated POM and PA 66 polymer composites with the use of a twin-disc machine (two polymer discs were running against each other) [62]. They applied 200-300 N load, 1000 rpm sliding speed, 10^7 cycles and 0-30% slip ratio. The matrix crystallinity and the material composition influenced the friction and wear of the glass fibre reinforced composites. Samples with 40 wt% glass fibre content have a higher wear rate than materials with 30 wt%. Composites with high crystallinity matrix show significantly higher wear rate compared to low crystallinity matrix. Specimens with glass fibre have a lower coefficient of friction than specimens with carbon and aramid fibres. In case of unreinforced polymers, POM had longer component life and lower contact temperature than PA66. At PA 66 samples, deep cracks appeared at the surface of the component resulting in higher wear. These results are related only to polymer pairs [62].

In 1999 Kukureka *et al*. investigated the wear of PA 66 matrix with different reinforcement materials under dry rolling-sliding contact with a twin-disc machine [63]. They applied 50-600 N load, 1000 rpm sliding speed, 10^7 cycles and 0-30% slip ratio. In case of composite-composite contact, all reinforcements (glass, carbon and aramid fibres) increased the wear rate with one order of magnitude compared to the neat polyamide. Carbon and glass fibres reduced the coefficient of friction; in this way, higher loads and slips can be transferred before the melting temperature of the matrix material is reached. In contrast with the composite-composite contact, in composite-metallic contacts, the use of fibre reinforcements decreased the wear. The carbon and aramid fibre reinforced composites had a remarkably higher coefficient of friction than glass fibre composites resulting in a higher surface temperature [63].
In 2004 Schön measured the coefficient of friction and the wear of carbon fibre reinforced epoxy composites in sliding composite-composite contact [64]. The dominant factors of the wear mechanisms were the wear of the matrix and the crack propagation in the fibre-matrix interface which resulted delamination and broken fibres (Figure 2.4) [64].

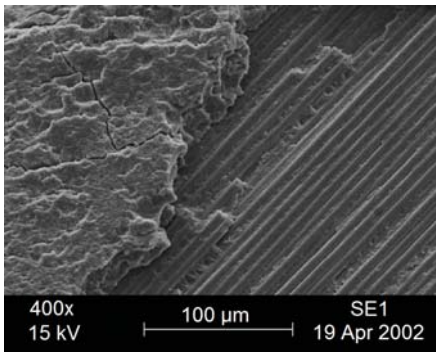

Figure 2.4. Groups of broken fibres on the worn surface [64].

In 2004 Unal *et al*. investigated the influence of speed and contact pressure on the friction and wear behaviour [65]. PA 66, POM, ultrahigh molecular weight polyethylene (UHMWPE), polyphenylene sulphide (PPS) with 30% glass fibre and aliphatic polyketone (APK) polymers were compared to each other by pin-on-disc tests. They applied 0.5 – 2.0 m/s sliding speed, 0.35 – 1.05 MPa contact pressure and 1000 m sliding distance at room temperature. The polymer specimens were tested against AISI D2 steel discs with 0.11 µm surface roughness (Ra) [65]. The coefficient of friction for all polymers linearly decreased as the contact pressure increased. The specific wear rates of UHMWPE, PPS with 30% glass fibre and APK were in the order of 10^{-5} mm^3/Nm. The wear rate value for PA 66 was in the order of 10^{-6} mm^3/Nm and for POM was in the order of 10^{-3} mm^3/Nm. PA 66 and POM showed micro-cutting and plastic deformation at their surfaces, PPS had a rough surface with glass fibre particles exposed in the matrix, while APK polymer showed a wavy morphology surface with peaks and valleys [65].

In 2007 Jia *et al*. published that the friction and wear behaviour of PA 66 - PA 66 pairs are strictly dependent on the pv value for the dry sliding condition, while the pv value has a slight effect on the tribological behaviour in case of oil-lubricated conditions [66]. The coefficients of friction of PTFE, PA 66 and PPS self-mated couples under liquid paraffin lubrication decreased by one order of magnitude compared to dry friction conditions. Liquid paraffin also decreased the wear of PTFE and PPS, while it increased the wear of PA 66. Frictional heat had a significant effect on the tribological behaviour of polymer-polymer combinations under dry friction. The external oil lubrication reduced the frictional heat during the sliding process, and hence decreased the friction and wear. The authors supposed that the higher wear of PA 66 under oil lubrication was due to the mechanical strength reduction because of the oil diffusion into the surface layer [66].

In 2011 Greco *et al*. investigated the tribological behaviour of PEEK disc samples against 440C stainless steel balls at 23-25°C temperature and 20-40% relative humidity [67]. They manually increased the speed from 0 up to 65 m/s, held the speed for 5 s at the maximal value, then they decreased the speed down to 0. The increasing and decreasing rate was 2.3 m/s^2. The tested materials were neat PEEK, PEEK with long woven carbon fibres and PEEK with short, randomly oriented carbon fibres. The short fibre reinforced PEEK included 10 wt% PTFE and 10 wt% graphite powder as well. All of the materials had a decreasing coefficient of friction trend as the load increased. PEEK with long woven fibres had the lowest coefficient of friction (Figure 2.5). The lower friction was related to the less abrasive morphology of the long woven fibres compared to the short randomly oriented fibres [67].

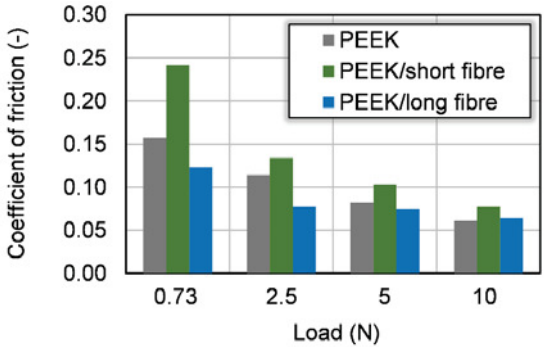

Figure 2.5. The coefficient of friction as a function of the load for neat PEEK, PEEK with long woven carbon fibres and PEEK with short, randomly orientated carbon fibres [67].

PEEK with short, randomly oriented fibres had the highest wear rate, neat PEEK had higher wear rate only at 10 N load. PEEK with long woven fibre had high wear resistance at 0.73 and 2.50 N load, but their wear rate increased remarkably at 5 and 10 N loads as the carbon fibres started to fracture (Figure 2.6 (a)). Abrasive wear caused by the fibres appeared on the steel

ball surfaces tested against both of the composite samples. At high loads the polymers softened and the carbon fibres were separated from the matrix, resulting in more pronounced abrasive action (Figure 2.6 (b)) [67].

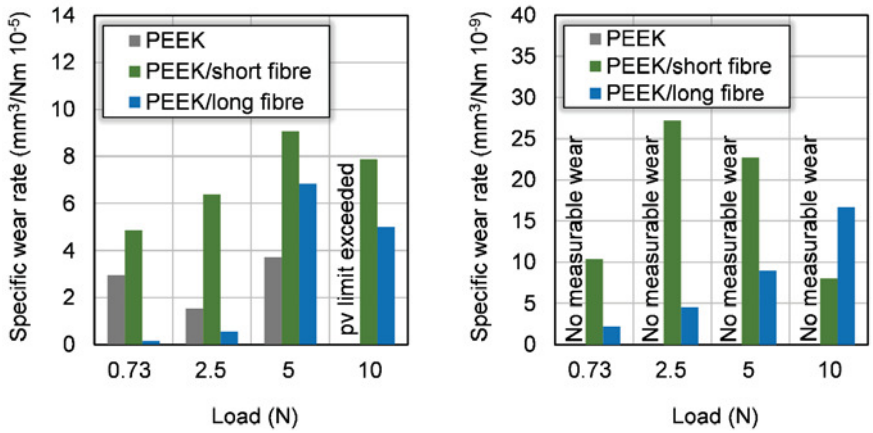

Figure 2.6. Specific wear rate as a function of load, (a) wear on the polymer disc surface and (b) wear on the steel ball surface [67].

2.3. Tribological characterisation of PTFE composites

2.3.1. *In situ* functionalization of PTFE during wear

Gong *et al.* published in 1990 that there is a tribo-chemical reaction between the transfer layer of PTFE and the metal counterface. The researchers carried out their analysis with X-ray photoelectron spectroscopy (XPS) [68]. They detected new chemical bonds in case of iron, silicon, zinc and aluminium counterfaces (active metals), but sliding against copper and silver was without detection of new bonds [68]. They supposed that the fluorine atoms of PTFE reacted with the active metallic atoms in the metal oxide layer, forming active metal fluoride [68]. Based on their results, we can suppose that those metals which are resistant to corrosion and oxidation are not able to react with the fluorine atoms of PTFE (e.g. gold, silver, platinum, copper and other noble metals). During wear, the long PTFE molecular chains undergo mechanical chain scission (Figure 2.7 (a) and (b)). On the PTFE chain ends carboxyl groups (COOH) are formed (*in situ* “carboxyl functionalization”) under the action of air and humidity [69-72]. With X-ray photoelectron spectroscopy (XPS) researchers observed the new peaks caused by the new chemical bonds formed during the wear process [45]. The terminal carboxyl groups, formed during wear, can chelate to the metal counterface to form a thin and robust transfer film (Figure 2.7 (f)) and with the functional groups of the filler (e.g. functionalized graphene filler) [45, 71-73].

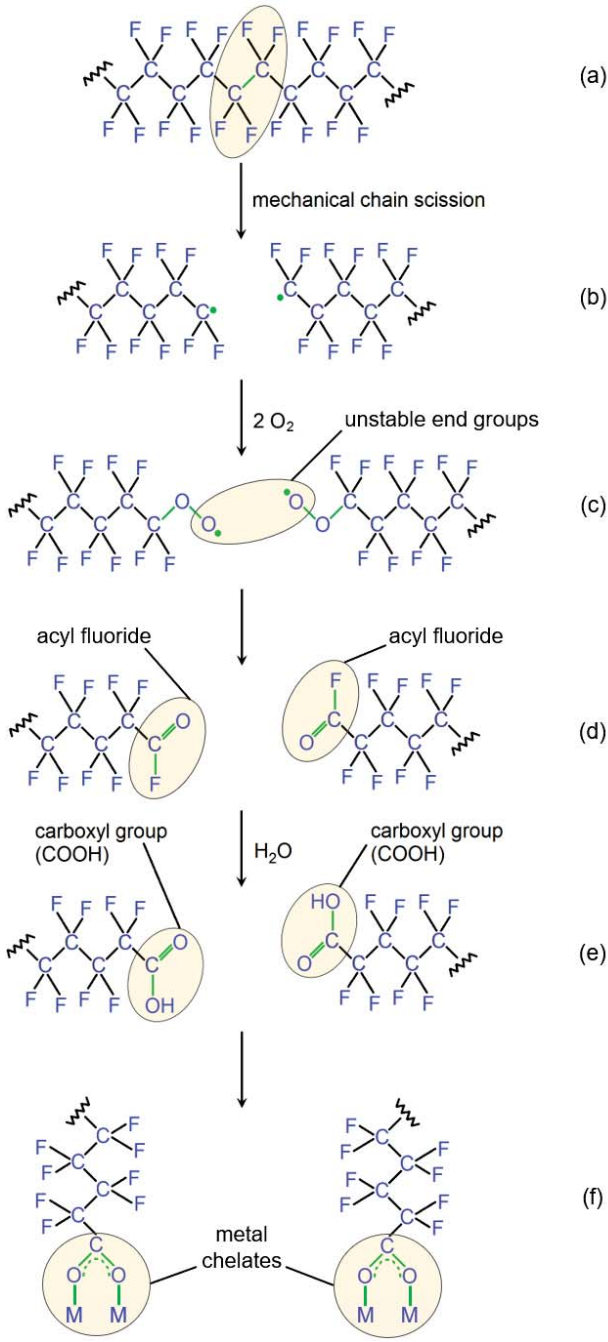

Figure 2.7. Mechanical chain scission and *in situ* carboxyl functionalization of PTFE chains in wear process [72].

There are two different models to explain the terminal carboxyl group formation on the PTFE chain ends. Both hypotheses suppose the importance of humidity in the tribo-chemical processes [72, 73]. According to the model of Harris *et al*. [72], after the mechanical chain scission of PTFE (Figure 2.7 (a) and (b)), the oxygen from the air reacts with the radicals of the chain ends forming unstable end groups (Figure 2.7 (c)). These unstable end groups decompose, and acyl fluoride is supposed to form (Figure 2.7 (d)). These acyl fluorides are hydrolysed by the moisture of the air to form carboxyl functional groups (Figure 2.7 (e)).

2.3.2. Wear resistance enhancement of PTFE

2.3.2.1. Potential fillers to decrease the wear rate of PTFE

A more uniform and adequate transfer layer can form when PTFE contains fillers. Some examples for these fillers are the graphene, alumina, lead monoxide (PbO), lead tetroxide (Pb_3O_4), copper(I) oxide (Cu_2O), iron(III) oxide (Fe_2O_3) and iron(II,III) oxide (Fe_3O_4) [69].
Table 2.1 and 2.2 introduce the tribo-test results of unfilled and filled PTFE samples from the literature. The applied counterface materials were steel, the tests were performed in air atmosphere, at room temperature, in dry contact. In Table 2.1, the coefficient of friction and wear rate values are given for both unfilled PTFE, as reference material, and filled PTFE. Table 2.2 shows the applied configurations and parameters. The average particle size of bronze, graphite, MoS_2 and copper fillers were in the range of few tens μm (Table 2.1). The introduced reference glass fibres had a diameter with average 7-10 μm, and length with average 50-100 μm [54, 74, 75]. The average particle size of the applied Al_2O_3 was 80 nm (Table 2.1, row 22-24) and 38 nm (Table 2.1, row 21 and 25-27). The average particle size and thickness of graphene nanoplatelets was 25 μm and 6-8 nm (Table 2.1, row 28-37), and a few μm and 2 nm (Table 2.1, row 38-41), respectively. Table 2.1, row 33-37 introduces the tribological results of oxyfluorinated graphene (OF) which contained functional groups. The relative humidity (RH%) was 2.5; 35 and 68% in tests introduced at row 22, 23 and 24, respectively. Figure 2.8 shows the pin-on-flat, pin-on-disc and block/plate-on-ring configurations presented in Table 2.2.
The wear resistance of PTFE is increased by 1-2 orders of magnitude with the incorporation of micro-fillers such as graphite, MoS_2 or copper. In comparison, the bronze increased it by three orders of magnitude (Table 2.1). In case of glass fibres, Blanchet *et al*. got three orders of magnitude improvement with pin-on-disc configuration, Khedkar *et al*. registered a wear rate of 10^{-4} mm^3/Nm for both neat PTFE and filled PTFE [74]. Klaas *et al*. reported a wear rate of 10^{-6} mm^3/Nm for glass fillers with different geometry and shape [76], they did not find significant differences as a function of the shape (Table 2.1). New-age research appeared related to wear rate decreasing of PTFE with the incorporation of nano-fillers [45, 46, 71-73, 77, 78]. With the application of Al_2O_3 and graphene significant wear rate decreasing was achieved with a value

of 3-4 orders of magnitude compared to the neat PTFE (Table 2.1). Furthermore, graphene reduced the coefficient of friction with approximately 50% [71]. Graphene increased the wear resistance up to three orders of magnitude improvement at 5 and 10 wt% filler content (Table 2.1) [46, 71]. The functional groups of oxyfluorinated graphene did not show a relevant enhancement compared to the conventional graphene [71, 79]. From Table 2.1, it can be seen that the relative humidity of the atmosphere significantly affects the wear rate of Al_2O_3. Applying the same test conditions and parameters, at 2.5% relative humidity the wear resistance increased with two orders of magnitude. In comparison, at 35 and 68% relative humidity, the wear resistance improvement reached or exceeded the three orders of magnitude (Table 2.1) [45]. It is noteworthy to mention here that these tests (Table 2.2, row 22-24) were performed with the same contact pressure and sliding speed against 304 stainless steel [45]. As transfer layer did not form in the absence of humidity, Krick *et al.* assumed the existence of chemical reaction at higher relative humidity [45]. When the relative humidity was not controlled, such a significant increase in wear resistance was not registered [80].

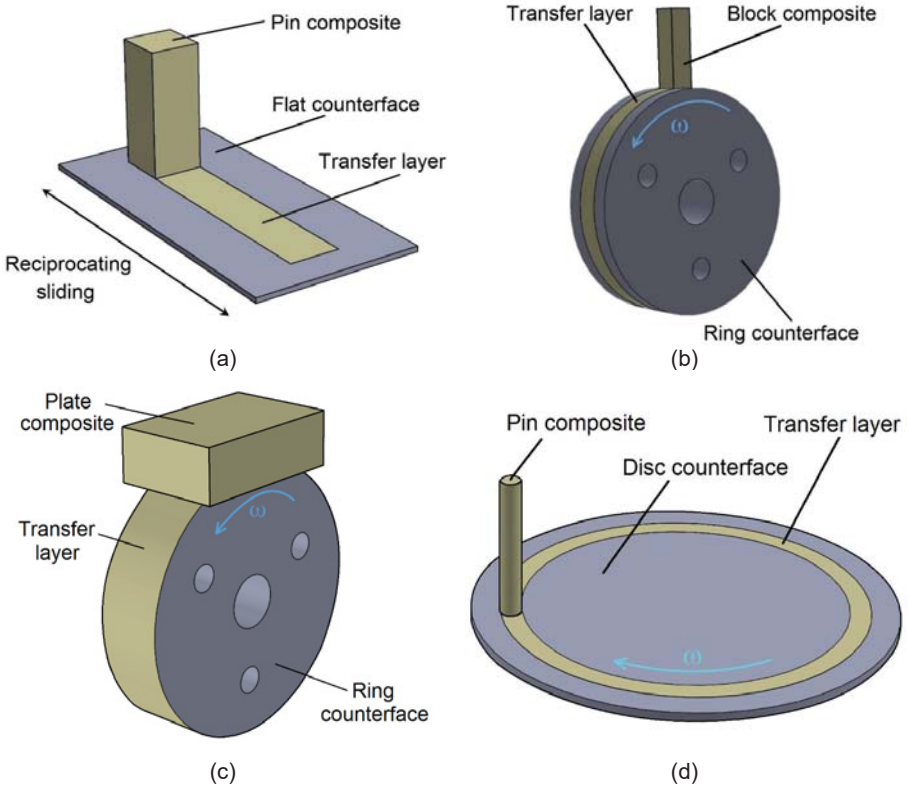

Figure 2.8. Schematic representation of pin-on-flat (a), block-on-ring (b), plate-on-ring (c) and pin-on-disc (d) configurations.

Table 2.1. Coefficient of friction and wear rate of PTFE composites in dry contact, air atmosphere, at room temperature. Yellow highlighted cells: 3 orders of magnitude decreasing of wear rate and 50% decreasing of the coefficient of friction. In row 33-37, OF graphene represents the oxyfluorinated graphene.

∗ Row 22, 23 and 24: relative humidity is 2.5; 35 and 68%, respectively [45].

	Filler	Filler content	Wear rate PTFE (ref.) (mm^3/Nm)	Wear rate Composite (mm^3/Nm)	Coefficient of friction PTFE (ref.) (-)	Coefficient of friction Composite (-)	
1	bronze	40 wt%	$8.0 \cdot 10^{-4}$	$2.0 \cdot 10^{-7}$	0.18	0.13	[74]
2	bronze	40 wt%	$3.0 \cdot 10^{-4}$	$6.0 \cdot 10^{-7}$	0.22	0.29	[75]
3	graphite	5 vol%	$7.3 \cdot 10^{-4}$	$5.8 \cdot 10^{-5}$	0.26	0.14	[81]
4	graphite	10 vol%	$7.3 \cdot 10^{-4}$	$2.0 \cdot 10^{-5}$	0.26	0.17	[81]
5	graphite	20 vol%	$7.3 \cdot 10^{-4}$	$1.5 \cdot 10^{-5}$	0.26	0.18	[81]
6	graphite	30 vol%	$7.3 \cdot 10^{-4}$	$8.0 \cdot 10^{-6}$	0.26	0.19	[81]
7	graphite	15 wt%	$8.0 \cdot 10^{-4}$	$5.0 \cdot 10^{-6}$	0.18	0.16	[74]
8	graphite	15 wt%	$3.0 \cdot 10^{-4}$	$4.0 \cdot 10^{-6}$	0.22	0.22	[75]
9	MoS_2	20 wt%	$3.0 \cdot 10^{-4}$	$1.0 \cdot 10^{-5}$	0.22	0.21	[75]
10	copper	5 vol%	$7.3 \cdot 10^{-4}$	$4.7 \cdot 10^{-5}$	0.26	0.22	[81]
11	copper	10 vol%	$7.3 \cdot 10^{-4}$	$8.0 \cdot 10^{-6}$	0.26	0.24	[81]
12	copper	20 vol%	$7.3 \cdot 10^{-4}$	$\sim 1 \cdot 10^{-6}$	0.26	0.20	[81]
13	copper	30 vol%	$7.3 \cdot 10^{-4}$	$\sim 1 \cdot 10^{-6}$	0.26	0.20	[81]
14	glass fibre	15 vol%	$9.0 \cdot 10^{-4}$	$7.0 \cdot 10^{-4}$	0.12	0.13	[54]
15	glass fibre	25 vol%	$9.0 \cdot 10^{-4}$	$3.0 \cdot 10^{-4}$	0.12	0.13	[54]
16	glass fibre	25 wt%	$8.0 \cdot 10^{-4}$	$5.0 \cdot 10^{-7}$	0.18	0.25	[74]
17	glass fibre	25 wt%	$3.0 \cdot 10^{-4}$	$1.0 \cdot 10^{-6}$	0.22	0.31	[75]
18	glass fibre	25 wt%	n/a	$1.3 \cdot 10^{-6}$	n/a	0.17	[76]
19	glass bead	25 wt%	n/a	$1.2 \cdot 10^{-6}$	n/a	0.18	[76]
20	glass flake	25 wt%	n/a	$4.7 \cdot 10^{-6}$	n/a	0.18	[76]
21	Al_2O_3	4 wt%	$4.8 \cdot 10^{-4}$	$2.0 \cdot 10^{-5}$	0.16	0.21	[80]
22∗	Al_2O_3	5 wt%	$6.3 \cdot 10^{-4}$	$4.4 \cdot 10^{-6}$	0.16	0.19	[45]
23∗	Al_2O_3	5 wt%	$4.3 \cdot 10^{-4}$	$5.6 \cdot 10^{-7}$	0.12	0.20	[45]
24∗	Al_2O_3	5 wt%	$4.9 \cdot 10^{-4}$	$2.4 \cdot 10^{-7}$	0.14	0.16	[45]
25	Al_2O_3	8 wt%	$4.8 \cdot 10^{-4}$	$1.0 \cdot 10^{-5}$	0.16	0.19	[80]
26	Al_2O_3	12 wt%	$4.8 \cdot 10^{-4}$	$3.0 \cdot 10^{-6}$	0.16	0.18	[80]
27	Al_2O_3	20 wt%	$4.8 \cdot 10^{-4}$	$1.0 \cdot 10^{-6}$	0.16	0.22	[80]
28	graphene	0.25 vol%	$1.6 \cdot 10^{-4}$	$2.7 \cdot 10^{-4}$	0.27	0.23	[71]
29	graphene	0.75 vol%	$1.6 \cdot 10^{-4}$	$2.8 \cdot 10^{-4}$	0.27	0.17	[71]
30	graphene	1 vol%	$1.6 \cdot 10^{-4}$	$2.4 \cdot 10^{-4}$	0.27	0.17	[71]
31	graphene	2 vol%	$1.6 \cdot 10^{-4}$	$1.7 \cdot 10^{-5}$	0.27	0.12	[71]
32	graphene	4 vol%	$1.6 \cdot 10^{-4}$	$6.6 \cdot 10^{-6}$	0.27	0.14	[71]
33	OF graphene	0.75 vol%	$2.0 \cdot 10^{-4}$	$2.6 \cdot 10^{-4}$	0.29	0.19	[79]
34	OF graphene	1 vol%	$2.0 \cdot 10^{-4}$	$5.1 \cdot 10^{-5}$	0.29	0.18	[79]
35	OF graphene	2 vol%	$2.0 \cdot 10^{-4}$	$1.1 \cdot 10^{-5}$	0.29	0.21	[79]
36	OF graphene	4 vol%	$2.0 \cdot 10^{-4}$	$5.5 \cdot 10^{-6}$	0.29	0.17	[79]
37	OF graphene	7 vol%	$2.0 \cdot 10^{-4}$	$1.2 \cdot 10^{-5}$	0.29	0.24	[79]
38	graphene	0.12 wt%	$4.0 \cdot 10^{-4}$	$4.0 \cdot 10^{-4}$	n/a	n/a	[46]
39	graphene	0.32 wt%	$4.0 \cdot 10^{-4}$	$3.0 \cdot 10^{-5}$	n/a	n/a	[46]
40	graphene	5 wt%	$4.0 \cdot 10^{-4}$	$4.0 \cdot 10^{-7}$	n/a	n/a	[46]
41	graphene	10 wt%	$4.0 \cdot 10^{-4}$	$1.0 \cdot 10^{-7}$	n/a	n/a	[46]

Table 2.2. The configurations and the parameters of wear tests with PTFE composites. The pin and block polymer samples were flat. Reciprocating movement is signed by (r).

∗ Row 22, 23 and 24: relative humidity is 2.5; 35 and 68%, respectively [45].

	Configuration	Counterface	Pressure	Sliding speed (m/s)	Sliding distance Composite (m)	
1	pin-on-disc	316, disc	6.55 MPa	0.05	n/a	[74]
2	pin-on-disc	mild steel, disc	1.4 MPa	0.50	n/a	[75]
3	block-on-ring	1Cr18Ni9Ti, ring	196 N	0.45	1602	[81]
4	block-on-ring	1Cr18Ni9Ti, ring	196 N	0.45	1602	[81]
5	block-on-ring	1Cr18Ni9Ti, ring	196 N	0.45	1602	[81]
6	block-on-ring	1Cr18Ni9Ti, ring	196 N	0.45	1602	[81]
7	pin-on-disc	316, disc	6.55 MPa	0.05	n/a	[74]
8	pin-on-disc	mild steel, disc	1.4 MPa	0.50	5000	[75]
9	pin-on-disc	mild steel, disc	1.4 MPa	0.50	n/a	[75]
10	block-on-ring	1Cr18Ni9Ti, ring	196 N	0.45	1602	[81]
11	block-on-ring	1Cr18Ni9Ti, ring	196 N	0.45	1602	[81]
12	block-on-ring	1Cr18Ni9Ti, ring	196 N	0.45	1602	[81]
13	block-on-ring	1Cr18Ni9Ti, ring	196 N	0.45	1602	[81]
14	ball-on-disc	440C, ball	5 N	0.10	5000	[54]
15	ball-on-disc	440C, ball	5 N	0.10	5000	[54]
16	pin-on-disc	316, disc	6.55 MPa	0.05	n/a	[74]
17	pin-on-disc	mild steel, disc	1.4 MPa	0.50	n/a	[75]
18	pin-on-flat	431, flat	6.4 MPa	0.20	5000 (r)	[76]
19	pin-on-flat	431, flat	6.4 MPa	0.20	5000 (r)	[76]
20	pin-on-flat	431, flat	6.4 MPa	0.20	5000 (r)	[76]
21	pin-on-flat	347, flat	6.4 MPa	0.05	1080 (r)	[80]
22∗	pin-on-flat	304, flat	6.3 MPa	0.05	2500 (r)	[45]
23∗	pin-on-flat	304, flat	6.3 MPa	0.05	2500 (r)	[45]
24∗	pin-on-flat	304, flat	6.3 MPa	0.05	2500 (r)	[45]
25	pin-on-flat	347, flat	6.4 MPa	0.05	1080 (r)	[80]
26	pin-on-flat	347, flat	6.4 MPa	0.05	2370 (r)	[80]
27	pin-on-flat	347, flat	6.4 MPa	0.05	30240 (r)	[80]
28	plate-on-ring	100Cr6, ring	1.0 MPa	1.00	14400	[71]
29	plate-on-ring	100Cr6, ring	1.0 MPa	1.00	14400	[71]
30	plate-on-ring	100Cr6, ring	1.0 MPa	1.00	14400	[71]
31	plate-on-ring	100Cr6, ring	1.0 MPa	1.00	14400	[71]
32	plate-on-ring	100Cr6, ring	1.0 MPa	1.00	14400	[71]
33	plate-on-ring	100Cr6, ring	0.5 MPa	1.00	14400	[79]
34	plate-on-ring	100Cr6, ring	0.5 MPa	1.00	14400	[79]
35	plate-on-ring	100Cr6, ring	0.5 MPa	1.00	14400	[79]
36	plate-on-ring	100Cr6, ring	0.5 MPa	1.00	14400	[79]
37	plate-on-ring	100Cr6, ring	0.5 MPa	1.00	14400	[79]
38	pin-on-flat	304, flat	3.13 MPa	0.10	1500 (r)	[46]
39	pin-on-flat	304, flat	3.13 MPa	0.10	20000 (r)	[46]
40	pin-on-flat	304, flat	3.13 MPa	0.10	65000 (r)	[46]
41	pin-on-flat	304, flat	3.13 MPa	0.10	80000 (r)	[46]

2.3.2.2. Tribo-chemical background of the wear rate decreasing effect

Table 2.1, row 22-24 introduces that the wear resistance of Al_2O_3 filled PTFE improved as the relative humidity increased [45]. To explain this phenomenon, first, we have to investigate the wear of neat PTFE. Due to the mechanical stress during wear, the long PTFE chains undergo mechanical chain scission. At the end of the chains, carboxyl functional groups (COOH) can form with the participation of the relative humidity [45, 71]. With the increasing number of these carboxyl functional groups, the potential chemical reactions are also increasing [45, 72, 73]. If we select the fillers and the counterfaces with the respect to this chemical background, an adequate and durable transfer layer can form. It is noteworthy to mention here that there is a model in literature which states that for the *in situ* formation of carboxyl groups in PTFE chain ends, not only the relative humidity but also oxygen is required [72]. In literature, however the coherence between the oxygen and wear rate is still not proven; the wear resistance values are almost the same in nitrogen (N_2) and nitrogen/oxygen (O_2) atmosphere considering similar relative humidity (Table 2.3) [45].

Table 2.3. The wear rate of PTFE/Al_2O_3 composites (5 wt%) in nitrogen and nitrogen/oxygen (80/20) atmosphere; all other test conditions were the same [45].

Atmosphere	Relative humidity (%)	Wear rate (mm^3/Nm)
Vacuum	~0	$3.5 \cdot 10^{-5}$
N_2	0.5	$1.4 \cdot 10^{-6}$
$N_2 + O_2$ (80/20)	2.5	$4.4 \cdot 10^{-6}$
N_2	30	$2.6 \cdot 10^{-7}$
$N_2 + O_2$ (80/20)	35	$5.6 \cdot 10^{-7}$
N_2	69	$1.0 \cdot 10^{-7}$
$N_2 + O_2$ (80/20)	68	$2.4 \cdot 10^{-7}$

In case of alumina (Al_2O_3), the *in situ* formed carboxyl groups of PTFE chain ends participate in a complex formation with the ions of the alumina, and make a complex with the atoms/ions of the metal counterfaces too [45, 72, 73]. The transfer layer of PTFE/Al_2O_3 composites (5 wt%) in nitrogen atmosphere as a function of relative humidity is shown in Figure 2.9 [45]. The relative humidity of Figure 2.9 (a) and (b) is 0.6% and 69%, respectively. A significant amount of wear debris is formed at 0.6% relative humidity, while at 69% relative humidity a durable and adequate transfer layer is formed, decreasing the quantity of the wear debris. The wear rates of the composites were $7 \cdot 10^{-6}$ (a) and $1 \cdot 10^{-7}$ (mm^3/Nm) (b) [45]. The formation of new functional groups and bonds during wear were registered by X-ray photoelectron spectroscopy (XPS) and Fourier-transform infrared spectroscopy (FTIR) as well [45].

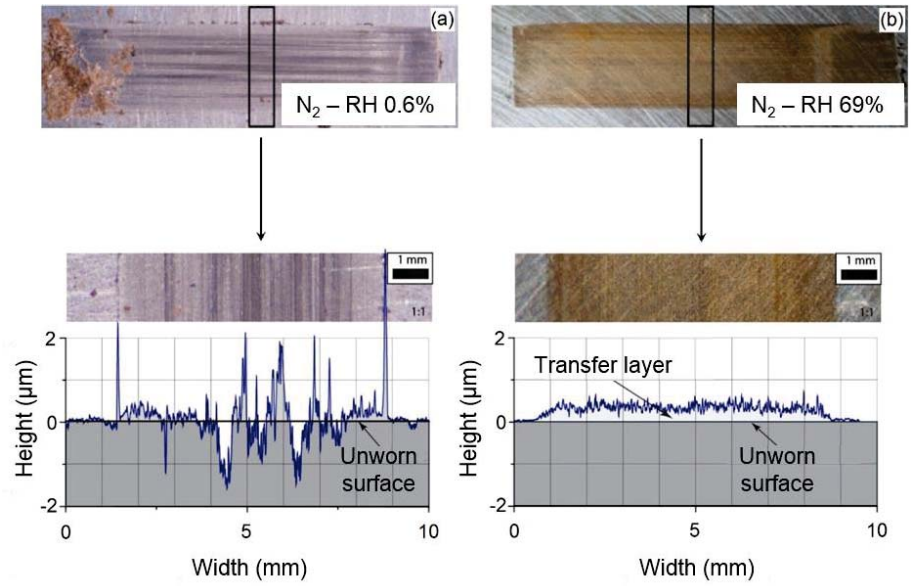

Figure 2.9. Transfer layers of PTFE/Al_2O_3 composites in 0.6% (a) and 69% (b) relative humidity (RH%) in nitrogen atmosphere [45].

2.3.2.3. The influence of functionalised graphene and carbon nanotubes

Regarding the functional groups, if the filler is functionalized graphene, a potential question concerns the influence of the functional groups on the transfer layer formation and consequently to the wear rate. Based on the research results presented above, we can suppose that if the graphene filler contains functional groups such as hydroxyl (OH), carboxyl (COOH) and epoxy functional groups, the wear rate can be further decreased. These reactive groups of graphene can make a complex with the carboxyl groups of the PTFE chain ends and with the atoms/ions of the metal counterfaces [46, 71]. Furthermore, it is also supposed that the nickel of the given metal counterface can react both with the mentioned functional groups of graphene and the carboxyl groups of the PTFE chain ends [74]. In the research of Padenko *et al*. the positive expectations related to the functionalised graphene are not so clear [71, 79]. The difference of the observed wear rate between the graphene and oxyfluorinated (functionalised) graphene filled PTFE was rather small [71, 79]. In contrast, Makowiec *et al*. reported a significant improvement in wear rate when they compared conventional and functionalised carbon nanotubes in the PTFE matrix. The functionalised nanotubes produced two orders of magnitude lower wear rate than nanotubes without functional groups [37].

2.3.2.4. Aluminium hydroxides as potential tribo-fillers

Aluminium hydroxides could be potential tribological fillers in PTFE matrix due to their hydroxyl functional groups, which can react with the *in situ* carboxyl groups of PTFE chains during wear. Chapter 1.3 introduces detailed information about this hypothesis.

Aluminium hydroxides are the hydrated precursors of metastable alumina [82]. These hydroxides can be, e.g. aluminium trihydroxides such as gibbsite (γ-$Al(OH)_3$), bayerite (α-$Al(OH)_3$) or aluminium monohydroxides such as boehmite (γ-AlO(OH)) and diaspore (α-AlO(OH)) [83, 84]. Boehmite, diaspore and gibbsite are the main constituents of bauxite minerals. Gibbsite and bayerite have three hydroxyl groups, which could be beneficial according to the hypothesis (Chapter 1.3). Their dehydration temperature is less than 300°C, in this way these fillers are not suitable in PTFE, due to the higher (360-380°C) sintering temperature of PTFE. Diaspore and boehmite have a higher dehydration temperature than the processing temperature of PTFE. Regarding the hardness, diaspore is much harder than boehmite, which can cause abrasive wear on some counterface materials. The Mohs scale hardness of diaspore and boehmite are ~6.5-7 and ~3-3.5, respectively. For comparison, Al_2O_3 has a Mohs hardness of ~9 [83-86]. Boehmite is a widely available material, and this nanofiller has a positive influence on the mechanical properties, thermal stability and scratch-resistance of polymers [82].

2.3.3. Effect of wear fragments and counter surface quality

The shape of the steel counterface asperities has a strong influence on the coefficient of friction, while the height and size of the asperities have a remarkable effect on the wear rate [87, 88]. Beside the counterface asperities, the wear rate of PTFE composites is governed by the shape and size of wear fragments [87, 89]. The debris is removed in flake form (smooth and thin layer) from neat PTFE, with a thickness of ~3 μm. In contrast with this, the wear fragments of particle-filled PTFE have particle form. The counterface quality has an influence on the wear mechanism in the aspect of wear fragments as well. The counter surface asperities can lock the particle fragments, forming a thin and durable transfer layer on the steel counterface. The fragmented flakes of neat PTFE formed on the steel counter surface can again easily be removed during the wear process [87, 89]. The wear rate is more sensitive for increased roughness if the surface groves (resulting from production technique such as e.g. grinding) are oriented perpendicular to the sliding direction [87, 90]. Besides the surface quality and transfer layer formation, the enhanced mechanical properties and the higher thermal conductivity of filled PTFE itself can also affect the wear rate [89].

Burris *et al.* tested alumina filled PTFE composites against 304 stainless steel [87]. They applied 0.05 m/s sliding speed and 250 N normal load. The wear rate decreased as the filler content increased because the increased filler content reduced the size of the debris, forming

a thinner and more uniform transfer layer. The coefficient of friction slightly increased as the filler content increased [87]. They hypothesized that as the higher filler content enhances wear resistance, a potential filler accumulation during wear at the contact surface would decrease the wear rate with the increasing sliding distance. The measured wear volume was a linear function of the normal load and sliding distance, so they supposed that the surface composition is more or less steady during wear process without filler accumulation [87]. It is noteworthy to mention that this suggestion was not confirmed by any chemical composition analysis.

Li *et al.* tested PTFE sliding against CuSn6 bronze disc in pin-on-disc configuration, in dry contact [91]. With polished discs the coefficient of friction is increased with 8-16%, while the wear rate decreased with 14-21%, compared to the non-polished surface. They had the same trend in three different counterface surface textures as well (Figure 2.10). The three surface textures were the following: grid groove, circle groove and asterisk groove. Compared with the smooth surface, the coefficient of friction of grid groove surface, circle groove surface and asterisk groove surface decreased by 10.55%, 9.50% and 6.03% while the wear rate increased by 47.05%, 27.21% and 41.48%, respectively [91].

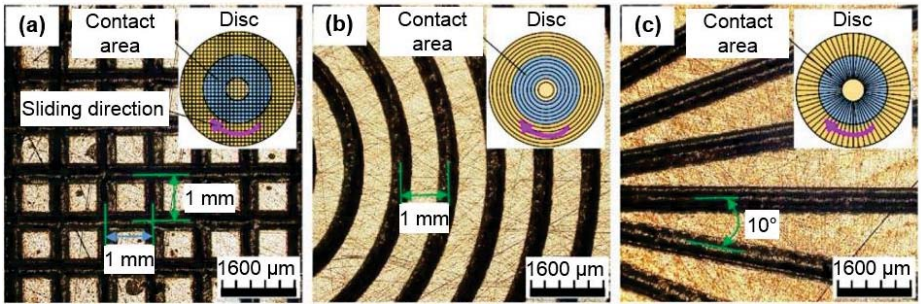

Figure 2.10. The investigated textured surfaces: grid groove (a), circle groove (b) and asterisk groove (c) [91].

2.4. Glass transition temperature of PTFE

The reported values for the glass transition temperature of PTFE are in the range of -110°C to 130°C, which is quite a broad range. Between -200°C and 380°C PTFE undergo four main relaxations, which are the following: γ relaxation at -103°C, β relaxation at 20-25°C, α relaxation at 116°C and the melting temperature at 330°C. It is universally accepted that β peak is a representative of crystalline transitions [92]. Below temperature of β relaxation, PTFE has a partially ordered hexagonal phase, while above this temperature, it converts into a pseudo-hexagonal disordered phase [93]. Eby *et al.* named both the γ and α relaxations as glass transition temperatures of PTFE [92, 94]. Other researchers proposed to consider the γ relaxation [95] or α relaxation [96] as the glass transition temperature of PTFE [94]. A theoretical way for the calculation of glass transition temperature of TFE copolymers also

exists. Equation (2.1) defines the glass transition temperature of PTFE based on the glass transition temperature and chemical composition of each monomer [92]:

$$1/T_g = w_1/T_{g1} + w_2/T_{g2} \quad (2.1)$$

where T_g is the glass transition temperature (°C) of the given TFE copolymer, w_1 and w_2 are the weight fraction (-) of each incorporated monomer, T_{g1} and T_{g2} are the corresponding glass transition temperatures (°C) of the applied homopolymers [92]. With the use of Equation (2.1), an intermediate value of glass transition was defined between Tγ and Tα (~-50°C) [92].
Calleja *et al.* investigated the loss factor of PTFE (Figure 2.11). The loss factor is influenced by the nature and amplitude of molecular motions, often named as internal friction or damping. It can be calculated with Equation (2.2) [92]:

$$tan\delta = G''/G' \quad (2.2)$$

where $tan\delta$ is the loss factor (-), G'' is the loss shear modulus (MPa), which is a measure of the viscous response of a material, while G' is the storage shear modulus (MPa), which is a measure of the elastic behaviour [92].

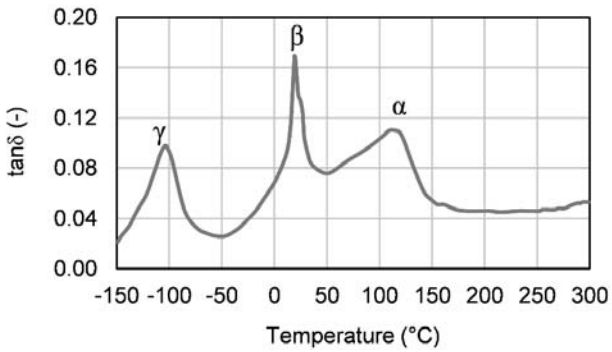

Figure 2.11. The loss factor of PTFE as a function of temperature [92].

Both γ and α relaxations are followed by a significant decreasing of G' storage modulus (Figure 2.12). In this way, none of these relaxations can be confused with a secondary rheological relaxation. The secondary relaxations do not have a significant effect on the storage modulus; these relaxations induce mechanical losses which appear as rheological peaks on the curve of G'' loss modulus. In contrast with this, the glass transition temperature has a significant effect on the storage modulus of the investigated sample. In this way, PTFE seems to have two glass transition domains [92].

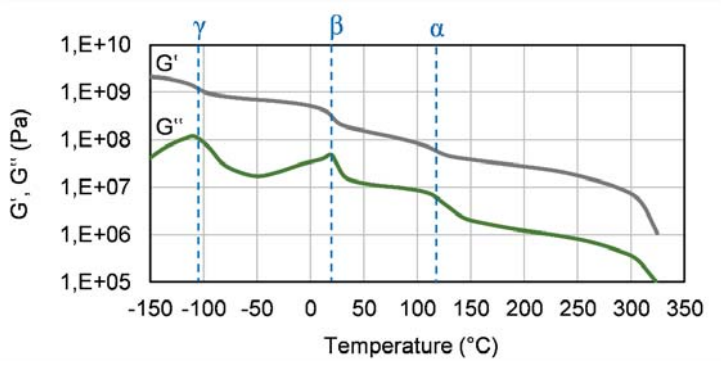

Figure 2.12. Storage shear modulus (G') and loss shear modulus (G'') of PTFE as a function of temperature [92].

For a better understanding of γ and α peaks, it is necessary to analyse the morphological structure of PTFE. Figure 2.13 displays the schematic illustration of PTFE [92]. Most of the semi-crystalline polymers can be considered as three-phase systems including mobile amorphous phase, rigid amorphous phase and crystalline phase. The rigid amorphous phase is the intermediate interfacial region between the mobile amorphous and crystalline phase. The molecular mobility of this rigid amorphous fraction is the intermediate between the mobile amorphous and crystalline fraction [92, 97].

The γ relaxation can be assigned to the mobile amorphous fraction, and α relaxation can be to the rigid amorphous fraction. The glass transition temperature of a polymer is defined as the amorphous phase being perfect glass; in this way it seems to be logical to determine Tγ (relaxation of the mobile amorphous phase) as glass transition temperature [92].

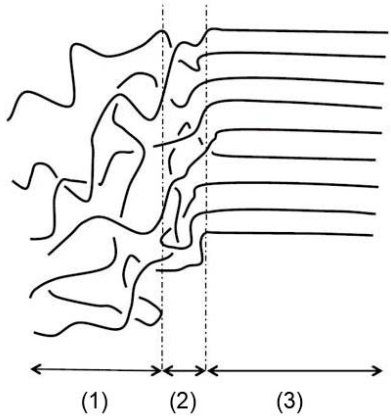

Figure 2.13. Schematic illustration of PTFE structure. Mobile amorphous phase (1), rigid amorphous phase (2) and crystalline phase (3) [92].

Figure 2.14 shows the tensile behaviour of PTFE at room temperature. PTFE shows a ductile behaviour during tensile test, with ~400% strain at break. This is in agreement with the assignment of glass transition temperature at T_γ (-103°C) [92].

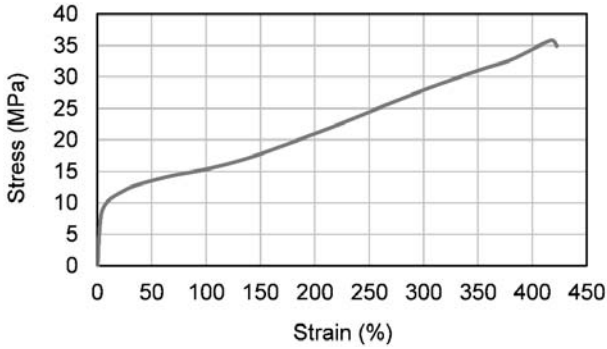

Figure 2.14. Tensile behaviour of PTFE at room temperature, 5 mm/min test speed [92].

2.5. Alumina and boehmite nanofillers in thermoplastic polymer matrices

Bhimaraj *et al.* tested alumina filled poly(ethylene) terephthalate (PET) against 347 stainless steel counterfaces (Ra ~0.1-0.2 μm) with a linear reciprocating tribometer. Al_2O_3 increased the wear resistance of PET matrix with approximately 100% and decreased the coefficient of friction with 10% [98]. The coefficient of friction and wear resistance improvement can be explained with the formation of a more coherent and adherent transfer layer. The wear rate of alumina filled PET had an optimum around 1-2 wt% filler content (Figure 2.15 (a)) which is the result of two competing factors such as the adequate transfer layer formation and the abrasive aggregate development [98]. Smaller Al_2O_3 particles can decrease the wear rate of PET more effectively than particles with a larger diameter (Figure 2.15 (a)). These smaller particles resulted in a lower coefficient of friction only at low filler content compared to larger particles (Figure 2.15 (b)) [99]. These results were concluded without varying the surface roughness of the steel counterfaces as a function of the alumina particle size. In this way, a potential question here is whether the superior wear performance of the smaller particles is valid at counterfaces with different roughness characteristics as well. Burris *et al.* investigated the influence of steel counterface asperities on the wear mechanism of neat PTFE and Al_2O_3 filled PTFE (Chapter 2.3.3) [87]. They stated that the countersurface roughness can lock the particle fragments of the tested filled PTFE. As a consequence, a thin and durable transfer layer is formed on the steel counterface. They observed that alumina with 80 nm particle size had 1-2 orders of magnitude lower wear rate compared to 44 nm and 500 nm alumina. Independently of the introduced wear mechanism, they concluded that the ratio of the root-mean-squared roughness to the filler diameter did not influence the wear rate of these composites [87].

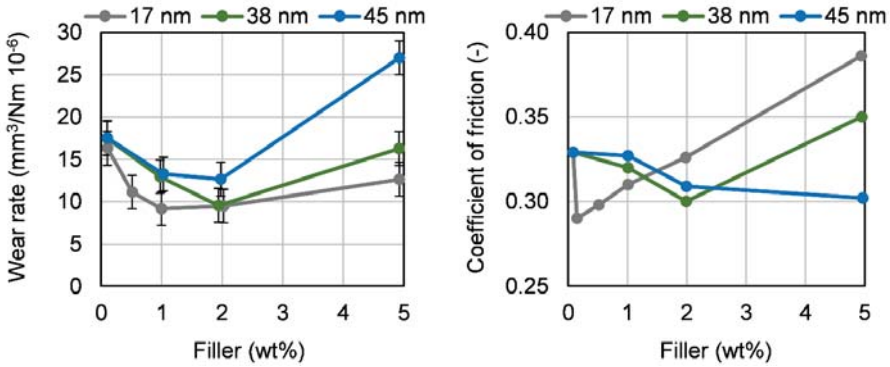

Figure 2.15. Wear rate (a) and coefficient of friction (b) of filled PET composites as a function of filler content and particle size [99].

POM is a widely used material in tribological applications because of its low coefficient of friction and low wear rate. The low coefficient of friction comes from the flexibility of the linear molecular chains, while the high wear resistance comes from the high crystallinity and high bond energy [100, 101]. Sun *et al.* investigated Al_2O_3 particles in POM matrix and compared the tribological performance in dry and oil-lubricated sliding conditions. Al_2O_3 particles had a positive influence on the tribological properties of POM only in oil-lubricated condition. In dry sliding condition both wear rate and coefficient of friction increased. The addition of 3% of Al_2O_3 particles increased the wear rate 22 times compared to neat POM. They explained that in dry condition, the alumina inhibits the adhesive wear mechanism of POM, the alumina particles do not peel off from the surface (filler accumulation), and they form agglomerates which further increase the abrasive wear [100]. This phenomenon is in contrast with the wear behaviour of alumina filled PTFE as a function of the filler accumulation, suggested by Burris *et al.* [87]. They supposed that a potential filler accumulation on the contact surface during the wear process would decrease the wear rate as the wear rate decreases as a function of the filler content increase. They registered that the measured wear rate is the linear function of the sliding distance, in this way they supposed that the filler accumulation is not a wear rate decreasing factor [87].

Derazkola *et al.* developed Al_2O_3 filled polymethyl methacrylate (PMMA) composites [102]. The application of alumina powder improved the tensile and flexural strength, hardness and impact energy of PMMA as a function of the alumina content (vol%) (Figure 2.16 (a)-(d)). The coefficient of friction and wear rate decreased as the alumina content increased in PMMA matrix, which is in contrast with the results of Sun *et al.* related to POM matrix [100].

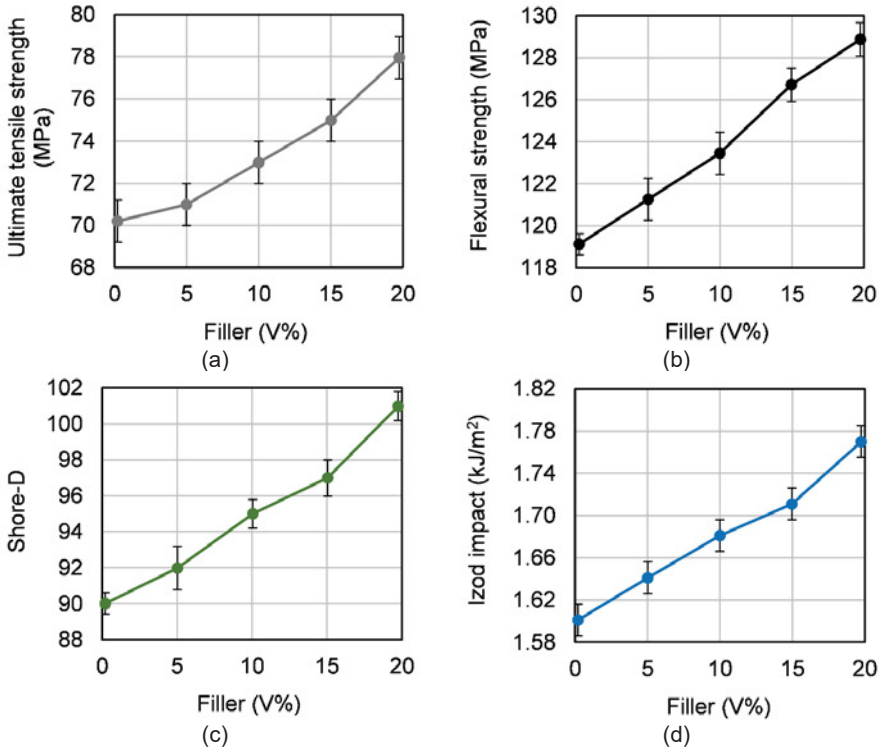

Figure 2.16. Ultimate tensile (a), flexural strength (b), Shore-D hardness (c) and impact energy (d) of PMMA/Al_2O_3 as a function of alumina content (vol%) [102].

Pedrazzoli *et al.* developed and tested boehmite alumina (BA) nanoparticle filled PP copolymer [103]. Table 2.4 shows the results of samples with 2.5, 5 and 10 wt% filler content. The yield strength increased with approximately 6%, independently of the filler content. The tensile modulus increased in 2.5, 5 and 10 wt% filler content with ~9%, ~13% and ~15%, respectively. This enhancement can be attributed to a rigid interphase formed between the PP and the boehmite particles.

Table 2.4. Tensile properties of boehmite alumina filled PP composites (2.5, 5 and 10 wt%) [103].

Sample	Tensile modulus (MPa)	Yield strength (MPa)	Elongation at break (%)
PP	901 ± 9	28.5 ± 0.4	127 ± 11
PP/BA40-2.5	987 ± 15	30.2 ± 0.2	168 ± 18
PP/BA40-5	1020 ± 32	30.4 ± 0.5	153 ± 18
PP/BA40-10	1034 ± 25	30.2 ± 0.2	149 ± 28

The elongation at break also increased; the observed improvements of 2.5, 5 and 10 wt% filler content were ~32%, ~20% and ~17%, respectively. The increased elongation at break comes from the failure method, where the particles first debond making voids in the matrix, followed by the fuse of these voids resulting in matrix fibrillation [103].

Table 2.5 shows the storage (E') and loss Young's modulus (E'') of the tested PP composites. At -50°C the storage modulus increased with ~4% and 32% in 5 and 10 wt% filler content samples, respectively. At +23°C, only the 10 wt% filler content PP increased the storage modulus; the other two materials had lower storage modulus than the reference sample [103].

Table 2.5. Storage (E') and loss Young's modulus (E'') values of boehmite filled PP composites evaluated at 1 Hz (2.5, 5 and 10 wt%) [103].

Sample	E' (-50°C) (MPa)	E' (+23°C) (MPa)	E'' (+23°C) (MPa)
PP	5160	2316	151
PP/BA40-2.5	5030	1980	122
PP/BA40-5	5380	2110	128
PP/BA40-10	6830	3020	173

The addition of boehmite improved the thermal and thermo-oxidative stability of PP copolymer; similar results from boehmite were reported for PE and LDPE [103-105]. Table 2.6 displays the differential scanning calorimetry (DSC) analysis of boehmite filled PP; boehmite resulted in a slight nucleation effect considering the initial temperature of the crystallisation. The degree of crystallinity slightly increased as the filler content increased both in the first and second heating cycles [103].

Table 2.6. DSC analysis of boehmite filled PP copolymers (2.5, 5 and 10 wt%) [103].

Sample	First melting		
	Melting peak temperature (°C)	Final temperature of melting (°C)	Degree of crystallinity (%)
PP	166.7	174.6	35.2
PP/BA40-2.5	166.6	173.8	37.1
PP/BA40-5	166.6	173.9	36.9
PP/BA40-10	166.1	173.8	38.3
Sample	Crystallization		
	Crystallization peak temperature (°C)	Initial temperature of crystallisation (°C)	Degree of crystallinity (%)
PP	122.2	129.8	37.8
PP/BA40-2.5	123.0	130.2	38.6
PP/BA40-5	124.1	131.0	39.4
PP/BA40-10	129.8	135.6	40.6
Sample	Second melting		
	Melting peak temperature (°C)	Final temperature of melting (°C)	Degree of crystallinity (%)
PP	167.3	174.8	38.2
PP/BA40-2.5	168.3	175.6	38.8
PP/BA40-5	166.9	174.4	40.1
PP/BA40-10	167.6	174.0	40.3

2.6. The effect of crystallinity and wear-induced crystallisation

The degree of crystallinity can vary due to the thermal and the mechanical antecedents of the polymer and affects its mechanical properties [43, 106, 107]. Because of the changes in mechanical properties and orientation of the molecular chains, the degree of crystallinity also has a significant effect on the transfer layer formation and behaviour, which may in turn affect the friction and wear characteristics [41, 43]. Due to ongoing wear, crystallinity can also vary with time. In this way, the degree of crystallinity is not a constant value during the lifecycle of a tribological component.

The relationships between the degree of crystallinity and the tribological characteristics of semi-crystalline thermoplastics are still not fully established. From the research with polyethylene terephthalate (PET) it is clear that the degree of crystallinity has an effect on the friction and wear behaviour [42, 98, 99]. Bhimaraj *et al.* reported that the coefficient of friction decreases and the wear rate increases with increasing degree of crystallinity [99]. A possible explanation is that the increase in the degree of crystallinity reduces the toughness and ductility. Hence the polymer surface loses its ability to sustain the local impacts and high strains, which leads to higher a wear rate [99], although the hardness and strength of polymers increase with increased crystallinity [108]. In case of ultra-high molecular weight polyethylene (UHMWPE) Kang *et al.* also introduced that higher crystallinity causes higher wear rate, by comparing slowly cooled samples to quenched ones [109]. In contrast to the results with PET, Karuppiah *et al.* showed that both the coefficient of friction and wear rate are decreasing with the increasing degree of crystallinity of UHMWPE [43]. It is noteworthy to mention that UHMWPE has a much lower hardness than PET. According to them, this increase in wear resistance of UHMWPE can be related to the increase in hardness and in elastic modulus [43]. The increase in hardness with the increased degree of crystallinity was also confirmed by nano-indentation tests [43]. Cartledge *et al.* investigated the wear resistance of polyamide 6 (PA6) as a function of the degree of crystallinity which was varied by the cooling condition of the manufacturing process [110]. It can be stated that the increase of crystallinity results in an increase in the wear resistance [110]. Chen *et al.* state that the crystalline regions in the debris are destroyed in both PA66 and PPS; therefore, the degree of crystallinity in the debris is significantly lower than for the original material [51].

2.7. Conclusions

PTFE is a widely used material in tribology. But besides its benefits, PTFE has a low wear resistance compared to other plastics. Some micro- and nano-fillers can increase the wear resistance of PTFE with orders of magnitude. There is however no clear agreement in the literature related to the friction and wear mechanism of nanoparticle filled thermoplastic matrices.

The literature is not in agreement on defining the most significant governing factors of wear. The transfer layer formation and the quality of the transfer layer has a huge influence on the tribological performance but the results related to the influence of the surface roughness and particle size of alumina on the wear mechanism are still not coherent [87, 99]. Some research focuses on the tribo-chemical background of the wear process with the use of functionalized graphene and alumina fillers [69-72]. Besides the above mentioned relevant factors, the wear resistance is affected by the physical, thermal, mechanical and morphological properties of the materials of interest. The correlation between the degree of crystallinity changes and the wear rate is not fully clarified yet. The wear-induced crystallisation is also an open question. Looking at real applications, it is possible that, due to the wear-induced crystallisation of the contact surfaces, after an initial sliding distance the material properties change in such a way that the material performance alters unexpectedly. In literature, a comprehensive investigation of the tribological characterisation of nanoparticle filled PTFE can be found but a detailed material characterisation is hardly available. In some publications, it is only mentioned that besides the roughness, the features of the debris, filler particle size and shape, some other properties such as the mechanical properties, thermal conductivity can also influence the wear resistance [54, 55, 89]. As a result, we lack a thorough understanding of this hybrid material.

None of the research related to the tribological performance of alumina and graphene filled PTFE investigated the thermal stability of the fillers and composites during the high-temperature sintering. Furthermore, the research did not discuss how they defined the production and sintering protocol. Both PTFE and alumina have high thermal stability at the sintering temperature (360-380°C), but a potential interaction between them at this temperature range can exist. Knowing that the used fillers can affect the thermal stability during sintering, the sensitivity analysis or in other words, the degradation analysis of this high-temperature process is crucial. The literature introduces many different sintering thermal profiles; however, the size and shape of the sintered samples were similar. Padenko *et al.* sintered unfilled/filled PTFE materials (~7.1 cm^3, ~16 g, 3 mm thickness and 55 mm diameter) at 380°C temperature with 4 hours dwelling time at the maximal temperature [1]. Krick *et al.* chose 380°C temperature with only 0.5 hours holding time (13 g) [2]. Ye *et al.* used 365°C maximal temperature with 3 hours dwelling time (~3.1 cm^3, 7 g, 25 mm thickness and 12.5 mm diameter) [3].

Burris *et al*. supposed that no filler accumulation appears on the sliding surface of alumina filled PTFE during wear. According to them, a potential filler accumulation during wear at the contact surface would decrease the wear rate with the increasing sliding distance [87]. Sun *et al.* explained that in dry condition, the alumina particles do not peel off from the surface resulting in filler accumulation, and the particles form agglomerates which further increase the

abrasive wear [100]. Based on these results and explanations, it seems that the existence and influence of filler accumulation of alumina particles during wear is also an open question.

In literature, the effect of the counterface material to the tribo-chemical reactions and the wear is still an open question. Generally, researchers used 100Cr6 steel and 304 stainless steel as counterface material [45, 46, 54, 71, 74, 76, 80]. The nickel and chromium content of 304 steel is much higher than 100Cr6. Blanchet and Kennedy suggested that nickel is a relevant factor related to the tribo-chemical reactions [74]. In contrast, Gong *et al.* found that only active metals can be beneficial in the aspect of tribo-chemical reactions as they can form oxide layer on the contact surface [68]. Following their suggestion, 304 stainless steel can be excluded from tribo-chemical related investigations. In contrast, Krick *et al.* concluded their tribo-chemical related results with the use of 304 stainless steel [45]. On the other hand, 304 stainless steel is not a typical shaft material; it is mostly used for e.g. sinks, cutlery, pans, tubing, nuts, screws, bolts and food/pharmaceutical production equipment. In this way, it is not a potential counterpart for a polymer bearing or a seal.

The influence of extra-functional groups on the wear rate in case of boehmite and graphene fillers is also an open question. These extra functional groups are supposed to react with the *in situ* functionalised PTFE carboxyl groups during wear process (Chapter 1) [79, 82]. In the research of Padenko *et al*., the difference of the observed wear rate between the graphene and oxyfluorinated (functionalised) graphene filled PTFE was slight [79, 81]. In contrast, Makowiec *et al*. presented two orders of magnitude lower wear rate in functionalised nanotubes compared to nanotubes without functional groups [37]. The hybrid effect of alumina, boehmite and graphene fillers for friction and wear behaviour is also a potential question to investigate.

The previously introduced open research questions and hypotheses are addressed in the present research work, and the following chapters try to answer them.

2.8. References

[1] A. van Beek: Advanced engineering design: lifetime performance and reliability. TU Delft (2015).

[2] I. Hutchings: Tribology: Friction and wear of engineering materials. Butterworth-Heinemann, 1st Edition (1992).

[3] C.H. da Silva, D.K. Tanaka, A. Sinatora: The effect of load and relative humidity on friction coefficient between high density polyethylene on galvanized steel — preliminary results. Wear 225–229 (1999) 339–342.

[4] K. Friedrich, Z. Lu, A.M. Hager: Overview on polymer composites for friction and wear application. Theoretical and Applied Fracture Mechanics 19 (1993) 1–11.

[5] D.H. Buckley, P.R. Aron: Characterization and measurement of polymer wear. NASA Tech. Memo. 83628, Lewis Res. Cent. (1984).

[6] https://www.corrosionpedia.com/ (19.10.2017).
[7] https://www.oerlikon.com/balzers/com/en/portfolio/surface-technologies/wear-tribology/ (19.10.2017).
[8] S. Toumi, S. Fouvry, M. Salvia: Prediction of sliding speed and normal force effects on friction and wear rate evolution in a dry oscillating-fretting PTFE/Ti-6Al-4V contact. Wear 376-377 (2017) 1365–1378.
[9] https://www.chemours.com/Teflon/en_US/products/history.html (20.10.2017).
[10] PTFE bearing materials. Modern Plastics 36 (1959) 123-127.
[11] W.D. Craig: Operation of PTFE bearings in seawater. Lubrication Engineering 20 (1964) 456-462.
[12] C.J. Speerschneider, C.H. Li: The role of filler geometrical shape in wear and friction of filled PTFE. Wear 5 (1962) 392-399.
[13] D. Tabor, D. E. W. Williams: The effect of orientation on the friction of polytetrafluoroethylene. Wear 4 (1961) 391-400.
[14] A.J. Stock: Graphite, molybdenum disulfide and PTFE: a comparison. Lubrication Engineering 19 (1963) 333-338.
[15] L. Zhang, H. Qi, G. Li, G. Zhang, T. Wang, Q. Wang: Impact of reinforcing fillers' properties on transfer film structure and tribological performance of POM-based materials. Tribology International 109 (2017) 58–68.
[16] R. J. Crawford: Plastics engineering. Pergamon Press (1987).
[17] K. A. Laux, A. Jean-Fulcrand, H. J. Sue, T. Bremner, J. S. S. Wong: The influence of surface properties on sliding contact temperature and friction for polyetheretherketone (PEEK). Polymer 103 (2016) 397-404.
[18] Z. Rymuza: Tribology of polymers. Archives of Civil and Mechanical Engineering 7 (2007) 177–184.
[19] H. Wang, B. Xu, J. Liu: Micro and nano sulfide solid lubrication. Science Press Beijing and Springer-Verlag Berlin Heidelberg, 2012.
[20] M. R. Hilton, P. D. Fleischauer: Applications of solid lubricant films in spacecraft. Surface and Coatings Technology 54/55 (1992) 435-441.
[21] E. Cigno, C. Magagnoli, M. S. Pierce, P. Iglesias: Lubricating ability of two phosphonium-based ionic liquids as additives of a bio-oil for use in wind turbines gearboxes. Wear 376-377 (2017) 756–765.
[22] C. Ye, W. Liu, Y. Chen, L. Yu: Room-temperature ionic liquids: a novel versatile lubricant. Chemical Communications 21 (2001) 2244–2245.
[23] J. L. Viesca, M. T. Mallada, D. Blanco, A. Fernandez-Gonzalez, J. Espina-Casado, R. Gonzalez, A. H. Battez: Lubrication performance of an ammonium cation-based ionic liquid used as an additive in a polar oil. Tribology International 116 (2017) 422–430.

[24] G. Huang, Q. Yu, Z. Ma, M. Cai, W. Liu: Probing the lubricating mechanism of oil-soluble ionic liquids additives. Tribology International 107 (2017) 152–162.

[25] K.D. Dearn, T.J. Hoskins, D.G. Petrov, S.C. Reynolds, R. Banks: Applications of dry film lubricants for polymer gears. Wear 298–299 (2013) 99–108.

[26] M. Zouari, M. Kharrat, M. Dammak: Wear and friction analysis of polyester coatings with solid lubricant. Surface and Coatings Technology 204 (2010) 2593–2599.

[27] X. Zheng, X. Wen, W. Wang, J. Gao, W. Lin, L. Ma, J. Yu: Creep-ratcheting behavior of PTFE gaskets under various temperatures. Polymer Testing 60 (2017) 229-235.

[28] Q.L. Huang, Y. Huang, C.F. Xiao, Y.W. You, C.X. Zhang: Electrospun ultrafine fibrous PTFE-supported ZnO porous membrane with self-cleaning function for vacuum membrane distillation. Journal of Membrane Science 534 (2017) 73–82.

[29] H. Liu, Q. Huang, Y. Wang, C. Xiao: PTFE conductive membrane for EVMD process and the application of electro-catalysis. Separation and Purification Technology 187 (2017) 327–333.

[30] J.K. Lancaster: Accelerated wear testing of PTFE composite bearing materials. Tribology International 12 (1979) 65-75.

[31] H. Sui, H. Pohl, U. Schomburg, G. Upper, S. Heine: Wear and friction of PTFE seals. Wear 224 (1999) 175–182.

[32] M. Furuta, A. Matsugaki, T. Nakano, I. Hirata, K. Kato, T. Oda, M. Sato, M. Okazaki: Molecular level analyses of mechanical properties of PTFE sterilized by Co- 60 γ-ray irradiation for clinical use. Radiation Physics and Chemistry 139 (2017) 126–131.

[33] M.K. Dubey, J. Bijwe, S.S.V. Ramakumar: PTFE based nano-lubricants. Wear 306 (2013) 80–88.

[34] M.K. Dubey, J. Bijwe, S.S.V. Ramakumar: Nano-PTFE: New entrant as a very promising EP additive. Tribology International 87 (2015) 121–131.

[35] M. Qu, Y. Yao, J. He, X. Ma, J. Feng, S. Liu, L. Hou, X. Liu: Tribological study of polytetrafluoroethylene lubricant additives filled with Cu microparticles or SiO_2 nanoparticles. Tribology International 110 (2017) 57–65.

[36] S. Palios, P.M. Cann, H.A. Spikes: Behaviour of PTFE suspensions in rolling/sliding contacts. Tribology Series 31 (1996) 141–152.

[37] M.E. Makowiec, T.A. Blanchet: Improved wear resistance of nanotube- and other carbon-filled PTFE composites. Wear 374-375 (2017) 77–85.

[38] K. Subramanian, R. Nagarajan, P. De Baets, S. Subramaniam, W. Thangiah, J. Sukumaran: Eco-friendly mono-layered PTFE blended polymer composites for dry sliding tribo – systems. Tribology International 102 (2016) 569–579.

[39] K. Tanaka, Y. Uchiyama, S. Toyooka: The mechanism of wear of polytetrafluoroethylene. Wear 23 (1973) 153-172.

[40] T. Czvikovszky, P. Nagy, J. Gaál: A polimertechnika alapjai. Kempelen Farkas Hallgatói Információs Központ (2007).

[41] M. Conte, B. Pinedo, A. Igartua: Role of crystallinity on wear behavior of PTFE composites. Wear 307 (2013) 81–86.

[42] Y. Yamada, K. Tanaka: Effect of the degree of crystallinity on the friction and wear of poly(ethylene terephthalate) under water lubrication. Wear 111 (1986) 63-72.

[43] K.S.K. Karuppiah, A.L. Bruck, S. Sundararajan, J. Wang, Z. Lin, Z.H. Xu, X. Li: Friction and wear behavior of ultra-high molecular weight polyethylene as a function of polymer crystallinity. Acta Biomaterialia 4 (2008) 1401-1410.

[44] J. G. Drobny: Technology of fluoropolymers. CRC Press, Taylor & Francis Group, second edition (2009).

[45] B.A. Krick, J.J. Ewin, G.S. Blackman, C.P. Junk, W.G. Sawyer: Environmental dependence of ultra-low wear behavior of polytetrafluoroethylene (PTFE) and alumina composites suggests tribochemical mechanisms. Tribology International 51 (2012) 42–46.

[46] S.S. Kandanur, M.A. Rafiee, F. Yavari, M. Schrameyer, Z. Yu, T.A. Blanchet, N. Koratkar: Suppression of wear in graphene polymer composites. Carbon 50 (2012) 3178–3183.

[47] Y. Wang, F. Yan: A study on tribological behaviour of transfer films of PTFE/bronze composites. Wear 262 (2007) 876–882.

[48] V.N. Aderikha, A.P. Krasnov, V.A. Shapovalov, A.S. Golub: Peculiarities of tribological behaviour of low-filled composites based on polytetrafluoroethylene (PTFE) and molybdenumdisulfide. Wear 320 (2014) 135–142.

[49] J. Sukumaran, J. De Pauw, P.D. Neis, L.F. Tóth, P. De Baets: Revisiting polymer tribology for heavy duty application. Wear 376-377 (2017) 1321–1332.

[50] P. Samyn, P. De Baets, G. Schoukens, I. Van Driessche: Friction, wear and transfer of pure and internally lubricated cast polyamides at various testing scales. Wear 262 (2007) 1433–1449.

[51] Z. Chen, T. Li, Y. Yang, X. Liu, R. Lv: Mechanical and tribological properties of PA/PPS blends. Wear 257 (2004) 696-707.

[52] K. Tanaka, Y. Uchiyama, S. Toyooka: The mechanism of wear of polytetrafluoroethylene. Wear 23 (1973) 153-172.

[53] M. K. Kar, S. Bahadur: Micromechanism of wear at polymer-metal sliding interface. Wear 46 (1978) 189-202.

[54] J. Khedkar, I. Negulescu, E.I. Meletis: Sliding wear behavior of PTFE composites. Wear 252 (2002) 361–369.

[55] M. Conte, A. Igartua: Study of PTFE composites tribological behavior. Wear 296 (2012) 568–574.

[56] S. K. Sinha, B. J. Briscoe: Polymer tribology. Imperial College Press, London (2009).

[57] N. Adams: Friction and deformation of nylon. I. Experimental. Journal of Applied Polymer Science 7 (1963) 2075–2103.

[58] G.V. Vinogradov, V.A. Mustafaev, Y.Y. Podolsky: A study of heavy metal-to-plastic friction duties and of the wear of hardened steel in the presence of polymers. Wear 8 (1965) 358–373.

[59] M. Watanabe, M. Karasawa, K. Matsubara: The frictional properties of nylon. Wear 12 (1968) 185–191.

[60] K. Tanaka: Transfer of semicrystalline polymers sliding against a smooth steel surface. Wear 75 (1982) 183–199.

[61] H. Voss, K. Friedrich: On the wear behaviour of short-fibre-reinforced PEEK composites. Wear 116 (1987) 1–18.

[62] C.J. Hooke, S.N. Kukureka, P. Liao, M. Rao, Y.K. Chen: The friction and wear of polymers in non-conformal contacts. Wear 200 (1996) 83–94.

[63] S.N. Kukureka, C.J. Hooke, M. Rao, P. Liao, Y.K. Chen: The effect of fibre reinforcement on the friction and wear of polyamide 66 under dry rolling–sliding contact. Tribology International 32 (1999) 107–116.

[64] J. Schon: Coefficient of friction and wear of a carbon fiber epoxy matrix composite. Wear 257 (2004) 395–407.

[65] H. Unal, U. Sen, A. Mimaroglu. Dry sliding wear characteristics of some industrial polymers against steel counterface. Tribology International 37 (2004) 727–732.

[66] B.B. Jia, T.S. Li, X.J. Liu, P.H. Cong: Tribological behaviors of several polymer–polymer sliding combinations under dry friction and oil-lubricated conditions. Wear 262 (2007) 1353–1359.

[67] A.C. Greco, R. Erck, O. Ajayi, G. Fenske: Effect of reinforcement morphology on high-speed sliding friction and wear of PEEK polymers. Wear 271 (2011) 2222–2229.

[68] D. Gong, B. Zhang, Q. Xue, H. L. Wang: Effect of tribochemical reaction of polytetrafluoroethylene transferred film with substrates on its wear behaviour. Wear 137 (1990) 267 – 273.

[69] G. Jintang: Tribochemical effects in formation of polymer transfer film. Wear 245 (2000) 100–106.

[70] Z. Zuo, Y. Yang, X. Qi, W. Su, X. Yang: Analysis of the chemical composition of the PTFE transfer film produced by sliding against Q235 carbon steel. Wear 320 (2014) 87–93.

[71] E. Padenko, L.J. Van Rooyen, B. Wetzel, J. Karger-Kocsis: “Ultralow” sliding wear polytetrafluoro ethylene nanocomposites with functionalized graphene. Journal of Reinforced Plastics and Composites 35 (2016) 892–901.

[72] K.L. Harris, A.A. Pitenis, W.G. Sawyer, B.A. Krick, G.S. Blackman, D.J. Kasprzak, C.P Junk: PTFE tribology and the role of mechanochemistry in the development of protective surface films. Macromolecules 48 (2015) 3739–3745.

[73] T. Onodera, K. Kawasaki, T. Nakakawaji, Y. Higuchi, N. Ozawa, K. Kurihara, M. Kubo: Effect of tribochemical reaction on transfer-film formation by poly(tetrafluoroethylene). The Journal of Physical Chemistry 118 (2014) 11820–11826.

[74] T.A. Blanchet, F.E. Kennedy: Sliding wear mechanism of polytetrafluoroethylene (PTFE) and PTFE composites. Wear 153 (1992) 229-243.

[75] K. Tanaka, S. Kawakami: Effect of various fillers on the friction and wear of polytetrafluoroethylene-based composites. Wear 79 (1982) 221–234.

[76] N.V. Klaas, K. Marcus, C. Kellock: The tribological behaviour of glass filled polytetrafluoroethylene. Tribology International 38 (2005) 824–833.

[77] F. Song, Z. Yang, G. Zhao, Q. Wang, X. Zhang, T. Wang: Tribological performance of filled PTFE-based friction material for ultrasonic motor under different temperature and vacuum degrees. Journal of Applied Polymer Science 45358 (2017) 1-10.

[78] V.N. Aderikha, A.P. Krasnov, A.V. Naumkin, V.A. Shapovalov: Effects of ultrasound treatment of expanded graphite (EG) on the sliding friction, wear resistance, and related properties of PTFE-based composites containing EG. Wear 386–387 (2017) 63–71.

[79] E. Padenko, L. J. van Rooyen, J. Karger-Kocsis: Transfer film formation in PTFE/oxyfluorinated graphene nanocomposites during dry sliding. Tribology Letters 65:36 (2017) 1-11.

[80] W.G. Sawyer, K.D. Freudenberg, P. Bhimaraj, L.S. Schadler: A study on the friction and wear behavior of PTFE filled with alumina nanoparticles. Wear 254 (2003) 573–580.

[81] F. Li, F. Yan, L. Yu, W. Liu: The tribological behaviors of copper-coated graphite filled PTFE composites. Wear 237 (2000) 33–38.

[82] J. Karger-Kocsis, L. Lendvai: Polymer/boehmite nanocomposites: A review. Journal of Applied Polymer Science 45573 (2017) 1-31.

[83] M. Digne, P. Sautet, P. Raybaud, H. Toulhoat, E. Artacho: Structure and stability of aluminum hydroxides: a theoretical study. The Journal of Physical Chemistry B 106 (2002) 5155-5162.

[84] S.-H. Cai, S. N. Rashkeev, S. T. Pantelides, K. Sohlberg: Phase transformation mechanism between γ- and θ-alumina. Physical Review B 67, 224104 (2003) 1-10.

[85] K. A. Matori, L. C. Wah, M. Hashim, I. Ismail, M. H. M. Zaid: Phase transformations of α-alumina made from waste aluminum via a precipitation technique. International Journal of Molecular Sciences 13 (2012) 16812-16821.

[86] J. T. Kloprogge, H. D. Ruan, R. L. Frost: Thermal decomposition of bauxite minerals: infrared emission spectroscopy of gibbsite, boehmite and diaspore. Journal of Materials Science 37 (2002) 1121 – 1129.

[87] D. L. Burris, W. G. Sawyer: Tribological sensitivity of PTFE/alumina nanocomposites to a range of traditional surface finishes. Tribology Transactions 48 (2005) 147-153.

[88] W. Wieleba: The statistical correlation of the coefficient of friction and wear rate of PTFE composites with steel counterface roughness and hardness. Wear 252 (2002) 719-729.

[89] S. Bahadur, D. Tabor: The wear of filled polytetrafluoroethylene. Wear 98 (1984) 1-13.

[90] S. E. Franklin, A. de Kraker: Investigation of counterface surface topography effects on the wear and transfer behaviour of a POM–20% PTFE composite. Wear 255 (2003) 766-773.

[91] J. Li, S. Liu, A. Yu, S. Xiang: Effect of laser surface texture on CuSn6 bronze sliding against PTFE material under dry friction. Tribology International 118 (2018) 37–45.

[92] G. Calleja, A. Jourdan, B. Ameduri, J.-P. Habas: Where is the glass transition temperature of poly(tetrafluoroethylene)? A new approach by dynamic rheometry and mechanical tests. European Polymer Journal 49 (2013) 2214–2222.

[93] M. Conte, B. Pinedo, A. Igartua: Frictional heating calculation based on tailored experimental measurements. Tribology International 74 (2014) 1-6.

[94] R. K. Eby, K. M. Sinnott: Transitions and relaxations in polytetrafluoroethylene. Journal of Applied Physics 32 (1961) 1765-1771.

[95] S. F. Lau, H. Suzuki, B. Wunderlich: The thermodynamic properties of polytetrafluoroethylene. Journal of Polymer Science Part B Polymer Physics 22 (1984) 379-405.

[96] Y. Araki: Thermal expansion coefficient of polytetrafluoroethylene in the vicinity of its glass transition at about 400°K. Journal of Applied Polymer Science 9 (1965) 421-427.

[97] G. C. Rutledge, E. Piorkowska: Handbook of polymer crystallization. John Wiley & Sons Inc., New Jersey (2013).

[98] P. Bhimaraj, D. L. Burris, J. Action, W. G. Sawyer, C. G. Toney, R. W. Siegel, L. S. Schadler: Effect of matrix morphology on the wear and friction behavior of alumina nanoparticle/poly(ethylene) terephthalate composites. Wear 258 (2005) 1437–1443.

[99] P. Bhimaraj, D. Burris, W.G. Sawyer, C.G. Toney, R.W. Siegel, L.S. Schadler: Tribological investigation of the effects of particle size, loading and crystallinity on poly(ethylene) terephthalate nanocomposites. Wear 264 (2008) 632–637.

[100] L.-H. Sun, Z.-G. Yang, X.-H. Li: Study on the friction and wear behavior of POM/Al_2O_3 nanocomposites. Wear 264 (2008) 693–700.

[101] H. S. Benabdallah: Reciprocationg sliding friction and contact stress of some thermoplastic against steel. Journal of Materials Science 32 (1997) 5069–5083.

[102] H. A. Derazkola, A. Simchi: Effects of alumina nanoparticles on the microstructure, strength and wear resistance of poly(methyl methacrylate)-based nanocomposites prepared by friction stir processing. Journal of the Mechanical Behavior of Biomedical Materials 79 (2018) 246-253.

[103] D. Pedrazzoli, V. M. Khumalo, J. Karger-Kocsis, A. Pegoretti: Thermal, viscoelastic and mechanical behavior of polypropylene with synthetic boehmite alumina nanoparticles. Polymer Testing 35 (2014) 92–100.

[104] V. M. Khumalo, J. Karger-Kocsis, R. Thomann: Polyethylene/synthetic boehmite alumina nanocomposites: structure, thermal and rheological properties. Express Polymer Letters 4 (5) (2010) 264-274.

[105] E. Vuorinen, N. Nhlapo, T. Mafa, J. Karger-Kocsis: Thermooxidative degradation of LDPE nanocomposites: effect of surface treatments of fumed silica and boehmite alumina. Polymer Degradation and Stability 98 (11) (2013) 2297-2305.

[106] B. H. Stuart: Review Polymer crystallinity studied using Raman spectroscopy. Vibrational Spectroscopy 10 (1996) 79-87.

[107] D. G. M. Wright, R. Dunk, D. Bouvart, M. Autran: The effect of crystallinity on the properties of injection moulded polypropylene and polyacetal. Polymer 29 (1988) 793-796.

[108] K. Balani, V. Verma, A. Agarwal, R. Narayan: Biosurfaces: a materials science and engineering perspective. First edition, The American Ceramic Society, John Wiley & Sons, 2015.

[109] P. H. Kang, Y. C. Nho: The effect of gamma-irradiation on ultra-high molecular weight polyethylene recrystallized under different cooling conditions. Radiation Physics and Chemistry 60 (2001) 79-87.

[110] H. C. Y. Cartledge, C. Baillie, Y. W. Mai: Friction and wear mechanisms of a thermoplastic composite GF/PA6 subjected to different thermal histories. Wear 194 (1996) 178-184.

CHAPTER 3

MATERIALS, EQUIPMENT AND METHODOLOGY

This chapter describes the applied materials such as the neat PTFE, the chosen fillers and the steel counterfaces. It is followed by a detailed description of the used equipment for the material development/characterisation, the transfer layer and the tribological characterisation. This chapter also introduces the methodology and the test plan for the tribological characterisation, highlighting the four phases of the wear tests. The chemical composition and the hardness of the steel counterfaces and the surface roughness of the unworn polymer samples and the steel counterfaces can be also found in this chapter.

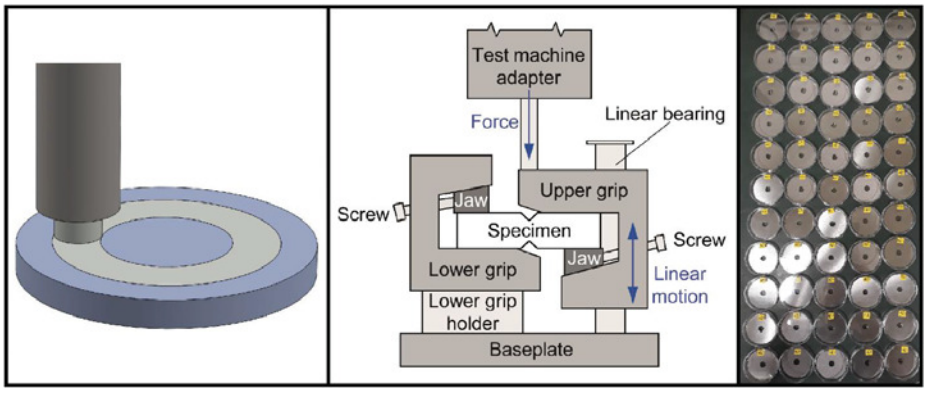

3.1. Materials and production protocol

3M™ Dyneon™ TFM™ 1700 polytetrafluoroethylene (PTFE) powder was used with ~25 μm average particle size, produced by 3M Company (Minnesota Mining and Manufacturing Company, Maplewood, Minnesota, U.S.).

xGnP® Graphene Nanoplatelets Grade M was used from XG Sciences (Lansing, Michigan, U.S.). The average particle size was ~25 μm, the average thickness was 6-8 nanometers, while their specific surface area was around 120-150 m^2/g. According to the manufacturer, these nanoplatelets had naturally occurring functional groups like ethers, carboxyls, or hydroxyls that can react with atmospheric humidity to form acids or other compounds. Their oxygen content was less than 1%, and their residual acid content was less than 0.5 wt%. The 1015WW alpha-alumina (Al_2O_3) with 99.5% purity was produced by Nanostructured & Amorphous Materials Inc. (Houston, Texas, U.S.). The average nanoparticle size was between 27 and 43 nm; the specific surface area was ~35 m^2/g. The boehmite alumina (aluminium hydroxide oxide-AlO(OH)) was Disperal® 80 (BA80) from Sasol (Johannesburg, South Africa) with ~35 μm average particle size, ~80 nm average crystallite size and ~80 m^2/g specific surface area. Al_2O_3 content of BA80 was 80%. Pural® MG70 hydrotalcite (MG70) from Sasol (Johannesburg, South Africa) has double-layered metal hydroxide structure including magnesium and aluminium hydroxides (70:30 wt%, respectively) (Figure 3.1). It had ~45 μm average particle size and ~180 m^2/g specific surface area.

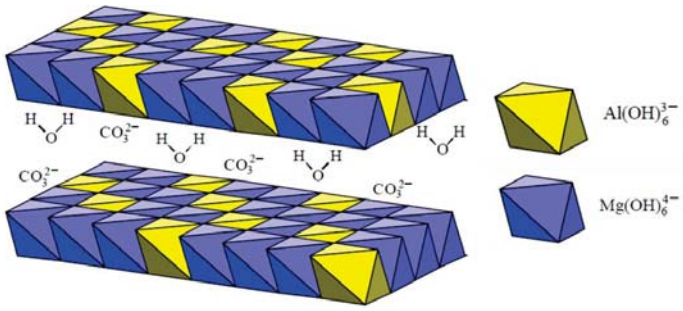

Figure 3.1. Double layered metal hydroxide structure of hydrotalcite.

The composition of the produced PTFE based materials can be seen in Table 3.1. All mono-filled materials had 1/4/8/16/30 wt% filler content. As graphene has a high volume ratio, PTFE filled with 0.25 wt% was also investigated. The hybrid-filled PTFE composites included 4-0.25/2-2/4-4 wt% alumina and graphene, respectively. The applied production technique was a room temperature pressing – free sintering method. Chapter 4 introduces the final production protocol; this protocol was used for all of the developed samples. PTFE and filler powders were blended by intensive dry mechanical stirring, which is a less hazardous and more environment-friendly alternative than solvent blending method. Stirring was provided by a rotating blade

grinder (180 W power); the stirring time was 30 seconds. The pressing was carried out with a Zwick Z250 universal tester (Zwick Roell Group, Ulm, Germany) at room temperature. The pressing speed was 2 mm/min until reaching 12.5 MPa pressure. Subsequently, 3 minutes of dwelling time was held at the same level of pressure. The sintering procedure was carried out in an oven, in air atmosphere. The sintering cycle was the following: 90 °C/h heating rate from room temperature to 370°C, 2 h dwelling time at 370°C temperature and 30 °C/h cooling rate. Disc-shaped samples were pressed with 10/120 mm diameter and 4 mm thickness. Specimens with 10 mm diameter were used for compressive tests and density measurements, while all other test specimens were cut out or milled from the samples with 120 mm diameter.

Table 3.1. The produced neat PTFE and filled PTFE materials.

Materials	Matrix	Filler(s)	Filler content (wt%)
PTFE	PTFE	---	---
PTFE/Graphene-0.25	PTFE	Graphene	0.25
PTFE/Graphene-1	PTFE	Graphene	1
PTFE/Graphene-4	PTFE	Graphene	4
PTFE/Graphene-8	PTFE	Graphene	8
PTFE/Graphene-16	PTFE	Graphene	16
PTFE/Graphene-30	PTFE	Graphene	30
PTFE/Al_2O_3-1	PTFE	Alumina (Al_2O_3)	1
PTFE/Al_2O_3-4	PTFE	Alumina (Al_2O_3)	4
PTFE/Al_2O_3-8	PTFE	Alumina (Al_2O_3)	8
PTFE/Al_2O_3-16	PTFE	Alumina (Al_2O_3)	16
PTFE/Al_2O_3-30	PTFE	Alumina (Al_2O_3)	30
PTFE/BA80-1	PTFE	Boehmite alumina (BA80)	1
PTFE/BA80-4	PTFE	Boehmite alumina (BA80)	4
PTFE/BA80-8	PTFE	Boehmite alumina (BA80)	8
PTFE/BA80-16	PTFE	Boehmite alumina (BA80)	16
PTFE/BA80-30	PTFE	Boehmite alumina (BA80)	30
PTFE/MG70-1	PTFE	Hydrotalcite (MG70)	1
PTFE/MG70-4	PTFE	Hydrotalcite (MG70)	4
PTFE/MG70-8	PTFE	Hydrotalcite (MG70)	8
PTFE/MG70-16	PTFE	Hydrotalcite (MG70)	16
PTFE/MG70-30	PTFE	Hydrotalcite (MG70)	30
PTFE/G/A-0.25/4	PTFE	Graphene + alumina (Al_2O_3)	0.25 + 4
PTFE/G/A-2/2	PTFE	Graphene + alumina (Al_2O_3)	2 + 2
PTFE/G/A-4/4	PTFE	Graphene + alumina (Al_2O_3)	4 + 4

3.2. Material development and characterisation, transfer layer characterisation

3.2.1. Chemical composition

Energy-dispersive X-ray spectroscopy (EDS) investigations were carried out with a JEOL JSM 6380LA device (JEOL, Tokyo, Japan) with 15 kV accelerating voltage, 10 sweep counts and 0.1 ms dwell time. The sufficient electron conductivity of the samples was provided by

sputtering of the surface with gold (Au) in a JEOL FC-1200 device. In Chapter 3.3.3, the chemical composition was also measured by a WAS Lab Spectrotest – PMI Master Sort portable optical emission spectrometer (SPECTRO Analytical Instruments, Kleve, Germany).

3.2.2. Compressive tests

The compressive properties of the produced samples were measured by a Zwick Z020 universal tester (Zwick Roell Group, Ulm, Germany) equipped with a 20 kN load cell. The crosshead speed during test was 2 mm/min. The average and standard deviations (σ) were calculated from 5 samples, the error bars in graphs represent ±1σ. The compressive stress values were calculated at 5 and 10% compressive deformation for comparison according to Equation (3.1):

$$\sigma_{x\%} = 4 \cdot F_{x\%}/(D_{in}^2\pi) \tag{3.1}$$

where $\sigma_{x\%}$ is the compressive stress (MPa) calculated at $x\%$ compressive deformation (%), $F_{x\%}$ is the acting normal force (N) at $x\%$ compressive deformation (%), D_{in} is the initial diameter of the tested samples (mm).

The compressive creep properties of PTFE/Al_2O_3-4 samples were measured by a Zwick Z005 universal tester (Zwick Roell Group, Ulm, Germany) equipped with a 5 kN load cell. The applied load and testing time were 3 MPa and 167 min, which are the same as the used contact pressure and testing time during the wear tests in Chapter 6. The error bars in graphs represent ±1σ.

3.2.3. Density measurements

The density of the sintered samples was estimated by the immersion method (ISO 1183 1:2012). The mass of the samples was measured first in air, and afterwards immersed in ethanol. In case of each material, the average and standard deviations (σ) were calculated from 5 samples, the error bars in graphs represent ±1σ. The density was calculated using Equation (3.2)-(3.4):

$$\rho_{et} = -0.0008544 \cdot T_{et} + 0.80641 \tag{3.2}$$

$$V_s = (m_{s,air} - m_{s,et})/\rho_{et} \tag{3.3}$$

$$\rho_s = m_{s,air}/V_s \tag{3.4}$$

where ρ_{et} is the density of ethanol (g/cm^3), T_{et} is the measured temperature in ethanol (°C), V_s is the volume of the sample (cm^3), $m_{s,air}$ is the measured sample mass in air (g), $m_{s,et}$ is the measured sample mass in ethanol (g), while ρ_s is the calculated density of the sample (g/cm^3).

3.2.4. Differential scanning calorimetry (DSC)

DSC measurements were carried out with a TA Instruments Q2000 device (TA Instruments, New Castle, Delaware, USA) according to three different protocols.

- Protocol 1 included a heat/cool/heat module between 0 and 370°C temperature, with 5 °C/min heating and cooling rate. The enthalpy of fusion was evaluated between 290°C and 335°C for both of the heating cycles, while the enthalpy of crystallisation was evaluated between 280°C and 325°C. This protocol was used for sintered samples.
- Protocol 2 was a modulated DSC, involving only one heating cycle from -90°C to 400°C temperature, with 2 °C/min heating rate, 1°C amplitude and 60 s period time.
- Protocol 3 included a heat/cool/heat module, the first heating and the cooling cycle simulated the sintering process. This protocol was carried out between 23 and 370°C temperature with 90 °C/h heating rate in the first cycle, 1440 / 720 / 360 / 60 / 30 / 20 / 15 °C/h cooling rate in the second cycle and 5 °C/min heating rate in the third cycle. The enthalpy of fusion was evaluated between 310°C and 350°C for the first heating cycle and between 290°C and 335°C for the second heating cycle. This protocol was used for unsintered samples.

Samples were placed in aluminium pans and tested in 50 ml/min nitrogen flow in all protocols. The degree of crystallinity was calculated by Equation (3.5):

$$X = \frac{\Delta H_m - \Delta H_{CC}}{\Delta H_f \cdot (1-\alpha)} \cdot 100 \quad (3.5)$$

where X is the degree of crystallinity (%), ΔH_m is the enthalpy of fusion (J/g), ΔH_{CC} is the enthalpy of cold-crystallisation (J/g), ΔH_f is the enthalpy of fusion for 100% crystalline PTFE (J/g) and α is the mass fraction of the fillers (-). As PTFE did not show any cold-crystallization, ΔH_{CC} was counted as zero. The degree of crystallinity was evaluated with 69 J/g enthalpy of fusion for 100% crystalline PTFE [1].

The molecular weight of PTFE was evaluated using Equation (3.6) from Suwa *et al.* [2]:

$$M_n = 2.1 \cdot 10^{11} \cdot \Delta H_c^{-5.16} \cdot \frac{1}{(1-\alpha)} \quad (3.6)$$

where M_n is the molecular weight (g/mol), ΔH_c is the enthalpy of crystallization (cal/g) and α is the mass fraction of the fillers (-). Equation (3.6) can be used for PTFE respecting the following limitation: the molecular weight of PTFE is recommended to be between 10^5 and 10^7 g/mol [3].

3.2.5. Dynamic mechanical analysis (DMA)

DMA was carried out with a TA Instruments DMA Q800 device (TA Instruments, New Castle, Delaware, USA) in multi-frequency-strain mode. 3-point bending setup was used, the length of the support was 20 mm. The temperature range was between -120°C and 330°C with 3 °C/min heating rate and 1 Hz frequency. The isothermal dwelling time at -120°C was 5 minutes. The oscillation strain was 0.05% with 6 N static force.

3.2.6. Fourier-transform infrared spectroscopy (FTIR)

FTIR analyses were carried out by a Bruker Tensor 37 FTIR spectrometer (Bruker, Billerica, Massachusetts, USA) with deuterated triglycine sulfate (DTGS) detector, and Specac Golden Gate single reflection monolithic diamond attenuated total reflection (ATR) sampling system. The spectroscopic transmission range was between 4000 and 600 cm^{-1} with 4 cm^{-1} resolution in wavenumbers.

3.2.7. Hardness measurements

Hardness measurements of the polymer samples were carried out with a Zwick H04.3150.000 digital hardness tester (Zwick Roell Group, Ulm, Germany) in Shore-D measurement range. The Vickers hardness of the steel counterfaces was measured by a KB 250 BVRZ universal hardness testing machine (KB Prüftechnik, Hochdorf-Assenheim, Germany) according to EN ISO 6507-1 standard (HV 10). The error bars in graphs represent ±1σ.

3.2.8. Moisture content measurement

Brabender Messtechnik Aquatrac-3E moisture meter (Brabender Messtechnik, Duisburg, Germany) was used to observe the moisture content of the polymer samples. The measurement principle is based on a chemical reaction between the absorbed water and calcium hydride reagent producing hydrogen. The device measures the gas pressure of hydrogen, which is proportional to the water content of the sample.

3.2.9. Raman spectroscopy

Raman spectrometry was carried out with a Horiba Jobin Yvon Labram 300 spectrometer (Horiba, Kyoto, Japan) equipped with charge-coupled device (CCD) detector and 532 nm Nd-YAG LASER. The grating was 1800 grooves/mm. The investigated spectrum range was between 1789 and 346 cm^{-1} in wavenumbers.

3.2.10. Shear tests

The applied technique is the Iosipescu shear test method. All tests were run according to ASTM D 5379-05 standard. The error bars in graphs represent ±1σ. The strain measurement was performed with a Digital Image Correlation (DIC) measurement system (Mercury Monet with

5 MP camera, Sobriety, Czech Republic). The shear properties of the polymer samples were measured by a Zwick Z020 universal tester (Zwick Roell Group, Ulm, Germany) equipped with a 20 kN load cell. The crosshead speed during the test was 2 mm/min. With this test method the shear properties of materials can be determined by the use of V-notched beams. The test arrangement can be seen in Figure 3.2.

The shear stress can be calculated with Equation (3.7) and (3.8):

$$\tau_{1,2} = F_{shear}/A_s \tag{3.7}$$

$$A_s = w \cdot t_s \tag{3.8}$$

where $\tau_{1,2}$ is the evaluated shear stress (MPa), F_{shear} is the measured shear force by the load cell (N), A_s is the area of the sample cross-section (mm^2), w is the notched beam width (mm) and t_s is the thickness (mm) of the V-notched beams.

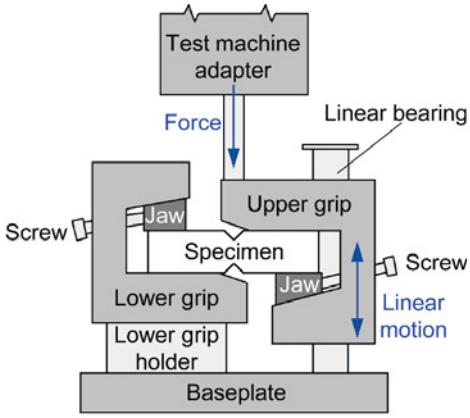

Figure 3.2. Test arrangement of Iosipescu shear test.

The shape and sizes of the V-notched specimens can be found in Figure 3.3. The main features are the following: 76 mm length, 4 mm thickness (t_s), 20 mm base width and 10 mm V-notched beam width (w).

The shear strains were measured by DIC system. Strain gauges could not have been used due to the high deformation of unfilled/filled PTFE specimens and the adhesion issues on PTFE. The applied four measuring points were positioned according to Figure 3.4. For DIC system, an inhomogeneous sample surface is required to provide sufficient contrast for the cameras. Therefore, the specimens were textured with a sprayed paint (Figure 3.5).

The axes of the chosen shear strains (green, dashed lines) are symmetrical with the respect of the horizontal axis, and they have an angle of 45° with the horizontal axis of the sample. The axes of shear strains were perpendicular with each other.

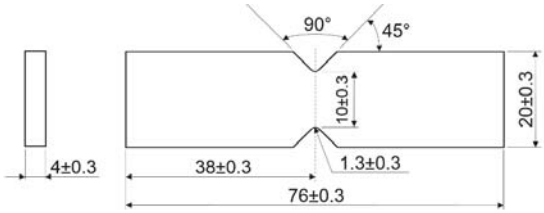

Figure 3.3. Iosipescu shear test specimens.

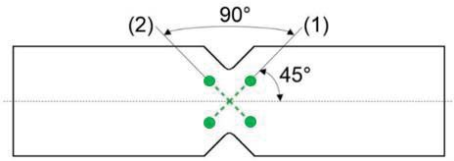

Figure 3.4. The position of the measured shear strains. (1) and (2) refers to the directions of strain measurement.

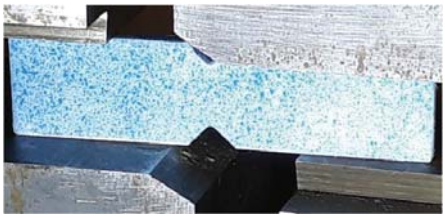

Figure 3.5. Textured Iosipescu shear test specimen.

The shear strain can be calculated with Equation (3.9):

$$\gamma_{xy} = \frac{2\cdot(\varepsilon_1 - \varepsilon_2)}{\sin(2\theta_1) - \sin(2\theta_2)} \tag{3.9}$$

As the shear strain axes are positioned in 45°, Equation (3.9) is simplified according to Equation (3.10):

$$\gamma_{xy} = \frac{2\cdot(\varepsilon_1 - \varepsilon_2)}{\sin(2\cdot 45) - \sin(-2\cdot 45)} = \frac{2\cdot(\varepsilon_1 - \varepsilon_2)}{2} = \varepsilon_1 - \varepsilon_2 \tag{3.10}$$

where γ_{xy} is the calculated shear strain (-), ε_1 and ε_2 are the measured strains (-), θ_1 and θ_2 are the angles (°) between the horizontal axis and the axes of ε_1 and ε_2, respectively.

3.2.11. Surface topography and roughness

The scanning electron microscope (SEM) measurements were carried out by a JEOL JSM 6380LA device (JEOL, Tokyo, Japan). The sufficient electron conductivity of the samples was provided by sputtering of the surface with gold (Au) in a JEOL FC-1200 device. The investigated surfaces were prepared by two different methods:

- Method 1 was the freeze-fracturing (cryo-fracturing) of the samples, which were pre-cooled in liquid nitrogen until 2 minutes.
- Method 2 was the microtome cutting of the investigated samples, which was carried out at -40°C temperature by a Leica EM UC6/FC7 microtome (Leica, Wetzlar, Germany) mounted with a glass blade.

White-light interferometry (WLI): Taylor Hobson CCI HD non-contact optical white-light interferometry (Taylor Hobson, Leicester, United Kingdom) was used to take 3D wear maps of polymer samples and steel counterfaces. In Chapter 3.3.4 the average and standard deviations (σ) were calculated from 5 measurements, applying 10x magnification which corresponds to 1.65 x 1.65 mm observed surface area. All of the calculated deviations were related to ±1σ.

3.2.12. Tensile tests

The tensile properties of the filled/unfilled PTFE samples were measured by a Zwick Z250 universal tester (Zwick Roell Group, Ulm, Germany) equipped with a 20 kN load cell (EN ISO 527-2). The crosshead speed was 10 mm/min until 0.5% strain to provide a low test speed for Young`s modulus measurement and 100 mm/min after 0.5% strain up to break. The error bars in graphs represent ±1σ.

3.2.13. Thermal conductivity measurements

The thermal conductivity of the unfilled/filled PTFE was measured by a thermal conductivity measurement device (Figure 3.6), developed at the Department of Polymer Engineering of BME (Budapest, Hungary) [4, 5].

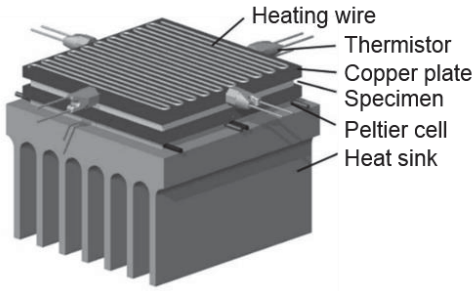

Figure 3.6. Schematic representation of thermal conductivity measurement device [5].

The measurements were carried out according to the transient hot plate method. The measured sample is mounted between two 80 mm x 80 mm sized copper plates. The upper one is heated by aluminium-chromium (AlCr) heating wire, while the lower one is cooled by four Peltier cells. The plates and the samples were placed in an isolated chamber. The temperature was registered by 2-2 built-in NTC thermistors (Epcos B57045K) at the upper and lower sides. The upper plate was tempered to 50°C. Each polymer sample was covered with

thermally conductive silicone grease to decrease the thermal contact resistance. The thermal conductivity was calculated with Equation (3.11) based on Fourier`s law:

$$\lambda = \frac{P}{2A} \cdot \frac{0.001 \cdot t_s}{\Delta T_m} \tag{3.11}$$

where λ is the thermal conductivity (W/mK), P is the heating power (W), t_s is the sample thickness (mm), A is the surface of the sample (m^2) perpendicular to the heat flux and ΔT_m is the temperature difference (K). The error bars in graphs represent ±1σ.

3.2.14. Thermogravimetric analysis (TGA)

TGA was carried out with a TA Instruments Q500 device (TA Instruments, New Castle, Delaware, USA) in nitrogen or air atmosphere depending on the type of test. The purge gas was nitrogen with 40 ml/min flow. The samples were placed in platinum pans and tested in 60 ml/min nitrogen or air flow.

The thermal stability analyses were carried out in two major aspects. The first was related to a conventional thermal stability/decomposition analysis with 10 °C/min heating rate from room temperature to 1000°C. The other kind of thermal analyses simulated the conditions of the sintering protocol to gain information on the thermal stability and decomposition at 370°C maximal sintering temperature.

The thermal stability/decomposition of the materials was observed by four different TGA protocols.

- Protocol 1 was a conventional thermal stability analysis with 10 °C/min heating rate from room temperature to 1000°C.
- Protocol 2 simulated the sintering process with the following parameters: 90 °C/h (1.5 °C/min) heating rate from 30°C to 370°C, two hours dwelling time at 370°C maximum temperature and 30 °C/h (0.5 °C/min) cooling rate from 370°C to 70°C.
- Protocol 3 simulated the sintering process with an extended dwelling time at the maximal sintering temperature. This analysis included the following steps: 90 °C/h (1.5 °C/min) heating rate from 30°C to 370°C, ten hours dwelling time at 370°C maximum temperature. This protocol did not focus on the cooling rate.
- Protocol 4 was related to the detailed investigation of BA80 particles to gain information about the content of humidity and those contaminants which can vaporize under 200°C. This protocol was the following: 10 °C/min heating rate from room temperature to 200°C, 10 hours dwelling time at 200°C and 10 °C/min heating rate from 200°C to 1000°C.

3.2.15. Wettability and surface free energy (SFE)

The wettability properties of the unfilled/filled PTFE and steel counterfaces were characterised by drop shape analyser (DSA30, KRÜSS, Hamburg, Germany) using sessile drop method and drop-build-up technique. The used liquid was distilled water and both advancing (10 µl drop volume) and receding contact angles (5 µl removing volume from the previously applied 10 µl drop) were measured. The measurements were performed in a chamber providing 95% relative humidity and 22°C temperature. The SFE was calculated by the software of the analyser based on both of the advancing and receding contact angles using the equation of state (EoS) method (Equation (3.12) and Equation (3.13)):

$$\sigma_s = \sigma_{sl} + \sigma_l \cdot cos\theta \tag{3.12}$$

$$\sigma_{sl} = \sigma_l + \sigma_s - 2\sqrt{\sigma_l \cdot \sigma_s} \cdot e^{-\beta(\sigma_l - \sigma_s)^2} \tag{3.13}$$

where σ_s is the surface free energy (SFE) of the solid (mN/m), σ_{sl} is the interfacial tension between the liquid and the solid (mN/m), σ_l is the surface tension of the used liquid (mN/m), θ is the measured contact angle (°) and β is a constant (0.0001247). The surface tension of the used water was counted as 72.3 mN/m (22°C, the correlated phase is air). The error bars in graphs represent ±1σ.

3.3. Tribological characterisation

3.3.1. Tribometer

Tribological characterisation was performed by a Wazau TRM 1000 tribometer (Dr.-Ing. Georg Wazau Mess- und Prüfsysteme GmbH, Berlin, Germany). The normal force can be applied by counter weights with a drive-spindle system in the range of 5-1000 N. The tribometer is driven by a servomotor adjustable from 0.1 to 3000 rpm. The mode and type of the applied motion is continuous sliding motion.

3.3.2. Test configuration and parameters

The applied configuration was pin-on-disc with rotating cylindrical polymer pin and stationary steel disc counterface (Figure 3.7). The investigated polymer pin samples had a diameter of 8 mm with 4 mm thickness, while the counterfaces had a diameter of 50 mm. The wear track centreline on the steel discs was at 30 mm diameter. Five samples were tested from each kind of material, the error bars in graphs represent ±1σ. The raw data exported from Wazau tribometer was processed by MATLAB R2015b, the Matlab code can be seen in Appendix A. The bulk temperature was measured by thermocouples, at the backside of the steel counterfaces, in 5 mm distance from the contact surface.

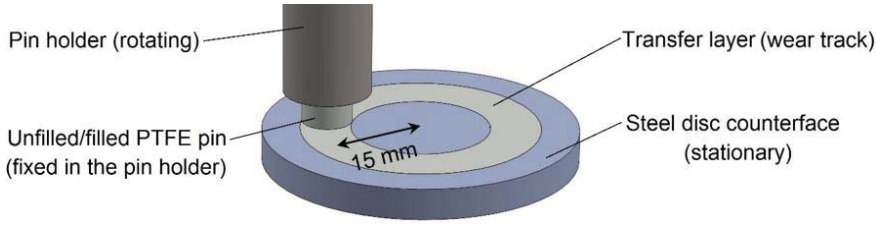

Figure 3.7. Schematic representation of wear test arrangement.

The coefficient of friction is calculated during wear test by the tribometer with Equation (3.14):

$$CoF = \frac{Fr}{F_N} \tag{3.14}$$

where CoF is the coefficient of friction (-), Fr is the friction force (N) calculated by the tribometer and F_N is the applied normal force (N) measured by the tribometer. As the pin rotating was continuous, the introduced friction values are related to the dynamic coefficient of friction.
The friction force is calculated by the tribometer with Equation (3.15):

$$Fr = 1000 \cdot \frac{M}{r} \tag{3.15}$$

where Fr is the friction force (N), M is the torque (Nm) measured by the tribometer and r is the radius of wear track centreline (mm).

The specific wear rate of polymer samples were calculated after wear test by using Equation (3.16):

$$k = \frac{\Delta m}{\rho \cdot F_N \cdot d_s} \tag{3.16}$$

where k is the specific wear rate (mm^3/Nm), Δm is the measured mass loss (g) by a weight balance after wear test, ρ is the density of the pin sample (g/mm^3), F_N is the applied normal force (N) measured by the tribometer and d_s is the total sliding distance (m) calculated by the tribometer. None of the polymer samples were dried before the wear tests (Chapter 3.3.5).

The total sliding distance is calculated by the tribometer with Equation (3.17):

$$d_s = v_s \cdot t_{test} \tag{3.17}$$

where d_s is the sliding distance (m), v_s is the sliding speed (m/s) calculated by the tribometer and t_{test} is the test time (s) measured by the tribometer.

The sliding speed is calculated by the tribometer with Equation (3.18):

$$v_s = \omega \cdot D_{wt} \cdot \pi \,/\, 1000 \tag{3.18}$$

where v_s is the sliding speed (m/s), ω is the rotational speed (revolutions per minute, rpm) measured by the tribometer and D_{wt} is the diameter of wear track centreline (mm).

The contact pressure can be calculated with Equation (3.19):

$$p = \frac{F_N}{A_S} \tag{3.19}$$

where p is the contact pressure (MPa), F_N is the applied normal force (N) measured by the tribometer and A_S is the corresponding area (cross section) of the polymer pin sample (mm^2).

The corresponding area of the polymer pin can be calculated with Equation (3.20):

$$A_S = \frac{D^2 \cdot \pi}{4} \tag{3.20}$$

where A_S is the corresponding area (cross section) of the polymer pin sample (mm^2) and D is the diameter of the polymer pin sample (mm).

The pv value (MPa · m/s) of the polymers was calculated with Equation (3.21):

$$pv = p \cdot v_S \tag{3.21}$$

where p is the contact pressure (MPa) and v_S is the sliding speed (m/s).

3.3.3. Chemical composition and hardness of the steel counterfaces

The following steels were used as disc counterfaces at this research work: 42CrMo4 (EN 1.7225), 34CrNiMo6 (EN 1.6582) and AISI 304 (EN 1.4301) stainless steel. Table 3.2 introduces the standard chemical composition of these steels [6-7] while Table 3.3 and 3.4 shows the measured chemical composition as a preliminary investigation of the unworn steel counterfaces. Table 3.3 introduces the EDS (Chapter 3.2.1) results, while as a comparison Table 3.4 shows the chemical composition taken by a portable optical emission spectrometer (Chapter 3.2.1). 42CrMo4 and 34CrNiMo6 are widely used construction steels (e.g. shafts) and in this way are potential counterparts of the developed PTFE based composites in the industry. 304 stainless steel was investigated as reference material as it has a relatively high chromium and nickel content which can be a relevant factor considering tribo-chemical reactions. The measured Vickers hardness of the steel discs is introduced in Table 3.5 (Chapter 3.2.7).

Table 3.2. Standard chemical composition of the steel disc counterfaces. Acronyms are the following: carbon (C), manganese (Mn), silicon (Si), phosphorus (P), sulphur (S), chromium (Cr), molybdenum (Mo) and nickel (Ni) [6-7].

Steels	C	Mn	Si	P	S	Cr	Mo	Ni
42CrMo4	0.38 0.45	0.60 0.90	max 0.40	max 0.025	max 0.035	0.90 1.20	0.15 0.30	---
34CrNiMo6	0.30 0.38	0.50 0.80	max 0.40	max 0.025	max 0.035	1.30 1.70	0.15 0.30	1.30 1.70
304	max 0.07	max 2.00	max 1.00	max 0.045	max 0.015	17.50 19.50	---	8.00 10.50

Table 3.3. The measured chemical composition (EDS) of steel counterfaces. Acronyms are the following: manganese (Mn), silicon (Si), chromium (Cr), molybdenum (Mo) and nickel (Ni).

	Mn	Si	Cr	Mo	Ni
42CrMo4	0.85 ± 0.14	0.22 ± 0.02	1.17 ± 0.09	0.15 ± 0.10	---
34CrNiMo6	0.78 ± 0.15	0.22 ± 0.03	1.72 ± 0.06	0.16 ± 0.12	1.44 ± 0.15
304	1.69 ± 0.05	0.56 ± 0.03	19.64 ± 0.04	---	7.63 ± 0.17

Table 3.4. The measured chemical composition (WAS Lab Spectrotest - PMI Master Sort) of the steel disc counterfaces. Acronyms are the following: manganese (Mn), silicon (Si), chromium (Cr), molybdenum (Mo) and nickel (Ni).

Steels	Mn	Si	Cr	Mo	Ni
42CrMo4	0.61	0.10	0.91	0.16	---
34CrNiMo6	0.53	0.10	1.41	0.17	1.46
304	1.54	0.41	18.70	---	7.26

Table 3.5. The measured Vickers hardness of the steel disc counterfaces.

	Hardness (HV)
42CrMo4	308 ± 2
34CrNiMo6	363 ± 3
304	227 ± 1

3.3.4. The surface roughness of the unworn polymers and steel counterfaces

All disc counterfaces were surface finished by turning for a Sa 0.3 – 0.4 µm average surface roughness in a spiral pattern. Further details from the surface roughness of the steels can be found in Table 3.6 and 3.7. Table 3.8 and 3.9 introduce the surface roughness of the developed polymers. These surface roughness values were measured by white light interferometer (Chapter 3.2.11) as a preliminary investigation of the unworn steel counterfaces and polymer samples. Sa (µm) is the arithmetical mean height of the analysed surface, Sq (µm) is the root mean square height in a given area and Sz (µm) is the sum of the largest peak height and the largest pit depth value. Sku (Kurtosis, µm) represents the sharpness of the roughness profile, if Sku<3, Sku=3 or Sku>3, the height distribution is skewed, normal or spiked, respectively. Sp (µm) is the maximum peak height of the analysed surface, Sv (µm) is the maximum pit height of the given area, while St (µm) is the sum of Sp and Sv [8].

Table 3.6. Surface roughness (Sa, Sq, Sz and Sku) of the steel counterfaces. All data measured by white light interferometer, 10x magnification, 1.65 x 1.65 mm surface area.

Steels	Sa (µm)	Sq (µm)	Sz (µm)	Sku (µm)
42CrMo4	0.42 ± 0.03	0.52 ± 0.03	2.39 ± 0.17	2.81 ± 0.20
34CrNiMo6	0.31 ± 0.02	0.39 ± 0.02	2.20 ± 0.18	3.20 ± 0.25
304	0.32 ± 0.04	0.41 ± 0.05	2.30 ± 0.37	3.40 ± 0.59

Table 3.7. Surface roughness (Sp, Sv and St) of the steel counterfaces. All data measured by white light interferometer, 10x magnification, 1.65 x 1.65 mm surface area.

Steels	Sp (μm)	Sv (μm)	St (μm)
42CrMo4	1.40 ± 0.10	0.99 ± 0.08	2.39 ± 0.17
34CrNiMo6	1.08 ± 0.11	1.12 ± 0.12	2.20 ± 0.18
304	1.28 ± 0.35	1.01 ± 0.07	2.30 ± 0.37

Table 3.8. Surface roughness (Sa, Sq, Sz and Sku) of the developed polymer samples. All data measured by white light interferometer, 10x magnification, 1.65 x 1.65 mm surface area.

Polymer samples	Sa (μm)	Sq (μm)	Sz (μm)	Sku (μm)
PTFE	1.77 ± 0.15	2.20 ± 0.20	11.07 ± 0.94	2.77 ± 0.12
PTFE/Graphene-1	1.95 ± 0.16	2.52 ± 0.23	15.37 ± 1.86	3.85 ± 0.52
PTFE/Graphene-4	2.01 ± 0.17	2.57 ± 0.24	15.17 ± 1.70	3.57 ± 0.50
PTFE/Al_2O_3-1	1.64 ± 0.16	2.05 ± 0.21	10.86 ± 1.08	2.92 ± 0.00
PTFE/Al_2O_3-4	1.95 ± 0.28	2.42 ± 0.35	12.26 ± 1.47	2.73 ± 0.04
PTFE/BA80-1	1.60 ± 0.22	1.99 ± 0.26	10.25 ± 0.96	2.77 ± 0.19
PTFE/BA80-4	1.56 ± 0.15	1.96 ± 0.17	10.37 ± 0.92	2.93 ± 0.13
PTFE/MG70-1	1.93 ± 0.16	2.39 ± 0.22	12.17 ± 1.10	2.72 ± 0.14
PTFE/MG70-4	1.90 ± 0.31	2.37 ± 0.37	13.19 ± 1.55	3.03 ± 0.30

Table 3.9. Surface roughness (Sp, Sv and St) of the developed polymer samples. All data measured by white light interferometer, 10x magnification, 1.65 x 1.65 mm surface area.

Polymer samples	Sp (μm)	Sv (μm)	St (μm)
PTFE	5.59 ± 0.61	5.83 ± 0.80	11.42 ± 1.38
PTFE/Graphene-1	6.11 ± 0.46	9.40 ± 1.46	15.51 ± 1.88
PTFE/Graphene-4	6.24 ± 0.34	8.98 ± 1.50	15.22 ± 1.71
PTFE/Al_2O_3-1	5.31 ± 0.70	5.71 ± 0.46	11.02 ± 1.16
PTFE/Al_2O_3-4	5.94 ± 0.70	6.46 ± 0.89	12.40 ± 1.58
PTFE/BA80-1	5.01 ± 0.25	5.28 ± 0.75	10.29 ± 0.97
PTFE/BA80-4	5.26 ± 0.86	5.16 ± 0.12	10.43 ± 0.93
PTFE/MG70-1	6.08 ± 0.47	6.22 ± 0.74	12.30 ± 1.18
PTFE/MG70-4	6.72 ± 0.90	6.62 ± 0.71	13.34 ± 1.53

3.3.5. Methodology

The wear of the polymers was measured during the tribo-tests by a displacement sensor, in this way, on-line wear graphs are available. The measured wear graphs were linear after a short running-in period, which means that the wear rate was quasi-steady-state during the sliding distance. In this way, the wear rate was only calculated after the wear test (off-line) from the measured mass loss of the filled/unfilled PTFE pin samples. For this evaluation, the mass of the pin sample was measured by an analytical scale 5-5 times before and after wear tests. In both cases, the mass of the polymer samples was measured together with the pin holder. With this technique, the possible mass removal from the polymer sample, caused by the

mounting or demounting from the steel holder, can be avoided. After the mass measurement of the unworn sample, the polymer pin and the steel counterface were mounted to the tribometer.

The polymer samples were not dried as the relative humidity – and in this way, the absorbed water content of the samples – is an important factor for the fillers according to the working hypothesis (Chapter 1.3). Another reason is that the potential products made from these materials (e.g. sliding bearings, guide rings, seals) are working mostly in environmental conditions. Focusing on the wear rate evaluation, the mass of the escaped water content during wear test has a negligible influence on the accuracy of mass loss measurement. The moisture content of the polymers was observed by a moisture meter (Chapter 3.2.8). Table 3.10 shows the observed moisture content of the samples. The mass of the filled/unfilled PTFE pin samples was ~0.5 g; the accuracy of the weight balance was 0.2 mg. The highest ratio between the moisture content and the mass loss during wear was calculated for PTFE/Graphene-16; these samples were tested only in Phase 1 (3 MPa contact pressure, 0.1 m/s sliding speed) where the measured bulk temperature was between 30°C and 40°C. It means that in this low temperature, most of the moisture content could not migrate from the polymer sample.

The relative humidity was between 50±5 RH%, while the temperature was 23±2°C. Before wear tests, the filled/unfilled PTFE pins were cleaned with isopropanol while the steel counterfaces were cleaned with acetone and isopropanol.

Table 3.10. The moisture content of PTFE samples with 4 and 16 wt% filler content. The weight of the moisture content is related to 0.5 g. The mass loss is related to 3 MPa contact pressure and 0.1 m/s sliding speed with ~38°C bulk temperature during wear.

Polymer samples	Moisture content (wt%)	Moisture content (mg)	Mass loss during wear (mg)	Ratio (%)
PTFE	0.001	0.005	176.25	0.003
PTFE/Graphene-4	0.013	0.065	15.75	0.413
PTFE/Graphene-16	0.048	0.240	2.37	10.127
PTFE/Al_2O_3-4	0.013	0.065	2.75	2.364
PTFE/BA80-4	0.022	0.110	63.31	0.174
PTFE/BA80-16	0.088	0.440	37.43	1.176
PTFE/MG70-4	0.013	0.065	144.00	0.045

3.3.6. Test plan for the tribological characterisation – research phases

The tribological characterisation was divided into four different phases with increasing complexity of the applied test parameters and the composition of the tribo-composites (Figure 3.8 and Table 3.11). This approach allows to gain insight into the effect of different mono- and hybrid fillers and leads to knowledge build-up on the level of material composition.

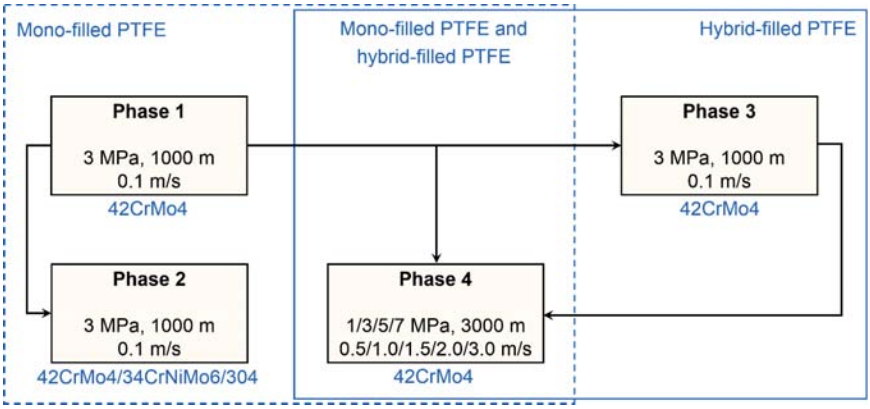

Figure 3.8. Test plan for tribological investigation.

Table 3.11. Main test plan for the developed unfilled and filled PTFE samples.

Materials	Production related sensitivity analysis of the materials	Material characterisation		Tribological characterisation			
	Applicable?	Mono-filled PTFE	Hybrid-filled PTFE	Phase 1	Phase 2	Phase 3	Phase 4
	Chapter 4, 7	Chapter 5	Chapter 7	Chapter 6	Chapter 6	Chapter 7	Chapter 7
PTFE	Yes	Tested	---	Tested	Tested	---	Tested
PTFE/Graphene-0.25	Yes	Tested	---	Tested	---	---	---
PTFE/Graphene-1	Yes	Tested	---	Tested	---	---	---
PTFE/Graphene-4	Yes	Tested	---	Tested	Tested	---	Tested
PTFE/Graphene-8	Yes	Tested	---	Tested	---	---	Tested
PTFE/Graphene-16	Yes	Tested	---	Tested	---	---	---
PTFE/Graphene-30	Reference	---	---	---	---	---	---
PTFE/Al_2O_3-1	Yes	Tested	---	Tested	---	---	---
PTFE/Al_2O_3-4	Yes	Tested	---	Tested	Tested	---	Tested
PTFE/Al_2O_3-8	No	---	---	---	---	---	---
PTFE/Al_2O_3-16	No	---	---	---	---	---	---
PTFE/Al_2O_3-30	Reference	---	---	---	---	---	---
PTFE/BA80-1	Yes	Tested	---	Tested	---	---	---
PTFE/BA80-4	Yes	Tested	---	Tested	Tested	---	---
PTFE/BA80-8	Yes	Tested	---	Tested	---	---	---
PTFE/BA80-16	Yes	Tested	---	Tested	---	---	---
PTFE/BA80-30	Reference	---	---	---	---	---	---
PTFE/MG70-1	No	Tested	---	Tested	---	---	---
PTFE/MG70-4	No	Tested	---	Tested	---	---	---
PTFE/MG70-8	No	---	---	---	---	---	---
PTFE/MG70-16	No	---	---	---	---	---	---
PTFE/MG70-30	Reference	---	---	---	---	---	---
PTFE/G/A-0.25/4	Yes	---	Tested	---	---	Tested	---
PTFE/G/A-2/2	Yes	---	Tested	---	---	Tested	---
PTFE/G/A-4/4	Yes	---	Tested	---	---	Tested	Tested

Phase 1 and 2 were performed with mono-filled PTFE composites, Phase 3 was done with hybrid-filled samples, while Phase 4 was performed with both mono- and hybrid-filled PTFE composites. The sliding distance in Phase 1, 2 and 3 was 1000 m which corresponds to 10273 rotation cycles, while in Phase 4 was 3000 m which correspond to 30819 cycles. In Phase 3 the fillers of the hybrid-filled composites were selected from the experience of Phase 1 and 2. Those fillers which had the lowest wear rate in Phase 1, were chosen as hybrid fillers for Phase 3. This hybridisation aimed to see the interaction between the used fillers and how it would affect the tribological behaviour of the developed PTFE composites.
In Phase 2 those PTFE samples with 4 wt% filler content were investigated which had remarkably lower wear rate than neat PTFE in Phase 1. In this phase, samples were tested with three different kinds of steel counterfaces. Phase 4 was a parametrical study with four different contact pressures (1/3/5/7 MPa), five sliding speeds (0.5/1/1.5/2/3 m/s), which corresponds to pv values between 0.5 and 21 MPa·m/s for each tested material. In this phase, three mono-filled and a hybrid-filled PTFE composite were investigated.

3.3.6.1. Phase 1

The tribological characterisation at Phase 1 was done with 42CrMo4 steel disc counterface. The roughness of the surface finished steel counterfaces was between Sa 0.3-0.4 µm. The sliding speed was 61 rpm which corresponds to 0.1 m/s (at track centreline) while the applied normal force was 151 N which corresponds to 3 MPa contact pressure. The sliding distance was set up to 1000 m, which corresponds to ~167 minutes. Five repeated tests were provided for each kind of material. The tested materials in this phase can be seen in Table 3.11.

3.3.6.2. Phase 2

The tribological characterisation at Phase 2 was done with 42CrMo4/34CrNiMo6/304 steel discs counterface. In this phase, those 4 wt% filler content samples were tested, which had a remarkably lower wear rate in Phase 1 compared to neat PTFE (Figure 3.8, Table 3.11). The roughness of the surface finished steel counterfaces was between Sa 0.3 – 0.4 µm. The sliding speed was 61 rpm which corresponds to 0.1 m/s (at track centreline) while the applied normal force was 151 N which corresponds to 3 MPa contact pressure. The sliding distance was set to 1000 m; the test time was ~167 minutes.

3.3.6.3. Phase 3

Hybrid-filled PTFE composites were tested in Phase 3 to investigate the combined effect of the chosen fillers (Table 3.11 and Figure 3.8). The fillers were selected from the experiences of Phase 1 and Phase 2. The roughness of the surface finished steel counterfaces was Sa 0.3-0.4 µm. The rotational speed was 61 rpm which corresponds to 0.1 m/s (at track

centreline) while the applied normal force was 151 N which corresponds to 3 MPa contact pressure. The sliding distance was set up to 1000 m; the test time was ~167 minutes. The counterface was 42CrMo4 steel.

3.3.6.4. Phase 4

Parametric tribological characterisation was done at Phase 4 with materials chosen from the experience of Phase 1 and 3 (Figure 3.8, Table 3.11). Four different contact pressures and five different sliding speeds were chosen. The sliding speeds and contact pressures were 0.5/1.0/1.5/2.0/3.0 m/s (at track centreline) and 1/3/5/7 MPa, respectively. The roughness of the surface finished steel counterfaces was Sa 0.3 – 0.4 µm. The sliding distance was set up to 3000 m. The counterface was 42CrMo4 steel.

3.4. References

[1] X. Q. Wang, D. R. Chen, J. C. Han, S. Y. Du: Crystallization behavior of polytetrafluoroethylene (PTFE). Journal of Applied Polymer Science 83 (2002) 990–996.

[2] T. Suwa, M. Takehisa, S. Machi: Melting and crystallization behavior of poly (tetrafluoroethylene). New method for molecular weight measurement of poly (tetrafluoroethylene) using a differential scanning calorimeter. Journal of Applied Polymer Science 17 (11) (1973) 3253-3257.

[3] U. Lappan, U. Geißler, L. Haußler, G. Pompe, U. Scheler: The estimation of the molecular weight of polytetrafluoroethylene based on the heat of crystallisation. A comment on Suwa's Equation. Macromolecular Materials and Engineering 289 (2004) 420–425.

[4] A. Suplicz, J. G. Kovács: Development of thermally conductive polymer materials and their investigation. Materials Science Forum 729 (2013) 80-84.

[5] J. G. Kovacs, A. Suplicz: Thermally conductive polymer compounds for injection moulding: the synergetic effect of hexagonal boron-nitride and talc. Journal of Reinforced Plastics and Composites 32 (16) (2013) 1234–1240.

[6] EN 10083-3:2006 Steels for quenching and tempering. Technical delivery conditions for alloy steels.

[7] EN 10088-2:2005 Stainless steels. Technical delivery conditions for sheet/plate and strip of corrosion resisting steels for general purposes.

[8] https://www.keyence.com/ss/products/microscope/roughness/surface/sp-maximum-peak-height.jsp (24.01.2021)

CHAPTER 4

DEVELOPMENT AND SENSITIVITY ANALYSIS OF FREE SINTERING PRODUCTION PROTOCOL

The purpose of this chapter is to introduce the development and sensitivity analysis of the production protocol. The applied production method is room temperature pressing – free sintering technique which is well known in PTFE-based material production.

The following articles were published based on this chapter:
Tóth Levente Ferenc, Szebényi Gábor, Patrick De Baets: Kísérleti gyártástechnológia fejlesztése PTFE szobahőmérsékletű préselésére és szinterelésére. Polimerek, 2018, 4, 155-160 (in Hungarian).
Levente Ferenc Tóth, Patrick De Baets, Gábor Szebényi: Processing Analysis of Nanoparticle Filled PTFE: Restrictions and Limitations of High Temperature Production. Polymers, 2020, 12, 2044, 1-14.

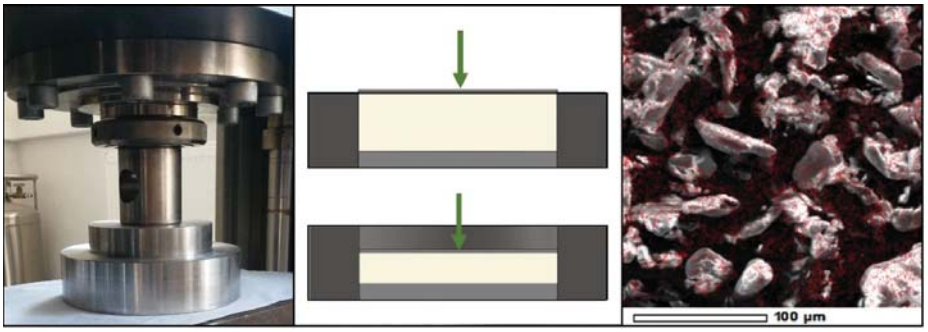

4.1. Introduction

A widely used production technique for polytetrafluoroethylene (PTFE) is the so-called room temperature pressing – free sintering method, which is preceded by a dry or solvent blending procedure when PTFE contains fillers. The quality of the final products depends on the applied blending efficiency, which affects the particle dispersion. The final material properties also highly depend on the protocol of the sintering process. Critical parameters of the sintering cycles are the heating rate, maximal temperature, dwelling time at maximal temperature and the cooling rate. The maximal sintering temperature range of PTFE is between 360 and 380°C; the thermal profile of the sintering cycle depends on the shape and volume of the material. The literature introduces many different sintering thermal profiles; however, the size and shape of their sintered samples were similar to each other [1-3]. Knowing that the used fillers can affect the thermal stability during sintering, the sensitivity analysis of this high-temperature process is crucial for the definition of the final production protocol.

4.2. Materials and methods

4.2.1. Materials

Table 4.1 introduces the developed and investigated samples in this chapter. More details about the materials can be found in Chapter 3.1. Composites with 1 wt% filler content were not investigated in this chapter as the mass losses of these composites were too low for a precise thermogravimetric analysis (TGA) analysis. For a more accurate recording of mass loss and IR spectra, 30 wt% filled composites were also analysed. Due to this high filler content, the registered mass loss of the composites and the FTIR peaks of the fillers are more significant.

Table 4.1. The developed neat PTFE and PTFE composites.

Materials	Matrix	Filler(s)	Filler content (wt%)
PTFE	PTFE	---	---
PTFE/Graphene-4	PTFE	Graphene	4
PTFE/Graphene-8	PTFE	Graphene	8
PTFE/Graphene-16	PTFE	Graphene	16
PTFE/Graphene-30	PTFE	Graphene	30
PTFE/Al_2O_3-4	PTFE	Alumina (Al_2O_3)	4
PTFE/Al_2O_3-8	PTFE	Alumina (Al_2O_3)	8
PTFE/Al_2O_3-16	PTFE	Alumina (Al_2O_3)	16
PTFE/Al_2O_3-30	PTFE	Alumina (Al_2O_3)	30
PTFE/BA80-4	PTFE	Boehmite alumina (BA80)	4
PTFE/BA80-8	PTFE	Boehmite alumina (BA80)	8
PTFE/BA80-16	PTFE	Boehmite alumina (BA80)	16
PTFE/BA80-30	PTFE	Boehmite alumina (BA80)	30
PTFE/MG70-4	PTFE	Hydrotalcite (MG70)	4
PTFE/MG70-8	PTFE	Hydrotalcite (MG70)	8
PTFE/MG70-16	PTFE	Hydrotalcite (MG70)	16
PTFE/MG70-30	PTFE	Hydrotalcite (MG70)	30

4.2.2. Production protocol and sensitivity analysis

This chapter introduces, in the aspect of the sensitivity analysis, the results of scanning electron microscopy (SEM), density measurements, compressive and hardness tests, thermogravimetric analysis (TGA), Fourier-transform infrared spectroscopy (FTIR) and differential scanning calorimetry (DSC). Further information about the production method and equipment can be found in Chapter 3.1 and 3.2, respectively.

4.2.2.1. Sensitivity analysis of neat PTFE

For the sensitivity analysis of the pressing protocol, samples were pressed with 5/12.5/20/35/50 MPa in order to investigate the effect of the applied pressure (Figure 4.1 (a)). The sensitivity analysis of the sintering protocol was performed with samples pressed by 12.5 MPa pressure. At the first step, the cooling rate was varied (Figure 4.1 (b)) to get information about the degree of crystallinity as a function of the cooling time. Besides the various cooling rates, the sintering protocol included a dwelling time of four hours at 370°C and 90 °C/h heating rate. Four cooling rates were compared to each other: 15/20/30/60 °C/h, which corresponds to 4/3/2/1 h cooling time from 370°C to 310°C. At the second step, the dwelling time was varied to gain knowledge about the required minimal dwelling time and the thermal stability at the maximal sintering temperature. The compared dwelling times were the following: 0.5/1/2/3/4/6/8 hours with 90 °C/h and 30 °C/h heating and cooling rate, respectively (Figure 4.1 (c)).

4.2.2.2. Sensitivity analysis of neat fillers and filled PTFE

The sensitivity analysis of fillers and filled PTFE was carried out by TGA measurements, followed by FTIR analysis. Chapter 4 introduces the thermal stability/decomposition of the materials observed by TGA using Protocol 1-4. More details about the used protocols are presented in Chapter 3.2.14. The results observed in neat fillers and filled PTFE were compared to the reference neat PTFE.

4.2.2.3. Final production protocol

The final production protocol is based on the results of the sensitivity analyses. The applied pressure is 12.5 MPa. The room temperature pressing was followed by a sintering cycle. The purpose was to choose a relatively short but sufficient dwelling time at 370°C maximal temperature to provide enough time for the fusion of the PTFE particles. The relatively slow heating rate had a role in avoiding the warping caused by the thermal stress during the heating cycle. The thermal profile of the sintering process was asymmetric, as the cooling rate was lower than the heating rate (Figure 4.1 (d)). This slow cooling rate aimed to minimise the residual thermal stress and maximise the degree of crystallinity of the sintered samples. The final sintering protocol was the following: 90 °C/h (1.5 °C/min) heating rate, two hours dwelling

time at 370°C maximum temperature and 30 °C/h (0.5 °C/min) cooling rate (Figure 4.1 (d)). All sintering processes were carried out in an oven, in air atmosphere, without the mould and without applying pressure.

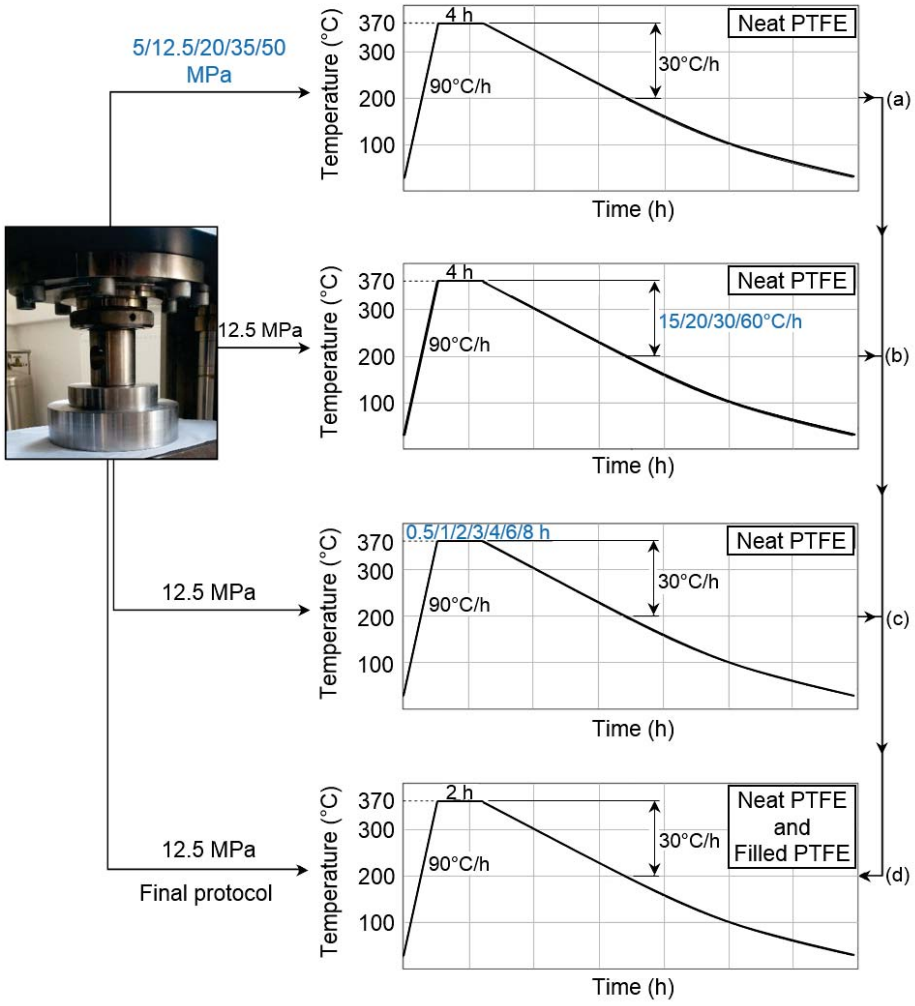

Figure 4.1. Sensitivity analysis of room temperature pressing – free sintering process for neat PTFE, the variables are marked by blue. This figure introduces the sensitivity analysis of applied pressure (a), cooling rate (b), dwelling time (c) and it also shows the final production protocol (d).

4.3. Results and discussion

4.3.1. Basic principles of the pressing protocol

The production method of unfilled/filled PTFE was a room temperature pressing – free sintering technique. The room temperature pressing of PTFE samples was carried out with 12.5 MPa pressure at the final production protocol. The aim was to provide a progressive pressing (from 0 to 12.5 MPa), with low initial pressure and low pressing speed. The construction of the mould was cylindrical to get a uniform clearance between the die and the punches. Figure 4.2. shows the steps of the final (12.5 MPa) pressing protocol.

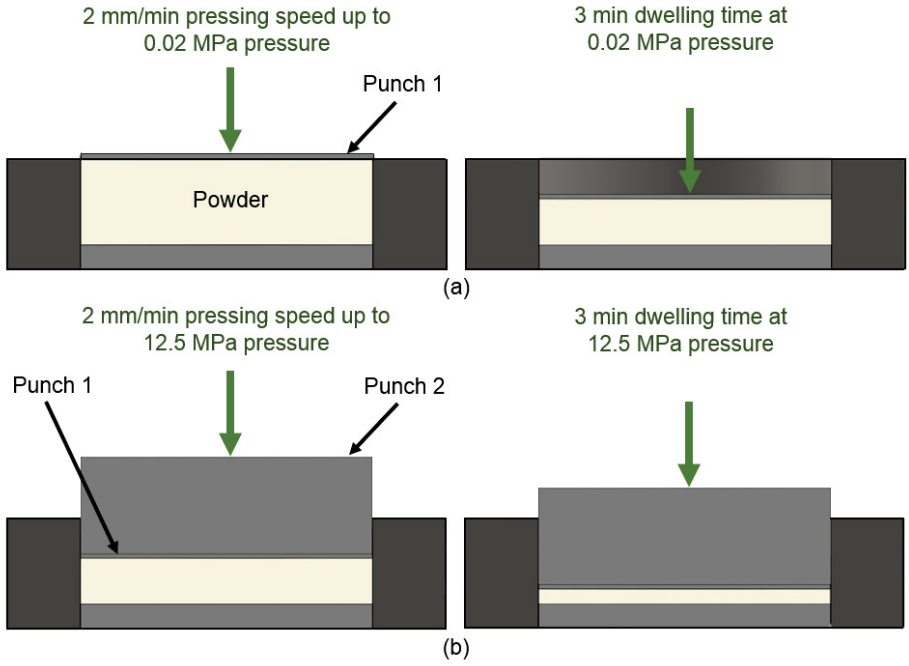

Figure 4.2. Pressing protocol for samples with 120 mm diameter in a cylindrical mould.

This paragraph introduces the pressing protocol applying 12.5 MPa pressure. As a first step, only Punch 1 was placed on the top of the neat/blended PTFE powder. Punch 1 had 120 mm diameter, 1 mm thickness and 0.09 kg (0.9 N) weight, providing only ~0.08 Pa initial pressure on the powder. With this low initial pressure, it was possible to minimise the escaping of fine powder from the system across the clearance between the mould and the punch. The second step was the pressing of the Punch 1 with 2 mm/min up to 0.02 MPa. After reaching this pressure, three minutes of dwelling time was maintained at 0.02 MPa. After the three minutes of dwelling time, the mould was unloaded. This 0.02 MPa pressure was high enough to restrict the freedom of the particles avoiding the escaping of some powder caused by the higher weight

of Punch 2. At the third step, Punch 2 was placed on the top of Punch 1. Punch 2 had 120 mm diameter, 40 mm thickness and 3.6 kg (36 N) weight, providing ~3.20 Pa pressure on the powder. This 3.20 Pa pressure is significantly lower than the applied 0.02 MPa pressing, respecting the proposed progressive increase of the pressure. The fourth step was the pressing of Punch 2 with 2 mm/min up to 12.5 MPa. Punch 1 would have been too thin to transfer without deformation this 12.5 MPa pressure. After the three minutes of dwelling time, the mould was unloaded, removed from the universal testing machine, and the pressed 'green' material was ready for the sintering process.

4.3.2. Sensitivity analysis of neat PTFE – pressing protocol

The sensitivity analysis of the pressing protocol is focusing on the effect of the applied pressure. The samples were produced according to the protocol showed in Figure 4.1 (a).

4.3.2.1. Density and porosity

Figure 4.3 shows the SEM micrographs of the pressed (12.5 MPa) and unsintered neat PTFE samples. These micrographs introduce the PTFE particles (~25 μm average particle size) and indicate the high porosity of the unsintered material. The PTFE particles are mostly discrete and separated as the samples are still unsintered.

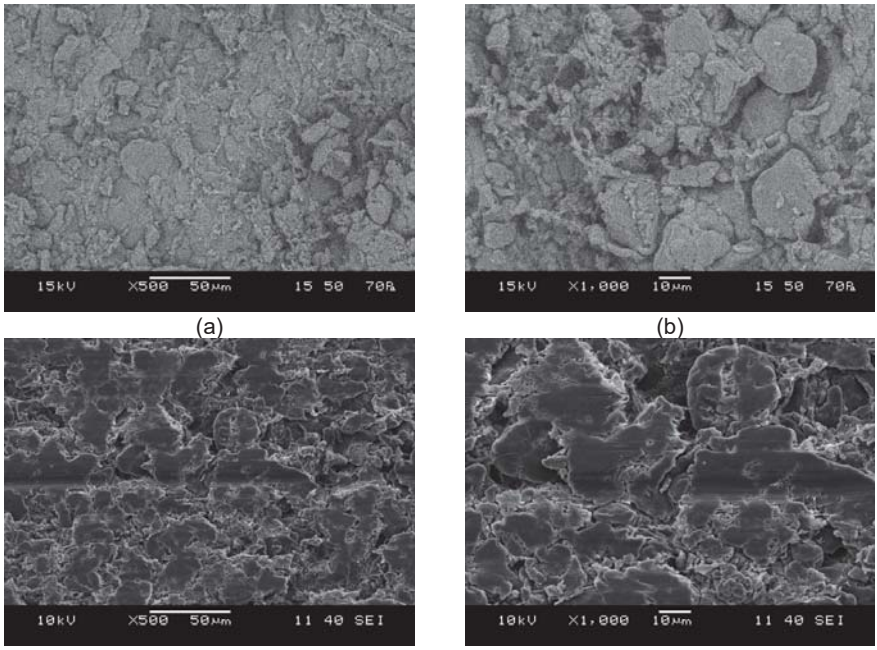

Figure 4.3. Micrographs of 12.5 MPa pressed neat PTFE, before sintering process. Cryo-fractured surface: (a) and (b), microtome cut surface: (c) and (d).

Figure 4.3 (a) and (b) present the cryo-fractured surfaces of the samples (Chapter 3.2.11, Method 1). The SEM analysis was carried out in low vacuum mode (70 Pa), as in high vacuum mode, the investigation of the discrete and loosed particles on the cryo-fractured surfaces was not possible due to their instability.

For the precise porosity analysis, a well-prepared smooth surface is required, therefore the microtome cut surfaces were analysed as well (Chapter 3.2.11, Method 2). As the cutting edge pressed the particles, they were more integrated into the surface; in this way, it was possible to use high vacuum mode. It can be seen from the micrographs, that a precise porosity and surface analysis can not be carried out even with this technique (Figure 4.3 (c) and (d)). The glass transition temperature of PTFE (-103°C) is much lower than the applied microtome cutting temperature (-40°C). In this way, the particles deformed due to the shear stress during cutting.

The density of neat PTFE can indicate the tendency of porosity as a function of the pressing pressure. Figure 4.4 and Table B.1 (Appendix B) introduce the average density of unsintered and sintered samples. All of the measured specimens had a diameter of 10 mm, and they were sintered according to the protocol introduced in Figure 4.1 (a). Only the density of the unsintered materials correlated with the applied pressure; their density increased as the pressure increased. The sintered materials had closely the same density regardless of the pressing pressure. This phenomenon comes from the nature of the free-sintering method, where no pressure was applied on the samples during sintering. At this sintering process, PTFE overpasses its melting temperature range, and the particles fuse, minimising the residual porosity and maximising the density. Below 35 MPa, the density of the pressed PTFE samples was lower than the theoretically 2.2. g/cm^3 due to their high porosity, in this way, the density increased during the sintering process. Above 35 MPa, the density of PTFE samples decreased during the sintering process. This reduction is supposed to come from the high applied pressure. These samples were pressed with 50 MPa, which achieved the theoretically 2.2. g/cm^3 density. When the PTFE melted, due to the free movement of the molecular chains, the volume of the material increased compared to the overpressed condition of unsintered samples. Rooyen *et al.* registered similar tendencies in the density of sintered and unsintered PTFE [4].

Besides the average density, the density distribution of PTFE sample with 120 mm diameter was also investigated to gain knowledge about the uniformity of the developed materials. Figure 4.5 and 4.6 introduce the density map of unsintered and sintered neat PTFE, respectively. The sample was pressed with 20 MPa pressure and the unsintered PTFE disc was cut into 10x10 mm pieces, as far as possible. After the density measurements of these unsintered 10x10 mm pieces, they were heat-treated according to the sintering protocol introduced in Figure 4.1 (a), and their density was measured again.

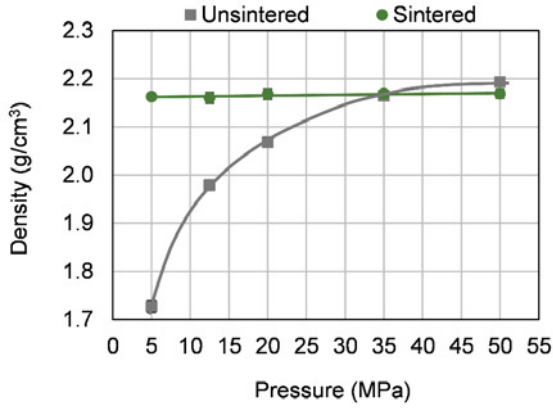

Figure 4.4. The average density of unsintered and sintered neat PTFE. The samples are sintered with 90 °C/h heating rate, 4 h dwelling time and 30 °C/h cooling rate.

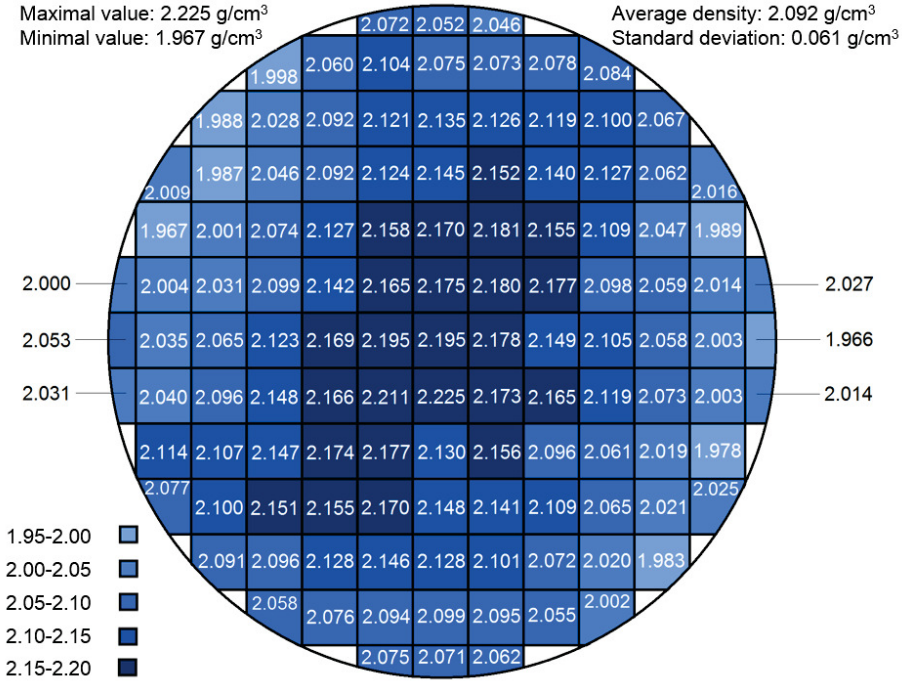

Figure 4.5. Density map of unsintered neat PTFE disc with 120 mm diameter, pressed with a pressure of 20 MPa.

The average density of the unsintered PTFE sample was 2.092 g/cm^3, with 0.061 g/cm^3 standard deviation (Figure 4.5). It is in agreement with the previously introduced density values, which were measured in small samples (Figure 4.4 and Table B.1). The lowest

measured density of the disc was 1.967 g/cm^3, while the highest value reached 2.225 g/cm^3. The middle of the specimen achieved the highest density, while due to the edge effect, the density is lower in the outer ranges. The different colours indicate the density ranges from 1.95 to 2.20 g/cm^3.

The average density of the sintered PTFE pieces was 2.161 g/cm^3, with 0.003 g/cm^3 standard deviation (Figure 4.6). It is also in agreement with the previously introduced density values, which were measured in small samples (Figure 4.4 and Table B.1). The lowest measured density of the disc was 2.156 g/cm^3, while the highest value reached 2.168 g/cm^3. This density map confirms that after the sintering process, the density of the sample is more homogeneous. It is in agreement with Figure 4.4, which shows that independently of the initial density of the pressed samples, the final density values of the sintered samples are approximately the same.

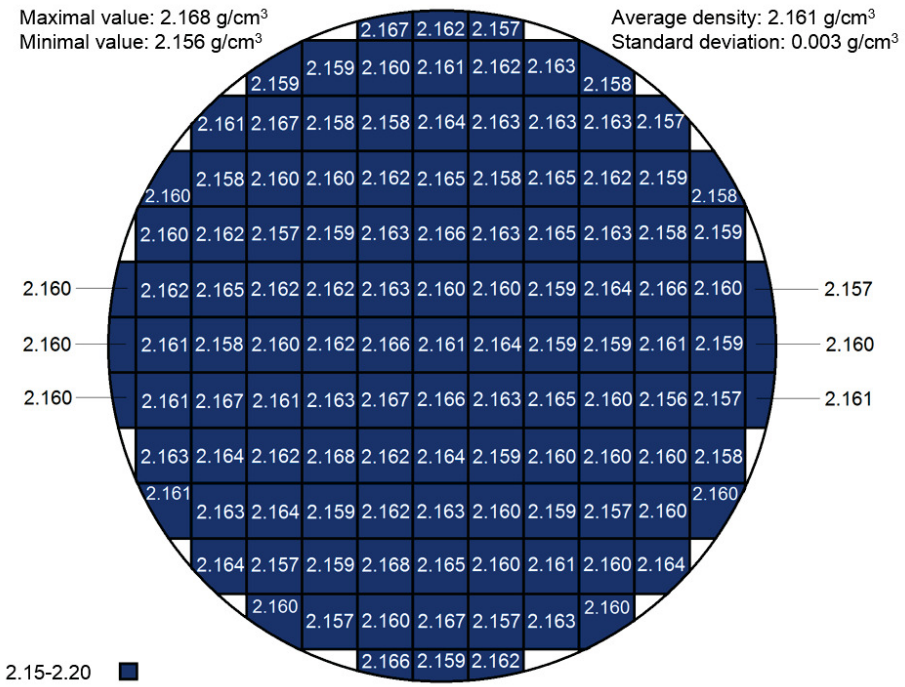

Figure 4.6. Density map of sintered neat PTFE disc with 120 mm diameter. Pressed with a pressure of 20 MPa, followed by 90 °C/h heating rate, 4 h dwelling time, 30 °C/h cooling rate.

4.3.2.2. Compressive stress and modulus

Figure 4.7 and Table B.2 introduce the compressive stress and modulus of the neat PTFE samples as a function of the applied pressure at pressing protocol. There are no remarkable differences in compressive stress and modulus; this is in agreement with the observed results of the density (Figure 4.4). As the density and in this way the porosity is closely the same in the sintered PTFE samples, caused by the overpassing of the melting temperature range, the fusion of the PTFE particles is the same independently of the applied pressure. In this way, no remarkable differences can be expected as a function of the pressure during pressing.

The average compressive stress at 5% and 10% deformation as a function of the applied pressure was between 12.74-13.74 MPa and 18.69-19.46 MPa, respectively. The average compressive modulus as a function of the pressure was between 356.7-362.6 MPa (Figure 4.7).

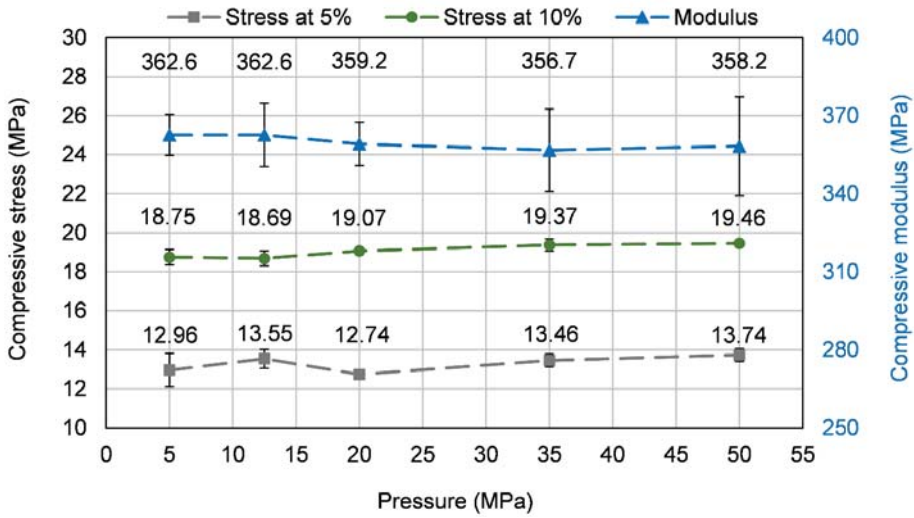

Figure 4.7. Compressive stress at 5 and 10% deformation and compressive modulus of sintered neat PTFE as a function of the applied pressure (90 °C/h heating rate, 4 h dwelling time, 30 °C/h cooling rate).

4.3.2.3. Hardness

The hardness of the neat PTFE samples is introduced in (Figure 4.8 and Table B.3). The applied pressure did not influence the hardness of the sintered samples. There are only slight differences between the measured values, as the influence of the applied pressing pressure is neutralised by the melting during the sintering process. The observed hardness of the specimens was between 56.4 and 57.9 MPa.

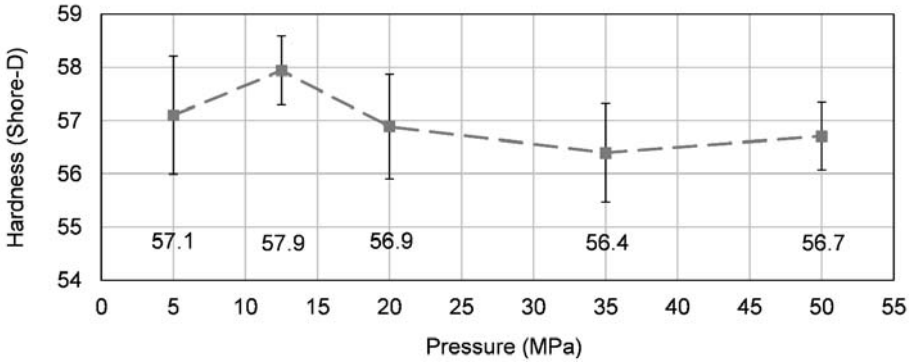

Figure 4.8. The hardness of the sintered neat PTFE as a function of the applied pressure (90 °C/h heating rate, 4 h dwelling time, 30 °C/h cooling rate).

4.3.3. Sensitivity analysis of neat PTFE – sintering protocol

The sensitivity analysis of the sintering protocol is focusing on the effect of the cooling rate and the dwelling time at maximal sintering temperature. The samples for the sensitivity analysis of cooling rate and dwelling time were produced according to the protocols introduced in Figure 4.1 (b) and (c).

4.3.3.1. Decomposition of neat PTFE

Figure 4.9 shows the thermal stability of neat PTFE, measured by TGA applying Protocol 1 (Chapter 3.2.14). Remarkable decomposition was initiated from ~490°C, where the observed mass loss reached 1%. The registered total mass loss of PTFE was ~100%.

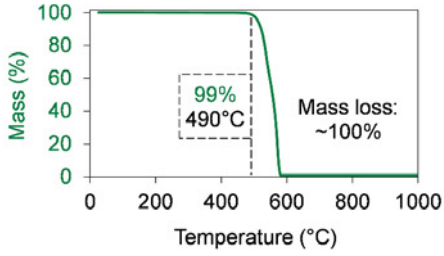

Figure 4.9. Thermal stability of neat PTFE in air atmosphere, measured by TGA with 10 °C/min heating rate up to 1000°C (Protocol 1, Chapter 3.2.14).

The thermal stability of neat PTFE was analysed at the sintering cycle as well with performing the sintering process of the 'green' unsintered PTFE by TGA (Figure 4.10 (a)) according to Protocol 2 (Chapter 3.2.14). The observed mass loss was only 0.01%, which means that PTFE had high thermal stability at the sintering temperature; and this is in agreement with the literature [5]. Figure 4.10 (b) illustrates the thermal stability of PTFE, measured by TGA,

applying Protocol 3 (Chapter 3.2.14). These results show that even in case of the extended ten hours dwelling time, the observed mass loss was only 0.11%. This low value indicates that PTFE has high thermal stability independently of the length of the dwelling time.

Figures 4.11 introduces the FTIR analysis of the unsintered and sintered (by TGA) neat PTFE. The FTIR spectra confirmed the high thermal stability of PTFE, as the results did not indicate a remarkable degradation.

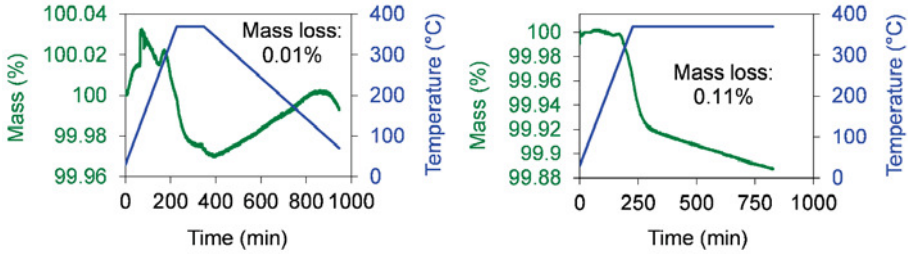

Figure 4.10. Thermal stability of neat PTFE in air atmosphere, measured by TGA, according to Protocol 2 (a) and Protocol 3 (b) (Chapter 3.2.14).

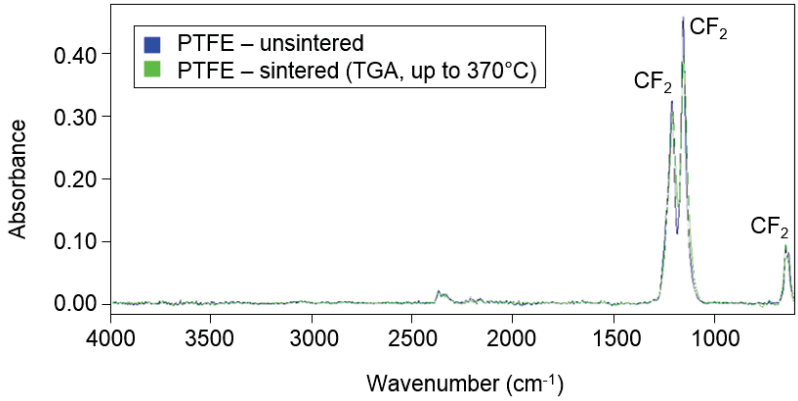

Figure 4.11. FTIR spectra of unsintered neat PTFE – blue; and sintered PTFE (TGA, Protocol 2, Chapter 3.2.14) – green.

4.3.3.2. Density

The unsintered samples had ~1.98 (g/cm^3), while the sintered ones have ~2.16-2.17 (g/cm^3) average density independently of the cooling rate and dwelling time (Figure 4.12 and 4.13; Table B.4 and B.5). When the cooling rate was varied (Figure 4.12), the density values were between 2.157-2.160 g/cm^3. A slight decreasing of density (from 2.170-2.158 g/cm^3) with the increase of the dwelling time can be seen in Figure 4.13, which is in agreement with the small

mass loss of TGA at 370°C (Figure 4.10). The observed slight mass loss is caused by the decomposition of PTFE, which can slightly increase the porosity due to the gas formation.

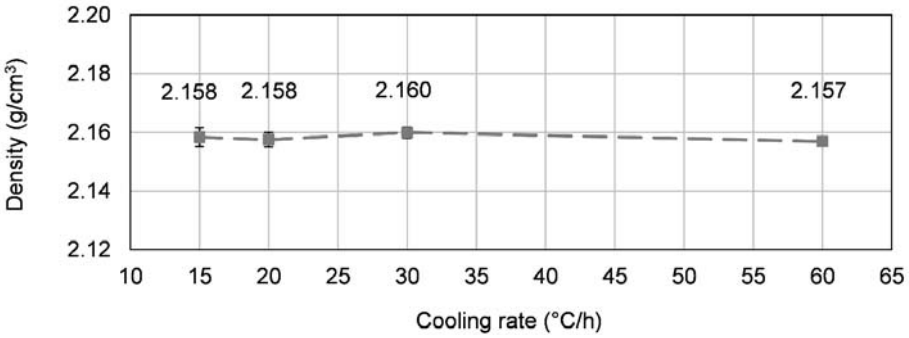

Figure 4.12. The density of the sintered neat PTFE as a function of the cooling rate (12.5 MPa pressure, 90 °C/h heating rate, 4 h dwelling time).

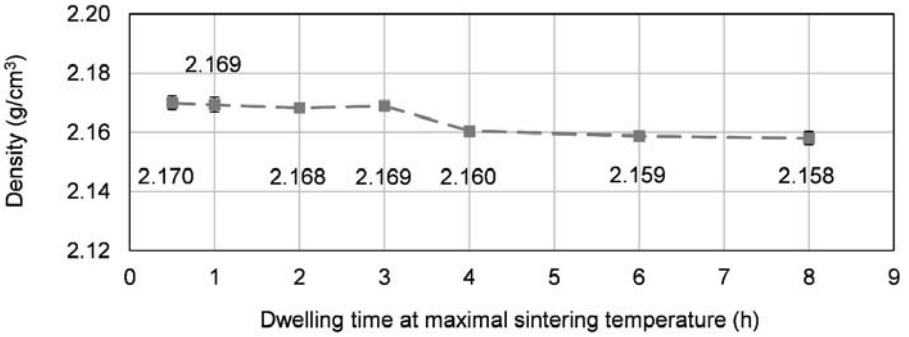

Figure 4.13. The density of the sintered neat PTFE as a function of the dwelling time (12.5 MPa pressure, 90 °C/h heating rate, 30 °C/h cooling rate).

4.3.3.3. Compressive stress and modulus

The compressive stress and modulus of the PTFE samples are introduced in Figure 4.14 and 4.15; Table B.6 and B.7. There are not any significant changes in compressive stress as a function of cooling rate and dwelling time. The unsintered specimens had 5.97 MPa and 3.42 MPa compressive stress at 5% and 10% deformation, respectively. The average compressive stress at 5% and at 10% deformation as a function of cooling rate was between 12.84-13.74 MPa and 18.69-19.33 MPa, respectively (Figure 4.14). The average compressive stress at 5% and at 10% deformation as a function of dwelling time was between 13.55-14.67 MPa and 18.69-19.78 MPa, respectively (Figure 4.15).

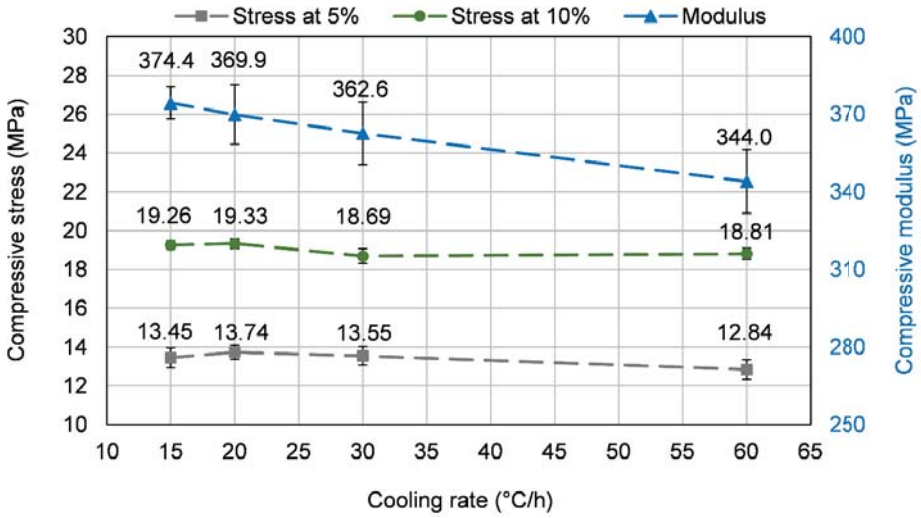

Figure 4.14. Compressive stress at 5 and 10% deformation and compressive modulus of sintered neat PTFE as a function of the cooling rate (12.5 MPa pressure, 90 °C/h heating rate, 4 h dwelling time).

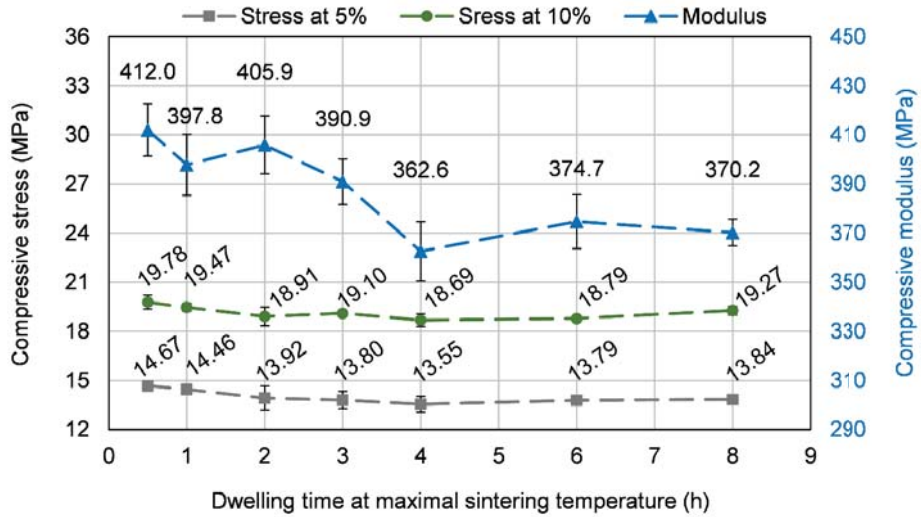

Figure 4.15. Compressive stress at 5 and 10% deformation and compressive modulus of sintered neat PTFE as a function of the dwelling time (12.5 MPa pressure, 90 °C/h heating rate, 30 °C/h cooling rate).

The average compressive modulus decreased as a function of increasing cooling rate; it was 374.4 MPa and 344.0 MPa at 15 °C/h and 60 °C/h, respectively (Figure 4.14). The average

compressive modulus decreased as a function of increasing dwelling time; it was 408.9 MPa and 372.0 MPa at 0.5 h and 8 h, respectively (Figure 4.15). From these results, it can be concluded that the optimal cooling rate has to be between 15 and 30 °C/h while the optimal dwelling time has to be between 0.5 and 3 hours in the viewpoint of compressive modulus.

Figure 4.16 introduces the compressive stress-deformation curves of the reference (unsintered) and sintered sample. The applied maximal deformation was 50%. The unsintered PTFE had much lower deformation compared to the sintered PTFE; the measured value was 10.5%. The unsintered samples reached a maximal deformation during the test; and overpassing this maximal value, the crack propagation was so significant, that it caused the failure of these materials. The test results of the sintered samples did not show this phenomenon, these materials deformed elastically, without reaching a local maximum during the test.

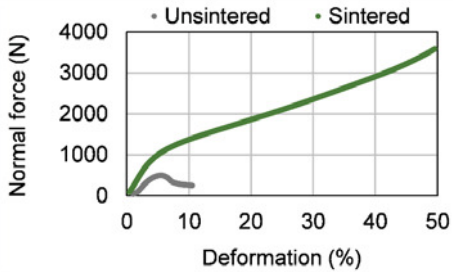

Figure 4.16. Compressive force as a function of the deformation; unsintered (grey) and sintered specimens (green) are pressed with 12.5 MPa; the sintered samples were heat-treated with 90 °C/h heating rate, four hours dwelling time, 30 °C/h cooling rate.

4.3.3.4. Hardness

The hardness of the PTFE samples is introduced in Figure 4.17 and 4.18; Table B.8 and B.9. No significant changes were found in hardness as a function of the cooling rate (Figure 4.17).

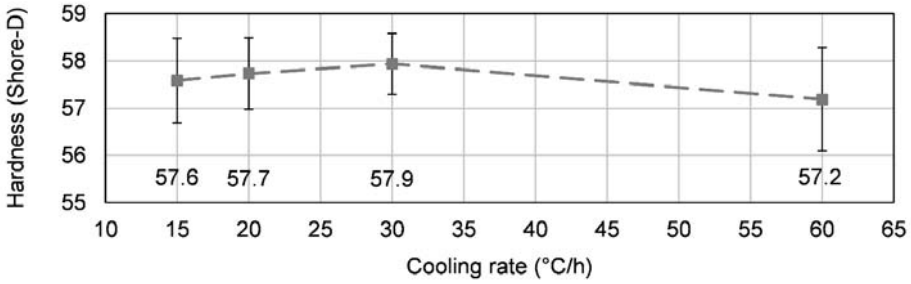

Figure 4.17. The hardness of the sintered neat PTFE as a function of the cooling rate (12.5 MPa pressure, 90 °C/h heating rate, 4 h dwelling time).

The average hardness as a function of dwelling time was increasing. At 0.5, 1, 2 and 3 hours it was 51.0, 53.5, 54.3 and 53.9 Shore-D, respectively, while at 4, 6 and 8 hours it was 57.9, 58.3 and 57.0 Shore-D, respectively (Figure 4.18).

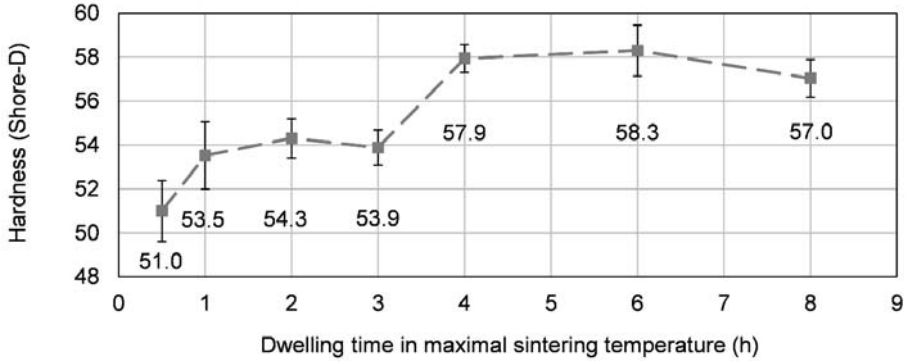

Figure 4.18. The hardness of the sintered neat PTFE as a function of the dwelling time (12.5 MPa pressure, 90 °C/h heating rate, 30 °C/h cooling rate).

4.3.3.5. Melting temperature and degree of crystallinity

The thermal and crystallisation properties of unsintered PTFE were observed by DSC analysis following Protocol 1 (Chapter 3.2.4). The melting peak temperature of neat PTFE was ~338°C in the first heating cycle and ~324°C in the second heating cycle. The first heating cycle is related to the behaviour of the unsintered material. After the first heating cycle, the PTFE already overpassed its melting temperature range; in this way, the second heating cycle represents the thermal properties of the sintered PTFE. The melting peak temperature of the sintered PTFE was ~324°C, which is in agreement with the literature [6, 7]. The crystallization peak temperature of neat PTFE was ~310°C.

Figure 4.19 introduces the first heating cycle of neat unsintered PTFE, focusing on the reversible and non-reversible heat flow. This modulated DSC analysis was carried out with Protocol 2 (Chapter 3.2.4). The investigated temperature range was between -90°C and 400°C. No glass transition temperature was observed in this range, which means that the 116°C (α relaxation) is not the glass transition temperature of PTFE, which is in agreement with the literature [8].

DSC analysis was carried out between 23 and 370°C temperature with the same protocol as the sintering process to observe the degree of crystallinity as a function of the cooling rate (Table 4.2 and 4.3). This analysis also involved some relatively high cooling rate as a comparison. The materials were analysed using Protocol 3 (Chapter 3.2.4). The enthalpy of fusion for 100% crystalline PTFE is 69 J/g [9].

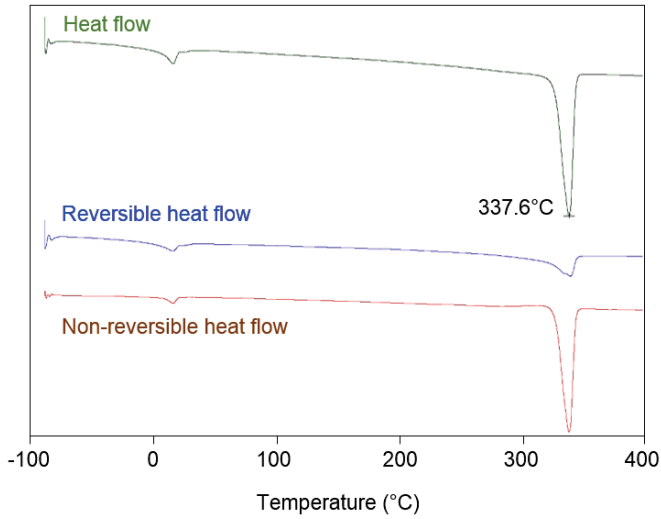

Figure 4.19. Modulated Differential Scanning Calorimetry (MDSC) analysis of unsintered PTFE powder (Protocol 2, Chapter 3.2.4).

Table 4.2 and 4.3 show that the degree of crystallinity is between 81 and 91% in the first heating cycle (unsintered PTFE samples), while 32 and 46% in the second heating cycle (sintered PTFE samples). In the second heating cycle, the thermal history was the same for all of the samples (as in the first heating cycle PTFE reached its melting temperature range), excluding the cooling rate, which were varied between 1440 and 15 °C/h. The degree of crystallinity increased as the cooling rate decreased. At 30 °C/h cooling rate, the degree of crystallinity reached 44.3%. The degree of crystallinity did not change significantly with the further decreasing cooling rate. In this way, the 30 °C/h cooling rate seems to be slow enough for the final sintering protocol.

Table 4.2. DSC analysis of neat PTFE as a function of the cooling rate, first heating cycle (Protocol 3, Chapter 3.2.4).

Cooling rate (°C/h)	Cooling time (h)	Enthalpy of fusion 1st heating (J/g)	Melting peak temperature 1st heating (°C)	Degree of crystallinity 1st heating (%)
1440	0.26	59.96	337.4	86.9
720	0.51	55.97	337.4	81.1
360	1.02	60.82	337.6	88.1
60	6.17	60.15	337.4	87.2
30	12.33	62.93	337.4	91.2
20	18.50	62.93	337.4	91.2
15	24.67	58.52	337.6	84.8

Table 4.3. DSC analysis of neat PTFE as a function of the cooling rate, second heating cycle (Protocol 3, Chapter 3.2.4). The green marked cell shows that value from where considerable changes in the degree of crystallinity was not registered any more.

Cooling rate (°C/h)	Cooling time (h)	Enthalpy of fusion 2nd heating (J/g)	Melting peak temperature 2nd heating (°C)	Degree of crystallinity 2nd heating (%)
1440	0.26	22.28	322.7	32.3
720	0.51	22.03	323.1	31.9
360	1.02	25.41	323.6	36.8
60	6.17	27.99	324.5	40.6
30	12.33	30.55	325.2	44.3
20	18.50	31.47	325.8	45.6
15	24.67	29.49	326.1	42.7

4.3.4. Sensitivity analysis of neat fillers – sintering protocol

The sensitivity analysis of neat fillers is related to the sintering protocol. It is focusing on the thermal stability of the fillers and on the effect of the dwelling time at maximal sintering temperature.

4.3.4.1 Decomposition of graphene

Figure 4.20 introduces the mass loss of graphene as a function of the temperature measured by TGA, applying Protocol 1 (Chapter 3.2.14). Significant decomposition is recorded only from 343°C, on where the observed mass loss still only reached 1% value (Figure 4.20 (a)). The decomposition procedure can be separated into two steps. The first is between ~343-500°C and comes from the decomposition of the amorphous carbon content [10], while the second step is in the range of ~570-800°C, and comes from the decomposition of structured graphene. The total mass loss of graphene is ~100%. The detected mass loss at the first step was ~19% (Figure 4.20 (a)). The initiation of the second decomposition is defined at 80% mass loss.
The decomposition of graphene was also measured by TGA during the sintering cycle according to Protocol 2 (Chapter 3.2.14). The measured mass loss was 19.28%, which means that during the sintering cycle, most of the amorphous carbon content decomposed (Figure 4.20 (b)). Table 4.4 shows the residual mass (m_r) of graphene after Protocol 1 and Protocol 2 (Chapter 3.2.14).

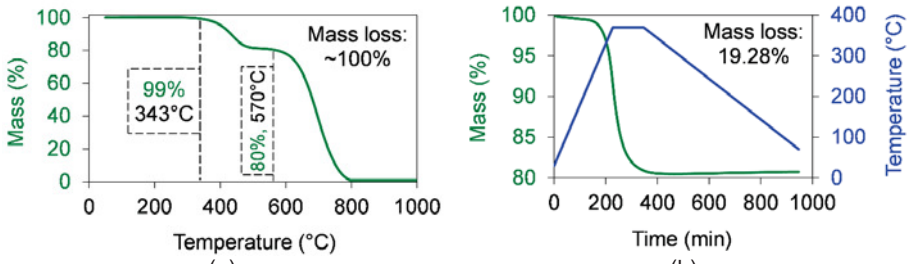

(a) (b)

Figure 4.20. Thermal stability of graphene in air atmosphere, measured by TGA, according to Protocol 1 (a) and Protocol 2 (b) (Chapter 3.2.14).

4.3.4.2. Decomposition of alumina (Al_2O_3)

Figure 4.21 introduces the mass loss of Al_2O_3, measured by TGA. Figure 4.21 (a) shows that the total mass loss was 2.69% when Protocol 1 (Chapter 3.2.14) was used. According to the manufacturer's datasheet, the purity of the used Al_2O_3 is around 99.5%; in other words, ~0.5% contaminants can be found in this filler. In the range of 200-240°C, a higher mass loss rate is recorded, which can come from the adsorbed humidity and from some contaminants. Around 590°C, a slight mass increase can be seen, which is supposed to come from the oxidation of some contaminants in the filler.

The thermal stability of Al_2O_3 was also analysed during the sintering cycle according to Protocol 2 (Chapter 3.2.14). The measured mass loss was 1.70% which is in agreement with the expected high thermal stability of alumina (Figure 4.21 (b)). Table 4.4 shows the residual mass (m_r) of alumina after Protocol 1 and Protocol 2 (Chapter 3.2.14).

The FTIR spectra of reference Al_2O_3, Al_2O_3 measured by TGA up to 370°C (Protocol 2), and Al_2O_3 measured by TGA up to 1000°C (Protocol 1) were measured. The FTIR spectra confirmed the high thermal stability of alumina, as the results did not indicate a significant decomposition (Figure 4.22).

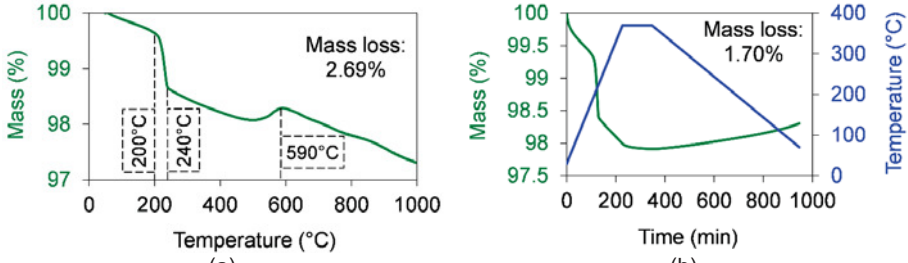

(a) (b)

Figure 4.21. Thermal stability of alumina in air atmosphere, measured by TGA, according to Protocol 1 (a) and Protocol 2 (b) (Chapter 3.2.14).

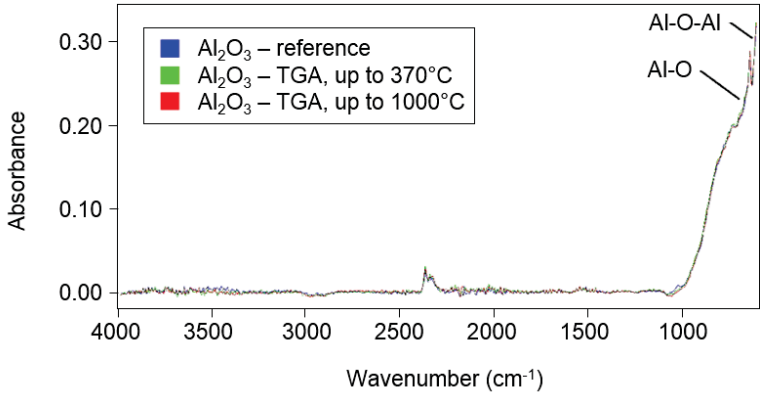

Figure 4.22. FTIR spectra of the reference Al_2O_3 – blue; Al_2O_3 measured by TGA up to 370°C (Protocol 2, Chapter 3.2.14) – green, and Al_2O_3 measured by TGA up to 1000°C (Protocol 1, Chapter 3.2.14) – red.

4.3.4.3. Decomposition of boehmite alumina (BA80, AlO(OH))

Theoretically BA80 decomposes to alumina and water according to the following chemical reaction (Equation (4.1)):

$$2AlO(OH) \rightarrow Al_2O_3 + H_2O \quad (4.1)$$

The mass percentage of H_2O is the theoretical mass loss, which can be measured by TGA. The atomic mass of aluminium (27 Da), oxygen (16 Da) and hydrogen (1 Da) was considered to get information about the theoretical mass loss. In this way, the mass of the molecules in Equation (4.1) is introduced by Equation (4.2):

$$120\ (Da) \rightarrow 102\ (Da) + 18\ (Da) \quad (4.2)$$

The theoretical mass loss can be calculated from the ratio of H_2O and $2AlO(OH)$ (Equation (4.3)):

$$18/120 = 0.15 \rightarrow 15\% \quad (4.3)$$

According to Equation (4.1)-(4.3), the theoretical mass percentage of water is 15%. The measured mass loss by TGA (Protocol 1, Chapter 3.2.14) was in the range of the calculated theoretical mass loss and equalled 16.65% (Figure 4.23 (a) and Table 4.4). This mass loss is slightly higher than the theoretical value. This difference comes from the humidity and contaminants in the analysed sample. In Figure 4.23 (a) it can be seen that the decomposition of boehmite alumina starts to be relevant from 288°C, which is significantly lower than the sintering temperature (370°C). The initiation of the decomposition is defined at 1% mass loss, similarly to the introduced previous analyses. TGA measurement was performed with a heat

hold at 200°C to get information about the content of humidity and about those contaminants which can vaporize under 200°C (Protocol 4, Chapter 3.2.14). The total mass loss is 16.68% (Figure 4.23 (b)) which correlates well to the 16.65% mass loss (Figure 4.23 (a)) presented earlier. After 10 hours of dwelling time at 200°C, the additional mass loss was only 0.75%; and the rest of the mass loss was 15.93% between 200-1000°C, which correlates well to the theoretical 15% mass loss.

The percentage of the decomposed material during the sintering cycle was investigated by simulating the sintering process with TGA (Figure 4.23 (c)), applying Protocol 2 (Chapter 3.2.14). The measured mass loss was 4.65%, which is around 28% (=4.65/16.65) of the total measured mass loss (Figure 4.23 (a)). It means that, although some of the hydroxyl (OH) functional groups decomposed during the sintering cycle, most of them persist. This can be beneficial in the wear process according to the introduced hypothesis related to the complex formation with the carboxyl groups of the PTFE chain ends during wear (Chapter 1.3). Table 4.4 shows the residual mass (m_r) of BA80 after Protocol 1 and Protocol 2. The samples taken out from TGA were also analysed by FTIR to confirm the persistence of OH groups.

The mass loss of BA80 was analysed for 10 hours dwelling time at maximal 370°C temperature as well to gain information about a broader scale of the sintering process (Figure 4.23 (d)). The applied method was Protocol 3, introduced in Chapter 3.2.14. The mass loss slightly increased during the 10 hours dwelling time, but it is still 34.6% of the total measured mass loss (Figure 4.23 (a)).

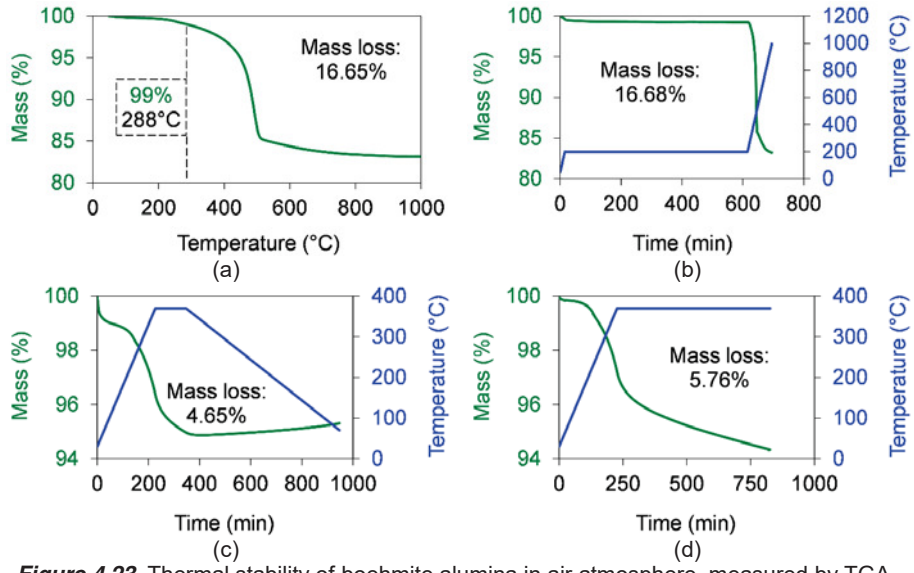

Figure 4.23. Thermal stability of boehmite alumina in air atmosphere, measured by TGA, according to Protocol 1 (a), Protocol 4 (b), Protocol 2 (c) and Protocol 3 (d) (Chapter 3.2.14).

Figure 4.24 shows the FTIR spectra for the samples of reference BA80, BA80 heat treated during TGA up to 370°C (Protocol 2) and BA80 heat treated during TGA up to 1000°C (Protocol 1). The last two samples were those which had already been investigated by TGA. Two significant peaks attributed to –OH bonds were detected in the range of 3000-3400 cm^{-1}, which is in agreement with the literature [11]. These peaks can be seen in both of the reference and TGA (370°C, Protocol 2) samples. These spectra confirm that most of the OH functional groups survived the sintering process, but not the 1000°C TGA test.

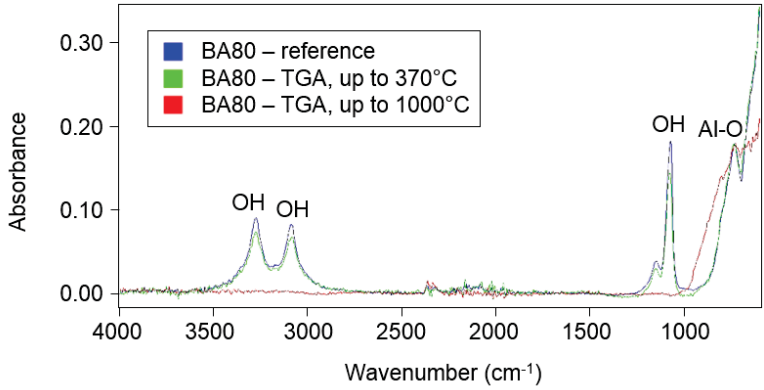

Figure 4.24. FTIR spectra of the reference BA80 – blue; BA80 measured by TGA up to 370°C (Protocol 2, Chapter 3.2.14) – green, and BA80 measured by TGA up to 1000°C (Protocol 1, Chapter 3.2.14) – red.

4.3.4.4. Decomposition of hydrotalcite (MG70)

Figure 4.25 and Table 4.4 shows the mass percentages and residual mass (m_r) of MG70, measured by TGA. Significant decomposition is recorded from 104°C, on where the observed mass loss reached 1% (Figure 4.25 (a)). The total mass loss during MG70 decomposition is 44.91% (Protocol 1, Chapter 3.2.14), while this value in case of simulated sintering procedure is 35.17% (Figure 4.25 (b), Protocol 2, Chapter 3.2.14). It means that the mass loss during sintering process is around ~78% of the total mass loss of MG70. Focusing on high-temperature production of PTFE, due to the observed high decomposition of MG70 during the sintering process, this material is not a promising filler in PTFE.

Figure 4.26 compares the FTIR spectra of reference MG70, MG70 measured by TGA up to 370°C (Protocol 2) and of MG70 measured by TGA up to 1000°C (Protocol 1). Regarding to the sintered MG70, due to their decomposition the intensity of the OH peaks decreased significantly compared to the original material.

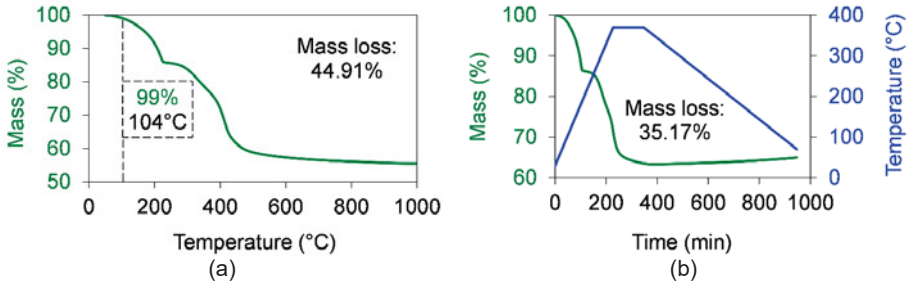

Figure 4.25. Thermal stability of MG70 in air atmosphere, measured by TGA, according to Protocol 1 (a) and Protocol 2 (b) (Chapter 3.2.14).

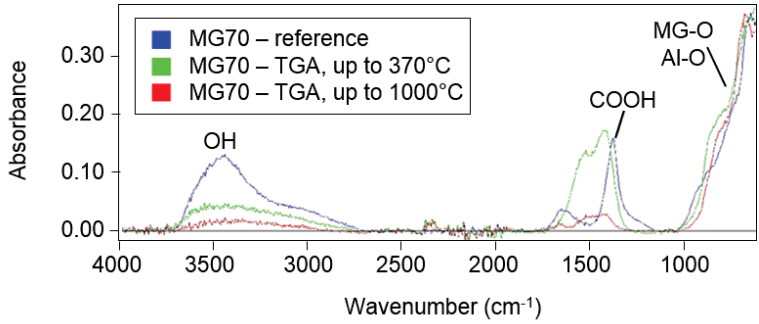

Figure 4.26. FTIR spectra of the reference MG70 – blue; MG70 measured by TGA up to 370°C (Protocol 2, Chapter 3.2.14) – green, and MG70 measured by TGA up to 1000°C (Protocol 1, Chapter 3.2.14) – red.

Table 4.4. Residual mass (m_r) of filled PTFE after sintering process (Protocol 2, Chapter 3.2.14) and after 1000°C test (Protocol 1, Chapter 3.2.14), measured by TGA.

Materials	m_r after sintering (%)	m_r at 1000°C (%)
PTFE	99.99	~0
Graphene	80.72	~0
Al_2O_3	98.30	97.31
BA80	95.35	83.35
MG70	64.83	55.09

4.3.5. Sensitivity analysis of filled PTFE – sintering protocol

The sensitivity analysis of the filled composites is focusing on the thermal stability of the fillers and on the effect of the dwelling time at maximal sintering temperature. The samples were pressed with 12.5 MPa pressure at room temperature.

4.3.5.1. PTFE with high filler contents

In this section, the decomposition and the thermal stability of filled PTFE were analysed during the sintering cycle by TGA (Figure 4.27, Protocol 2, Chapter 3.2.14), followed by FTIR spectroscopy (Figure 4.28-4.30). For a more accurate recording of mass loss and IR spectra, 30 wt% filled composites were analysed. Figure 4.27 introduces the thermal stability of unfilled/filled PTFE during the sintering cycle. The following mass loss values were registered at the end of the sintering process: 7.85% (PTFE/Graphene-30), 4.65% (PTFE/Al_2O_3-30), 2.09% (PTFE/BA80-30) and 10.46% (PTFE/MG70-30). Table 4.5 shows the observed temperature and the sintering time at 1%, 3% and 5% mass loss. PTFE had only a slight mass loss, which was around 0.01% (Figure 4.10 (a)). Regarding the filled PTFE samples, PTFE/Al_2O_3-30 was the most stable material at the heating cycle; it reached the 1% mass loss only at 370°C, after ~247 minutes. In the overall sintering process, PTFE/BA80-30 showed the highest thermal stability as it did not reach the 3% mass loss.

Table 4.5. Registered temperatures and sintering time at 1%, 3% and 5% mass loss in air atmosphere, measured by TGA (Protocol 2, Chapter 3.2.14).

Materials	Temperature at 1% mass loss (°C)	Temperature at 3% mass loss (°C)	Temperature at 5% mass loss (°C)
PTFE	---	---	---
PTFE/Graphene-30	306.9	370.0	370.0
PTFE/Al_2O_3-30	370.0	370.0	---
PTFE/BA80-30	335.0	---	---
PTFE/MG70-30	109.3	161.8	275.2
Materials	**Sintering time at 1% mass loss (min)**	**Sintering time at 3% mass loss (min)**	**Sintering time at 5% mass loss (min)**
PTFE	---	---	---
PTFE/Graphene-30	184.9	228.0	254.9
PTFE/Al_2O_3-30	246.7	322.3	---
PTFE/BA80-30	203.6	---	---
PTFE/MG70-30	53.2	88.2	163.8

PTFE/Al_2O_3-30 sample had 4.65% (Figure 4.27 (b)) mass loss and if it is supposed that all decomposition comes from the fillers, the mass loss in proportion to the Al_2O_3 content will be 15.50% (=100*4.65/30). This 15.50% is much higher than the total 2.69% mass loss of Al_2O_3 in case of 1000°C (Figure 4.21 (a)), in this way the mass loss of the composites during the sintering cycle comes from both of the fillers and the PTFE matrix material. Chapter 4.3.5.2 and 4.3.5.3 further discuss this phenomenon.

In case of PTFE/BA80-30 composite (Figure 4.27 (c)), even if the measured full mass loss comes from the BA80 filler decomposition, the calculated mass loss of BA80 filler is 6.97%, as the highest case. This 6.97% mass loss is around ~41.9% (=6.97/16.65) of the total measured mass loss (Figure 4.23 (a)). It means that around ~58.1% of the OH functional groups persist,

which is beneficial according to the introduced research hypothesis (Chapter 1.3). PTFE/BA80-30 material taken out from TGA was analysed by FTIR as well (Figure 4.29), to confirm the persisting functional groups. Both sintered and unsintered samples had significant peaks between 3000 and 3500 cm^{-1}, which come from the persisting OH bonds.

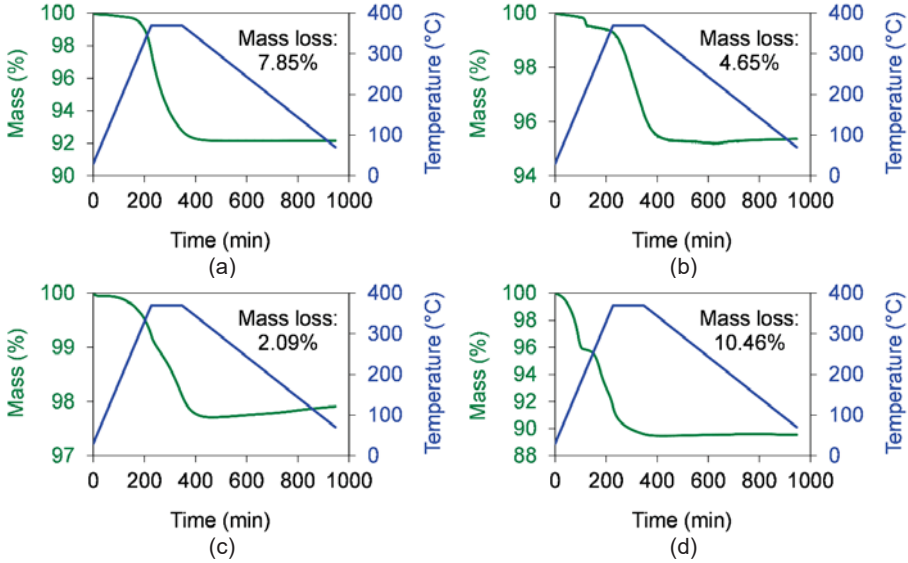

Figure 4.27. Mass loss of PTFE/Graphene-30 (a), PTFE/Al_2O_3-30 (b), PTFE/BA80-30 (c) and PTFE/MG70-30 (d) materials in air atmosphere, measured by TGA (Protocol 2, Chapter 3.2.14).

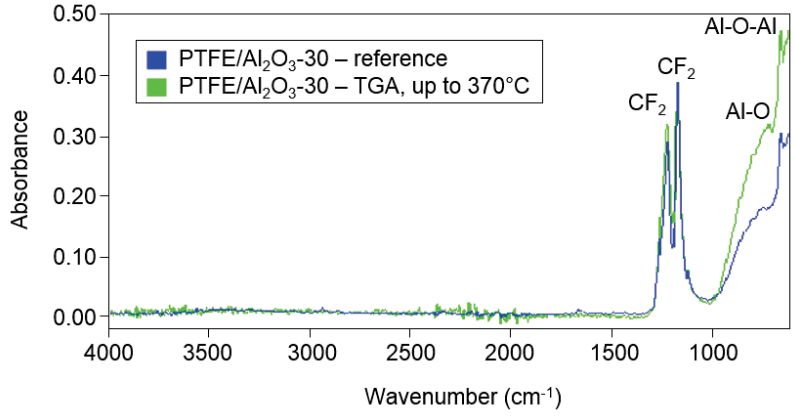

Figure 4.28. FTIR spectra of the reference PTFE/Al_2O_3-30 – blue and PTFE/Al_2O_3-30 measured by TGA up to 370°C (Protocol 2, Chapter 3.2.14) – green.

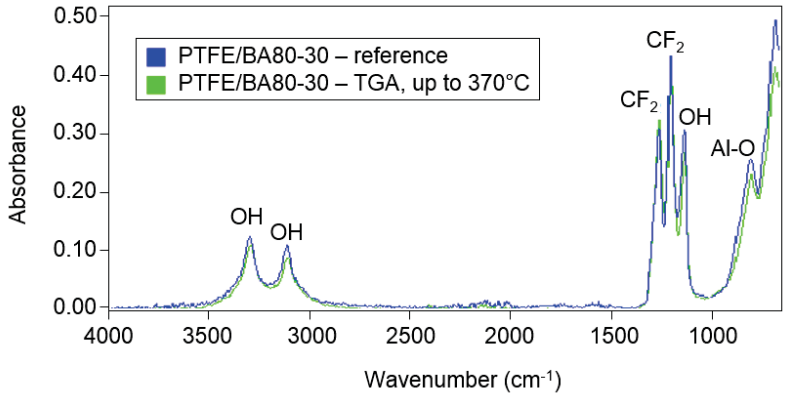

Figure 4.29. FTIR spectra of the reference PTFE/BA80-30 – blue and PTFE/BA80-30 measured by TGA up to 370°C (Protocol 2, Chapter 3.2.14) – green.

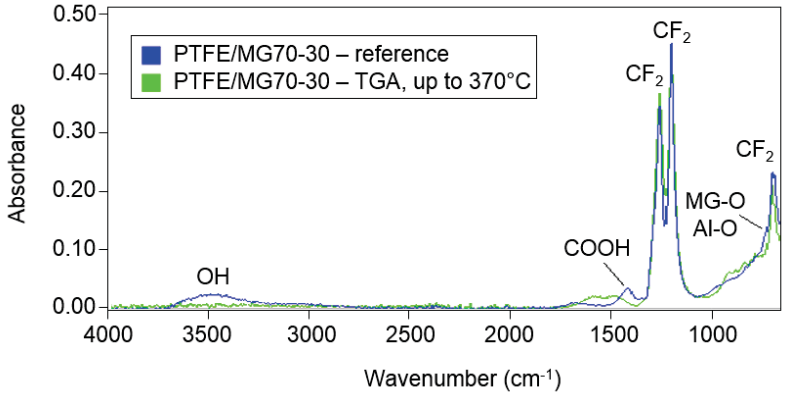

Figure 4.30. FTIR spectra of the reference PTFE/MG70-30 – blue and PTFE/MG70-30 measured by TGA up to 370°C (Protocol 2, Chapter 3.2.14) – green.

The FTIR spectra of PTFE/Al_2O_3-30 (Figure 4.28) and PTFE/BA80-30 (Figure 4.29) shows that all of the bonds (peaks) are still significant after the sintering process. The spectra of PTFE/MG70-30 (Figure 4.30) indicates a considerable decomposition of MG70 filler which confirms the conclusion of Chapter 4.3.4.4 that this material is not a promising filler for PTFE.

4.3.5.2. Unfilled/filled PTFE

Table 4.4 and 4.6 show the residual mass (m_r) in case of neat fillers, and unfilled/filled PTFE. All results introduced in Table 4.6 were measured by TGA, according to Protocol 2 (Chapter 3.2.14). The residual mass is evaluated at the beginning of the hold time, at the beginning of the cooling (after 2 hours heat dwelling) and after the final sintering process.

Table 4.6. Residual mass (m_r) during the sintering process, measured by TGA (Protocol 2, Chapter 3.2.14).

Materials	m_r at the beginning of hold time at 370°C (%)	m_r at the beginning of cooling at 370°C (%)	Final m_r after sintering (%)
Section 1: Neat PTFE and neat fillers – measured by TGA			
PTFE	100.00	99.97	99.99
Graphene	91.35	80.93	80.72
Al_2O_3	98.03	97.96	98.30
BA80	96.37	95.01	95.35
MG70	71.26	63.42	64.83
Section 2: Filled PTFE – measured by TGA			
PTFE/Graphene-30	97.40	92.63	92.15
PTFE/Graphene-16	98.65	95.92	95.60
PTFE/Graphene-8	99.04	97.63	97.62
PTFE/Graphene-4	99.59	98.86	98.86
PTFE/Al_2O_3-30	99.22	96.28	95.35
PTFE/Al_2O_3-16	99.83	98.64	98.20
PTFE/Al_2O_3-8	99.73	98.92	98.66
PTFE/Al_2O_3-4	99.64	99.25	99.17
PTFE/BA80-30	99.07	97.96	97.91
PTFE/BA80-16	99.39	98.85	98.66
PTFE/BA80-8	99.65	99.34	99.32
PTFE/BA80-4	99.75	99.48	99.45
PTFE/MG70-30	91.51	89.58	89.54
PTFE/MG70-16	95.19	93.93	94.11
PTFE/MG70-8	97.71	97.10	96.97
PTFE/MG70-4	98.58	98.23	98.32
Section 3: Calculated based on the filler contents and m_r in Section 1 – Theoretical values			
PTFE/Graphene-30	97.41	94.26	94.21
PTFE/Graphene-16	98.62	96.92	96.91
PTFE/Graphene-8	99.31	98.45	98.45
PTFE/Graphene-4	99.65	99.21	99.22
PTFE/Al_2O_3-30	99.41	99.37	99.48
PTFE/Al_2O_3-16	99.68	99.65	99.72
PTFE/Al_2O_3-8	99.84	99.81	99.85
PTFE/Al_2O_3-4	99.92	99.89	99.92
PTFE/BA80-30	98.91	98.48	98.60
PTFE/BA80-16	99.42	99.18	99.25
PTFE/BA80-8	99.71	99.57	99.62
PTFE/BA80-4	99.85	99.77	99.80
PTFE/MG70-30	91.38	89.01	89.44
PTFE/MG70-16	95.40	94.12	94.36
PTFE/MG70-8	97.70	97.05	97.18
PTFE/MG70-4	98.85	98.51	98.58
Section 4: Difference between theoretical and measured values (= Section 3 - Section 2)			
PTFE/Graphene-30	0.01	1.63	***2.06*** *
PTFE/Graphene-16	-0.03	1.00	***1.31*** *
PTFE/Graphene-8	0.27	0.82	0.83
PTFE/Graphene-4	0.06	0.35	0.36
PTFE/Al_2O_3-30	0.19	3.09	***4.13*** *
PTFE/Al_2O_3-16	-0.15	1.01	***1.52*** *
PTFE/Al_2O_3-8	0.11	0.89	***1.19*** *
PTFE/Al_2O_3-4	0.28	0.64	0.75
PTFE/BA80-30	-0.16	0.52	0.69
PTFE/BA80-16	0.03	0.33	0.59
PTFE/BA80-8	0.06	0.23	0.30
PTFE/BA80-4	0.10	0.29	0.35
PTFE/MG70-30	-0.13	-0.58	-0.10
PTFE/MG70-16	0.21	0.19	0.25
PTFE/MG70-8	-0.01	-0.05	0.21
PTFE/MG70-4	0.27	0.28	0.26

In Table 4.6, the theoretical sample mass were calculated from the measured residual mass of neat PTFE and neat fillers. The highlighted numbers in Table 4.6 (Section 4) reflect those final m_r values, where the difference between theoretical and measured values was higher than 1%. Composites with 1 wt% filler content were not investigated here because the mass losses of these composites were too low for a precise analysis.

As it can be seen, there is a gap between the calculated results of the theoretical and the measured residual mass of the developed composites. In case of graphene and Al_2O_3 filled samples, the measured residual mass was higher than it was expected from the mass loss of the PTFE and the given fillers. PTFE/Al_2O_3-30 sample had the most significant difference. These higher values indicate that there is an interaction between graphene or Al_2O_3 filler and PTFE, and consequently, a higher decomposition was observed compared to the neat materials.

4.3.5.3. Unfilled/filled PTFE – extended heat dwelling (10 and 48 hours)

This section introduces the decomposition analysis of PTFE composites, measured by TGA, simulating a sintering process with 10 hours dwelling time at the maximal 370°C temperature (Protocol 3, Chapter 3.2.14). The residual mass were registered in Table 4.7 at the start of the dwelling time (0 h) and after 2/4/6/8/10 h dwelling time. With this long interval, it is possible to get a more detailed insight into the thermal stability of the composites during the sintering process.

Table 4.7. Registered residual mass during dwelling time at 370°C in air atmosphere, measured by TGA (Protocol 3, Chapter 3.2.14).

Materials	Residual mass (m_r) at elapsed dwelling time (%)					
	0 h	2 h	4 h	6 h	8 h	10 h
PTFE	99.96	99.92	99.91	99.90	99.90	99.89
Graphene	90.80	80.37	79.57	79.33	79.19	79.09
Al_2O_3	97.92	97.81	97.79	97.79	97.79	97.79
BA80	96.65	95.32	94.83	94.46	94.14	93.84
MG70	69.18	64.17	63.44	62.99	62.80	62.61
PTFE/Graphene-30	97.17	92.33	90.97	90.27	89.70	89.19
PTFE/Al_2O_3-30	99.30	96.37	92.85	89.40	86.00	82.70
PTFE/BA80-30	98.83	97.38	95.93	94.74	93.68	92.73
PTFE/MG70-30	90.85	88.90	88.47	88.15	87.89	87.66
PTFE/Graphene-16	98.39	95.65	94.93	94.46	94.04	93.64
PTFE/Al_2O_3-16	99.65	97.84	96.04	94.38	92.84	91.38
PTFE/BA80-16	99.40	98.65	97.75	96.85	95.98	95.14
PTFE/MG70-16	95.27	94.16	93.91	93.72	93.56	93.43
PTFE/Graphene-8	99.19	97.79	97.25	97.10	96.90	96.71
PTFE/Al_2O_3-8	99.73	98.79	97.77	96.86	95.97	95.12
PTFE/BA80-8	99.71	99.26	98.69	98.10	97.49	96.89
PTFE/MG70-8	97.54	96.93	96.79	96.70	96.62	96.56
PTFE/Graphene-4	99.61	99.02	98.83	98.65	98.47	98.26
PTFE/Al_2O_3-4	99.87	99.44	99.02	98.58	98.16	97.73
PTFE/BA80-4	99.76	99.31	98.86	98.41	98.00	97.61
PTFE/MG70-4	98.73	98.41	98.33	98.27	98.21	98.16

As it can be seen in Table 4.7 and 4.8, the mass of graphene, Al_2O_3 and BA80 filled samples is significantly decreasing with the increasing dwelling time during the full 10 hours. In contrast with this, only slight mass losses were registered in case of unfilled PTFE and neat Al_2O_3, which are only 0.07% and 0.13% during the 10 hours dwelling time at 370°C temperature, respectively. PTFE/MG70 samples show moderate mass decrease in this 10 h interval, because most of the decomposition occurred at the heating period, before the dwelling time. The most significant influence of the dwelling time on the decomposition was registered in case of PTFE/Al_2O_3-30 sample where this value was 16.60%. The theoretical value based on the thermal degradation of neat materials and filler is only 0.09% (Table 4.8), which means that the rest of the material loss comes from an interaction between PTFE and Al_2O_3. These results clearly show that in case of the applied fillers, the longer the dwelling time, the higher the decomposed material mass, which can have a negative effect on the final material properties. The largest difference between the measured and theoretical values was registered for Al_2O_3 filled samples in case of 4/8/16/30 wt% filler content as well (Table 4.8, highlighted numbers).

Table 4.8. Registered mass loss during the dwelling time at 370°C in air atmosphere, measured by TGA (Protocol 3, Chapter 3.2.14). The theoretical values in Column 3 are calculated based on the basis of filler contents and mass loss of the neat PTFE and neat fillers. Column 4 introduces the difference between theoretical (Column 3) and measured values (Column 2).

Materials	Mass loss (0-10 h) Measured by TGA (%)	Mass loss (0-10 h) Theoretical (%)	Mass loss (0-10 h) Difference (%) = Measured – Theoretical
PTFE	0.07	---	---
Graphene	11.71	---	---
Al_2O_3	0.13	---	---
BA80	2.81	---	---
MG70	6.57	---	---
PTFE/Graphene-30	7.98	3.56	4.42
PTFE/Al_2O_3-30	16.60	0.09	***16.51 ****
PTFE/BA80-30	6.10	0.89	5.21
PTFE/MG70-30	3.19	2.02	1.17
PTFE/Graphene-16	4.75	1.93	2.82
PTFE/Al_2O_3-16	8.27	0.08	***8.19 ****
PTFE/BA80-16	4.26	0.51	3.75
PTFE/MG70-16	1.84	1.11	0.73
PTFE/Graphene-8	2.48	1.00	1.48
PTFE/Al_2O_3-8	4.61	0.07	***4.54 ****
PTFE/BA80-8	2.82	0.29	2.53
PTFE/MG70-8	0.98	0.59	0.39
PTFE/Graphene-4	1.35	0.54	0.81
PTFE/Al_2O_3-4	2.14	0.07	***2.07 ****
PTFE/BA80-4	2.15	0.18	1.97
PTFE/MG70-4	0.57	0.33	0.24

PTFE/Al_2O_3-30 material was analysed with a more extended heat dwelling (48 h) to get information about the mass loss in a broader range. It can be seen from Figure 4.31 that the measured mass loss was 70.95 wt%, which is the total mass of the PTFE. The FTIR spectrum (Figure 4.32) confirms that all of the PTFE was decomposed during this long sintering process as no PTFE related peaks were registered in case of the sintered sample (TGA). In this way, a potential explanation is that Al_2O_3 filler catalysed the decomposition of PTFE matrix during the sintering process.

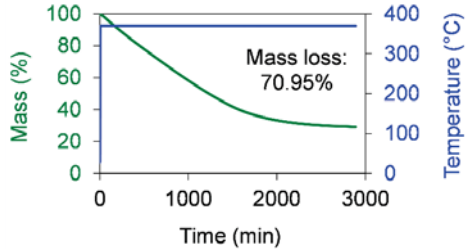

Figure 4.31. Mass loss PTFE/Al_2O_3-30 material in air atmosphere, 48 h dwelling time at 370°C maximal temperature, measured by TGA.

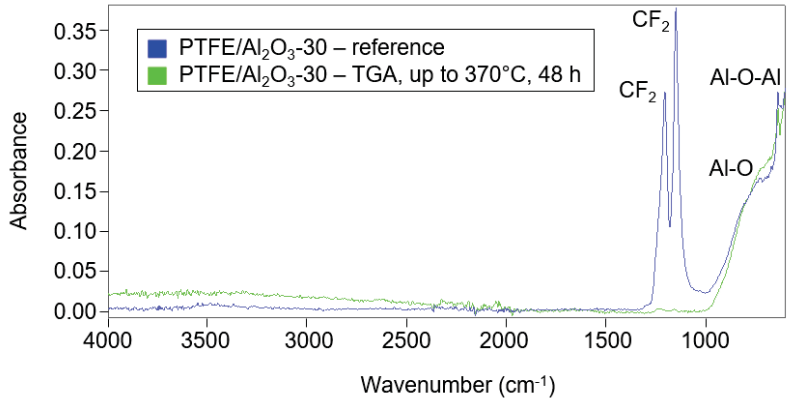

Figure 4.32. FTIR spectra of the reference PTFE/Al_2O_3-30 – blue and PTFE/Al_2O_3-30 measured by TGA up to 370°C with 48 h dwelling time – green.

4.3.6. Applicable materials and final production protocol

The chosen pressure for the room temperature pressing was 12.5 MPa, as this value is high enough to provide appropriate materials. The increase of the applied pressure influenced remarkably none of the density, compressive properties and hardness of PTFE. The sintering protocol includes 90 °C/h heating rate up to 370°C, two hours dwelling time at 370°C and 30 °C/h cooling rate. The purpose was to choose a relatively short dwelling time, as most of the developed filled PTFE composites had low thermal stability during the dwelling time. At

30 °C/h cooling rate, the degree of crystallinity reached 44.3%, which value is remarkably higher compared to the investigated faster cooling rates. Further decrease in the cooling rate did not influence the degree of crystallinity significantly. Regarding PTFE discs with 120 mm diameter, at this cooling rate, no warping was observed during the sintering cycle. The compressive strength and modulus decreased as a function of the dwelling time. The two hours dwelling time and the 30 °C/h cooling rate did not decrease the compressive strength and modulus of PTFE remarkably.

Based on the introduced sensitivity analysis, PTFE/Al_2O_3-8, PTFE/Al_2O_3-16, PTFE/MG70-8 and PTFE/MG70-16 materials are excluded from the further investigations, as they had low thermal stability during the sintering cycle. These samples were also produced as discs with 120 mm diameter, to get more information about the consequences of their low thermal stability during sintering. After the sintering process, due to the significant decomposition, the samples were deformed, crack formation and brown/black spots on their surfaces were observed (Figure 4.33 and 4.34). The rest of the materials were further characterised; the following chapters introduce their results. PTFE/MG70-1 and PTFE/MG70-4 composites also had remarkably low thermal stability, but they were further investigated to provide a full-scale analysis for materials with 1 and 4 wt% filler content.

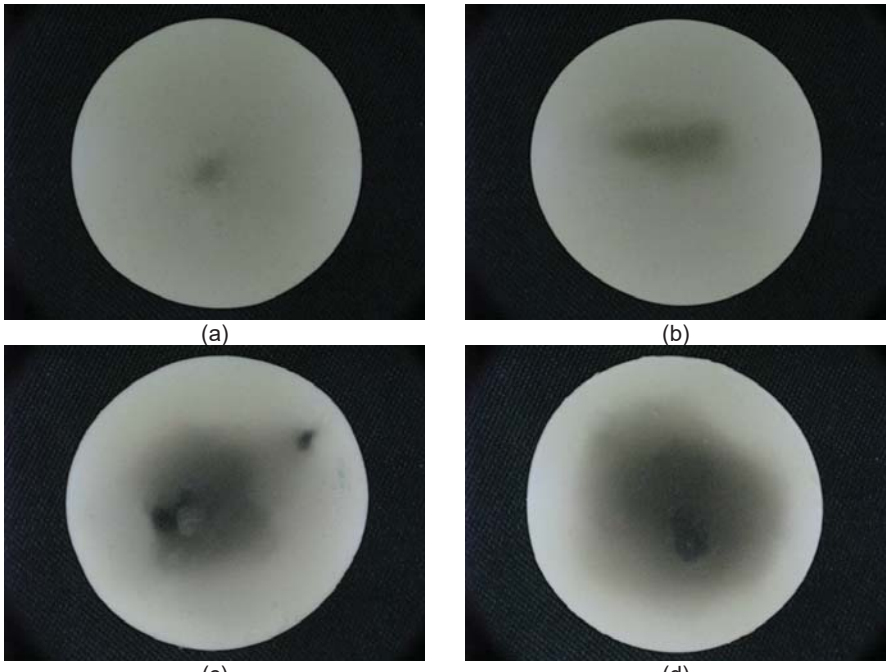

Figure 4.33. Brown/black spots on PTFE/Al_2O_3-8 (a), PTFE/Al_2O_3-16 (b), PTFE/MG70-8 (c) and PTFE/MG70-16 (d) materials (discs with diameter of 120 mm).

Figure 4.34. Crack formation (circled by blue) on PTFE/Al_2O_3-16.

4.4. Conclusions

In this chapter, a production protocol was developed for unfilled/filled PTFE, followed by a sensitivity analysis of the production. The variation of the applied pressure, dwelling time at maximal temperature and cooling rate had no significant influence on the investigated mechanical properties and density of the sintered neat PTFE. Only the compressive strength and modulus decreased as the dwelling time increased.

The final room temperature pressing – free sintering protocol is the following:

- 12.5 MPa pressure at room temperature,
- 90 °C/h heating rate up to 370°C,
- two hours dwelling time at 370°C,
- 30 °C/h cooling rate.

Decomposition of neat PTFE and neat filler during sintering process measured by TGA (370°C maximal sintering temperature) and followed by FTIR spectroscopy:

- As it was expected, neat PTFE and neat Al_2O_3 filler had high thermal stability during the sintering process, in case of neat PTFE no mass loss was measured.
- BA80-filler can be used in PTFE matrix; most of the hydroxyl (OH) functional groups survived the applied sintering process.
- The decomposition analysis indicates that MG70-filler cannot be used in PTFE matrix, as the thermal stability of MG70 is too low under the conditions of the sintering process.

Decomposition of filled PTFE materials during sintering process measured by TGA (370°C maximal sintering temperature) and followed by FTIR spectroscopy:

- Low thermal stability was observed in case of Al_2O_3 filled PTFE materials; the mass losses of these materials are remarkably higher than it was expected from the results of neat PTFE and Al_2O_3. It indicates that there is an interaction between the thermally

stable PTFE and Al_2O_3 at 370°C. The mass loss and in this way, the decomposition of these materials was increasing as the filler content increased.

- The sintering process with 10 hours dwelling time confirmed the low thermal stability of Al_2O_3 filled PTFE materials. During the 10 hours dwelling time at 370°C, a significant increase in mass loss was observed. It means that these materials are sensitive to the applied dwelling time at the maximal sintering temperature (370°C).
- PTFE/Al_2O_3-8, PTFE/Al_2O_3-16, PTFE/MG70-8 and PTFE/MG70-16 materials were excluded from the further investigations, as they had low thermal stability during the sintering cycle.

4.5. References

[1] E. Padenko, L.J. Van Rooyen, B. Wetzel, J. Karger-Kocsis: “Ultralow” sliding wear polytetrafluoro ethylene nanocomposites with functionalized graphene. Journal of Reinforced Plastics and Composites 35 (2016) 892–901.

[2] B.A. Krick, J.J. Ewin, G.S. Blackman, C.P. Junk, W.G. Sawyer: Environmental dependence of ultra-low wear behavior of polytetrafluoroethylene (PTFE) and alumina composites suggests tribochemical mechanisms. Tribology International 51 (2012) 42–46.

[3] J. Ye, H.S. Khare, D.L. Burris: Transfer film evolution and its role in promoting ultra-low wear of a PTFE nanocomposite. Wear 297 (2013) 1095–1102.

[4] L.J. van Rooyen, H. Bissett, M.C. Khoathane, J. Karger-Kocsis: Preparation of PTFE/graphene nanocomposites by compression moulding and free sintering: A guideline. Journal of Applied Polymer Science 43369 (2016) 1-9.

[5] K.A. Klinedinst, W.M. Vogel, P. Stonehart: Rheological characterization and thermal degradation of PTFE. Journal of Material Science 11 (1976) 794-800.

[6] S. Feng, Z. Zhong, Y. Wang, W. Xing, E. Drioli: Progress and perspectives in PTFE membrane: Preparation, modification, and applications. Journal of Membrane Science 549 (2018) 332–349.

[7] S. A. Khatipov, S. P. Kabanov, E. M. Konova, S. A. Ivanov, S. A. Serov: Effect of PTFE irradiation above the melting point on ITS porosity. Radiation Physics and Chemistry 81 (2012) 273–277.

[8] G. Calleja, A. Jourdan, B. Ameduri, J.-P. Habas: Where is the glass transition temperature of poly(tetrafluoroethylene)? A new approach by dynamic rheometry and mechanical tests. European Polymer Journal 49 (2013) 2214–2222.

[9] X. Q. Wang, D. R. Chen, J. C. Han, S. Y. Du: Crystallization behavior of polytetrafluoroethylene (PTFE). Journal of Applied Polymer Science 83 (2002) 990–996.

[10] S. Chen, Y. Xin, Y. Zhou, F. Zhang, Y. Ma, H. Zhou, L. Qi: Branched CNT @ SnO_2 nanorods @ carbon hierarchical heterostructures for lithium ion batteries with high reversibility and rate capability. J. Mater. Chem. A, 2014, 2, 15582–15589.

[11] C. Liu, K. Shih, Y. Gao, F. Li, L. Wei: Dechlorinating transformation of propachlor through nucleophilic substitution by dithionite on the surface of alumina. J Soils Sediments (2012) 12, 724–733.

CHAPTER 5

DEVELOPMENT AND MATERIAL CHARACTERISATION OF MONO-FILLED PTFE COMPOSITES

The purpose of this chapter is to introduce the material characterisation results, focusing on the thermal stability, physical, thermal, morphological and mechanical properties of the developed unfilled and filled PTFE.

The following article was published based on this chapter:
Levente Ferenc Tóth, Patrick De Baets, Gábor Szebényi: Thermal, Viscoelastic, Mechanical and Wear Behaviour of Nanoparticle Filled Polytetrafluoroethylene: A Comparison. Polymers, 2020, 12, 1940, 1-17.

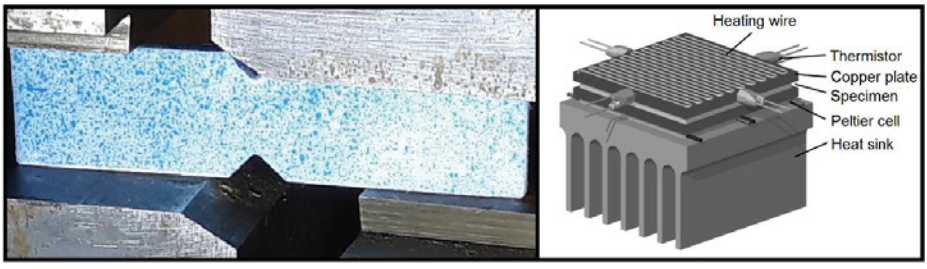

5.1. Introduction

Some material properties such as the density (porosity), thermal conductivity, crystallinity, viscoelastic behaviour, hardness, compressive/shear/tensile strength and modulus can influence the friction and wear behaviour of polymers. In this way, a well detailed tribological characterisation has to include the investigations of these material features for the fundamental understanding of friction and wear influencing factors.

5.2. Materials and methods

5.2.1. Materials and production method

Table 5.1 shows the developed and investigated samples related to this chapter. Chapter 3.1 introduces more details about the materials and production protocol.

Table 5.1. The developed unfilled and filled polytetrafluoroethylene (PTFE).

Materials	Matrix	Filler(s)	Filler content (wt%)
PTFE	PTFE	---	---
PTFE/Graphene-0.25	PTFE	Graphene	0.25
PTFE/Graphene-1	PTFE	Graphene	1
PTFE/Graphene-4	PTFE	Graphene	4
PTFE/Graphene-8	PTFE	Graphene	8
PTFE/Graphene-16	PTFE	Graphene	16
PTFE/Al_2O_3-1	PTFE	Alumina (Al_2O_3)	1
PTFE/Al_2O_3-4	PTFE	Alumina (Al_2O_3)	4
PTFE/BA80-1	PTFE	Boehmite alumina (BA80)	1
PTFE/BA80-4	PTFE	Boehmite alumina (BA80)	4
PTFE/BA80-8	PTFE	Boehmite alumina (BA80)	8
PTFE/BA80-16	PTFE	Boehmite alumina (BA80)	16
PTFE/MG70-1	PTFE	Hydrotalcite (MG70)	1
PTFE/MG70-4	PTFE	Hydrotalcite (MG70)	4

5.2.2. Material characterisation

This chapter introduces the results of the following tests: thermogravimetric analysis (TGA), scanning electron microscopy (SEM), Raman spectroscopy, energy-dispersive X-ray spectroscopy (EDS), density, thermal conductivity, differential scanning calorimetry (DSC), dynamic mechanical analysis (DMA), hardness and compressive/shear/tensile properties. This chapter also introduces a highlight about the wear properties to provide a comprehensive material characterisation for a thorough understanding of the correlation of material and wear properties. Further information about the material characterisation, applied methods and equipment can be found in Chapter 3.2 and 3.3.

5.3. Results and discussion

5.3.1. Thermal stability

The comparison of the developed unfilled/filled PTFE in air and nitrogen atmosphere is shown in Figure 5.1 and 5.2, respectively. All filled materials included fillers in a nominal content of 4 wt%. The residual mass percentages in air atmosphere correlate well with the TGA measurements of neat fillers (Figure 4.20 (a), 4.21 (a), 4.23 (a) and 4.25 (a)). In case of neat PTFE and PTFE/Graphene-4, the observed decomposition was 100%. In PTFE/Graphene-4, an approximately 3% mass loss is registered in the range of 600-800°C, which correlates well with the second step of graphene decomposition (Figure 4.20 (a)).

Table 5.2 and 5.3 show the registered temperature measured at 1%, 10% and 50% mass loss for all analysed materials in air and nitrogen atmosphere, respectively. All fillers decreased the temperature at 1% and 10% mass loss with respect to the reference neat PTFE, except PTFE/graphene-4, where the temperature at 10% mass loss was higher than in case of neat PTFE. These results indicate lower thermal stability both in air and nitrogen atmosphere.

Table 5.2. The registered temperatures in case of 1%, 10% and 50% mass loss in air atmosphere, measured by TGA (Protocol 1, Chapter 3.2.14).

Materials	Temperature at 1% mass loss (°C)	Temperature at 10% mass loss (°C)	Temperature at 50% mass loss (°C)
PTFE	489.9	521.2	556.4
PTFE/Graphene-4	488.4	524.3	551.7
PTFE/Al_2O_3-4	485.2	518.7	544.1
PTFE/BA80-4	483.9	518.1	540.9
PTFE/MG70-4	464.3	516.2	545.3

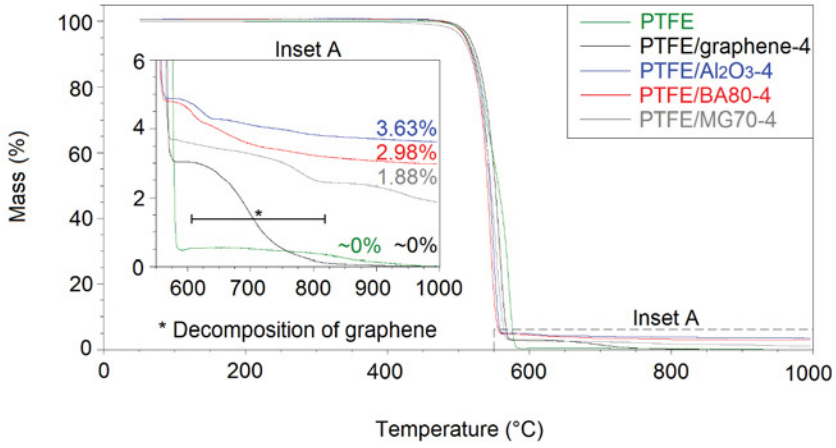

Figure 5.1. Decomposition analysis of filled/unfilled PTFE in air atmosphere, measured by TGA (Protocol 1, Chapter 3.2.14). PTFE/Graphene-4 had approximately 3% mass loss in the range of 600-800°C, which correlates well with the second step of graphene decomposition.

Table 5.3. The registered temperature in case of 1%, 10% and 50% mass loss in nitrogen atmosphere, measured by TGA (Protocol 1, Chapter 3.2.14).

Materials	Temperature at 1% mass loss (°C)	Temperature at 10% mass loss (°C)	Temperature at 50% mass loss (°C)
PTFE	492.8	528.2	556.7
PTFE/Graphene-4	488.4	524.4	555.5
PTFE/Al_2O_3-4	482.7	526.3	565.6
PTFE/BA80-4	479.5	513.0	546.6
PTFE/MG70-4	484.6	527.6	558.6

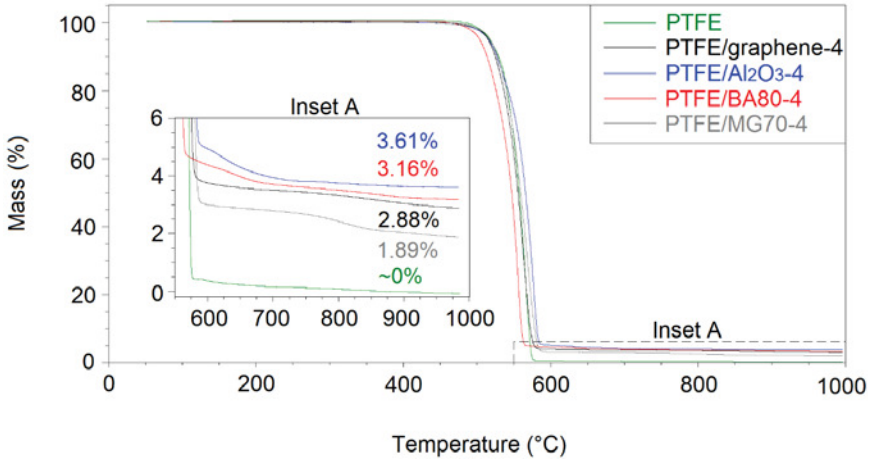

Figure 5.2. Decomposition analysis of filled/unfilled PTFE in nitrogen atmosphere, measured by TGA (Protocol 1, Chapter 3.2.14).

5.3.2. Micrographs of the fillers and developed composites

Figure 5.3 introduces the particles of PTFE powder and Al_2O_3/graphene/BA80 fillers. These SEM micrographs show the original materials, before any treatment. The accelerating voltage was 10 kV, micrographs were taken in high vacuum mode. As Figure 5.3 (a) introduces the particles of 3M PTFE were around ~25 µm, which is in agreement with the producer datasheet. The Al_2O_3 agglomerates are in the range of 1-20 µm (Figure 5.3 (c)), while the graphene/BA80 agglomerates are in the range of 1-50 µm (Figure 5.3 (b) and (d)).

Figure 5.4 introduces the freeze-fractured (cryo-fractured) surfaces of neat PTFE, PTFE/graphene-4, PTFE/Al_2O_3-4, PTFE/BA80-4 and PTFE/MG70-4 samples. The fracture surfaces indicate that all the fillers were homogeneously dispersed in the PTFE base material. A few humps and cavities in the range of few ten µm can be seen in PTFE/BA80-4 and PTFE/MG70-4 samples, which originates from some larger particles of the fillers. Chapter 5.3.3 introduces a more detailed dispersion analysis of these materials, carried out by Raman spectroscopy and EDS.

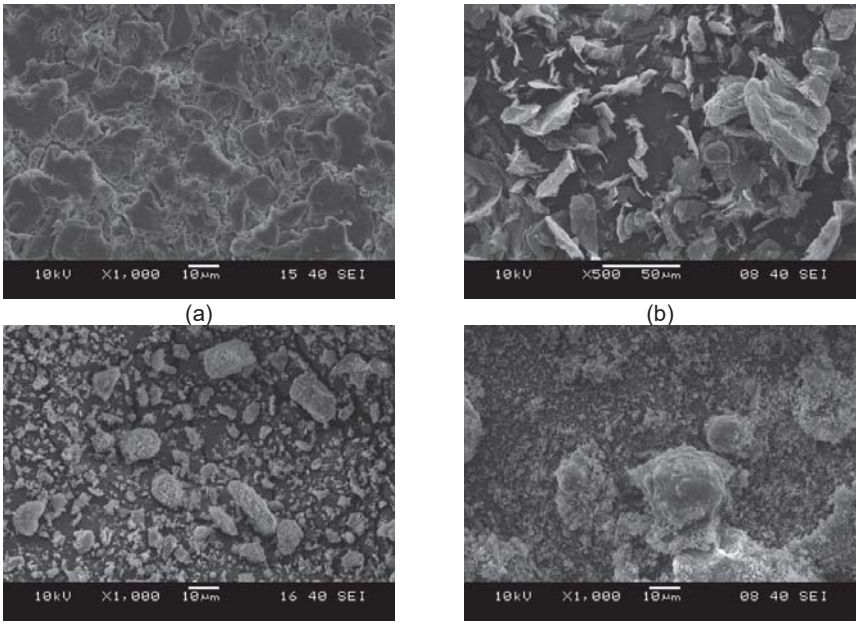

Figure 5.3. SEM micrographs from 3M-PTFE (a), graphene (b), Al_2O_3 (c) and BA80 (d) powders.

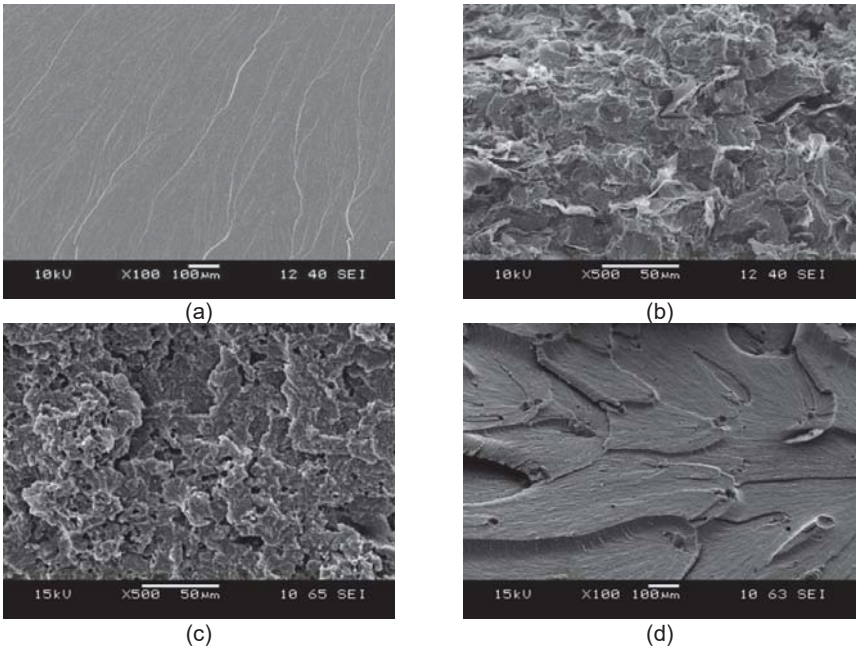

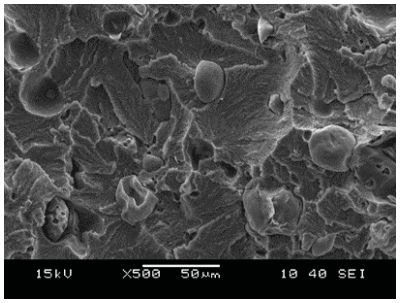

(e)

Figure 5.4. SEM micrographs of cryo-fractured neat PTFE (a), PTFE/Graphene-4 (b), PTFE/Al_2O_3-4 (c), PTFE/BA80-4 (d) and PTFE/MG70-4 (e) materials.

5.3.3. Dispersion analysis of the fillers

This section discusses the efficiency of the applied mechanical stirring in the aspect of the filler dispersion. The cryo-fractured surfaces of PTFE/graphene-4, PTFE/Al_2O_3-4, PTFE/BA80-4 and PTFE/MG70-4 samples were analysed by Raman spectroscopy or EDS.

5.3.3.1. Dispersion of graphene

Figure 5.5 introduces the Raman mapping of PTFE/Graphene-4 freeze-fractured surface. The white colour indicates the graphene-rich areas, while the black shows the PTFE-rich areas. The size of the mapped surface is 1.0x1.1 mm.

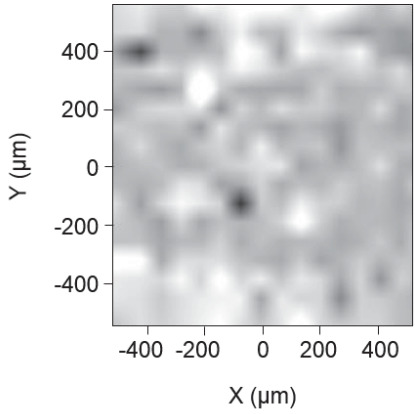

Figure 5.5. Raman-microscopy mapping of PTFE/Graphene-4.

Figure 5.6 (a) displays the Raman spectra of PTFE/Graphene-4. The size of the analysed area in one measurement point is 50x50 µm. The graphene dispersion was checked in 8 locations of the cross-section at different depths from the pressed surface (Figure 5.6 (b)). In all

measured areas of the cryo-fractured surface, there is a significant peak close to 1600 cm^{-1}, which comes from the graphene content of the area. These spectra indicate that there was no significant graphene migration or diffusion from the core to the edge (pressed surface of the sample) neither at the room temperature pressing nor at sintering temperature.

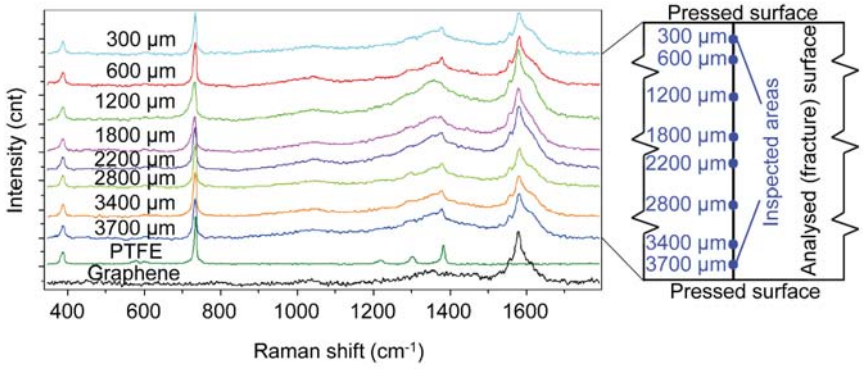

(a) (b)

Figure 5.6. Raman spectra of PTFE/Graphene-4 sample in different depth on the cryo-fractured surface (a), the investigated locations in PTFE/Graphene-4 (b). The reference spectra of the neat graphene and PTFE are introduced at the bottom of the diagram.

5.3.3.2. Dispersion of alumina (Al_2O_3)

The dispersion of Al_2O_3-filler in PTFE/Al_2O_3-4 was analysed by EDS mapping in four locations of the cross-section at different depths from the pressed surface. Figure 5.7 (a) shows the original cryo-fractured surface, while Figure 5.7 (b) and (c) introduce the aluminium and fluorine content, respectively. The fluorine atoms come from the PTFE backbone. Figure 5.7 (b) and (c) have black spots in the same positions, with similar shape and size. From these areas, an insufficient number of reflected X-ray photons reached the detector caused by surface topology (Figure 5.7 (a)). The dispersion of aluminium, representing the Al_2O_3 particles, realized by the rotating blade grinder, is shown in Figure 5.7 (b).

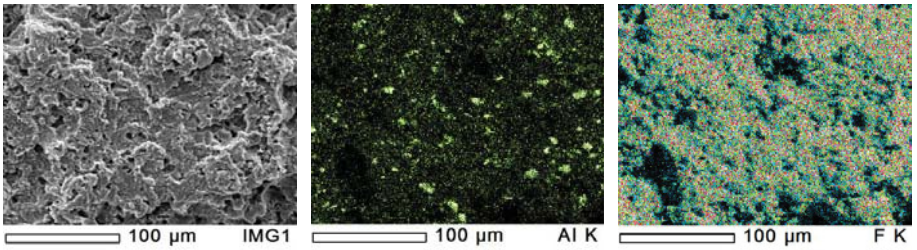

(a) (b) (c)

Figure 5.7. EDS analysis of PTFE/Al_2O_3-4 sample with 500x magnification; original cryo-fractured surface (a), aluminium content (b) and fluorine content (c).

Further EDS analyses were performed at three other locations of the cryo-fractured surface. All inspections showed similar results and similar dispersion. Besides the larger particles in the range of 10 µm, finer homogeneously dispersed Al_2O_3-powder can be also seen. The size of these finer filler particles was below 1 µm. The EDS spectrum also showed a significant aluminium peak (Al-K, where K represents the K electron shell). The total detected percentage of aluminium was 3.77%, 3.89%, 4.32% and 3.39% at the four locations, which means that the dispersion effect of the dry mechanical stirring was successful at macro- and micro-level.

5.3.3.3. Dispersion of boehmite alumina (BA80, AlO(OH))

Figure 5.8 depicts the dispersion of BA80-filler in PTFE/BA80-4 sample. Figure 5.8 (a-c) displays the cryo-fractured surface and the aluminium and fluorine content, respectively. The average size of the filler agglomerates was below 1 µm. On the other hand, Figure 5.4 (d) shows that some larger agglomerates (in the range of 10 µm) still exist besides the nanoparticles. The presence of an aluminium peak (Al-K, where K represents the K electron shell) was significant in the EDS spectra. The total percentage of aluminium was 2.73%, 2.17%, 2.53% and 2.09% at the four locations, which indicate efficient dispersion of the fine filler powder.

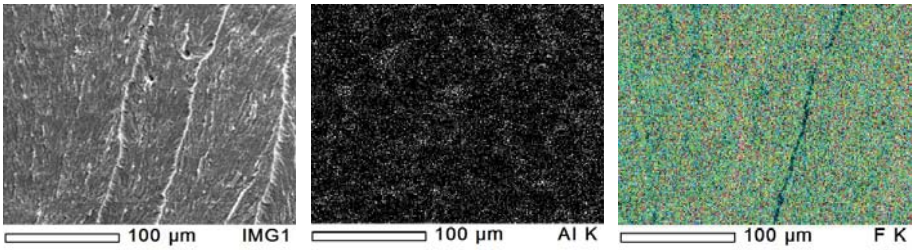

(a) (b) (c)

Figure 5.8. EDS analysis of PTFE/BA80-4 sample with 500x magnification; original cryo-fractured surface (a), aluminium content (b) and fluorine content (c).

5.3.3.4. Dispersion of hydrotalcite (MG70)

Figure 5.9 presents the dispersion of MG70-filler in PTFE/MG70-4. Figure 5.9 (a-c) shows the cryo-fractured surface and the magnesium and fluorine content, respectively. The dispersion of magnesium provided by the rotating blade grinder can be seen in Figure 5.9 (b). Similarly to Figure 5.7, Figure 5.9 (b) and (c) have black spots from, where an insufficient number of reflected X-ray photons reached the detector. From the given cryo-fractured surface, four EDS tests were performed, all of them with similar results. The magnesium peak (MG-K, where K represents the K electron shell) was significant in the EDS spectra. The total percentage of magnesium was 2.65%, 3.02%, 2.68% and 3.10%. All EDS mappings indicate that the

dispersion of MG70-filler was efficient. Figure 5.4 (e) displays that PTFE/MG70-4 also includes some larger agglomerates besides the nanoparticles.

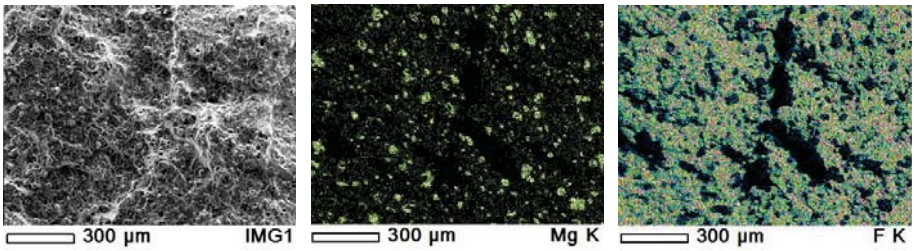

(a) (b) (c)

Figure 5.9. EDS analysis of PTFE/MG70-4 sample with 100x magnification; original cryo-fractured surface (a), magnesium content (b) and fluorine content (c).

5.3.4. Density

Figure 5.10 and Table B.10 introduce the density of neat PTFE, PTFE/graphene, PTFE/Al_2O_3, PTFE/BA80 and PTFE/MG70. The reference (neat) PTFE had 2.168 g/cm^3 density, which is in agreement with the literature [1, 2]. In case of graphene filled samples, the density decreased as the filler content increases due to the low density of graphene filler. The density of PTFE/Graphene-16 sample was only 1.946 g/cm^3, which is ~10% lower compared to neat PTFE. Both Al_2O_3 and BA80 increased the density compared to neat PTFE, due to the higher density of alumina and boehmite alumina. These increases were observed as slight changes in density. The lower density of PTFE/MG70 samples is supposed to come from the decomposition of the functional groups of MG70 filler in the sintering process. During decomposition of MG70-filler, some of the produced gas cannot escape from the PTFE increasing the final material porosity and thus lowering its density.

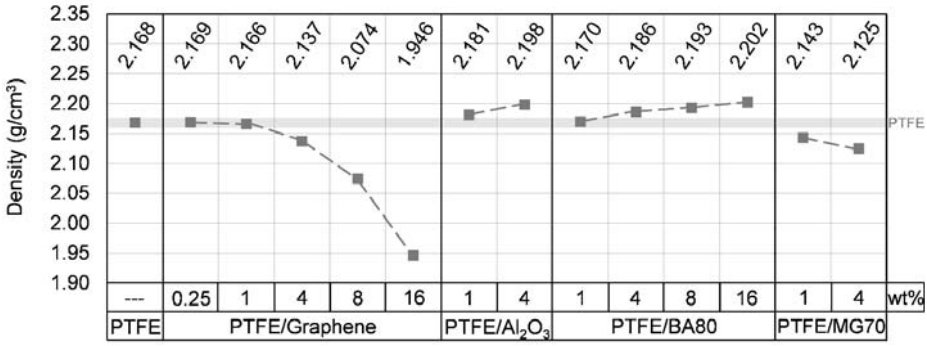

Figure 5.10. The density of unfilled/filled PTFE samples. The grey transparent line displays the measured density of the reference (neat) PTFE.

5.3.5. Thermal conductivity

Figure 5.11 and Table B.10 display the thermal conductivity of unfilled and filled PTFE materials. Neat PTFE had a thermal conductivity of 0.243 (W/mK), which is in agreement with the literature [2, 3]. Graphene in 4/8/16 wt% filler content increased the thermal conductivity with ~29/~84/~157 %, respectively. The excellent thermal properties of graphene caused this phenomenon. This higher thermal conductivity can be beneficial, e.g. in wear process as more frictional heat can be transferred from the contact surface. As a result, the surface temperature of the polymer is decreasing, which results in a smaller reduction in the mechanical properties of the polymer. Al_2O_3, BA80 and MG70 fillers only slightly increased the thermal conductivity.

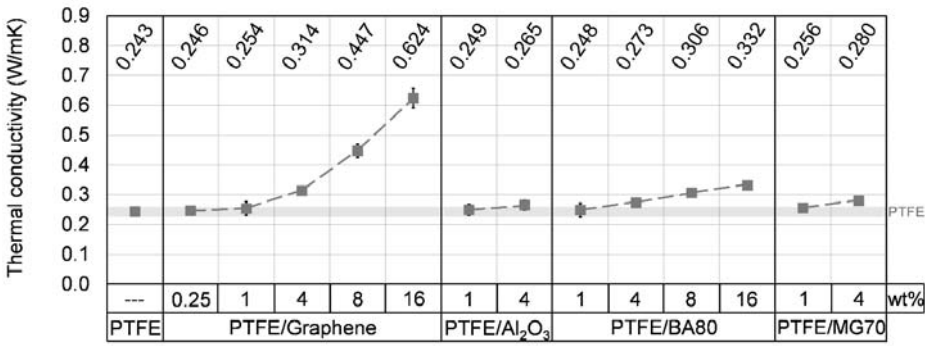

Figure 5.11. The thermal conductivity of unfilled/filled PTFE samples. The grey transparent line displays the measured thermal conductivity of the reference (neat) PTFE.

5.3.6. Melting temperature and degree of crystallinity

The degree of crystallinity is an essential feature of semi-crystalline polymers. It has a significant influence on the mechanical properties of the material. Therefore DSC measurements were carried out in heat/cool/heat cycle from room temperature (23°C) to 370°C to simulate the sintering process according to Protocol 3 (Chapter 3.2.4). The applied cooling rate was 30 °C/h. The DSC provided a more precise control for the sintering process, compared to the used conventional oven, but here a nitrogen atmosphere was applied. Table 5.4 introduces the second heating cycle of these simulated sintering processes focusing on the reference (neat) PTFE and PTFE materials with 4 wt% filler content. At the second heating cycle, the unfilled and filled PTFE was already sintered due to the first heating cycle. No remarkable change in the degree of crystallinity was registered. The fillers only slightly increased the degree of crystallinity. The evaluated degree of crystallinity of neat PTFE was 40.5%, which is similar to the previously introduced value (Chapter 4.3.3.5, Table 4.3). Table 4.3 displayed that the degree of crystallinity was 44.3% for that neat PTFE, which was measured with the same protocol.

Table 5.4. Simulation of the sintering process by DSC analysis (Protocol 3, Chapter 3.2.4).

Samples	Second heating			
	Initial temperature of melting (°C)	Melting peak temperature (°C)	Enthalpy of fusion (J/g)	Degree of crystallinity (%)
PTFE	319.8	324.9	27.96	40.5
PTFE/graphene-4	319.4	324.8	28.54	43.1
PTFE/Al_2O_3-4	319.3	324.9	30.93	46.7
PTFE/BA80-4	319.0	324.7	29.17	44.0
PTFE/MG70-4	319.9	324.9	28.71	43.3

As a second step, DSC analyses were carried out with samples sintered in a conventional oven in air atmosphere. The applied module was heat/cool/heat cycle from 0 to 370°C, according to Protocol 1 (Chapter 3.2.4). The initial and peak temperature of melting/crystallisation, the enthalpy of fusion/crystallisation (integrated peak area) and the degree of crystallinity of the developed materials are shown in Table 5.5. In the first heating cycle, the thermal and mechanical history of the samples originates from the room temperature pressing – free sintering production method. After having reached the melting range in the first heating cycle of the DSC and cooling down the samples with the same cooling rate, in the second heating cycle all samples had exactly the same thermal history which was provided by the DSC process. As the heating and cooling cycles of the sintering process were different compared to the DSC-cycle, the melting temperature and degree of crystallinity also differed in the first and second heating cycle. In the second heating cycle, all the measured degrees of crystallinity were lower than in the first heating cycle. This phenomenon comes from the different cooling cycles. In case of the sintering process, the cooling rate was 0.5 °C/min, which is only 10% of the cooling rate of the DSC analysis. In this way, more time was provided for the crystallisation of PTFE during the real sintering cycle than during the DSC analysis.

There is no significant difference in the melting peak temperature of the tested polymers in the first heating cycle (Table 5.5). In the first heating, the melting peak temperature was between 325-327°C, while in the second heating cycle it was between 323-325°C, in case of all materials. At 19-21°C, an endothermal peak was detected at both melting cycles (Figure 5.12). The crystallisation peak temperature of the samples was between ~308 and 310°C. The initial temperature of crystallisation was higher in case of all filled PTFE samples than the unfilled reference PTFE. It indicates a small nucleation effect of the incorporated fillers. The melting behaviour, the melting peak temperature and the crystallisation peak temperature were not significantly influenced by the fillers.

In the first heating cycle, PTFE/Al_2O_3-4 sample had the highest enthalpy of fusion with 37.20 J/g, which correlates to 56.2% degree of crystallinity (Table 5.5). It was confirmed in the second heating cycle as well, where the enthalpy of fusion was 32.12 J/g, while the degree of

crystallinity was 48.5%. In the first heating cycle, the neat PTFE sample had the second highest degree of crystallinity with 53.4%, while in the second heating cycle, this value was 43.4%. PTFE/MG70-1 sample had the lowest degree of crystallinity in both heating cycles. Graphene and BA80 fillers decreased the degree of crystallinity compared to neat PTFE. Only PTFE/graphene-4 sample had a moderately higher degree of crystallinity in the second heating cycle. The enthalpy of fusion for 100% crystalline PTFE is 69 J/g [4].

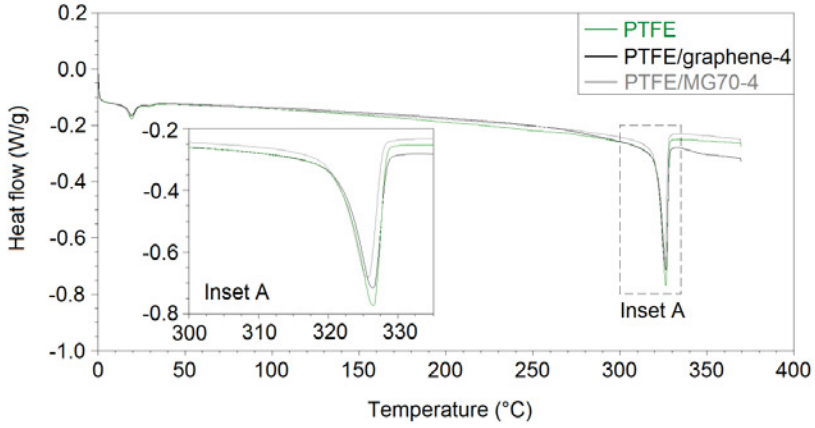

(a)

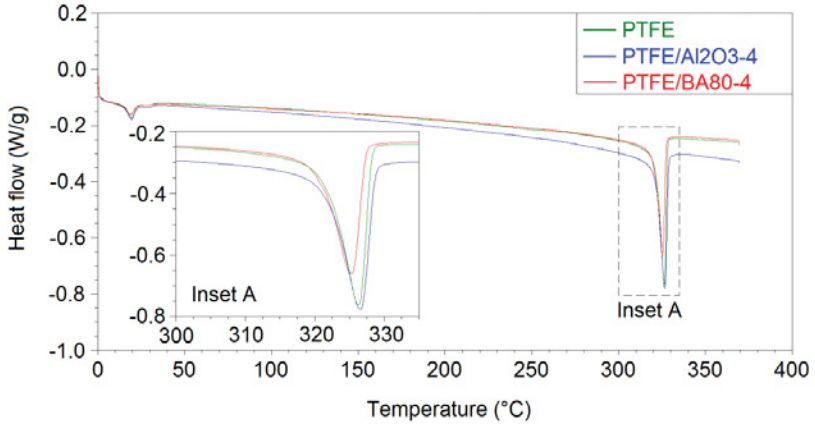

(b)

Figure 5.12. DSC analysis of unfilled/filled PTFE, applying Protocol 1 (Chapter 3.2.4).

In Table 5.4, the second heating can be considered as the first heating in Table 5.5, as both of these cycles were preceded by a sintering protocol. Those materials, which were analysed by Protocol 1 (Table 5.5) had a higher degree of crystallinity than the ones by Protocol 3 (Table 5.4). The reason of this phenomenon can be that in Protocol 3 the sintering process

was carried out with a more precise DSC, in nitrogen atmosphere, while in Protocol 1 the sintering was done in a conventional oven, in air atmosphere.

Table 5.5. DSC analysis of sintered filled/unfilled PTFE samples, applying Protocol 1 (Chapter 3.2.4).

	First heating			
	Initial temperature of melting (°C)	Melting peak temperature (°C)	Enthalpy of fusion (J/g)	Degree of crystallinity (%)
PTFE	321.4	326.3	36.82	53.4
PTFE/graphene-0.25	320.8	326.1	32.52	47.2
PTFE/graphene-1	320.5	325.5	34.95	51.2
PTFE/graphene-4	321.5	326.2	33.09	50.0
PTFE/graphene-8	321.1	326.1	28.48	44.9
PTFE/graphene-16	320.6	326.1	29.15	50.3
PTFE/Al_2O_3-1	320.5	325.7	35.45	51.9
PTFE/Al_2O_3-4	321.4	326.6	37.20	56.2
PTFE/BA80-1	320.4	325.6	31.95	46.8
PTFE/BA80-4	320.3	325.3	31.15	47.0
PTFE/BA80-8	321.3	326.2	32.20	50.7
PTFE/BA80-16	320.9	326.4	27.79	47.9
PTFE/MG70-1	320.3	325.1	27.43	40.2
PTFE/MG70-4	320.6	325.5	32.81	49.5
	Second heating			
PTFE	319.5	324.0	29.93	43.4
PTFE/graphene-0.25	319.1	324.0	27.70	40.2
PTFE/graphene-1	318.7	323.7	29.99	43.9
PTFE/graphene-4	319.4	324.2	27.59	41.7
PTFE/graphene-8	319.0	324.2	26.08	41.1
PTFE/graphene-16	318.7	324.3	24.93	43.0
PTFE/Al_2O_3-1	318.8	323.8	28.25	41.4
PTFE/Al_2O_3-4	320.1	324.8	32.15	48.5
PTFE/BA80-1	318.6	323.8	27.18	39.8
PTFE/BA80-4	318.5	323.6	26.95	40.7
PTFE/BA80-8	319.3	324.3	27.27	43.0
PTFE/BA80-16	318.8	324.3	23.36	40.3
PTFE/MG70-1	318.4	323.3	24.36	35.7
PTFE/MG70-4	318.7	323.7	28.54	43.1
	First cooling			
	Initial temperature of crystallisation (°C)	Crystallisation peak temperature (°C)	Enthalpy of crystallisation (J/g)	Degree of crystallinity (%)
PTFE	310.6	308.8	31.25	45.3
PTFE/graphene-0.25	314.7	308.0	29.56	42.9
PTFE/graphene-1	314.6	308.8	30.12	44.1
PTFE/graphene-4	314.4	309.6	26.95	40.7
PTFE/graphene-8	314.6	308.7	26.08	41.1
PTFE/graphene-16	314.9	309.2	25.32	43.7
PTFE/Al_2O_3-1	314.5	308.2	28.28	41.4
PTFE/Al_2O_3-4	314.6	308.4	29.71	44.9
PTFE/BA80-1	312.0	307.8	26.36	38.6
PTFE/BA80-4	312.8	308.3	28.06	42.4
PTFE/BA80-8	313.4	309.6	29.10	45.8
PTFE/BA80-16	313.6	309.4	24.79	42.8
PTFE/MG70-1	314.8	308.8	24.44	35.8
PTFE/MG70-4	314.5	308.4	29.18	44.1

5.3.7. Viscoelastic properties

DMA analysis was performed for neat PTFE and for all filled PTFE samples with 4 wt% filler content. The storage modulus and tangent delta (loss factor) as a function of temperature can be seen in Figure 5.13. The storage moduli of the materials at -50°C, 20°C and 150°C temperature are presented in Table 5.6.

All filled PTFE samples had markedly higher storage moduli concerning the reference unfilled PTFE. Graphene, Al_2O_3, BA80 and MG70 improved the storage modulus at 20°C by ~138%, ~33%, ~54% and ~67%, respectively (Table 5.6). The reason for this improvement can be the restriction of the molecular chain motion due to the filler particles. Three main steps in the storage modulus curve and three main peaks on the loss factor (tangent delta) curve can be observed in Figure 5.13. The three significant peaks of the tangent delta can be found at -95-85°C, 18-20°C and 117-121°C temperature, depending on the given material (Figure 5.13 and Table 5.6). It is in agreement with the literature [5]. The temperature peaks correspond to the phase transitions of PTFE: the first peak is the γ-transition, the second one is the β-transition, while the third one is the α-transition [5-7]. At γ-transition, localized bond movements such as bending and stretching can occur. At β-transition where the crystal structure changes from triclinic to hexagonal, the side groups begin to move. It can be related to the toughness of the polymer. At α-transition, large scale chain movements occur in the amorphous part. In other words, the α-transition is the glass transition of the amorphous parts [5-7]. A significant difference in the α/β-transition peak temperature as a function of the filler was not found. The peak temperature of β-transition is in agreement with the measured endotherm peak of DSC (Figure 5.12).

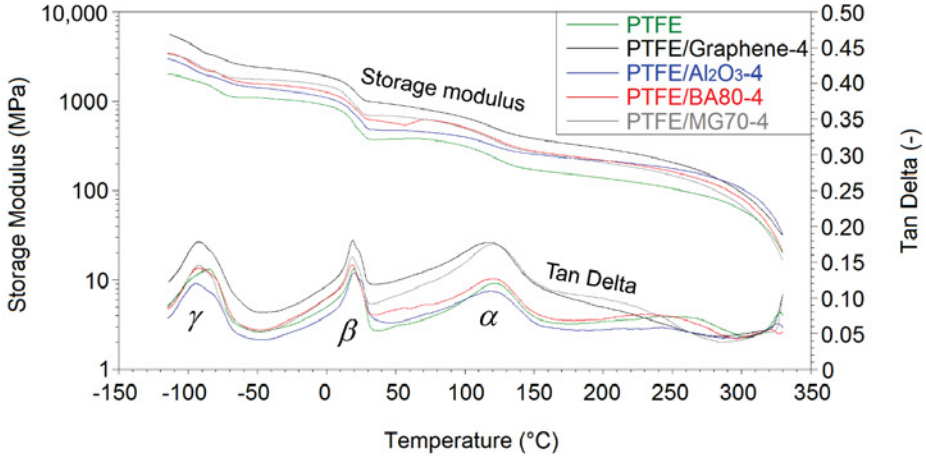

Figure 5.13. DMA characterisation of sintered filled/unfilled PTFE specimens in 3-point bending setup, 3 °C/min heating rate and 1 Hz frequency.

Table 5.6. DMA analysis of sintered filled/unfilled PTFE specimens in 3-point bending setup, 3 °C/min heating rate and 1 Hz frequency.

	Storage modulus, MPa (-50°C)	Storage modulus, MPa (20°C)	Storage modulus, MPa (150°C)
PTFE	1102	545	170
PTFE/graphene-4	2412	1297	381
PTFE/Al_2O_3-4	1413	723	254
PTFE/BA80-4	1567	842	277
PTFE/MG70-4	1773	908	266
	Peak temperature (γ) (°C)	Peak temperature (β) (°C)	Peak temperature (α) (°C)
PTFE	-85.4	19.7	121.3
PTFE/graphene-4	-92.9	18.9	117.0
PTFE/Al_2O_3-4	-94.9	20.1	117.9
PTFE/BA80-4	-92.5	18.5	120.7
PTFE/MG70-4	-92.3	18.6	119.9

5.3.8. Hardness

Figure 5.14 and Table B.11 introduce the hardness values of the sintered materials. The reference unfilled PTFE had 54.3 (Shore-D) hardness, which is in agreement with the literature [1-3]. The developed graphene filled materials had slightly higher hardness compared to neat PTFE, except for 16 wt% filler content where the hardness was slightly lower; this can originate from the high volume fraction of graphene filler, which comes from the low density of graphene. Al_2O_3 and BA80 filled materials reached a higher hardness, and this value was increased as the filler content increases. The highest hardness was measured in PTFE/BA80-16, PTFE/BA80-8 and PTFE/Al_2O_3-4 samples, as 60.0, 59.1 and 58.8 (Shore-D), respectively. PTFE/MG70-1 and PTFE/MG70-4 samples had the same values as the reference unfilled PTFE.

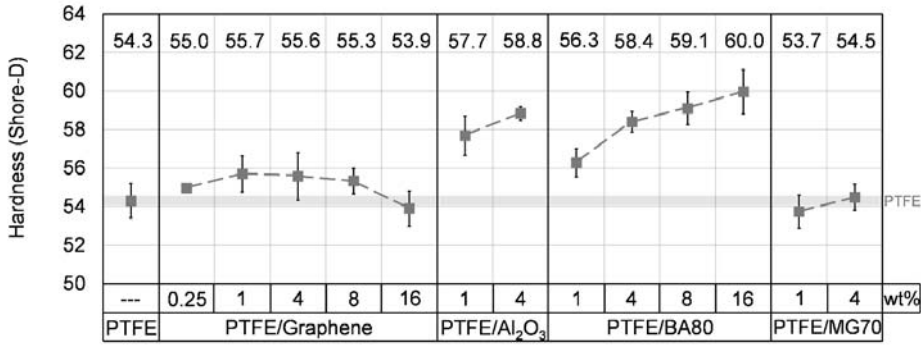

Figure 5.14. The hardness of unfilled/filled PTFE samples. The grey transparent line displays the measured hardness of the reference (neat) PTFE.

5.3.9. Compressive properties

The compressive properties of the sintered samples are introduced in Figure 5.15, Figure 5.16, Table 5.7 and Table B.11. The measured compressive stress of the reference PTFE at 5% and 10% deformation is 13.92 and 18.91 MPa respectively, while its compressive modulus is 405.9 MPa, which is in agreement with the literature [1, 3]. PTFE/Al_2O_3-1 and PTFE/Al_2O_3-4 samples did not reach significantly higher compressive stress compared to neat PTFE, while their compressive modulus increased remarkably. MG70 filler decreased both the compressive stress and modulus. Graphene with low filler content (0.25, 1 and 4 wt%) did not change the compressive properties remarkably, while BA80 in 1 and 4 wt% increased the compressive modulus significantly compared to neat PTFE. At higher filler content, BA80 is observed superior compared to graphene filler. Samples with 8 and 16 wt% BA80 reached the same level of compressive modulus as neat PTFE, while the application of graphene in higher percentages decreased both compressive stress and compressive modulus significantly. This is attributed to the low density of graphene, which resulted in a high volume fraction of graphene in the developed PTFE/Graphene-8 and PTFE/Graphene-16 samples. PTFE/Al_2O_3-1, PTFE/BA80-4 and PTFE/Al_2O_3-4 samples reached the most remarkable improvement in compressive modulus, which was ~34.2%, 33.1% and 32.6% higher compared to neat PTFE, respectively.

As it is introduced in Chapter 5.3.7, regarding the β-transition of PTFE, the peak temperature can be found around 19-20°C. Between 0°C and 50°C a slope in the storage modulus graph is registered, which caused a significant decrease in these modulus values. As the peak temperature of β-transition is relatively close to room temperature (23°C) where all of the static mechanical tests were done, further compressive tests were carried out at 50°C with 4 wt% filler content samples (Table 5.7). As it is expected from DMA, the compressive stress and modulus values were lower at 50°C. An important conclusion is that the tendencies of the measured compressive properties are similar in case of both room temperature and 50°C, which is in agreement with the DMA results (Figure 5.13).

Table 5.7. Compressive stress at 5% and 10% deformation and compressive modulus of the sintered unfilled and 4 wt% filled PTFE at 50°C.

Samples	Compressive stress at 5% deformation (MPa, 50°C)	Compressive stress at 10% deformation (MPa, 50°C)	Compressive modulus (MPa, 50°C)
PTFE	11.13 ± 0.27	16.00 ± 1.34	318.4 ± 12.7
PTFE/graphene-4	11.00 ± 0.27	16.39 ± 0.17	351.0 ± 7.7
PTFE/Al_2O_3-4	12.47 ± 0.12	17.06 ± 0.19	422.5 ± 17.3
PTFE/BA80-4	12.02 ± 0.55	16.53 ± 0.19	422.0 ± 13.0
PTFE/MG70-4	11.21 ± 0.62	15.99 ± 0.09	325.9 ± 10.0

5.3.10. Shear properties

The shear properties of the unfilled and filled PTFE samples are introduced in Figure 5.15-5.17 and in Table B.12. All of the filler increased the shear stress at 2% and 5% strain and the shear modulus as the filler content increases. In agreement with the observed changes in the stress and modulus values, the elongation of the samples decreased as the filler content increases. The reason for this phenomenon can be that due to the fillers, the movement of the PTFE molecular chains is restricted, which results in an increased modulus and decreased elongation. The higher shear modulus confirms the changes in storage modulus measured by DMA (Figure 5.13). Because the elongation of PTFE based samples was so high and given the limited displacement range of the tensile tester, it was not possible to reach a local maximal value for shear stress. In this way, the elongation was compared at 7 MPa stress as this level of shear stress was reached by all of the tested samples (Figure 5.17). BA80 and graphene in high filler content (8 and 16 wt%) modified the shear properties at the same level. PTFE/BA80-16, PTFE/Graphene-16, PTFE/BA80-8 and PTFE/Graphene-8 samples had the lowest elongation, 1.86%, 1.95%, 2.67% and 2.29% (Figure 5.17), respectively, while their shear modulus was the highest, 611.4 MPa, 657.4 MPa, 418.9 MPa and 507.8 MPa (Figure 5.16), respectively. In comparison, neat PTFE had 9.28% elongation at 7 MPa stress and 223.2 MPa shear modulus.

5.3.11. Tensile properties

Figure 5.18 shows a tensile curve of a PTFE/Al_2O_3-1 sample as an example. The tensile stress values were calculated at 2% strain, which is at the middle of the linear interval and at 5% strain which is after the proportional point. The yield strength and the elongation was calculated at the first local maximum.

The tensile properties of the unfilled and filled PTFE samples are introduced in Figure 5.15-5.17 and in Table 5.8 and Table B.13. The tendencies of the measured tensile stress at 2% and 5% strain, the tensile modulus and the elongation at yield are in agreement with the shear properties and the results of DMA tests (Figure 5.13). In case of neat PTFE, 512 MPa tensile modulus, 25.4% elongation at yield and 288% elongation at break were determined. Compared to the reference neat PTFE, PTFE/Graphene-16 and PTFE/BA80-16 samples reached ~216% and ~161% improvement in tensile modulus (Figure 5.16), which can be explained again with the restricted movement of the long PTFE molecular chains. Another explanation for the higher modulus can be the aggregation of nanoparticles which have a stiffness increasing mechanism [8]. The tensile modulus enhancement achieved by graphene filler is also in agreement with the literature [9]. PTFE/Graphene-16 and PTFE/BA80-16 specimens had one order of magnitude lower elongation at yield compared to neat PTFE (Figure 5.17). Remarkable tendencies in the yield strength were not registered. Compared to

the reference neat PTFE, PTFE/Graphene-8 and PTFE/Graphene-16 samples decreased the stress at break significantly, and their elongation at break was one and two orders of magnitude lower, respectively. When the elongation at break for BA80 filled specimens are considered, with respect to the reference neat PTFE, it can be stated that the elongation is increased, which is in agreement with the literature [10].

Table 5.8. The yield strength, elongation at yield, tensile stress at break and elongation at break of the sintered materials.

Samples	Yield strength MPa	Elongation at yield %	Tensile stress at break MPa	Elongation at break %
PTFE	12.69 ± 0.12	25.39 ± 0.93	20.06 ± 1.26	288.0 ± 15.3
PTFE/graphene-0.25	14.52 ± 0.19	24.26 ± 2.36	24.81 ± 2.99	348.8 ± 35.9
PTFE/graphene-1	12.67 ± 0.28	22.55 ± 1.57	23.35 ± 1.34	356.9 ± 67.0
PTFE/graphene-4	13.32 ± 0.21	15.24 ± 1.20	17.15 ± 0.74	226.0 ± 22.1
PTFE/graphene-8	15.17 ± 0.74	7.60 ± 0.26	13.05 ± 1.35	15.4 ± 0.8
PTFE/graphene-16	13.06 ± 0.95	2.36 ± 0.38	13.69 ± 1.51	2.5 ± 0.4
PTFE/Al_2O_3-1	12.60 ± 0.20	22.55 ± 0.96	24.11 ± 2.22	369.9 ± 3.0
PTFE/Al_2O_3-4	12.60 ± 0.13	12.43 ± 2.06	20.17 ± 1.72	306.5 ± 25.8
PTFE/BA80-1	12.56 ± 0.22	24.46 ± 0.88	22.32 ± 1.31	378.2 ± 81.2
PTFE/BA80-4	12.21 ± 0.29	16.66 ± 1.15	22.05 ± 1.68	344.7 ± 43.9
PTFE/BA80-8	13.98 ± 0.56	6.44 ± 0.96	23.16 ± 0.53	368.2 ± 8.7
PTFE/BA80-16	14.51 ± 0.62	3.96 ± 0.24	17.50 ± 0.95	320.0 ± 13.0
PTFE/MG70-1	11.93 ± 0.27	23.84 ± 1.13	21.78 ± 1.58	319.6 ± 36.2
PTFE/MG70-4	12.05 ± 0.38	19.73 ± 2.11	23.40 ± 2.36	438.9 ± 73.6

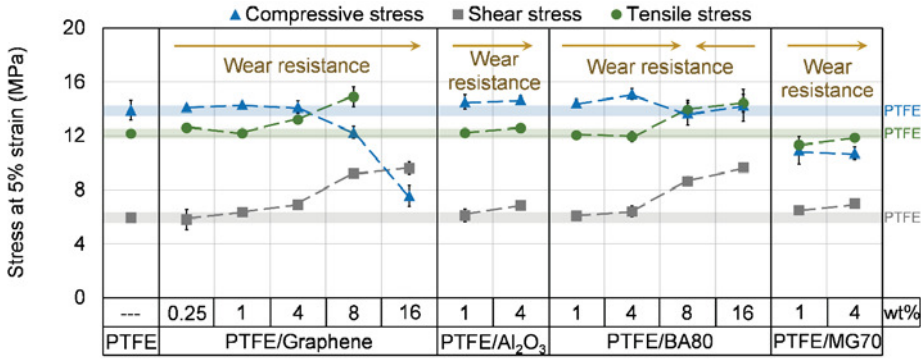

Figure 5.15. Compressive, shear and tensile stress of unfilled and filled PTFE samples at 5% strain. The blue, grey and green transparent lines display the compressive, shear and tensile stress of the neat PTFE at 5% strain, respectively. The introduced wear resistance is discussed in Chapter 5.3.12.

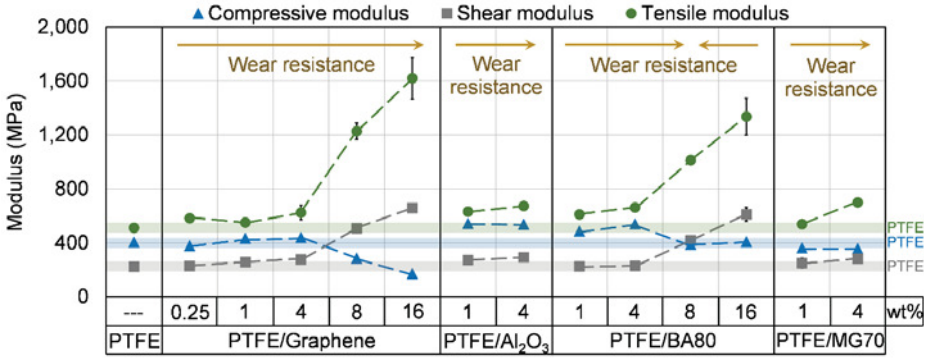

Figure 5.16. Compressive, shear and tensile modulus of unfilled and filled PTFE samples. The blue, grey and green transparent lines display the compressive, shear and tensile modulus of the neat PTFE, respectively. The introduced wear resistance is discussed in Chapter 5.3.12.

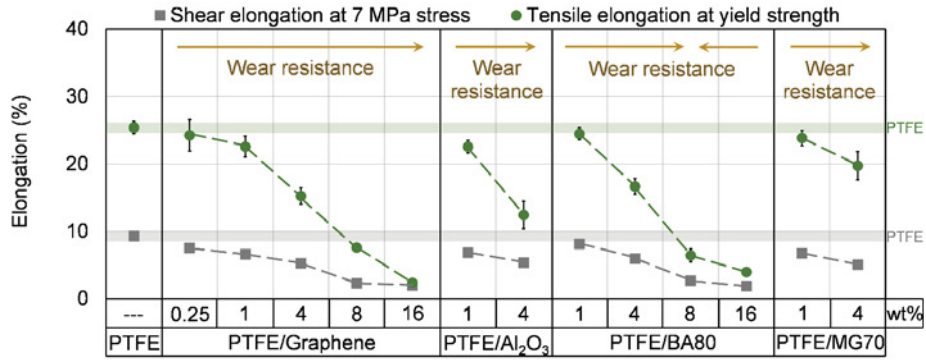

Figure 5.17. Shear and tensile elongation of unfilled and filled PTFE samples. The grey and green transparent lines display the shear and tensile elongation of the neat PTFE, respectively. The introduced wear resistance is discussed in Chapter 5.3.12.

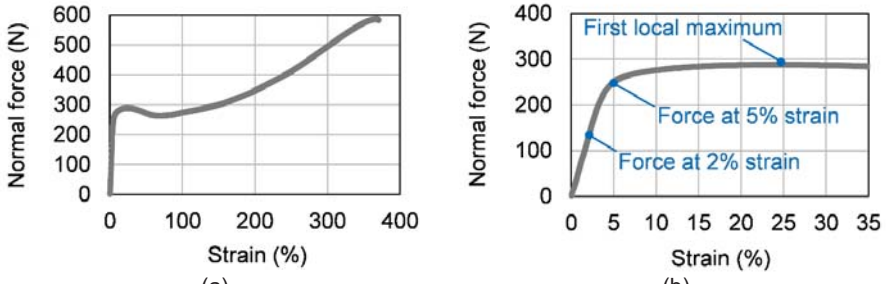

Figure 5.18. The full-scale tensile curve of a PTFE/Al_2O_3-1 sample (a) and the localization of the calculated tensile stress and yield strength values (b).

5.3.12. Wear behaviour

The calculated specific wear rates of the tested unfilled/filled PTFE samples are presented in Table 5.9. Neat PTFE had $5.16 \cdot 10^{-4}$ (mm^3/Nm) wear rate. The lowest wear rate was reached with PTFE/Al_2O_3-4 polymer samples with a value of $2.91 \cdot 10^{-6}$ (mm^3/Nm), which is more than two orders of magnitude improvement compared to the reference neat PTFE. PTFE/Al_2O_3-1 had ~82% reduction in wear rate compared to unfilled PTFE. Graphene in 4/8/16 wt% filler content also significantly decreased the wear, the reduction was around 1-2 orders of magnitude with a value of $4.72 \cdot 10^{-5}$, $3.17 \cdot 10^{-5}$ and $8.51 \cdot 10^{-6}$ (mm^3/Nm), respectively. The wear rate of PTFE/graphene-0.25 and PTFE/graphene-1 was similar to the reference PTFE. PTFE/BA80 in 1/4/8/16 wt% filler content decreased the wear rate of neat PTFE by 53%, 61%, 86% and 78%, respectively. MG70 filler showed similar wear rate as the reference PTFE, which comes from its high decomposition at 370°C sintering temperature (Chapter 4.3.4 and 4.3.5). The wear rate improvements achieved by graphene and Al_2O_3 fillers are in agreement with the literature [11-13].

The wear rate as a function of the shear and compressive modulus is depicted in Figure 5.19. It can be seen that no clear relation exists between the compressive/shear modulus and the wear rate. PTFE/Al_2O_3-4 material had the lowest wear rate, with a low shear modulus and high compressive modulus compared to the other PTFE-based materials. In contrast with this PTFE/graphene-16 had the second lowest wear rate, but it has the highest shear modulus and the lowest compressive modulus. The low wear rate of PTFE/Al_2O_3-4 material can not come from its thermal conductivity, hardness or tensile modulus as these properties only slightly changed compared to neat PTFE. It means that focusing on the wear rate, the dominant factor can only be the type of the fillers (e.g. filler material, particle size and geometry) and the transfer layer formation. The filler and consequently, the transfer layer formation, can have a dominant (primary) role in the wear mechanism of the investigated materials.

It is also important to mention that the higher tensile/shear modulus and thermal conductivity can also affect the wear resistance of the materials. For example the higher thermal conductivity can indirectly be beneficial in the wear process as more frictional heat can be removed from the contact surface. As a result, the surface temperature of the polymer is decreasing, which results in a smaller reduction in the mechanical properties of the polymer. Focusing on the graphene filler, it can be seen that the wear rate was decreased as the filler content increases, and simultaneously the tensile/shear modulus and thermal conductivity were increased as the filler content increases. In opposition to this in case of BA80 filler, the wear rate was not significantly influenced by the increased filler content and accompanying increased shear and tensile modulus. As a conclusion, it can be stated that the shear/tensile

properties and thermal conductivity have only a secondary role in the wear mechanism of the investigated materials.

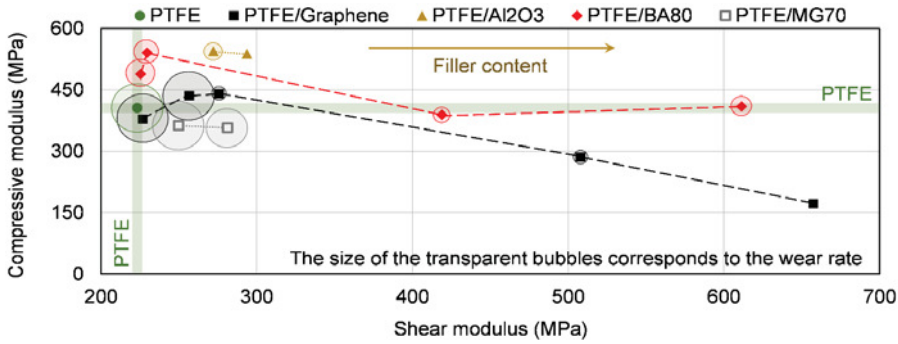

Figure 5.19. Compressive modulus as a function of the shear modulus of unfilled and filled PTFE samples. The size of the bubbles correlates to the wear rate of the samples.

Table 5.9. The measured wear rates of the tested unfilled/filled PTFE.

Materials	Wear rate (mm^3/mN)	
	Average	Deviation (%)
PTFE	$5.16 \cdot 10^{-4}$	8.8
PTFE/graphene-0.25	$5.47 \cdot 10^{-4}$	6.0
PTFE/graphene-1	$5.07 \cdot 10^{-4}$	20.6
PTFE/graphene-4	$4.72 \cdot 10^{-5}$	17.2
PTFE/graphene-8	$3.17 \cdot 10^{-5}$	25.6
PTFE/graphene-16	$8.51 \cdot 10^{-6}$	39.6
PTFE/Al_2O_3-1	$9.26 \cdot 10^{-5}$	12.5
PTFE/Al_2O_3-4	$2.91 \cdot 10^{-6}$	68.4
PTFE/BA80-1	$2.40 \cdot 10^{-4}$	10.9
PTFE/BA80-4	$2.01 \cdot 10^{-4}$	6.7
PTFE/BA80-8	$7.27 \cdot 10^{-5}$	10.3
PTFE/BA80-16	$1.12 \cdot 10^{-4}$	10.9
PTFE/MG70-1	$5.39 \cdot 10^{-4}$	2.2
PTFE/MG70-4	$4.49 \cdot 10^{-4}$	12.7

5.4. Conclusions

This chapter introduced the physical, thermal, viscoelastic, mechanical and wear analysis of unfilled and filled PTFE.

- The applied blending method was an intensive dry mechanical stirring, which is suitable to make homogeneous blends. The homogeneity of the powder blends was investigated by EDS/Raman spectrometry.

- Graphene filler, due to its excellent thermal properties, increased significantly the thermal conductivity of PTFE based samples. Compared to neat PTFE, graphene in 4/8/16 wt% improved the thermal conductivity with ~29/~84/~157 %, respectively.
- Compared to neat PTFE, the shear and tensile modulus of the developed mono-filled samples were increased together with the increase of the filler content. It is in line with the changes in storage modulus measured by DMA tests. All the fillers increased the storage modulus of PTFE. In agreement with the changes observed for the shear, tensile and storage modulus the elongation at yield and the measured elongation during shear tests were significantly reduced with decreasing filler content. This reduced ductility and the increase of the modulus values can be explained based on the restricted molecular chain motion caused by the fillers.
- Focusing on the compressive properties, with higher filler content (8 and 16 wt%) boehmite alumina is observed as a superior filler compared to graphene. Graphene significantly decreased the compressive stress and modulus compared to neat PTFE. Samples with lower alumina or boehmite content significantly increased the compressive modulus.
- As the peak temperature of β-transition of PTFE is close to room temperature (19-20°C), compressive tests at 50°C were carried out as a confirmation of the measurements run at room temperature. The tendencies of the registered compressive stress and modulus values between room temperature (23°C) and 50°C are close to each other. It means that at the temperature range of the β-transition of PTFE, the ratio of the mechanical performance of the measured specimens does not change significantly. This is in agreement with the measured storage modulus of the samples.
- PTFE/Al_2O_3-4 polymer samples had the lowest wear rate, reaching more than two orders of magnitude improvement compared to the neat PTFE. This ultra-low wear rate is not induced by the modified thermal conductivity, hardness or compressive/shear/tensile modulus as these values only slightly changed compared to the neat PTFE. It is supposed that this improvement comes from the modified transfer layer formation. Chapter 6 and 7 introduce further results about the tribological behaviour and transfer layer formation of these materials.
- The type of filler has a dominant (primary) role in wear mechanism. The increased shear/tensile properties and thermal conductivity have a lower influence on the wear mechanism (secondary role) in case of the investigated PTFE-based materials.

5.5. References

[1] http://catalog.wshampshire.com/Asset/psg_teflon_ptfe.pdf (16.05.2018).

[2] https://www.bearingworks.com/uploaded-assets/pdfs/retainers/ptfe-datasheet.pdf (16.05.2018).

[3] Teflon PTFE – fluoropolymer resin. DuPont, Properties Handbook, http://www.rjchase.com/ptfe_handbook.pdf (16.05.2018).

[4] X. Q. Wang, D. R. Chen, J. C. Han, S. Y. Du: Crystallization behavior of polytetrafluoroethylene (PTFE). Journal of Applied Polymer Science 83 (2002) 990–996.

[5] N. G. McCrum, B. E. Read, G. Williams: Anelastic and dielectric effects in polymeric solids. Dover Publications, Inc., New York (1991) 450-460.

[6] R. F. Boyer: Dependence of mechanical properties on molecular motion in polymers. Polymer Engineering and Science 8 (3) (1968) 161-185.

[7] K. P. Menard: Dynamic mechanical analysis: a practical introduction. CRC Press LLC, United States of America (1999).

[8] A. Dorigato, Y. Dzenis, A. Pegoretti: Nanofiller aggregation as reinforcing mechanism in nanocomposites, Procedia Eng. 10 (2011) 894-899.

[9] Y. S. Jun, J. G. Um, G. Jiang, A. Yu: A study on the effects of graphene nano-platelets (GnPs) sheet sizes from a few to hundred microns on the thermal, mechanical, and electrical properties of polypropylene (PP)/GnPs composites. Express Polymer Letters 12(10) (2018) 885–897.

[10] D. Pedrazzoli, V.M. Khumalo, J. Karger-Kocsis, A. Pegoretti: Thermal, viscoelastic and mechanical behavior of polypropylene with synthetic boehmite alumina nanoparticles. Polymer Testing 35 (2014) 92–100.

[11] B. A. Krick, J. J. Ewin, G. S. Blackman, C. P. Junk, W. G. Sawyer: Environmental dependence of ultra-low wear behavior of polytetrafluoroethylene (PTFE) and alumina composites suggests tribochemical mechanisms. Tribology International 51 (2012) 42-46.

[12] E. Padenko, L. J. Van Rooyen, B. Wetzel, J. Karger-Kocsis: “Ultralow” sliding wear polytetrafluoro ethylene nanocomposites with functionalized graphene. J. Reinf. Plast. Compos. 35 (2016) 892–901.

[13] S. S. Kandanur, M. A. Rafiee, F. Yavari, M. Schrameyer, Z. Z. Yu, T. A. Blanchet, N. Koratkar: Suppression of wear in graphene polymer composites. Carbon 50 (2012) 3178–3183.

CHAPTER 6

TRIBOLOGICAL CHARACTERISATION OF MONO-FILLED PTFE COMPOSITES

This chapter presents the friction and wear characterisation of the developed PTFE tribo-composites highlighting the transfer layer analysis of the worn polymer samples and steel counterfaces. The wear mechanism, the filler accumulation on the contact surface of the polymer sample and the wear-induced crystallinity are also discussed in a detailed way.

The following article was accepted based on this chapter:
Levente Ferenc Tóth, Gábor Szebényi, Jacob Sukumaran, Patrick De Baets: Tribological Characterisation of Nanoparticle Filled PTFE: Wear-Induced Crystallinity Increase and Filler Accumulation. Express Polymer Letters, 2021.

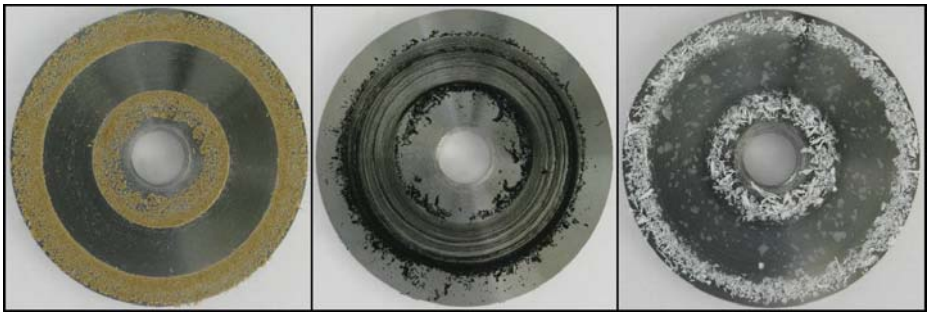

6.1. Introduction

Filler materials can significantly change the tribological behaviour of polymers, and in this way, the friction and wear properties of PTFE. The type of the filler has a dominant (primary) role in friction and wear mechanism of filled materials. These fillers also affect the friction stability, the transfer layer and debris formation, the homogeneity and uniformity of the transfer layer, the size and the amount of the formed debris. The composition of the steel counterfaces can also influence the tribological performance. This section focuses on the results of Phase 1 and 2, more explanation about these phases can be found in Chapter 3.3.6.

6.2. Materials and methods

6.2.1. Test materials

Table 6.1 shows the investigated samples related to this chapter. Chapter 3.1 introduces more details about the materials. The used disc steel counterfaces were 42CrMo4 / 304 / 34CrNiMo6 with a spiral surface pattern (Chapter 3.3.3).

Table 6.1. The tested unfilled and filled polytetrafluoroethylene (PTFE).

Materials	Matrix	Filler(s)	Filler content (wt%)
PTFE	PTFE	---	---
PTFE/Graphene-0.25	PTFE	Graphene	0.25
PTFE/Graphene-1	PTFE	Graphene	1
PTFE/Graphene-4	PTFE	Graphene	4
PTFE/Graphene-8	PTFE	Graphene	8
PTFE/Graphene-16	PTFE	Graphene	16
PTFE/Al_2O_3-1	PTFE	Alumina (Al_2O_3)	1
PTFE/Al_2O_3-4	PTFE	Alumina (Al_2O_3)	4
PTFE/BA80-1	PTFE	Boehmite alumina (BA80)	1
PTFE/BA80-4	PTFE	Boehmite alumina (BA80)	4
PTFE/BA80-8	PTFE	Boehmite alumina (BA80)	8
PTFE/BA80-16	PTFE	Boehmite alumina (BA80)	16
PTFE/MG70-1	PTFE	Hydrotalcite (MG70)	1
PTFE/MG70-4	PTFE	Hydrotalcite (MG70)	4

6.2.2. Friction and wear characterisation, transfer layer analysis

The tribological characterisation was carried out with a Wazau TRM 1000 tribometer. The applied test parameters: 3 MPa contact pressure and 0.1 m/s sliding distance. Chapter 3.3 introduces more information about the tribometer, test configuration, parameters, methodology and test plan. The creep tests of PTFE/Al_2O_3-4 were carried out with a Zwick Z005 universal tester. The transfer layer analysis was carried out with white-light interferometry (WLI), scanning electron microscopy (SEM), differential scanning calorimetry (DSC), energy-dispersive X-ray spectroscopy (EDS) and Fourier-transform infrared spectroscopy (FTIR). More details about the equipment are available in Chapter 3.2.

6.3. Results and discussion

6.3.1. Friction and wear

This section presents the coefficient of friction and the wear rate of the mono-filled PTFE materials related to Phase 1 and 2 (Chapter 3.3.6). At Phase 1, the applied counterface is 42CrMo4, while Phase 2 compares 42CrMo4 steel counterface to 304 and 34CrNiMo6 steels. In both phases, the contact pressure was 3 MPa, while the sliding speed was 0.1 m/s. All values were calculated according to the formulas in Chapter 3.3.2. The measured bulk temperature increase during the wear tests was not significant, their stabilised values were between 32°C and 38°C. In this way, in this chapter, the measured bulk temperatures are not discussed.

6.3.1.1. Coefficient of friction

Figure 6.1, 6.2 and Table B.14, B.15 depict the coefficient of friction of unfilled and filled PTFE. Besides the neat PTFE, only the friction properties of graphene and alumina filled PTFE are available in the literature, and the tendency of the measured results are in agreement with them [1, 2].

The neat PTFE had 0.093/0.096/0.100 (-) coefficient of friction against 42CrMo4 / 304 / 34CrNiMo6 steel counterfaces, respectively. The most remarkable reduction was achieved by PTFE/Graphene–1 material which had 0.078 (-) coefficient of friction against 42CrMo4 steel which is ~16% lower than the reference unfilled PTFE. The coefficient of friction reduction was slighter in case of PTFE/Graphene–4 samples. Their coefficient of friction were 0.088 / 0.088 / 0.092 (-) against 42CrMo4 / 304 / 34CrNiMo6 steel counterfaces, respectively. Graphene in 8 and 16 wt% filler content slightly increased the friction between the filled PTFE and the steel counterface. Al_2O_3 and MG70 filler also increased the coefficient of friction both in 1 and 4 wt%, independently of the counterface steel. PTFE/BA80-1 had similar friction values as unfilled PTFE; while BA80 in higher filler content increased the coefficient of friction. Regarding the three different steel counterfaces, polymers tested against 42CrMo4 steel disc had slightly lower coefficient of friction (Figure 6.2, Table B.15). In case of neat PTFE, PTFE/Graphene-4 and PTFE/Al_2O_3–4 samples, the highest coefficient of friction values were registered against 34CrNiMo6 steel counterface, still the differences are in the range of the deviation.

Analyses of variance (ANOVA) based on both Bonferroni-Holm and Holm-Šidák method were carried out to compare the coefficient of friction of filled PTFE materials to the reference neat PTFE. Both methods concluded that the measured differences in the coefficient of friction compared to the reference neat PTFE are not significant. This conclusion is valid for Phase 1 and Phase 2; the differences are not significant independently of the applied filled PTFE pin and of the used counterface steel disc (42CrMo4 / 304 / 34CrNiMo6).

The coefficient of friction graphs of the tested materials against 42CrMo4 steel disc can be seen in Figure 6.3. All of the materials reached steady-state friction during the applied 1000 m sliding distance (graphene filler reached quasi-steady-state friction). The importance of this steady-state condition is related to the reliability of the materials, and it is a good indicator for friction and wear stability. In this way, a persistent steady-state condition, besides the low coefficient of friction and low wear rate, is also a requirement in industrial applications.

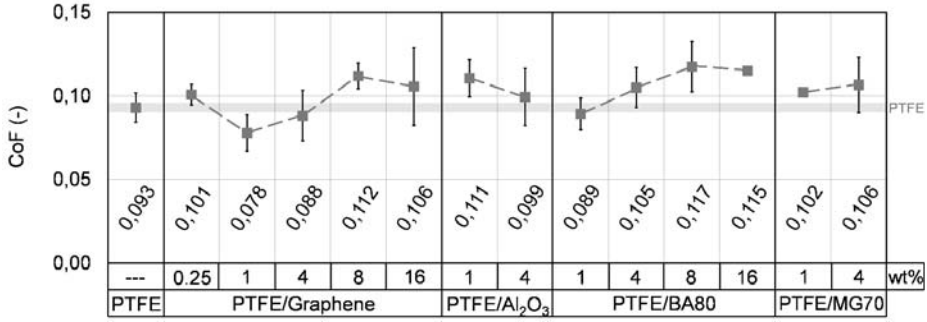

Figure 6.1. The coefficient of friction of unfilled/filled PTFE samples. The grey transparent line displays the measured coefficient of friction of the reference neat PTFE. Dry contact, 42CrMo4 steel counterface, 3 MPa contact pressure, 0.1 m/s sliding speed, 1000 m sliding distance (Phase 1, Chapter 3.3.6.1).

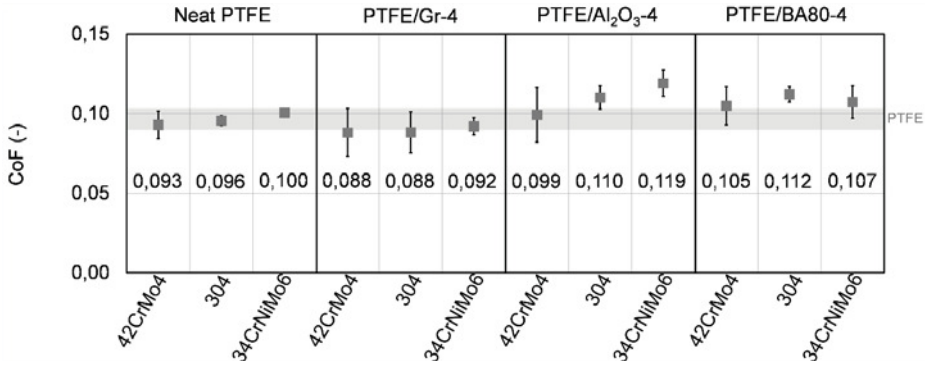

Figure 6.2. The coefficient of friction of unfilled/filled PTFE samples. The grey transparent line displays the measured coefficient of friction of the reference neat PTFE. Dry contact, 42CrMo4 / 304 / 34CrNiMo6 steel counterface, 3 MPa contact pressure, 0.1 m/s sliding speed, 1000 m sliding distance (Phase 2, Chapter 3.3.6.2).

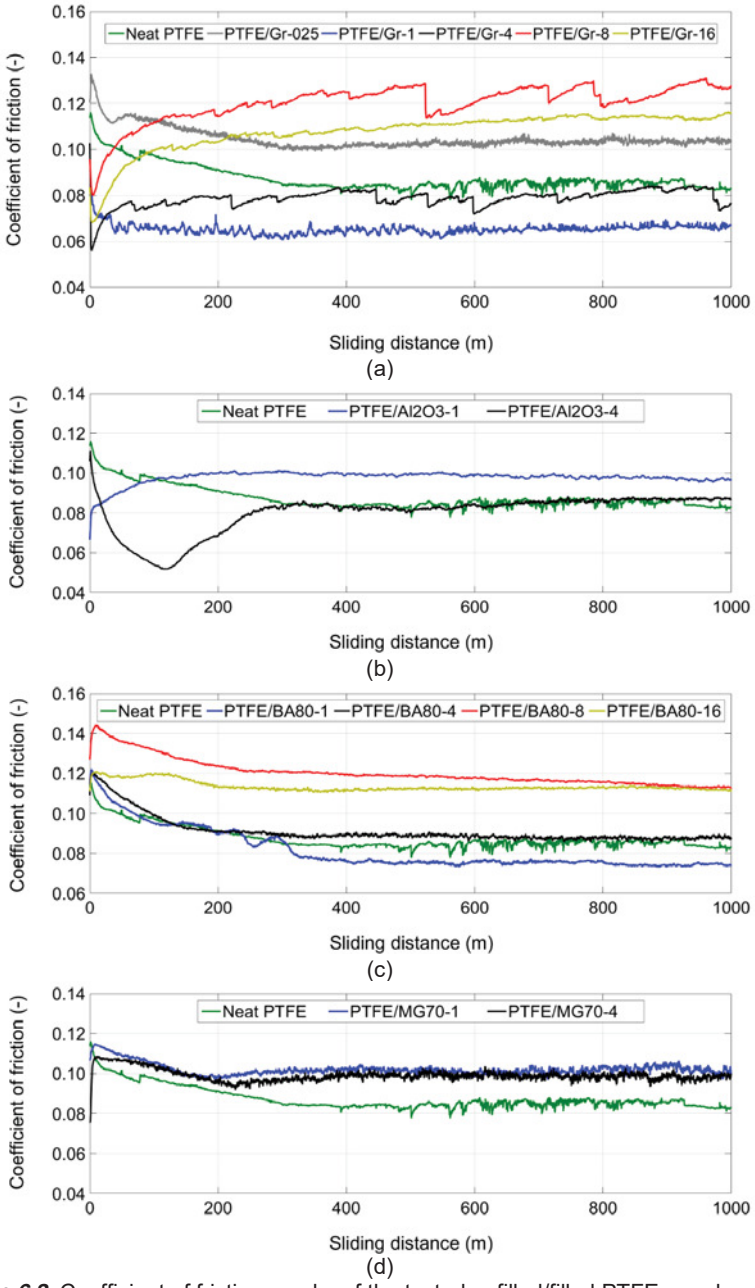

Figure 6.3. Coefficient of friction graphs of the tested unfilled/filled PTFE: graphene filled PTFE (a), Al_2O_3 filled PTFE (b), BA80 filled PTFE (c), and MG70 filled PTFE (d). Dry contact, 42CrMo4 steel counterface, 3 MPa contact pressure, 0.1 m/s sliding speed, 1000 m sliding distance (Phase 1, Chapter 3.3.6.1).

All of the tested unfilled and filled PTFE samples reached the steady-state friction after ~300-400 m sliding distances. Some examples for these curves are introduced in Figure 6.3. In case of PTFE/Graphene-4 and PTFE/Graphene-8 composites (Figure 6.3 (a)), rapid drops and slow raises can be seen periodically in friction graphs, which can be the influence of transfer layer formation. It is supposed that at a certain transfer layer thickness, the top layer of the transfer film is suddenly removed. Transfer layer formation is then continued on a thinner remaining layer. The duration of the rapid drops was around 2-5 rotational cycles, while the slower increasing periods were around 200-1500 cycles. The friction reduction of the mentioned drops is around 0.01 (-) or less. This behaviour of PTFE/Graphene-4 composites was also registered in case of 304/34CrNiMo6 counterfaces.

6.3.1.2. Wear rate

Figure 6.4, 6.5 and Table B.16, B.17 introduce the wear rate and wear depth of unfilled and filled PTFE. Neat PTFE had $5.16 \cdot 10^{-4}$ / $5.89 \cdot 10^{-4}$ / $5.10 \cdot 10^{-4}$ (mm^3/Nm) wear rate against 42CrMo4 / 304 / 34CrNiMo6 steels, respectively. PTFE/Al_2O_3-4 polymer samples reached the lowest wear rate independently of the applied steel counterfaces. The wear rate of PTFE/Al_2O_3-4 was $2.91 \cdot 10^{-6}$ / $3.17 \cdot 10^{-6}$ / $9.83 \cdot 10^{-7}$ (mm^3/Nm) against 42CrMo4 / 304 / 34CrNiMo6 disc counterfaces, respectively. It is more than two orders of magnitude improvement compared to the reference neat PTFE, which is in agreement with the literature [1]. Graphene in 4/8/16 wt% filler content also decreased the wear significantly; their reduction was around 1-2 orders of magnitude, which is in agreement with the literature [2]. PTFE/Graphene-4 sample had $4.72 \cdot 10^{-5}$ / $1.88 \cdot 10^{-5}$ / $2.19 \cdot 10^{-5}$ wear rate against 42CrMo4 / 304 / 34CrNiMo6 disc counterfaces, respectively. Chapter 4 and 5 indicates a sufficient material development for BA80 filled composites, which means that most of the functional groups of BA80 still exist after the sintering process, and the composites have appropriate material properties. In this way, it can be concluded that the functional groups of boehmite did not influence so much the wear rate as it was expected in the research hypothesis (Chapter 1.3). Because of the high wear rate of MG70 filled composites, Phase 2 did not include the further investigation of these materials.

Analyses of variance (ANOVA) based on both Bonferroni-Holm and Holm-Šidák method were evaluated to compare the wear rate of filled PTFE samples to the reference neat PTFE. Both methods concluded that most of the observed differences in the wear rate compared to the reference unfilled PTFE are significant. Only PTFE/Graphene-0.25, PTFE/Graphene-1, PTFE/MG70-1 and PTFE/MG70-4 had no significant difference related to the wear rate. This conclusion is valid for Phase 1 and Phase 2 (42CrMo4 / 304 / 34CrNiMo6).

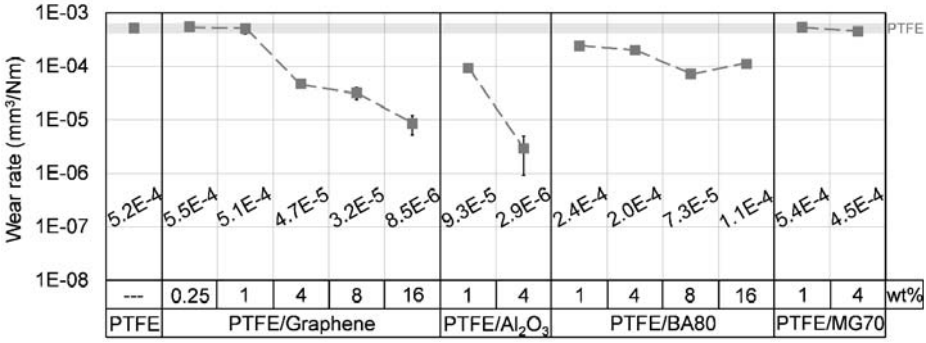

Figure 6.4. Wear rate of unfilled/filled PTFE samples. The grey transparent line displays the measured wear rate of the neat PTFE. Dry contact, 42CrMo4 steel counterface, 3 MPa contact pressure, 0.1 m/s sliding speed, 1000 m sliding distance (Phase 1, Chapter 3.3.6.1).

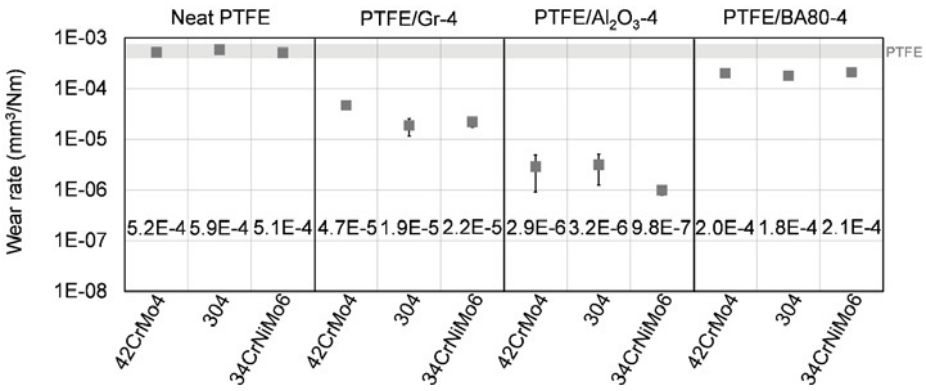

Figure 6.5. Wear rate of unfilled/filled PTFE samples. The grey transparent line displays the measured wear rate of the neat PTFE. Dry contact, 42CrMo4 / 304 / 34CrNiMo6 steel counterface, 3 MPa contact pressure, 0.1 m/s sliding speed, 1000 m sliding distance (Phase 2, Chapter 3.3.6.2).

Figure 6.6 shows the wear (displacement) graphs of the developed 4 wt% filler content materials; the tested counterface is 42CrMo4 steel. All the tested composites reached the steady-state wear during the 1000 m sliding distance. The running-in period had higher wear, and in this way higher wear rate, which can be seen in PTFE/Graphene-4 and PTFE/Al_2O_3-4 composites in Figure 6.6 (b). All of the on-line wear graphs were linear after a short running-in period (Figure 6.6 (a) and (b)), in this way, the wear rate was evaluated only after completing the proposed sliding distance, based on the measured mass loss. In case of PTFE/Al_2O_3-4 sample (Figure 6.6 (b)), a small increase can be seen in wear graphs. This phenomenon comes from the thermal expansion of the material, as the thickness of the removed (worn) material is

extremely low in case of the given PTFE/Al_2O_3-4 sample. The introduced phenomenon can be explained with the following example. The wear depth related to the mass loss during wear test was ~2 μm. The measured bulk temperature during wear was 34°C. The thermal expansion of neat PTFE is 1.70% at room temperature, while 2.09% at 34°C. In this way, the thickness change of a filled PTFE pin sample with 5 mm thickness caused by the temperature increase during wear (from 23°C to 34°C) is ~19.5 μm. This evaluation used the thermal expansion of neat PTFE, as only this was available in the literature. The measured creep of PTFE/Al_2O_3-4 material at the wear test conditions (3 MPa, 167 minutes) was ~14.5 ± 2.3 μm. In this way, the measured (total) wear depth by the displacement sensor was 3 μm. The wear depth was evaluated with Equation (6.1).

$$t_{c,total} = t_{c,thermal} - t_{c,wear} - t_{c,creep} = 19.5 - 2 - 14.5 = 3\ \mu m \quad (6.1)$$

In Equation (6.1), $t_{c,total}$ is the total change of thickness during the wear test (μm), which can be measured by the displacement sensor. $t_{c,thermal}$ is the change of thickness caused by the thermal expansion (μm), $t_{c,wear}$ is the change of thickness caused by the wear (wear depth, μm), which is calculated based on the measured mass loss, while $t_{c,creep}$ is the measured creep at the wear test conditions (μm).

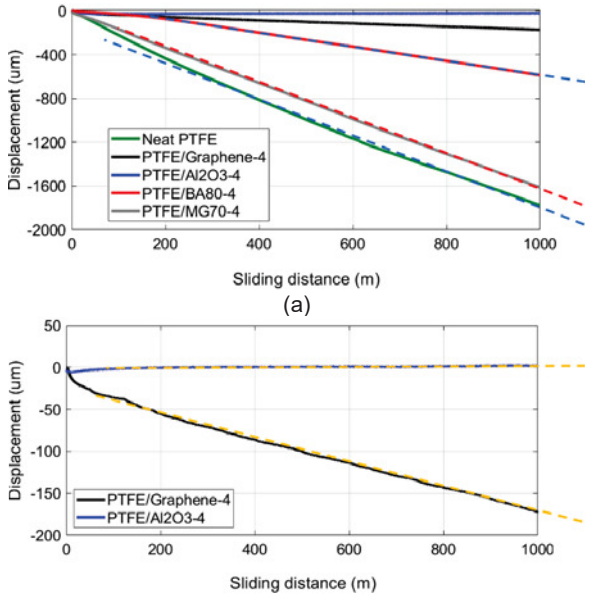

Figure 6.6. Wear (displacement) graphs of tested unfilled PTFE and PTFE composites with 4 wt% filler content. Dry contact, 42CrMo4 steel counterface, 3 MPa contact pressure, 0.1 m/s sliding speed, 1000 m sliding distance (Phase 1, Chapter 3.3.6.1).

6.3.1.3. Wettability and surface free energy (SFE)

Figure 6.7, 6.8 and Table B.18 introduce the measured advancing/receding contact angles and the calculated surface free energy of the developed unfilled and filled PTFE. The contact angles and the surface free energy of the steel counterparts can be found in Table B.18. 42CrMo4/304/34CrNiMo6 steels had a surface energy of 41.6/54.1/40.8 mN/m (based on the measured advancing contact angle), respectively.

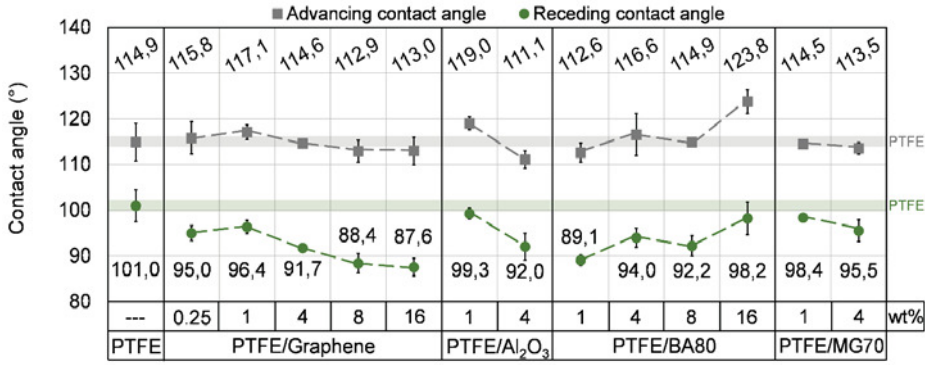

Figure 6.7. Advancing and receding contact angles of the unfilled and mono-filled PTFE materials. The grey/green transparent lines display the measured advancing/receding contact angle of the neat PTFE.

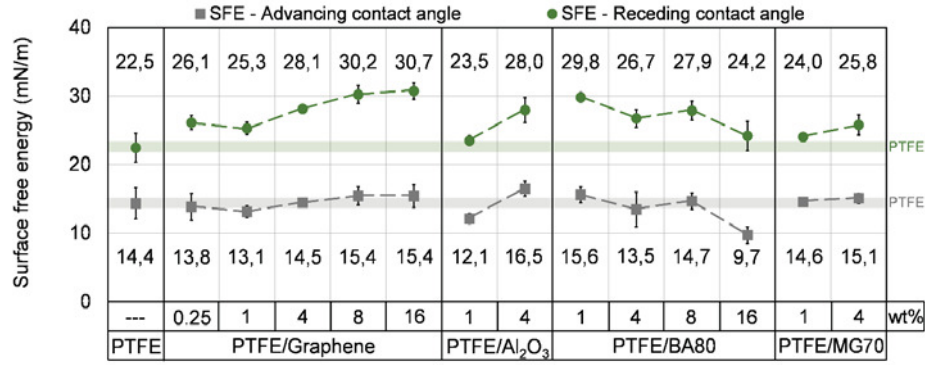

Figure 6.8. Surface free energy (SFE) based on the advancing and receding contact angles of the unfilled and mono-filled PTFE materials. The grey/green transparent lines display the measured SFE (advancing/receding) of the neat PTFE.

Unfilled PTFE had 114.9°/101.0° advancing/receding contact angles and 14.4/22.5 mN/m SFE (related to the advancing/receding contact angles), respectively. It can be seen that in most cases the fillers increased the surface energy compared to neat PTFE, which corresponds to a higher adhesion between the contact surfaces, in this way, the increase of the coefficient of friction and wear rate would be expected as well (Chapter 1.1) [3, 4]. Still, graphene, alumina and BA80 fillers just slightly changed the coefficient of friction, furthermore, they significantly decreased the wear rate in higher filler content. It means that the filler particles can compensate the effect of the increased surface energy, and even the used fillers can significantly improve the wear resistance.

6.3.2. Transfer layer analysis and wear mechanism

6.3.2.1. Wear track of the steel counterfaces – macrographs

Figure 6.9 displays the macrographs of the tested steel counterfaces for visualisation of the formed transfer layer. The macrographs show remarkable differences in the transfer layer formation, and in the shape and the size of the formed debris.

No transfer layer is formed on the surface of the neat PTFE steel disc (Figure 6.9 (a)). PTFE/graphene-1 and PTFE/BA80-1 steel counterfaces also showed a limited transfer layer formation (Figure 6.9 (b) and (f)). A more significant transfer layer formation was observed on the surface of PTFE/Al_2O_3-1, PTFE/BA80-4, PTFE/MG70-1 and PTFE/MG70-4 steels (Figure 6.9 (d), (g), (h) and (i)). The surface area of these transfer layers is however on the same scale as the formed debris, which indicates that a uniform and durable transfer layer formation was not possible with these materials. On the other hand, PTFE/ Al_2O_3-1 composite had a lower wear rate, which comes from the different debris formation mechanism. As it can be seen in Figure 6.9 (d), the size of the formed debris is smaller compared to BA80 or MG70 filled materials, which resulted in a thinner transfer layer as the smaller particles are able to fill the smaller asperity cavities of the steel. PTFE/graphene-4 counterface (Figure 6.9 (c)) had a partly uniform transfer layer and the wear debris were smaller than the debris of the PTFE/graphene-1. PTFE/Al_2O_3-4 shows the smallest polymer wear particles (debris) on the steel counterface (Figure 6.9 (e)). The observed transfer layer of the counterface tested against PTFE/Al_2O_3-4 polymer was uniform, and due to the small debris, the thickness was on the scale of the steel surface asperities.

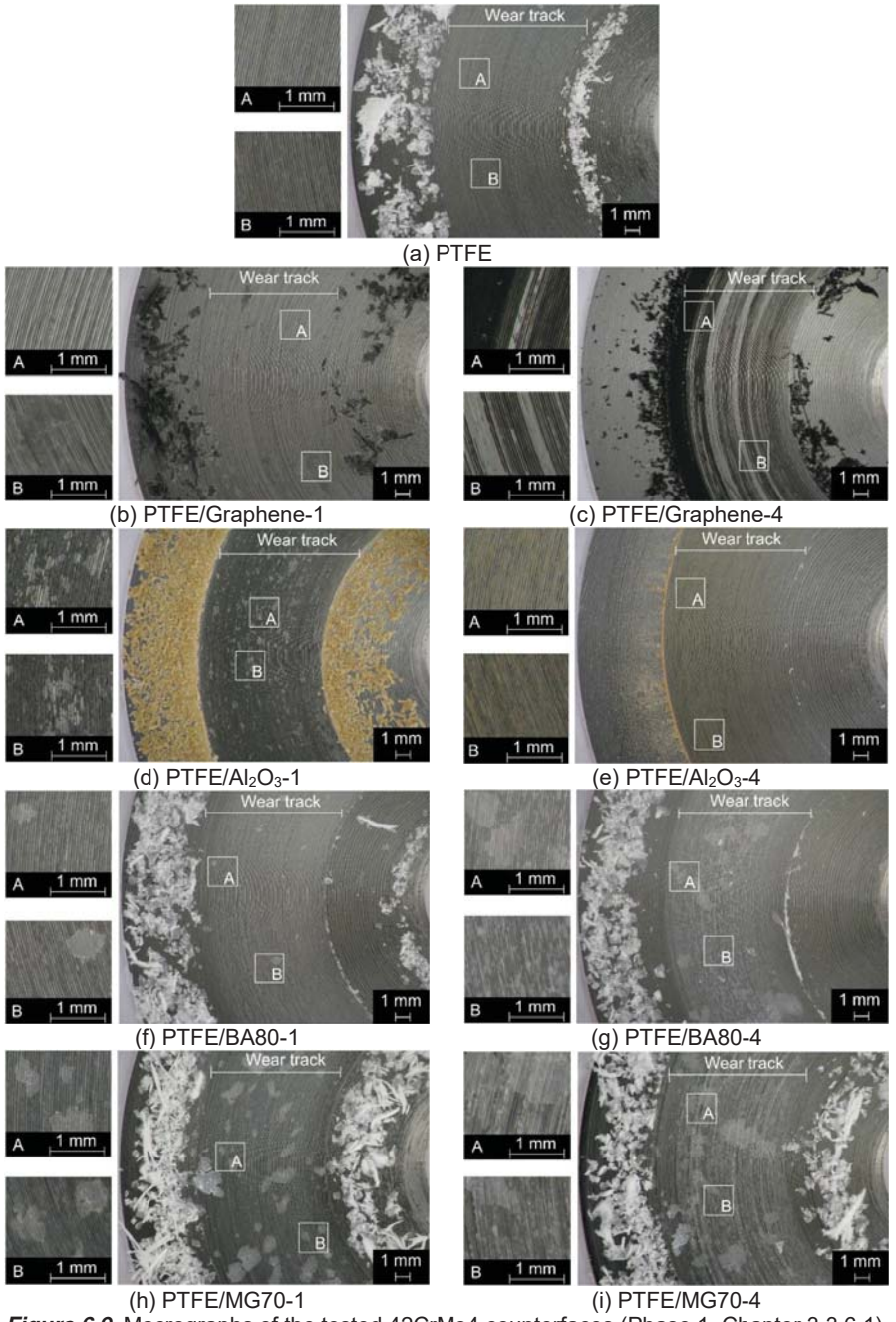

(a) PTFE

(b) PTFE/Graphene-1

(c) PTFE/Graphene-4

(d) PTFE/Al_2O_3-1

(e) PTFE/Al_2O_3-4

(f) PTFE/BA80-1

(g) PTFE/BA80-4

(h) PTFE/MG70-1

(i) PTFE/MG70-4

Figure 6.9. Macrographs of the tested 42CrMo4 counterfaces (Phase 1, Chapter 3.3.6.1). Neat PTFE (a), PTFE/graphene-1 (b), PTFE/graphene-4 (c), PTFE/Al_2O_3-1 (d), PTFE/Al_2O_3-4 (e), PTFE/BA80-1 (f), PTFE/BA80-4 (g), PTFE/MG70-1 (h) and PTFE/MG70-4 (i).

6.3.2.2. Wear track of the steel counterfaces – micrographs

Figure 6.10 introduces the micrographs of the tested counterfaces analysed by white light interferometry.

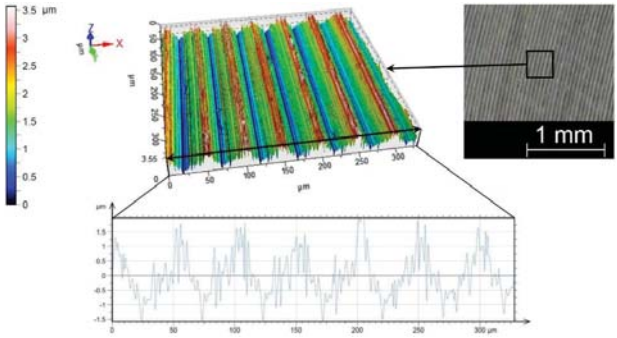

(a) Original unworn 42CrMo4 steel

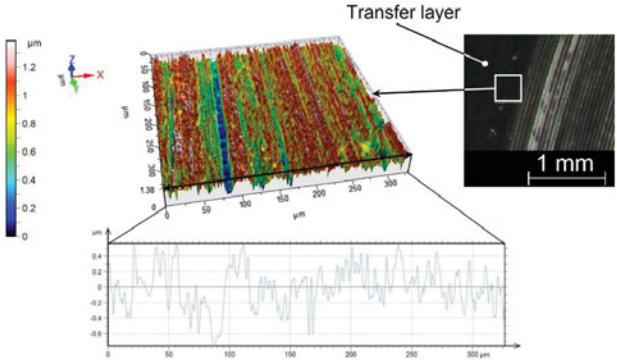

(b) PTFE/graphene-4 - 42CrMo4 steel wear track

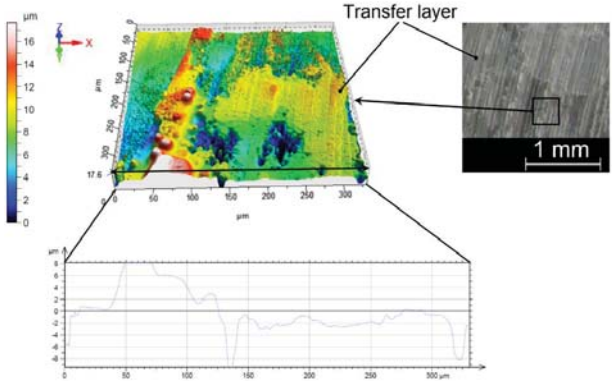

(c) PTFE/MG70-4 - 42CrMo4 steel wear track

Figure 6.10. 3D/2D macrographs of the original unworn surface (a), PTFE/graphene-4 steel counterface wear track (b) and PTFE/MG70-4 (c) steel counterface wear track (Phase 1, Chapter 3.3.6.1).

All counterfaces had spiral surface patterns as the surface finishing method was turning. The advantage of this surface finishing method is that in the aspect of the rotating polymer pin, the relative surface pattern of the steel is closely the same at the wear track during the wear process as it can be seen in real conditions such as e.g. shaft in bushing.

Figure 6.10 (a) shows the original, unworn surface pattern of a steel counterface. As the very limited wear of the steel counterfaces was not observable, the wear track of neat PTFE, PTFE/graphene-1 and PTFE/BA80-1 steel counterfaces were similar to Figure 6.10 (a), as no transfer layer formation was observed on these discs. PTFE/Al_2O_3-1 and PTFE/Al_2O_3-4 counterfaces had a thin transfer layer due to the small formed debris; in this way, significant differences were not recorded compared to the unworn, neat steel counterfaces.

Figure 6.10 (b) also confirms that only PTFE/graphene-4 sample formed a (partly uniform) transfer layer on the steel counterface. This transfer layer significantly modified the surface pattern of the wear track. PTFE/BA80-4, PTFE/MG70-1 and PTFE/MG70-4 steels had not uniform transfer layers, which were remarkably thicker due to the formed large debris during the wear test. Figure 6.10 (c) shows an example of this kind of transfer layer on PTFE/MG70-4 steel counterface. The observed transfer layer thickness was between 10-15 µm.

The transfer layer on the PTFE/graphene-4 counterface was further investigated by white light interferometer (Figure 6.11).

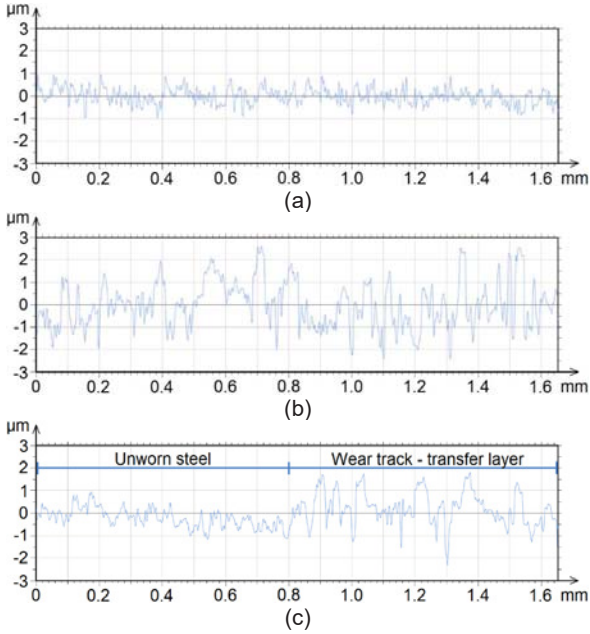

Figure 6.11. The unworn steel (a), the wear track/transfer layer (b), the interface of the unworn steel and the transfer layer (c) on 42CrMo4 steel counterface tested against PTFE/graphene-4 polymer sample (Phase 1, Chapter 3.3.6.1).

The scale of these figures is chosen uniform for a better comparison. The wear track was analysed in a range with 1.65 mm width. Figure 6.11 (a) displays the surface of the unworn steel counterface, while Figure 6.11 (b) shows the wear track in the steel counterface where significant deposits were detected. Figure 6.11 (c) introduces the interface of the unworn steel disc (left), and the wear track/transfer layer on the steel (right). This figure can help in making a basic estimation of the thickness of PTFE/graphene-4 transfer layer. The observed results indicate that the thickness of this transfer layer on the steel counterfaces was approximately 1-2 µm.

6.3.2.3. Wear mechanism of the polymer samples

Figure 6.12 displays the contact surface of some polymer samples. Figure 6.12 (a) introduces an unworn PTFE/Al_2O_3-4 surface, while (b) and (c) shows a PTFE/Al_2O_3-4 sample after the wear test. The surface pattern of the steel counterface just partly impressed on the contact surface of the PTFE/Al_2O_3-4 polymer; the original surface pattern of the polymer sample is still persisting (Figure 6.12 (b)). This phenomenon comes from the ultra-low wear rate of this material. Figure 6.12 (c) depicts some white areas on the PTFE/Al_2O_3-4 polymer surface, which can indicate alumina or iron-oxide rich regions formed during the wear process. All of the other polymer materials had a similar surface pattern (but different from PTFE/Al_2O_3-4) which comes from the used steel counterfaces (Figure 6.12 (d)-(f)).

Figure 6.13 and 6.14 introduce the surface pattern of PTFE/Al_2O_3-4 and PTFE/BA80-4 polymer pin samples in unworn stage and after 0.1 / 1 / 10 / 100 / 200 / 400 / 1000 m sliding distance. These two materials were chosen for comparison, as they had different transfer layer and debris formation and a different size of debris. This analysis was carried out with the use of white light interferometry. Figure 6.13 (a) and 6.14 (a) depicts the rough surface quality of the unworn polymer samples. Their characteristics come from the room temperature pressing. After 10 m sliding distance (Figure 6.13 and 6.14 (d)) the original surface characteristics disappear, and the dominant surface pattern of the polymer samples becomes similar to the steel counterface. It means that after 10 m sliding distance the original surface quality of the polymer samples does not affect the sliding process any more. If the applied sliding distance is 1000 m, the original rough surface quality of the polymer materials can influence the wear process only during the first ~1% of the sliding distance.

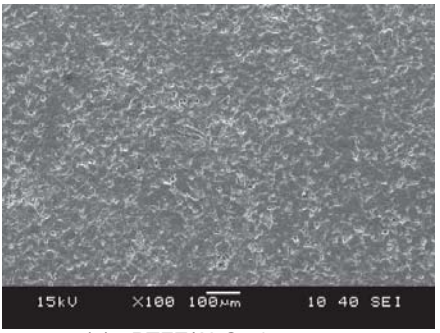

(a) - PTFE/Al_2O_3-4, unworn

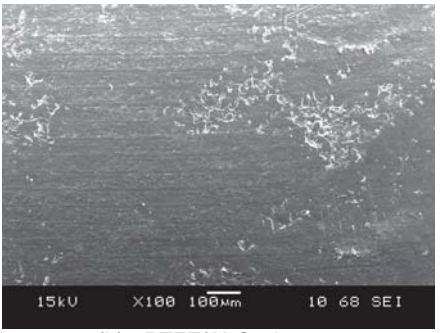

(b) - PTFE/Al_2O_3-4, worn

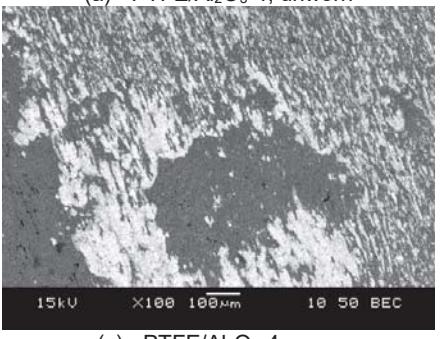

(c) - PTFE/Al_2O_3-4, worn

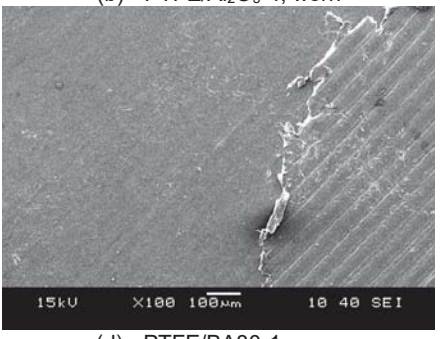

(d) - PTFE/BA80-1, worn

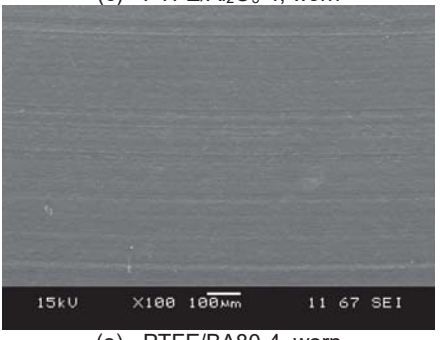

(e) - PTFE/BA80-4, worn

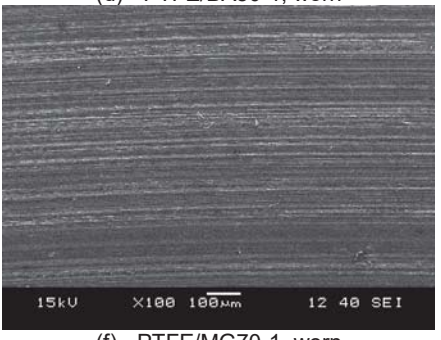

(f) - PTFE/MG70-1, worn

Figure 6.12. SEM micrographs from the contact surfaces of unworn PTFE/Al_2O_3-4 (a), worn PTFE/Al_2O_3-4 (b) and (c), worn PTFE/BA80-1 (d), worn PTFE/BA80-4 (e) and worn PTFE/MG70-1 (f) polymers samples against 42CrMo4 steel counterfaces (Phase 1, Chapter 3.3.6.1).

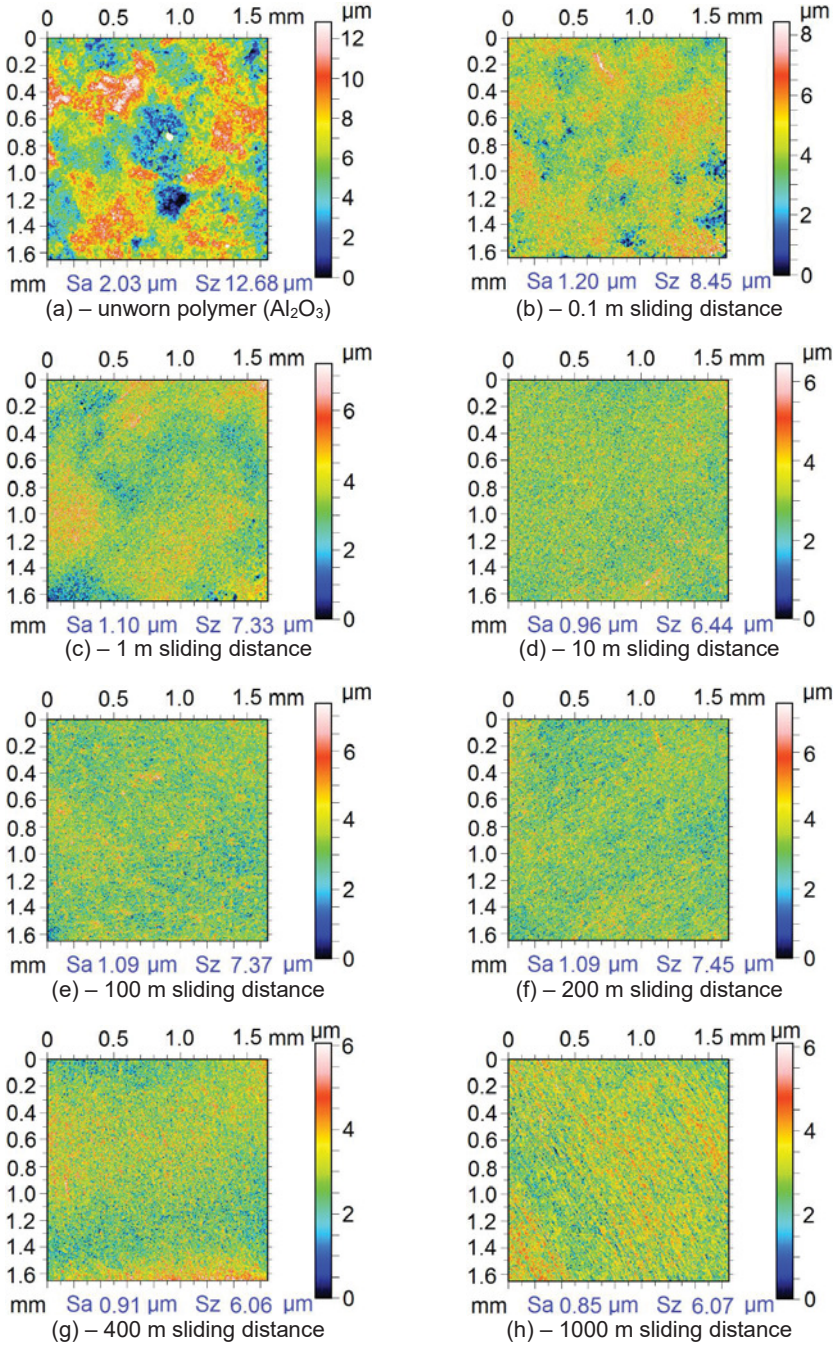

(a) – unworn polymer (Al_2O_3)
(b) – 0.1 m sliding distance
(c) – 1 m sliding distance
(d) – 10 m sliding distance
(e) – 100 m sliding distance
(f) – 200 m sliding distance
(g) – 400 m sliding distance
(h) – 1000 m sliding distance

Figure 6.13. The contact surface of PTFE/Al_2O_3-4 polymer samples against 42CrMo4 steel counterfaces (3 MPa contact pressure, 0.1 m/s sliding speed).

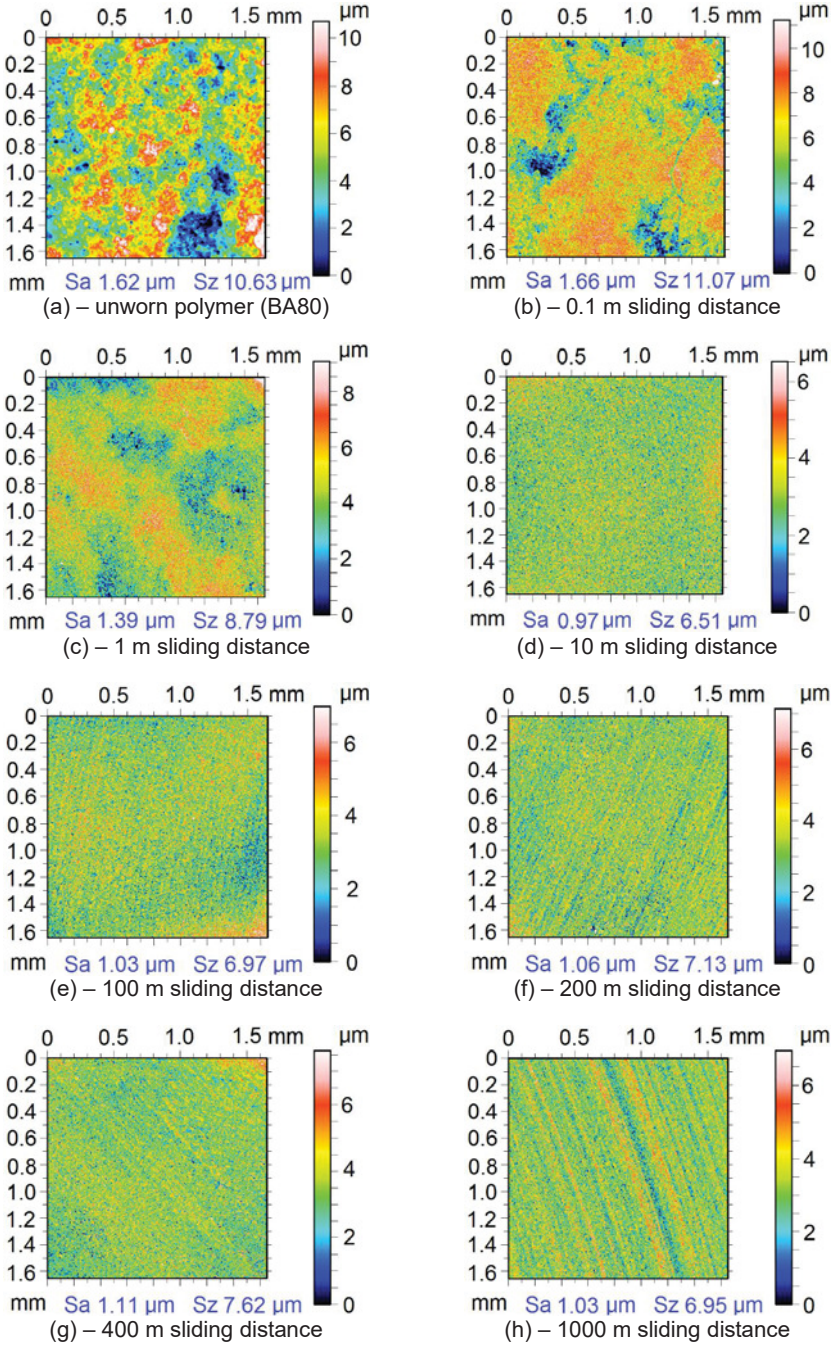

Figure 6.14. The contact surface of PTFE/BA80-4 polymer samples against 42CrMo4 steel counterfaces (3 MPa contact pressure, 0.1 m/s sliding speed).

6.3.2.4. The formed debris

Table 6.2 introduces the maximal size and shape of the formed debris, while Figure 6.15 shows some examples for the SEM micrographs of the formed polymer debris. The maximal size of the debris is in correlation with the tendency of the calculated wear rates (Figure 6.4 and 6.5). PTFE/Al_2O_3-4 polymer debris had the smallest size with < 50 μm. Most of the polymers formed debris with smooth and thin layer structure (flakes). The PTFE/Al_2O_3-1 debris Figure 6.15 (e) had mostly a waved and frilled layer structure while PTFE/Al_2O_3-4 debris Figure 6.15 (f) had particle-based shape.

Table 6.2. The maximal size and the dominant shape of the formed debris.

Materials	Max. size (μm)	Dominant shape	
PTFE	> 1000	smooth and thin layers (flakes)	Figure 6.15 (a)
PTFE/Graphene-0.25	> 1000	smooth and thin layers (flakes)	Figure 6.15 (b)
PTFE/Graphene-1	> 1000	smooth and thin layers (flakes)	Figure 6.15 (c)
PTFE/Graphene-4	300-600	smooth and thin layers (flakes)	Figure 6.15 (d)
PTFE/Al_2O_3-1	300-600	waved and frilled layers	Figure 6.15 (e)
PTFE/Al_2O_3-4	< 50	particle-based shape	Figure 6.15 (f)
PTFE/BA80-1	> 1000	smooth and thin layers (flakes)	Figure 6.15 (g)
PTFE/BA80-4	> 1000	smooth and thin layers (flakes)	Figure 6.15 (h)
PTFE/MG70-1	> 1000	smooth and thin layers (flakes)	Figure 6.15 (i)
PTFE/MG70-4	> 1000	smooth and thin layers (flakes)	Figure 6.15 (j)

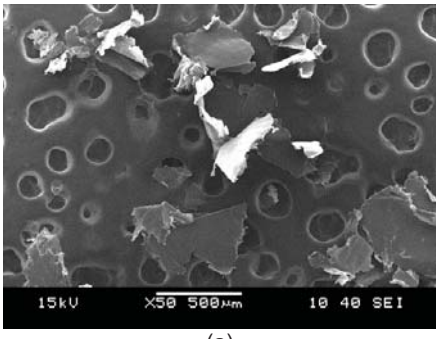

(a)

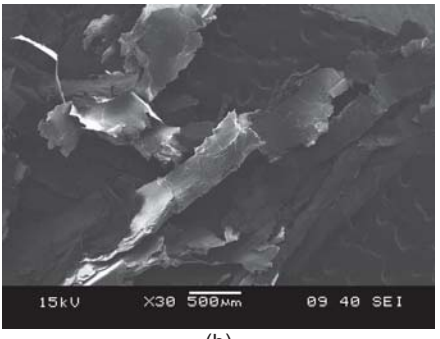

(b)

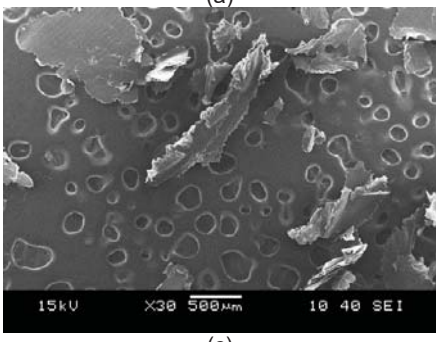

(c)

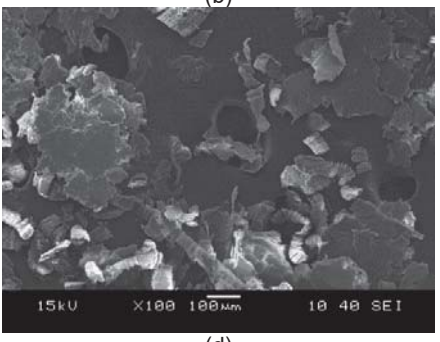

(d)

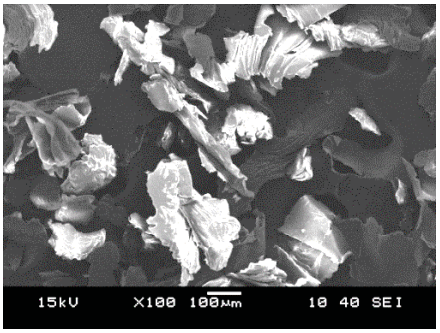

(e)

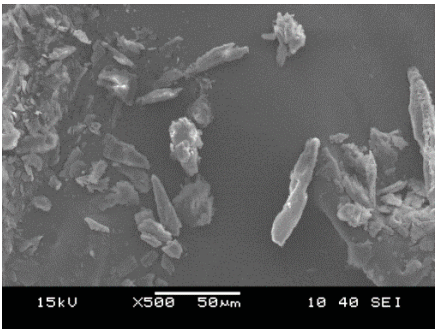

(f)

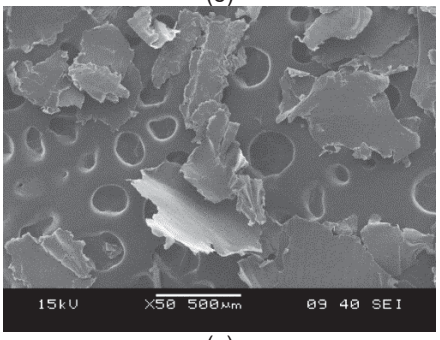

(g)

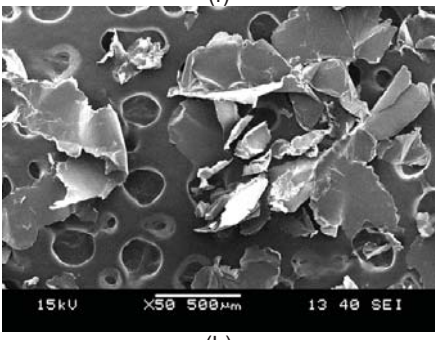

(h)

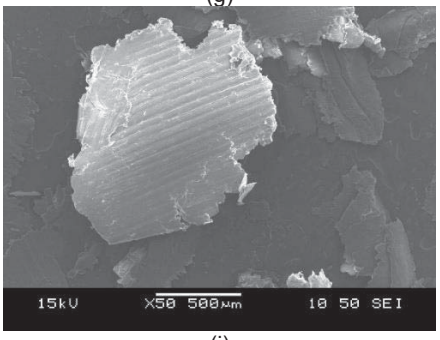

(i)

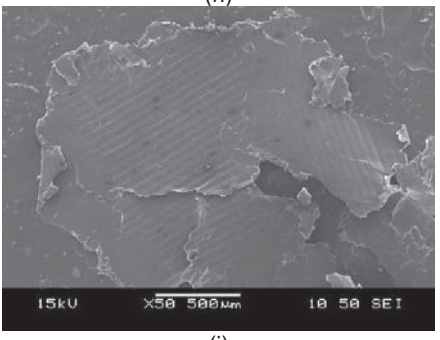

(j)

Figure 6.15. SEM micrographs from the debris of neat PTFE (a), PTFE/graphene-0.25 (b), PTFE/graphene-1 (c), PTFE/graphene-4 (d), PTFE/Al_2O_3-1 (e), PTFE/Al_2O_3-4 (f), PTFE/BA80-1 (g), PTFE/BA80-4 (h), PTFE/MG70-1 (i) and PTFE/MG70-4 (j) composites against 42CrMo4 counterfaces (Phase 1, Chapter 3.3.6.1).

6.3.2.5. Wear-induced crystallisation

The wear-induced crystallisation of the unfilled/filled PTFE materials was investigated by DSC (Protocol 1, Chapter 3.2.4). Table 5.5 introduces the DSC results of the unworn samples (Chapter 5.3.6); these samples were later tested against 42CrMo4 steel discs. Table 6.3 shows the DSC results of the polymer debris (42CrMo4 counterface).

Table 6.3. DSC results of the filled/unfilled PTFE debris (Phase 1, Chapter 3.3.6.1), applying Protocol 1 for the DSC analysis (Chapter 3.2.4). Here the enthalpy of fusion at the first heating cycle was evaluated between 300°C and 370°C.

Polymer debris (42CrMo4)	First heating			
	Initial temperature of melting (°C)	Melting peak temperature (°C)	Enthalpy of fusion (J/g)	Degree of crystallinity (%)
PTFE	327.6	334.2	54.55	79.1
PTFE/graphene-0.25	327.3	332.9	53.21	77.3
PTFE/graphene-1	327.0	332.6	53.96	79.0
PTFE/graphene-4	322.6	327.8	55.87	84.3
PTFE/graphene-8	---	---	---	---
PTFE/graphene-16	---	---	---	---
PTFE/Al_2O_3-1	317.2	327.2	51.39	75.2
PTFE/Al_2O_3-4	---	---	---	---
PTFE/BA80-1	326.1	333.5	52.95	77.5
PTFE/BA80-4	323.8	333.8	52.79	79.7
PTFE/BA80-8	321.9	326.4	49.65	78.2
PTFE/BA80-16	321.1	326.9	46.45	80.1
PTFE/MG70-1	326.0	334.0	47.96	70.2
PTFE/MG70-4	325.9	334.9	56.06	84.6
	Second heating			
PTFE	324.9	327.7	46.58	67.5
PTFE/graphene-0.25	325.1	327.9	48.64	70.7
PTFE/graphene-1	325.3	327.9	49.11	71.9
PTFE/graphene-4	324.7	327.2	52.89	79.8
PTFE/graphene-8	---	---	---	---
PTFE/graphene-16	---	---	---	---
PTFE/Al_2O_3-1	323.7	326.8	56.67	83.0
PTFE/Al_2O_3-4	---	---	---	---
PTFE/BA80-1	324.9	327.6	45.80	67.0
PTFE/BA80-4	325.7	327.9	53.31	80.5
PTFE/BA80-8	324.8	326.7	51.10	80.5
PTFE/BA80-16	324.8	326.7	51.47	88.8
PTFE/MG70-1	323.1	327.3	42.59	62.3
PTFE/MG70-4	324.6	327.7	49.34	74.5
	First cooling			
	Initial temperature of crystallisation (°C)	Crystallisation peak temperature (°C)	Enthalpy of crystallisation (J/g)	Degree of crystallinity (%)
PTFE	314.8	311.2	44.81	64.9
PTFE/graphene-0.25	315.5	311.9	46.12	67.0
PTFE/graphene-1	316.0	313.3	49.95	73.1
PTFE/graphene-4	320.2	317.7	46.57	70.3
PTFE/graphene-8	---	---	---	---
PTFE/graphene-16	---	---	---	---
PTFE/Al_2O_3-1	314.2	312.0	53.25	78.0
PTFE/Al_2O_3-4	---	---	---	---
PTFE/BA80-1	314.8	311.7	44.85	65.7
PTFE/BA80-4	315.8	313.5	51.73	78.1
PTFE/BA80-8	317.4	315.0	50.30	79.2
PTFE/BA80-16	317.7	316.1	47.89	82.6
PTFE/MG70-1	315.4	311.6	39.20	57.4
PTFE/MG70-4	316.7	313.0	49.27	74.4

The analysed unworn specimens and the wear debris come from the same polymer sample. The DSC specimens of the unworn material were cut from the opposite (unworn) side of the tested sample. Table B.19 and B.20 refer to polymer samples tested against 304 and 34CrNiMo6 counterface material. The DSC analysis did not include the debris of PTFE/graphene-8, PTFE/graphene-16 and PTFE/Al_2O_3-4 polymers as these materials had low wear rate; in this way, the amount of the formed debris was not sufficient for DSC analysis. In case of 34CrNiMo6 steel counterface, PTFE/graphene-4 debris was neither analysed due to its low wear rate.

The initial temperature of melting and the melting peak temperature of debris were higher both in the first and second heating cycle compared to the unworn material (Table 5.5, 6.3, B.18, B.19 and Figure 6.16). The debris also had a higher initial temperature of crystallisation and crystallisation peak temperature compared to the unworn materials. It means that the crystallisation process is initiated sooner in case of the debris compared to the original unworn samples (Table 5.5, 6.3, B.18, B.19).

In the first heating cycle, the degree of crystallinity of the debris increased between 23% and 42% compared to the unworn samples (Table 6.4). This increasing can come from the different thermal and mechanical antecedents. The surface temperature during wear tests can be so high which can affect the morphological structure of PTFE materials. Furthermore, the applied pressure and the sliding motion can also align the molecular chains due to the high shear stress during the wear process.

The increase of the degree of crystallinity was also confirmed by the results of the second heating cycle where, after the first melt, all the analysed samples had the same thermal history. In this way, the thermal history or the molecular chain aligning of the debris cannot be the reason for this significant increase of the degree of crystallinity. In the second heating cycle, the debris had 24-49% higher degree of crystallinity than the unworn samples (Table 6.4). The degree of crystallinity evaluated from the enthalpy of crystallisation also had an increase between 20% to 49% compared to the unworn samples (Table 6.4).

From these results, it can be concluded that this significant increase in the degree of crystallinity comes from the influence of high shear stress during the wear process. It is well known from the literature [1, 2, 5] that during wear process, the PTFE molecular chains undergo mechanical chain scission. This mechanical chain scission can cause a significant molecular length decrease in the formed debris. These shorter molecular chains of the debris can more efficiently reach an aligned arrangement than the longer chains of the unworn materials. In this way, the degree of crystallinity will be higher in both of the first and the second heating cycle.

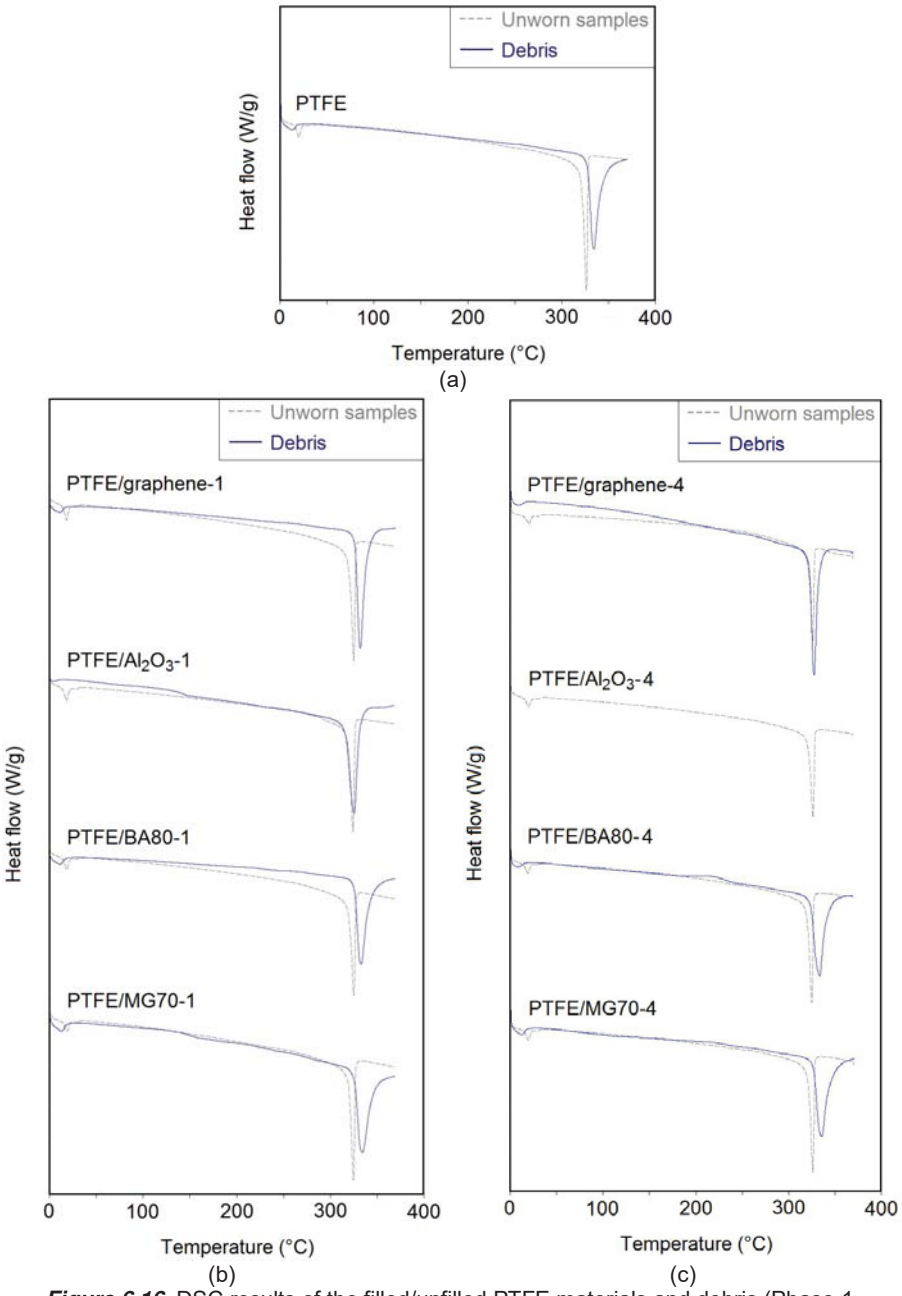

Figure 6.16. DSC results of the filled/unfilled PTFE materials and debris (Phase 1, Chapter 3.3.6.1), applying Protocol 1 for the DSC analysis (Chapter 3.2.4). Neat PTFE (a), PTFE with 1 wt% filler content (b) and PTFE with 4 wt% filler content (c), first heating cycle.

Table 6.4. DSC comparison of unworn polymer samples with their debris (Protocol 1, Chapter 3.2.4). Polymer samples were tested against 42CrMo4/304/34CrNiMo6 counterface material (Phase 1 and 2, Chapter 3.3.6.1 and 3.3.6.1).

Materials	Counterface material	Degree of crystallinity – increase = debris (%) – unworn (%)		
		First heating (%)	First cooling (%)	Second heating (%)
PTFE	42CrMo4	25.7	19.7	24.1
PTFE/graphene-0.25	42CrMo4	30.1	24.1	30.4
PTFE/graphene-1	42CrMo4	27.8	29.0	28.0
PTFE/graphene-4	42CrMo4	34.4	29.6	38.2
PTFE/graphene-8	42CrMo4	---	---	---
PTFE/graphene-16	42CrMo4	---	---	---
PTFE/Al_2O_3-1	42CrMo4	23.3	36.6	41.6
PTFE/Al_2O_3-4	42CrMo4	---	---	---
PTFE/BA80-1	42CrMo4	30.7	27.1	27.3
PTFE/BA80-4	42CrMo4	32.7	35.7	39.8
PTFE/BA80-8	42CrMo4	27.5	33.4	37.5
PTFE/BA80-16	42CrMo4	32.2	39.9	48.5
PTFE/MG70-1	42CrMo4	30.1	21.6	26.7
PTFE/MG70-4	42CrMo4	35.1	30.3	31.4
PTFE	304	37.1	29.1	28.1
PTFE	34CrNiMo6	36.6	24.9	29.2
PTFE/graphene-4	304	36.5	36.6	34.5
PTFE/graphene-4	34CrNiMo6	---	---	---
PTFE/Al_2O_3-4	304	---	---	---
PTFE/Al_2O_3-4	34CrNiMo6	---	---	---
PTFE/BA80-4	304	41.3	48.8	49.1
PTFE/BA80-4	34CrNiMo6	35.4	41.2	44.7

Table 6.5 introduces the calculated molecular weight of the unworn unfilled/filled PTFE samples and their debris. The molecular weight and in this way, the length of the PTFE molecular chains in the debris decreased by 1-2 orders of magnitude compared to the unworn materials. From the results, it can be seen that filled PTFE had a more significant decrease in molecular weight than the reference PTFE. The increase of filler content further decreased the molecular weight due to the hard particles which damaged with a higher rate the molecular chains. The details about the molecular weight calculation method can be found in Chapter 3.2.4. In general, the filler content also influences the calculated degree of crystallinity but here the difference between the filler content of the debris and the unworn material is negligible compared to the significant increase of the degree of crystallinity (Chapter 6.3.2.6). From the presented results, it can be concluded that the degree of crystallinity and the morphological structure of the tested materials changed during the wear process. It can influence the mechanical features as well. In case of a sliding bearing, as an example, after the first running period, the introduced characteristics of the PTFE top surface will change. It means that for the second running period the contact surface will have different morphological structure and mechanical features, which can influence the further tribological performance.

Table 6.5. The calculated molecular weight of unworn polymer samples compared to their debris. Polymer samples were tested against 42CrMo4/304/34CrNiMo6 counterface material (Phase 1 and 2, Chapter 3.3.6.1 and 3.3.6.2).

Materials	Counterface material	First cooling		
		Molecular weight - unworn (g/mol)	Molecular weight - debris (g/mol)	Molecular weight = debris/unworn (%)
PTFE	42CrMo4	6.57E+06	1.02E+06	15.6
PTFE/graphene-0.25	42CrMo4	8.78E+06	8.84E+05	10.1
PTFE/graphene-1	42CrMo4	8.03E+06	5.90E+05	7.4
PTFE/graphene-4	42CrMo4	1.47E+07	8.74E+05	5.9
PTFE/graphene-8	42CrMo4	1.82E+07	---	---
PTFE/graphene-16	42CrMo4	2.32E+07	---	---
PTFE/Al_2O_3-1	42CrMo4	1.11E+07	4.24E+05	3.8
PTFE/Al_2O_3-4	42CrMo4	8.89E+06	---	---
PTFE/BA80-1	42CrMo4	1.60E+07	1.03E+06	6.4
PTFE/BA80-4	42CrMo4	1.19E+07	5.08E+05	4.3
PTFE/BA80-8	42CrMo4	1.03E+07	6.13E+05	5.9
PTFE/BA80-16	42CrMo4	2.58E+07	8.65E+05	3.3
PTFE/MG70-1	42CrMo4	2.36E+07	2.06E+06	8.7
PTFE/MG70-4	42CrMo4	9.75E+06	6.53E+05	6.7
PTFE	304	1.27E+07	7.53E+05	5.9
PTFE	34CrNiMo6	8.86E+06	8.27E+05	9.3
PTFE/graphene-4	304	1.12E+07	4.56E+05	4.1
PTFE/graphene-4	34CrNiMo6	2.12E+07	---	---
PTFE/Al_2O_3-4	304	1.12E+07	---	---
PTFE/Al_2O_3-4	34CrNiMo6	1.18E+07	---	---
PTFE/BA80-4	304	1.73E+07	2.70E+05	1.6
PTFE/BA80-4	34CrNiMo6	1.23E+07	3.64E+05	3.0

6.3.2.6. Filler accumulation in the tested polymers

The aluminium accumulation in the worn polymer surface and debris was investigated by EDS analysis (Table 6.6 and 6.7). On the contact surfaces of the worn samples, filler accumulation was observed. In case of PTFE/Al_2O_3-4 polymer samples, the worn surfaces tested against 42CrMo4, 304 and 34CrNiMo6 steel discs, had ~82%, ~216% and ~118% higher aluminium content than the original unworn surfaces, respectively. In case of PTFE/BA80-4 polymer samples, the worn surfaces tested against 42CrMo4, 304 and 34CrNiMo6 steel discs, had ~262%, ~310% and ~303% higher aluminium content than the original unworn surfaces, respectively. In contrast to this, the formed debris of PTFE/Al_2O_3-4 polymer samples contains ~82%, ~59% and ~81% less aluminium than the original unworn samples, in case of 42CrMo4, 304 and 34CrNiMo6 steel discs, respectively. This filler content decrease cannot be seen in case of PTFE/BA80-4 polymer debris.

Table 6.6. EDS analysis of unworn samples, contact surfaces and debris (3 MPa contact pressure and 0.1 m/s sliding speed).

Materials	Counterface material	Aluminium content Unworn (%)	Aluminium content Worn surface (%)	Aluminium content Debris (%)	Iron (Fe) content Worn surface (%)
PTFE/Al_2O_3-4	42CrMo4	2.76	5.02	0.49	9.63
PTFE/Al_2O_3-4	304	2.32	7.34	0.94	13.63
PTFE/Al_2O_3-4	34CrNiMo6	2.87	6.27	0.55	9.80
PTFE/BA80-4	42CrMo4	2.14	7.75	1.97	~0
PTFE/BA80-4	304	2.04	8.37	2.56	~0
PTFE/BA80-4	34CrNiMo6	1.93	7.77	1.89	~0

Table 6.7. Aluminium content increase on the worn surfaces compared to the unworn materials (3 MPa contact pressure and 0.1 m/s sliding speed).

Materials	Counterface material	Aluminium content = worn/unworn (%)
PTFE/Al_2O_3-4	42CrMo4	181.9
PTFE/Al_2O_3-4	304	316.4
PTFE/Al_2O_3-4	34CrNiMo6	218.5
PTFE/BA80-4	42CrMo4	362.1
PTFE/BA80-4	304	410.3
PTFE/BA80-4	34CrNiMo6	402.6

The EDS analysis of PTFE/Al_2O_3-4 transfer layer on the polymer sample can be seen in Figure 6.17, where the applied counterface steel was 42CrMo4. Interestingly, Fe content around ~10% was also observed on the polymer contact surface, which comes from the steel counterface in case of all three kinds of steels. Figure 6.17 (c) indicates that the lighter areas of Figure 6.17 (a) have significant Fe content. The reason for this Fe content can be that during wear the hard alumina fillers can damage and partly remove the oxide layer of the steel counterface. The measured Vickers hardness of 42CrMo4/34CrNiMo6/304 steel counterfaces were 308/363/227 (HV 10), respectively, while according to the literature the Vickers hardness of alumina is between 1400 and 1800 (HV 10) [6]. On the transfer layer of PTFE/Graphene-4, PTFE/BA80-4 and PTFE/MG70-4 polymer samples, no Fe content was registered due to the less hard filler particles and relatively high wear rate of these samples. In other words, after the wear test of PTFE/Al_2O_3-4 polymer, an extremely low amount of material was removed from the polymer sample. In this way, the contact layer of PTFE/Al_2O_3-4 polymer could collect more Fe without losing the Fe rich top layer during the wear mechanism of the polymer.

The more significant aluminium and iron content were also confirmed by FTIR spectroscopy (Figure 6.18 and 6.19). The new peaks from the iron content can only be seen in Figure 6.18 (PTFE/Al_2O_3-4). The peaks of aluminium bonds are more intensive in case of the transfer layer (red) than in the bulk material (blue). The hydroxyl (OH) bonds of PTFE/BA80-4 transfer layer are also more visible compared to the unworn material due to the filler accumulation.

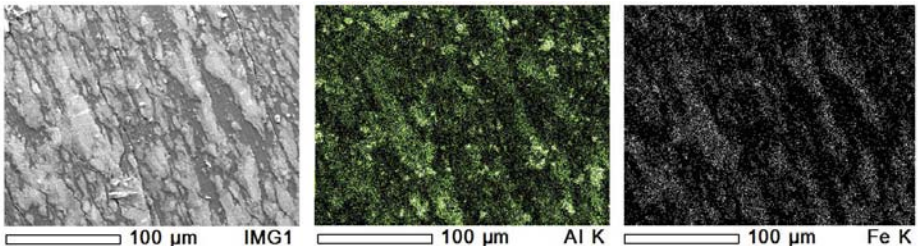

(a) (b) (c)

Figure 6.17. EDS analysis of PTFE/Al_2O_3-4 transfer layer on the polymer surface (42CrMo4 steel counterface, 3 MPa contact pressure and 0.1 m/s sliding speed).

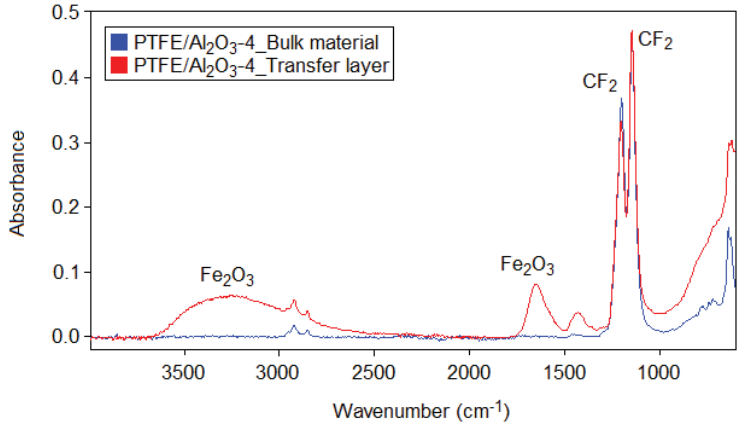

Figure 6.18. FTIR spectra of PTFE/Al_2O_3-4 bulk material (blue) and transfer layer (red). 304 steel counterface, 3 MPa contact pressure and 0.1 m/s sliding speed.

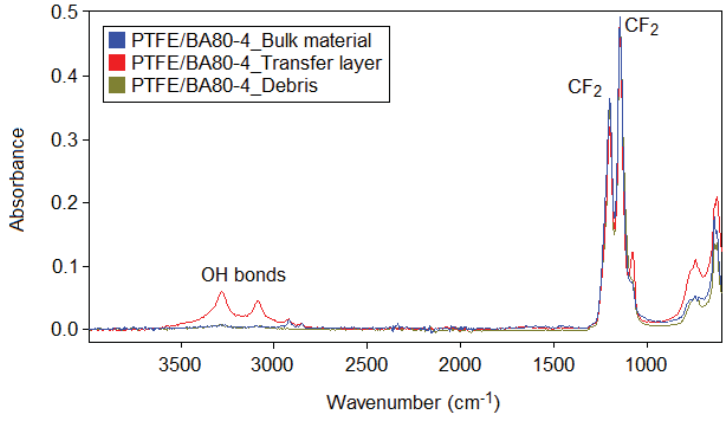

Figure 6.19. FTIR spectra of PTFE/BA80-4 bulk material (blue), transfer layer (red) and debris (olive). 304 steel counterface, 3 MPa contact pressure and 0.1 m/s sliding speed.

The filler content of worn surface of the polymer samples with 0.1/1/10/100/200/400 m sliding distance were analysed to collect more detailed information about the process of filler accumulation (Table 6.8 and 6.9). The filler content reached a significant increase even after 10 m sliding distance, and after this 10 m, there is only a slight increase in filler content. It means that almost the total registered accumulation occurs in the first 10 m. It indicates that a dynamic balance is reached between the detached and the eliminated wear debris, in other words, the recycled and the lost wear particles are in balance, which is in agreement with the solid third-body concept (Chapter 1.1) [7, 8].

Table 6.8. EDS analysis results of unworn samples and contact surfaces (3 MPa contact pressure and 0.1 m/s sliding speed).

Materials	Counterface material	Sliding distance (m)	Aluminium content Unworn (%)	Aluminium content Worn surface (%)	Iron (Fe) content Worn surface (%)
PTFE/Al_2O_3-4	42CrMo4	0.1	2.54	3.28	0.85
PTFE/Al_2O_3-4	42CrMo4	1	3.06	4.23	2.59
PTFE/Al_2O_3-4	42CrMo4	10	3.15	9.06	4.01
PTFE/Al_2O_3-4	42CrMo4	100	2.91	7.89	3.85
PTFE/Al_2O_3-4	42CrMo4	200	3.45	10.45	5.26
PTFE/Al_2O_3-4	42CrMo4	400	3.40	11.31	5.71
PTFE/BA80-4	42CrMo4	0.1	2.01	2.53	~0
PTFE/BA80-4	42CrMo4	1	2.10	2.64	~0
PTFE/BA80-4	42CrMo4	10	1.90	6.34	~0
PTFE/BA80-4	42CrMo4	100	1.89	7.74	~0
PTFE/BA80-4	42CrMo4	200	2.22	7.81	~0
PTFE/BA80-4	42CrMo4	400	1.97	7.40	~0

Table 6.9. Aluminium content increase on the worn surfaces compared to the unworn materials (3 MPa contact pressure and 0.1 m/s sliding speed).

Materials	Counterface material	Sliding distance (m)	Aluminium content = worn/unworn (%)
PTFE/Al_2O_3-4	42CrMo4	0.1	129.1
PTFE/Al_2O_3-4	42CrMo4	1	138.2
PTFE/Al_2O_3-4	42CrMo4	10	287.6
PTFE/Al_2O_3-4	42CrMo4	100	271.1
PTFE/Al_2O_3-4	42CrMo4	200	302.9
PTFE/Al_2O_3-4	42CrMo4	400	332.6
PTFE/BA80-4	42CrMo4	0.1	125.9
PTFE/BA80-4	42CrMo4	1	125.7
PTFE/BA80-4	42CrMo4	10	333.7
PTFE/BA80-4	42CrMo4	100	409.5
PTFE/BA80-4	42CrMo4	200	351.8
PTFE/BA80-4	42CrMo4	400	375.6

Figure 6.20 displays the contact surfaces of PTFE/Al_2O_3-4 polymer samples, the applied counterface was 42CrMo4 steel.

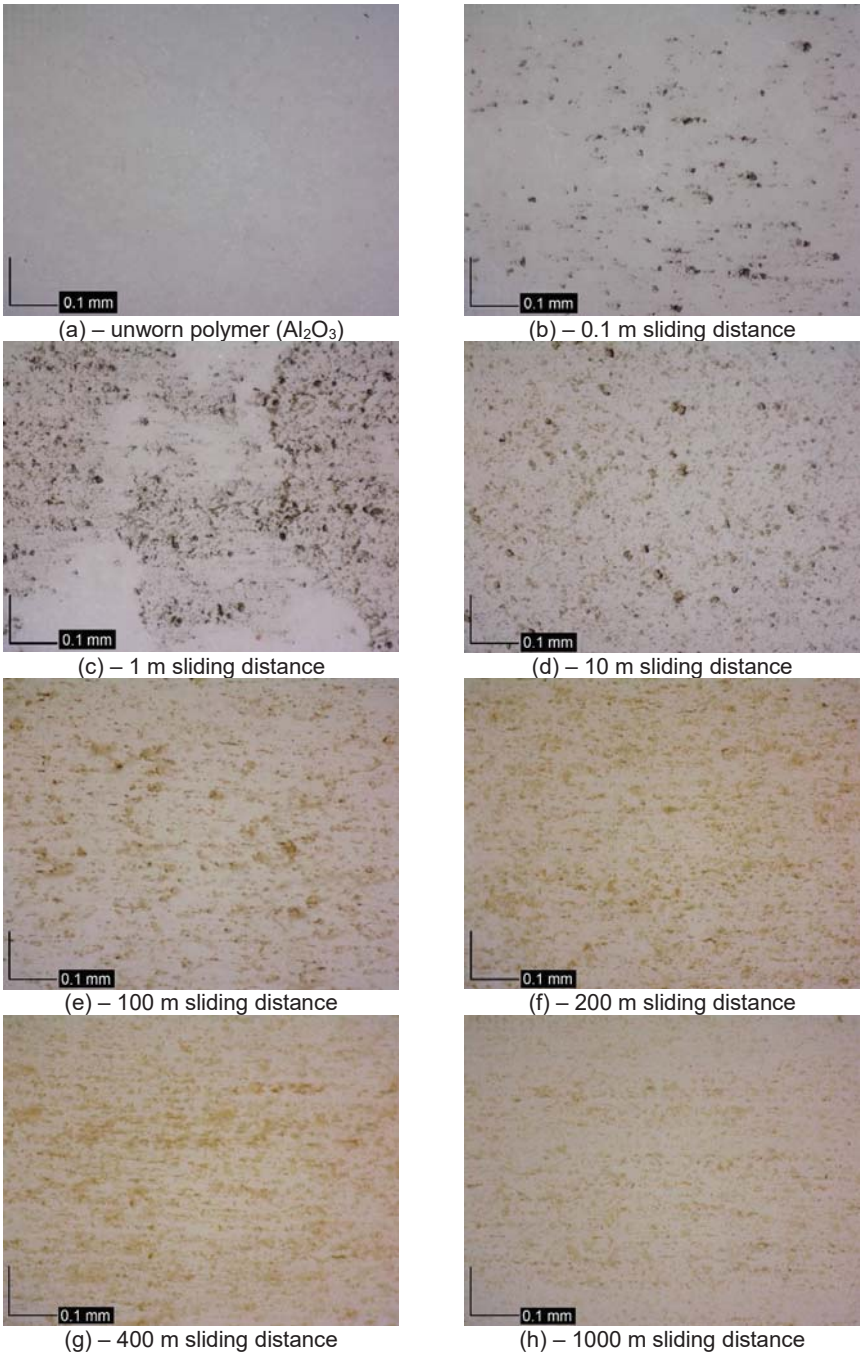

(a) – unworn polymer (Al_2O_3) (b) – 0.1 m sliding distance

(c) – 1 m sliding distance (d) – 10 m sliding distance

(e) – 100 m sliding distance (f) – 200 m sliding distance

(g) – 400 m sliding distance (h) – 1000 m sliding distance

Figure 6.20. Iron oxide accumulation on PTFE/Al_2O_3-4 polymer contact surface (42CrMo4 steel counterface, 3 MPa contact pressure and 0.1 m/s sliding speed).

The original, unworn polymer surface can be seen in Figure 6.20 (a) while the worn contact surfaces after 0.1/1/10/100/200/400/1000 m sliding distance are introduced in Figure 6.20 (b-h), respectively. In Figure 6.20 (b) it can be seen that even after 0.1 m sliding distance black spots appeared in the polymer contact surface which comes from the oxide layer of the steel counterface. In Figure 6.20 (b-d), an accumulation of the spots can be observed, which is in agreement with the results of EDS measurements (Table 6.8). After 10 m sliding distance (Figure 6.20 (d-h)) the black colour of iron oxide particles became orange. This change in their colour shows that the removed iron oxide particles are modified during the wear process. The black colour indicates that the iron oxide particles include basically Fe_3O_4 (iron(II,III) oxide) molecules; in other words, the original stage is magnetite. The orange colour indicates high Fe_2O_3 (iron(III) oxide) content which means that the iron oxide goes through an oxidation process during wear. Focusing on Fe_2O_3, λ-Fe_2O_3 can be found in maghemite (brown colour), and α-Fe_2O_3 are in hematite (red colour). Equation (6.2)-(6.4) introduce the background of these stages:

$$4\ Fe_3O_4 + O_2 \rightarrow 6\ \lambda\text{-}Fe_2O_3\ (200°C\text{-}400°C) \quad (6.2)$$

$$\lambda\text{-}Fe_2O_3 \rightarrow \alpha\text{-}Fe_2O_3\ (375°C\ \text{-}550°C) \quad (6.3)$$

$$4\ Fe_3O_4 + O_2 \rightarrow 6\ \alpha\text{-}Fe_2O_3\ (\text{from } 550°C) \quad (6.4)$$

These temperature values in Equation (6.2)-(6.4) indicate that the local contact temperature of the contact surfaces during the wear process reached a minimum of 375-400°C.

In case of PTFE/BA80-4 polymer samples, none of the contact surfaces included iron according to the EDS and optical measurements as well. It can have two different reasons, the first is that PTFE/BA80-4 sample had much higher wear rate compared to PTFE/Al_2O_3-4, in this way the top layer of the polymer with the iron content is removed. Here it is important to mention that even after 0.1/1/10 m sliding distance, no iron content was detected on the PTFE/BA80-4 polymer contact surfaces. In contrast with this, iron content accumulation was registered in the given sliding distances on the PTFE/Al_2O_3-4 contact surfaces. It means that even if a more significant material depth was removed from PTFE/BA80-4 samples, the worn contact surface of these polymers should have some iron content as the iron oxide is removed continuously from the counterface. In this way, the second potential explanation is that Al_2O_3 filler contains abrasive and hard particles. These particles can damage and remove the peaks of the steel counterface, resulting in an iron-oxide accumulation on the polymer contact surface.

Figure 6.21 and Table 6.10 shows the results of horizontal EDS mapping of PTFE/Al_2O_3-4 contact surface. These values indicate that the filler accumulation is independent from the sliding direction or from the position of the contact layer.

Table 6.10. EDS analysis of PTFE/Al_2O_3-4 contact surface, in 5 different position (42CrMo4 steel counterface, 3 MPa contact pressure and 0.1 m/s sliding speed).

Materials	Location	Aluminium content Worn surface (%)	Iron (Fe) content Worn surface (%)
PTFE/Al_2O_3-4	Centre	11.02	4.13
PTFE/Al_2O_3-4	0°	11.14	3.88
PTFE/Al_2O_3-4	90°	11.03	3.63
PTFE/Al_2O_3-4	180°	10.90	4.06
PTFE/ Al_2O_3-4	270°	11.06	3.59

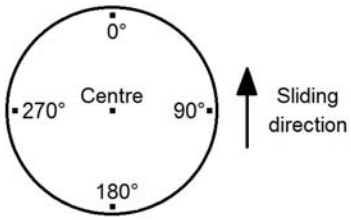

Figure 6.21. The measured five different positions of the transfer layer for EDS mapping.

Figure 6.22 indicates the aluminium content accumulation of PTFE/Al_2O_3-4 contact surface. Figure 6.22 (a) introduce the unworn surface while Figure 6.22 (b) shows the contact layer of the polymer sample.

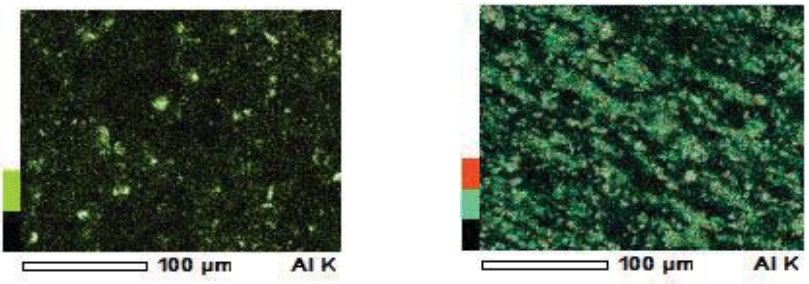

(a) (b)

Figure 6.22. EDS mapping of PTFE/Al_2O_3-4 polymer unworn sample (a) and contact layer (b). 1000 m sliding distance (42CrMo4 steel counterface, 3 MPa contact pressure and 0.1 m/s sliding speed).

A potential explanation for the alumina filler accumulation is that the softer PTFE particles can be torn easier from the contact surface than the hard metal oxide filler particles. In this way, the filler content of the contact surface is higher due to the still remaining fillers. Some of the torn or broken filler particles can also stick again as back transfer into the softer PTFE due to the high pressure and high temperature. This mechanism is illustrated in Figure 6.23. As less filler is removed from the contact surface of the polymer during wear, it is evident that the debris had lower filler content.

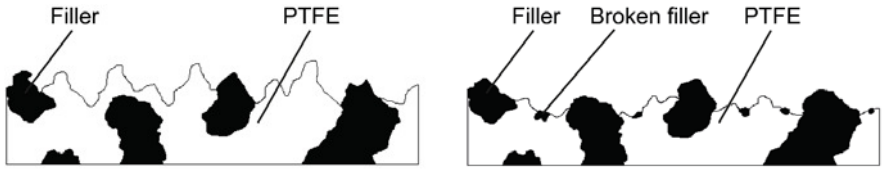

(a) (b)

Figure 6.23. Illustration of wear mechanism and filler accumulation of the top surface.

As on the polymer surfaces of PTFE/Al_2O_3-4 samples iron-oxide layer was detected, it can be assumed that the hard alumina particles significantly damage the steel counterfaces. All kinds of steel surface damage have to be avoided as in general the polymer surface (e.g. bearings and seals) is the sacrificial part, the softer polymer is required to wear off instead of the steel counterfaces (e.g. shafts) as their replacement is more complex and their prices are much higher compared to the bearings or the seals. The steel counterfaces were analysed by white-light interferometry and no damages were detected on the contact surfaces. Some examples of PTFE/Al_2O_3-4 samples are introduced in Figure 6.24.

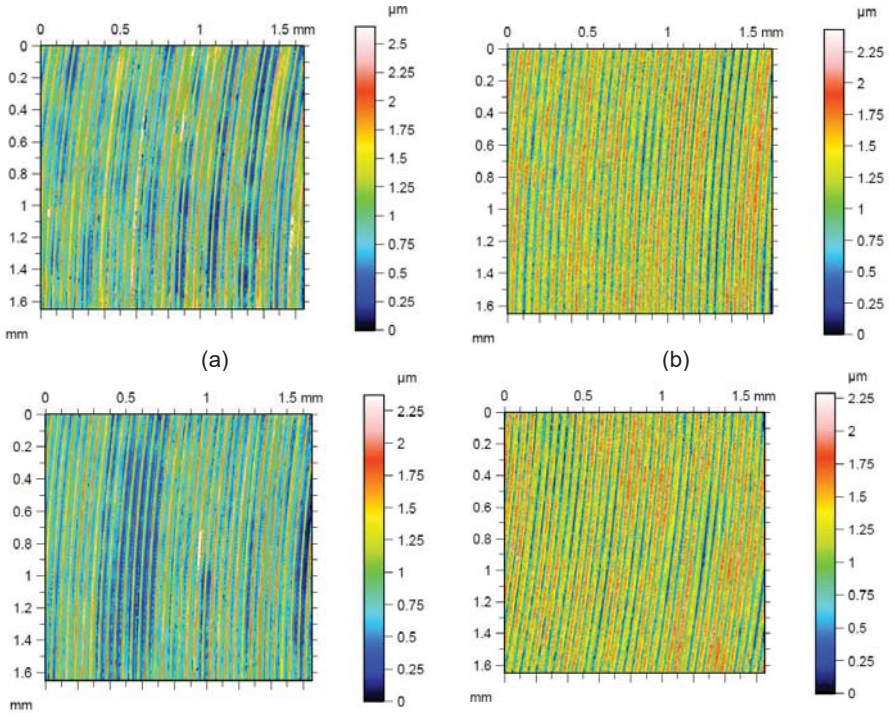

Figure 6.24. White light interferometer maps from the unworn (a), (c) and worn (b), (d) PTFE/Al_2O_3-4 steel counterfaces (42CrMo4), 3 MPa contact pressure, 0.1 m/s sliding speed, 1000 m sliding distance.

6.4. Conclusions

This chapter introduced the friction and wear characterisation and the transfer layer formation of unfilled and mono-filled PTFE (Phase 1 and 2, Chapter 3.3.6).

- PTFE/Al_2O_3-4 samples achieved the lowest wear rate with a decrease of more than two orders of magnitude compared to the neat PTFE independently of the applied steel counterfaces (42CrMo4/304/34CrNiMo6). Graphene in 4/8/16 wt% filler content reached 1-2 orders of magnitude reduction in wear rate. As Chapter 5 introduced, this ultra-low wear rate cannot be indicated by the modified hardness, compressive/shear/tensile properties or thermal conductivity. Independently of the applied fillers and steel counterface materials, the coefficient of friction did not change significantly compared to the neat PTFE.
- As Al_2O_3 and graphene filled PTFE specimens reached the lowest wear rate, these fillers were chosen to develop hybrid-filled PTFE materials. Chapter 7 introduces the material and tribological characterisation of these hybrid-filled PTFE samples.
- After 10 m sliding distance, the dominant surface pattern of the polymer samples becomes similar to the steel counterface. It means that if the sliding distance is 1000 m, the original rough surface quality of the polymer materials can influence the wear process only at the first ~1% of the sliding distance.
- After the wear tests, the degree of crystallinity of the debris increased by between 23% and 42% compared to the unworn samples. This increase comes from the influence of high shear stress in the wear process which causes mechanical chain scission in the molecular chains. Due to this phenomena, the molecular length shortened in the formed debris, which increased the degree of crystallinity.
- This chapter confirmed that the high wear rate improvement of PTFE/Al_2O_3-4 sample comes from the modified transfer layer formation. The first influencing factor is that this material had the smallest wear debris, with a maximal size of 50 µm. The second important factor is that on the contact surfaces of the worn samples, filler accumulation was observed. The filler content reached a significant increase even after 10 m sliding distance. The reason for this high filler accumulation is that the softer PTFE particles can be torn easier from the contact surface than the hard metal oxide filler particles. In this way, the filler content of the polymer contact surface is higher due to the still remaining fillers, which can serve as a more protective layer. The broken filler particles can also penetrate into the softer PTFE due to the high pressure and high temperature. The third wear rate decreasing factor is the iron accumulation, which was observed on the top layer of PTFE/Al_2O_3-4 polymers; the explanation for this phenomenon is that Al_2O_3 filler contains abrasive and hard particles. These particles can damage and

remove the peaks of the steel counterface, resulting in an iron-oxide accumulation on the polymer contact surface, which can enhance the protective role of the layer. No iron accumulation was registered in case of graphene, BA80 and MG70 fillers.

- The graphene decreased the wear rate in 4/8/16 wt% filler content as the debris formation was modified due to the applied filler resulted in smaller debris. As both graphene and PTFE contain carbon, it was not possible to investigate the filler accumulation on the top surface.

6.5. References

[1] B.A. Krick, J.J. Ewin, G.S. Blackman, C.P. Junk, W.G. Sawyer: Environmental dependence of ultra-low wear behavior of polytetrafluoroethylene (PTFE) and alumina composites suggests tribochemical mechanisms. Tribology International 51 (2012) 42–46.

[2] E. Padenko, L.J. Van Rooyen, B. Wetzel, J. Karger-Kocsis: “Ultralow” sliding wear polytetrafluoro ethylene nanocomposites with functionalized graphene. Journal of Reinforced Plastics and Composites 35 (2016) 892–901.

[3] S.K. Sinha, B.J. Briscoe: Polymer tribology. Imperial College Press, London, United Kingdom (2009).

[4] E.F. Finkin: Surface energy and the theory of the friction of solids. Applied Physics Letters 30 (1977) 436.

[5] K.L. Harris, A.A. Pitenis, W.G. Sawyer, B.A. Krick, G.S. Blackman, D.J. Kasprzak, C.P Junk: PTFE tribology and the role of mechanochemistry in the development of protective surface films. Macromolecules 48 (2015) 3739–3745.

[6] https://www.bce-special-ceramics.com/comparison/bce-material-table.htm (21.01.2021).

[7] M. Godet: The third-body approach: a mechanical view of wear. Wear 100 (1984) 437-452.

[8] Y. Berthier: Maurice Godet's third body. The Third Body Concept: Interpretation of Tribological Phenomena, First edition, Elsevier Science (1996) 21-30.

CHAPTER 7

MATERIAL AND TRIBOLOGICAL CHARACTERISATION OF HYBRID-FILLED PTFE COMPOSITES

This chapter presents the material, friction and wear characterisation of the developed hybrid-filled PTFE tribo-composites. The second half of this chapter introduces the parametrical study of the well-performing materials focusing on the influence of contact pressure and sliding speed.

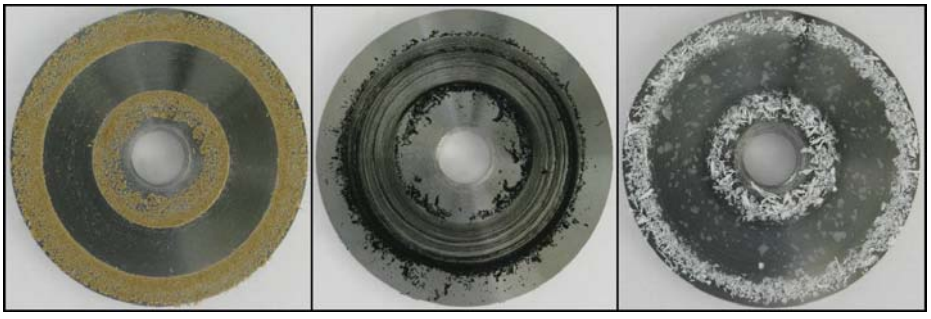

7.1. Introduction

As the use of graphene and (alumina) Al_2O_3 among the tested fillers the most efficiently decreased the wear rate of mono-filled polytetrafluoroethylene (PTFE), the goal of this chapter is to investigate the hybridisation of these fillers. Graphene/Al_2O_3 hybrid-filled PTFE composites were developed and investigated by material and tribological characterisation. The material characterisation includes the determination of density (porosity), thermal conductivity, hardness, compressive, shear and tensile properties. The tribological characterisation was carried out to measure and analyse the friction and wear properties and the transfer layer formation. A parametrical study of the best performing mono- and hybrid-filled PTFE, related to the influence of contact pressure and sliding speed, was also carried out. This section focuses on the results of Phase 3 and 4; more details about these phases can be found in Chapter 3.3.6.

7.2. Materials and methods

7.2.1. Materials and production method

Table 7.1 introduces the developed and investigated hybrid-filled PTFE samples (Phase 3, Chapter 3.3.6.3), while Table 7.2 shows mono- and hybrid-filled PTFE materials related to the parametrical study (Phase 4, Chapter 3.3.6.4). Detailed information about the matrix, fillers and production protocol can be found in Chapter 3.1.

Table 7.1. The developed and tested hybrid-filled PTFE samples (Phase 3, Chapter 3.3.6.3).

Materials	Matrix	Filler(s)	Filler content (wt%)
PTFE/G/A-0.25/4	PTFE	Graphene + alumina (Al_2O_3)	0.25 + 4
PTFE/G/A-2/2	PTFE	Graphene + alumina (Al_2O_3)	2 + 2
PTFE/G/A-4/4	PTFE	Graphene + alumina (Al_2O_3)	4 + 4

Table 7.2. The tested mono- and hybrid-filled PTFE samples (Phase 4, Chapter 3.3.6.4).

Materials	Matrix	Filler(s)	Filler content (wt%)
PTFE/Graphene-4	PTFE	Graphene	4
PTFE/Graphene-8	PTFE	Graphene	8
PTFE/Al_2O_3-4	PTFE	Alumina (Al_2O_3)	4
PTFE/G/A-4/4	PTFE	Graphene + alumina (Al_2O_3)	4 + 4

7.2.2. Material and tribological characterisation

The material characterisation was carried out with thermogravimetric analysis (TGA), density and thermal conductivity measurements, hardness and compressive/shear/tensile tests. The tribological characterisation and transfer analysis focused on the results of pin-on-disc tests, differential scanning calorimetry (DSC) and energy-dispersive X-ray spectroscopy (EDS).

Further information about the material and tribological characterisation, applied methods and equipment can be found in Chapter 3.2 and 3.3.

7.3. Results and discussion

7.3.1. Sensitivity analysis of the hybrid-filled PTFE materials

The sensitivity analysis of the hybrid-filled composites is focusing on the thermal stability of the fillers during the sintering process and on the influence of the dwelling time at maximal sintering temperature. The room temperature pressing of the hybrid-filled samples was carried out with 12.5 MPa pressure.

7.3.1.1. Sintering protocol

Table 7.3 shows the residual mass (m_r) of neat PTFE, graphene, Al_2O_3 and hybrid-filled PTFE. All the introduced results were measured by TGA, according to Protocol 2 (Chapter 3.2.14). The residual mass is evaluated at the beginning of the hold time, at the beginning of the cooling (after 2 hours heat dwelling) and after the final sintering process. In Table 7.3, the theoretical sample mass was calculated from the measured residual mass of neat PTFE and neat fillers. The highlighted numbers in Table 7.3 (Section 4) reflect those final m_r values, where the difference between theoretical and measured values was higher than 1%.

Table 7.3. Residual mass (m_r) during the sintering process, measured by TGA (Protocol 2, Chapter 3.2.14).

Materials	m_r at the beginning of hold time at 370°C (%)	m_r at the beginning of cooling at 370°C (%)	Final m_r after sintering (%)
Section 1: Neat PTFE and neat fillers – measured by TGA			
PTFE	100.00	99.97	99.99
Graphene	91.35	80.93	80.72
Al_2O_3	98.03	97.96	98.30
Section 2: Filled PTFE – measured by TGA			
PTFE/Graphene-4	99.59	98.86	98.86
PTFE/Graphene-8	99.04	97.63	97.62
PTFE/Al_2O_3-4	99.64	99.25	99.17
PTFE/G/A-0.25/4	99.97	99.07	98.79
PTFE/G/A-2/2	99.73	99.01	98.94
PTFE/G/A-4/4	99.44	98.22	97.99
Section 3: Calculated based on the filler contents and m_r in Section 1 – Theoretical values			
PTFE/Graphene-4	99.65	99.21	99.22
PTFE/Graphene-8	99.31	98.45	98.45
PTFE/Al_2O_3-4	99.92	99.89	99.92
PTFE/G/A-0.25/4	99.90	99.84	99.87
PTFE/G/A-2/2	99.79	99.55	99.57
PTFE/G/A-4/4	99.58	99.13	99.15
Section 4: Difference between theoretical and measured values (= Section 3 - Section 2)			
PTFE/Graphene-4	0.06	0.35	0.36
PTFE/Graphene-8	0.27	0.82	0.83
PTFE/Al_2O_3-4	0.28	0.64	0.75
PTFE/G/A-0.25/4	-0.07	0.77	***1.08 ****
PTFE/G/A-2/2	0.06	0.54	0.63
PTFE/G/A-4/4	0.14	0.91	***1.16 ****

As Table 7.3 shows, similarly to the mono-filled samples (Chapter 4.3.5.2), there is a gap between the calculated results of the theoretical and the measured residual mass of the developed composites. In case of all hybrid-filled PTFE samples, the measured residual mass was higher than it was expected from the mass loss of the PTFE, graphene and Al_2O_3 fillers.

7.3.1.2. Sintering protocol – extended heat dwelling (10 hours)

This section introduces the decomposition analysis of PTFE composites, measured by TGA, simulating a sintering process with 10 hours dwelling time at the maximal 370°C temperature (Protocol 3, Chapter 3.2.14). The residual mass was registered in Table 7.4 at the start of the dwelling time (0 h) and after 2/4/6/8/10 h dwelling time. With this long interval, it is possible to get a more detailed insight into the thermal stability of the composites during the sintering process.

As it can be seen in Table 7.4 and 7.5, the mass of hybrid-filled samples is considerably decreasing with increasing dwelling time during the full 10 hours. In contrast to this, only a slight mass loss was registered in case of unfilled PTFE and neat Al_2O_3, which are only 0.07% and 0.13% during the 10 hours dwelling time at 370°C temperature, respectively. The observed difference could come only from the graphene filler (as neat PTFE and neat Al_2O_3 had high thermal stability), but as it was represented in Chapter 4.3.5.3, the Al_2O_3 mono-filled PTFE also had a low thermal stability during the 10 hours dwelling time. The highest difference between the measured and theoretical values was registered for PTFE/G/A-4/4 sample (Table 7.5), with a value of 4.51%. This 4.51% mass loss of PTFE/G/A-4/4 sample is higher than the sum of the 0.81% mass loss of PTFE/Graphene-4 and the 2.07% mass loss of PTFE/Al_2O_3-4 (0.81 + 2.07 = 2.88%) but it is in line with the 4.54% mass loss of PTFE/Al_2O_3-8 (Table 4.8). These results clearly show that in case of the applied fillers, the longer is the dwelling time, the higher the decomposed material mass, which can have a negative effect on the final material properties.

Table 7.4. Registered residual mass during dwelling time at 370°C in air atmosphere, measured by TGA (Protocol 3, Chapter 3.2.14).

Materials	Residual mass (m_r) at elapsed dwelling time (%)					
	0 h	2 h	4 h	6 h	8 h	10 h
PTFE	99.96	99.92	99.91	99.90	99.90	99.89
Graphene	90.80	80.37	79.57	79.33	79.19	79.09
Al_2O_3	97.92	97.81	97.79	97.79	97.79	97.79
PTFE/Graphene-4	99.61	99.02	98.83	98.65	98.47	98.26
PTFE/Graphene-8	99.19	97.79	97.25	97.10	96.90	96.71
PTFE/Al_2O_3-4	99.87	99.44	99.02	98.58	98.16	97.73
PTFE/G/A-0.25/4	99.81	99.41	99.11	98.82	98.53	98.24
PTFE/G/A-2/2	99.78	99.03	98.53	98.00	97.46	96.87
PTFE/G/A-4/4	99.46	98.11	97.19	96.31	95.37	94.41

Table 7.5. Registered mass loss during the dwelling time at 370°C in air atmosphere, measured by TGA (Protocol 3, Chapter 3.2.14). The theoretical values in Column 3 are calculated based on the filler contents and mass loss of the neat PTFE and neat fillers. Column 4 introduces the difference between theoretical (Column 3) and measured values (Column 2).

Materials	Mass loss (0-10 h) Measured by TGA (%)	Mass loss (0-10 h) Theoretical (%)	Mass loss (0-10 h) Difference (%) = Measured – Theoretical
PTFE	0.07	---	---
Graphene	11.71	---	---
Al_2O_3	0.13	---	---
PTFE/Graphene-4	1.35	0.54	0.81
PTFE/Graphene-8	2.48	1.00	1.48
PTFE/Al_2O_3-4	2.14	0.07	2.07
PTFE/G/A-0.25/4	1.57	0.10	1.47
PTFE/G/A-2/2	2.91	0.30	2.61
PTFE/G/A-4/4	5.05	0.54	4.51

7.3.2. Material characterisation of the hybrid-filled PTFE materials

This section introduces the material characterisation focusing on the determination of density (porosity), thermal conductivity, hardness, compressive, shear and tensile properties.

7.3.2.1. Density

The density values of neat PTFE and hybrid-filled PTFE composites can be seen in Figure 7.1 and Table B.10. For the better comparison, graphene/Al_2O_3 mono-filled PTFE samples are also displayed in Figure 7.1.

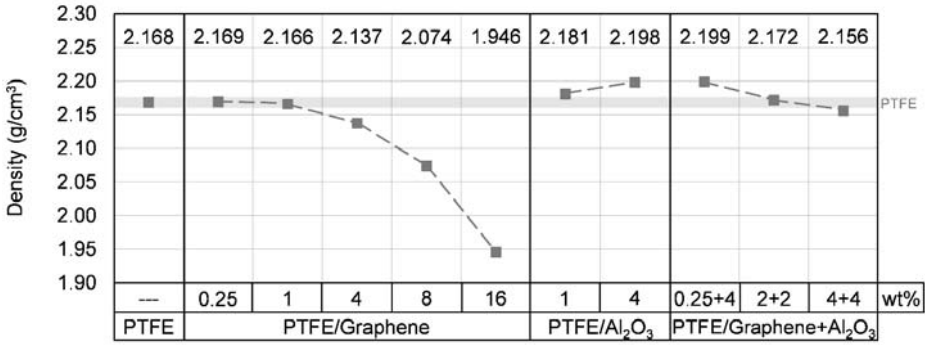

Figure 7.1. The density of unfilled and filled PTFE samples. The grey transparent line displays the measured density of the reference neat PTFE.

The fillers did not significantly modify the density of PTFE. PTFE/G/A-0.25/4 sample had 2.199 g/cm^3 density, which is similar to PTFE/Al_2O_3-4 material which reached 2.198 g/cm^3. The density of hybrid-filled PTFE samples decreased as the graphene content increases, but this

density reduction was compensated by Al_2O_3 filler. PTFE/G/A-2/2 and PTFE/G/A-4/4 materials had 2.172 g/cm^3 and 2.156 g/cm^3 density, respectively, while PTFE/Graphene-4 which includes only graphene filler reached 2.137 g/cm^3 density.

7.3.2.2. Thermal conductivity

The thermal conductivity of neat PTFE, graphene/Al_2O_3 mono-filled and hybrid-filled PTFE composites can be seen in Figure 7.2 and in Table B.10. The thermal conductivity of PTFE/Al_2O_3-4 and PTFE/G/A-0.25/4 samples were similar, both of them reached 0.265 W/mK, while PTFE/G/A-2/2 and PTFE/G/A-4/4 had 0.283 and 0.386 W/mK, respectively. As it is registered in graphene mono-filled PTFE, due to the high thermal conductivity of graphene, the increase of graphene content resulted in higher thermal conductivity in case of hybrid-filled PTFE as well. It means that graphene filler had a more dominant role in hybrid-filled composites compared to Al_2O_3. PTFE/G/A-4/4 had ~59% higher thermal conductivity compared to reference neat PTFE.

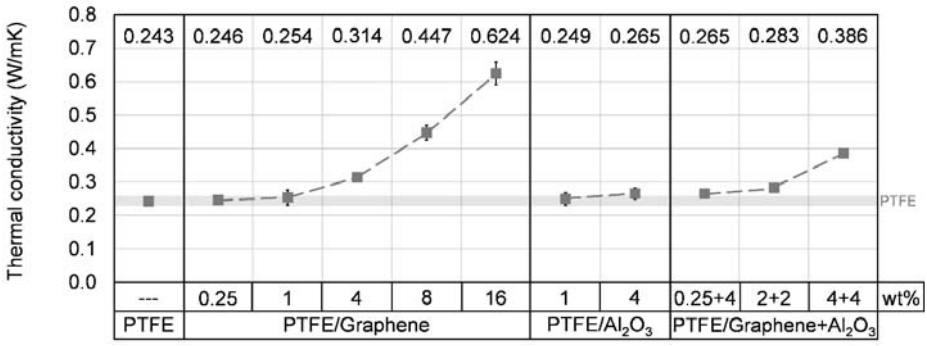

Figure 7.2. The thermal conductivity of unfilled and filled PTFE samples. The grey transparent line displays the measured thermal conductivity of the reference neat PTFE.

7.3.2.3. Hardness

The hardness of neat PTFE, graphene/Al_2O_3 mono-filled and hybrid-filled PTFE composites can be seen in Figure 7.3 and Table B.11. Al_2O_3 filler had a dominant influence on the hardness in case of the hybrid-filled composites. Similarly to mono-filled samples, the hardness is increasing as the Al_2O_3 filler content increases. PTFE/G/A-0.25/4, PTFE/G/A-2/2 and PTFE/G/A-4/4 samples had 56.6, 56.7 and 58.2 Shore-D hardness, respectively. Compared to the 54.3 Shore-D hardness of neat PTFE, the changes caused by the hybrid fillers are not remarkable.

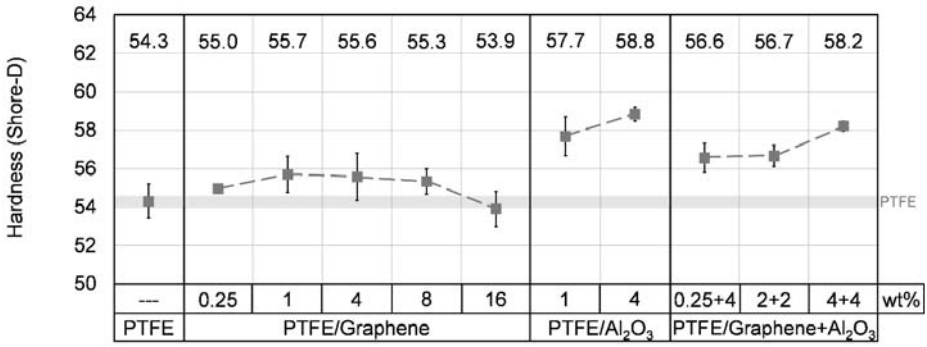

Figure 7.3. The hardness of unfilled and filled PTFE samples. The grey transparent line displays the measured hardness of the reference neat PTFE.

7.3.2.4. Compressive properties

The compressive properties of neat PTFE, graphene/Al_2O_3 mono-filled and hybrid-filled PTFE composites can be seen in Figure 7.4, Figure 7.5 and Table B.11. PTFE/Al_2O_3-1 and PTFE/Al_2O_3-4 samples reached higher compressive modulus compared to neat PTFE, while only a slight increase of the compressive stress was measured in these samples. Graphene with low filler content (0.25, 1 and 4 wt%) did not change the compressive properties remarkably compared to neat PTFE. All PTFE/G/A-0.25/4, PTFE/G/A-2/2 and PTFE/G/A-4/4 samples had slightly lower compressive modulus compared to neat PTFE. This phenomenon is not in agreement with the results of 1/4 wt% graphene/Al_2O_3 mono-filled samples but it is in line with the compressive modulus decreasing effect of graphene with high filler content (8/16 wt%). The observed changes in compressive stress at 5 and 10% deformation were similar to the tendency of compressive modulus; only a slight decrease was registered.

7.3.2.5. Shear properties

The shear properties of neat PTFE, graphene/Al_2O_3 mono-filled and hybrid-filled PTFE composites can be seen in Figure 7.4-7.6 and Table B.12. The main tendencies are similar to the mono-filled samples. The shear modulus and shear stress are increasing, and the elongation is decreasing as the filler content of hybrid-filled samples increases as it is expected from the results of mono-filled materials. The elongation of neat PTFE was 9.28%, while PTFE/G/A-0.25/4, PTFE/G/A-2/2 and PTFE/G/A-4/4 samples had significantly lower elongation such as 5.23, 3.99 and 3.09%, respectively. Their shear modulus improved with ~33%, 53% and 104%, respectively. The enhanced modulus values can be explained with the restricted molecular chain movements, which comes from the higher filler content.

It was not possible to reach a local maximal value for shear stress, as the elongation of PTFE based samples was remarkably high, and the displacement range of the tensile tester was

limited. In this way, the elongation was compared at 7 MPa stress as this level of shear stress was reached by all of the tested samples (Figure 7.6).

7.3.2.6. Tensile properties

The tensile properties of neat PTFE, graphene/Al_2O_3 mono-filled and hybrid-filled PTFE composites can be seen in Figure 7.4-7.6, Table 7.6 and B.13. The tendencies of the tensile stress at 2% and 5% strain, the tensile modulus and elongation at yield are in line with the results of shear tests (Chapter 7.3.2.5). Focusing on PTFE/G/A-0.25/4, PTFE/G/A-2/2 and PTFE/G/A-4/4 samples, the tensile modulus increased with ~33%, 73% and 123%, while the elongation at yield decreased with ~23%, 35% and 67%, respectively. It can be explained again with the restricted movement of the long PTFE molecular chains. Focusing on the modulus values, comparing PTFE/graphene-4, PTFE/Al_2O_3-4 and PTFE/G/A-4/4 samples, it could be supposed that there is a hybrid interaction between graphene and Al_2O_3 fillers. The reason is that PTFE/G/A-4/4 material had significantly higher tensile modulus than expected from the 4 wt% mono-filled samples. On the other hand, PTFE/graphene-8 had slightly higher modulus compared to PTFE/G/A-4/4, which means that the higher rate of the increase comes from the higher (8 wt%) filler content and not from a potential hybrid interaction between the fillers.

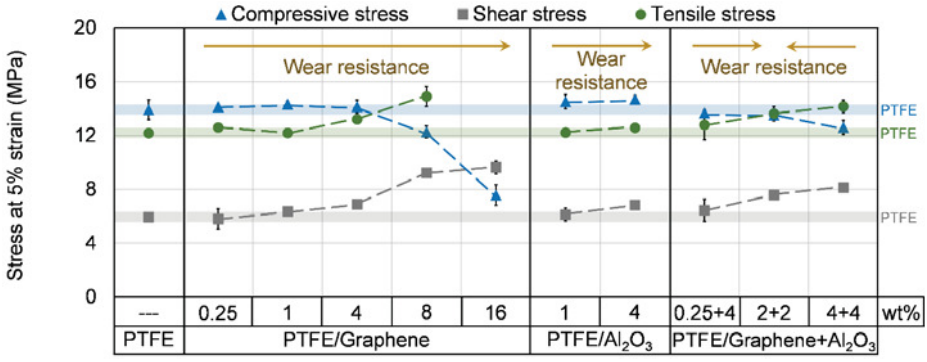

Figure 7.4. Compressive, shear and tensile stress of unfilled and filled PTFE samples at 5% strain. The blue, grey and green transparent lines display the compressive, shear and tensile stress of the neat PTFE at 5% strain, respectively. The introduced wear resistance is discussed in Chapter 7.3.3.2.

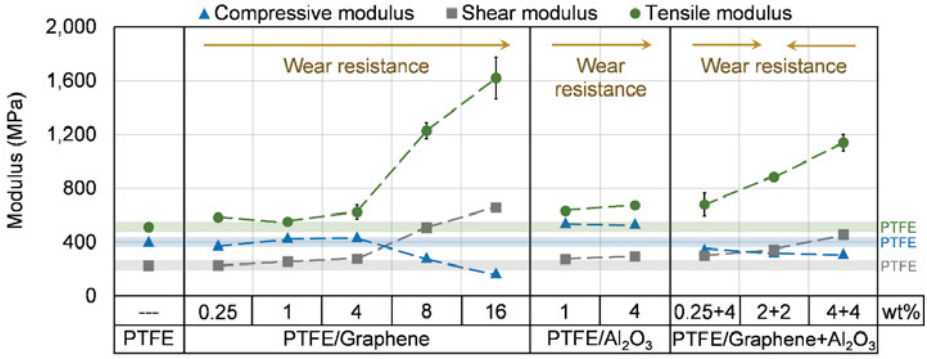

Figure 7.5. Compressive, shear and tensile modulus of unfilled and filled PTFE samples. The blue, grey and green transparent lines display the compressive, shear and tensile modulus of the neat PTFE, respectively. The introduced wear resistance is discussed in Chapter 7.3.3.2.

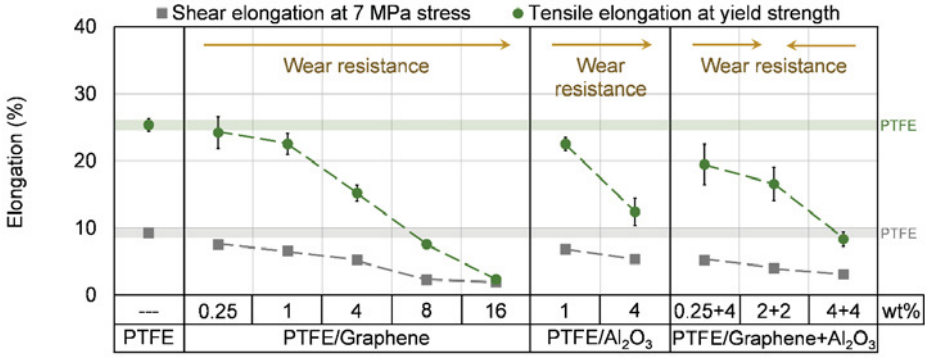

Figure 7.6. Shear and tensile elongation of unfilled and filled PTFE samples. The grey and green transparent lines display the shear and tensile elongation of the neat PTFE, respectively. The introduced wear resistance is discussed in Chapter 7.3.3.2.

Table 7.6. The yield strength, elongation at yield, tensile stress at break and elongation at break of the sintered materials.

Samples	Yield strength MPa	Elongation at yield %	Tensile stress at break MPa	Elongation at break %
PTFE/G/A-0.25/4	13.39 ± 1.26	19.48 ± 3.03	23.14 ± 3.10	354.2 ± 38.2
PTFE/G/A-2/2	14.50 ± 0.52	16.58 ± 2.50	22.77 ± 0.71	314.5 ± 14.9
PTFE/G/A-4/4	14.36 ± 0.44	8.35 ± 1.12	10.48 ± 2.70	49.6 ± 21.1

7.3.3. Friction and wear of the hybrid-filled PTFE materials

This section introduces the friction and wear characterisation of hybrid-filled PTFE samples with respect to the measured thermal and mechanical properties (Phase 3, Chapter 3.3.6.3).

7.3.3.1. Coefficient of friction

The coefficient of friction of neat PTFE, graphene/Al_2O_3 mono-filled and hybrid-filled PTFE composites can be seen in Figure 7.7 and Table B.14. All of the hybrid-fillers increased the coefficient of friction, and the observed increases were higher than expected from the results of mono-filled samples. The coefficient of friction graphs of the tested neat PTFE and hybrid-filled materials against 42CrMo4 steel disc can be seen in Figure 7.8. All of the materials reached the steady-state friction after ~300-400 m sliding distance (Figure 7.8).

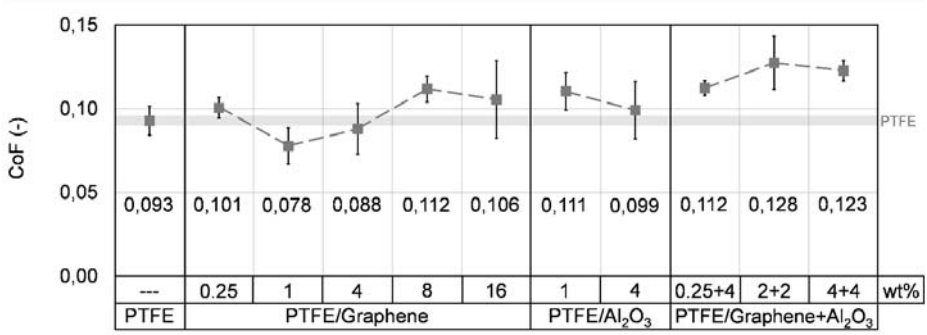

Figure 7.7. The coefficient of friction of unfilled/filled PTFE samples. The grey transparent line displays the measured coefficient of friction of the neat PTFE. Dry contact, 42CrMo4 steel counterface, 3 MPa contact pressure, 0.1 m/s sliding speed, 1000 m sliding distance (Phase 3, Chapter 3.3.6.3).

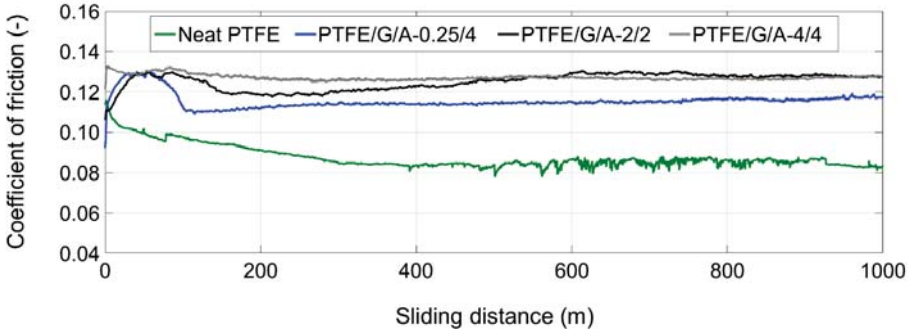

Figure 7.8. Coefficient of friction graphs of the tested unfilled and hybrid-filled PTFE. Dry contact, 42CrMo4 steel counterface, 3 MPa contact pressure, 0.1 m/s sliding speed, 1000 m sliding distance (Phase 3, Chapter 3.3.6.3).

Analyses of variance (ANOVA) based on both Bonferroni-Holm and Holm-Šidák method were carried out to compare the coefficient of friction of filled PTFE materials to the reference neat PTFE. Both methods concluded that the measured differences in the coefficient of friction compared to the reference neat PTFE are not significant.

7.3.3.2. Wear rate

The wear rate of the reference neat PTFE, graphene/Al_2O_3 mono-filled and hybrid-filled PTFE composites tested against 42CrMo4 steel can be seen in Figure 7.9 and Table B.16. Compared to neat PTFE, hybrid-filled samples reached 1-2 orders of magnitude improvement in wear resistance. The lowest wear rate from the hybrid-filled samples was observed in case of PTFE/G/A-4/4 material with a value of $4.3 \cdot 10^{-6}$ mm^3/Nm. It can be stated that the wear resistance enhancement of Al_2O_3 was slightly moderated by graphene filler. This can be explained with the modified transfer layer formation. Al_2O_3 as an abrasive and hard filler can remove the peaks of the steel counterfaces, and these removed iron-oxide particles are transferred to the top layer of the polymer resulting in a more resistance transfer layer which improves the wear resistance. A more detailed explanation is available in Chapter 6.3.2.6. It is assumed that graphene filler can moderate the abrasive effect of the Al_2O_3 particles, in this way it can modify the wear mechanism of Al_2O_3 filled PTFE, decreasing the wear resistance. Figure 7.10 displays the wear (displacement) graphs of the developed hybrid-filled PTFE materials. All the tested composites reached the steady-state wear during the 1000 m sliding distance.

Analyses of variance (ANOVA) based on both Bonferroni-Holm and Holm-Šidák method were evaluated to compare the wear rate of filled PTFE samples to the reference neat PTFE. Both methods concluded that all of the observed differences in the wear rate of the hybrid-filled PTFE materials compared to the reference unfilled PTFE are significant.

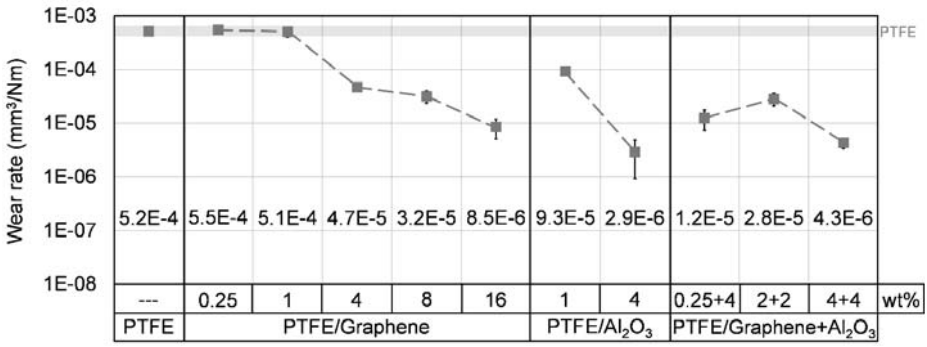

Figure 7.9. Wear rate of unfilled/filled PTFE samples. The grey transparent line displays the measured wear rate of the neat PTFE. Dry contact, 42CrMo4 steel counterface, 3 MPa contact pressure, 0.1 m/s sliding speed, 1000 m sliding distance (Phase 3, Chapter 3.3.6.3).

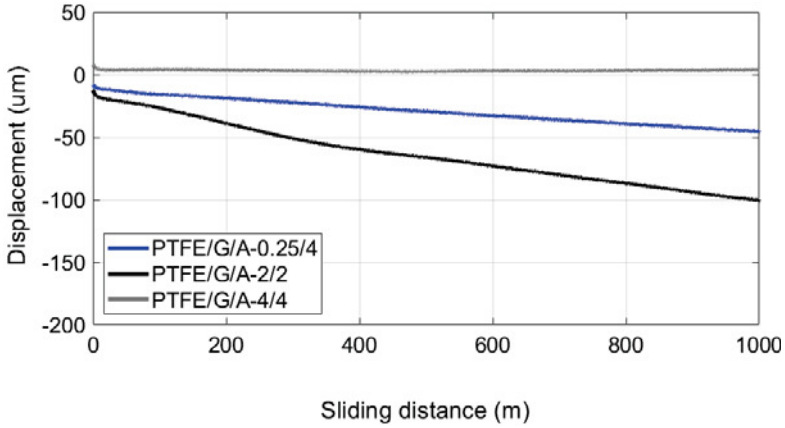

Figure 7.10. Wear (displacement) graphs of tested unfilled and hybrid-filled PTFE. Dry contact, 42CrMo4 steel counterface, 3 MPa contact pressure, 0.1 m/s sliding speed, 1000 m sliding distance (Phase 3, Chapter 3.3.6.3).

The wear rate as a function of the shear and compressive modulus is depicted in Figure 7.11. This figure confirms that no clear relation exists between the compressive/shear modulus and the wear rate (Chapter 5.3.12). The applied filler and consequently, the transfer layer formation has a dominant (primary) role in the wear mechanism of the investigated materials. The shear/tensile properties and thermal conductivity have only a secondary role in the wear mechanism of the investigated materials.

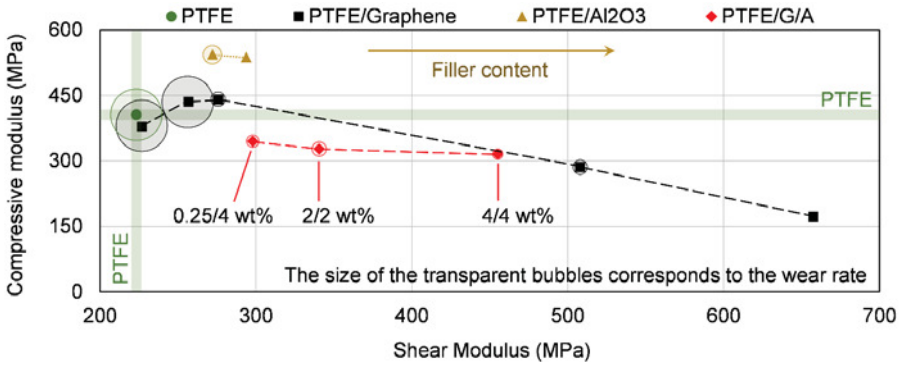

Figure 7.11. Compressive modulus as a function of the shear modulus of unfilled and filled PTFE samples. The size of the bubbles correlates to the wear rate of the samples.

7.3.3.3. Wettability and surface free energy

Figure 7.12, 7.13 and Table B.18 show the advancing and receding contact angles and the evaluated surface free energy of the unfilled/filled PTFE samples. Table B.18 introduces the

wettability and the surface free energy of the 42CrMo4/304/34CrNiMo6 steels. As it was observed in case of the mono-filled materials, the hybrid fillers reached similar or higher surface energy compared to neat PTFE. Still, graphene and alumina filled composites decreased the wear rate, which is not in agreement with the expectations which were introduced in Chapter 1.1 [1, 2] but it confirms the results of mono-filled PTFE materials Chapter 6.3.1.3.

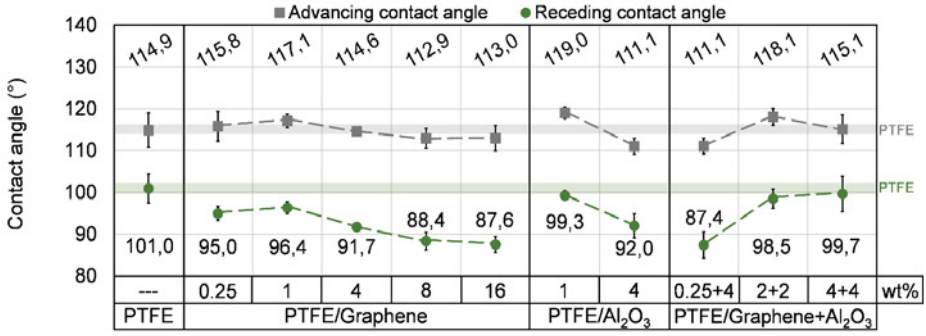

Figure 7.12. Advancing and receding contact angles of the unfilled and filled PTFE materials. The grey/green transparent lines display the measured advancing/receding contact angle of the neat PTFE.

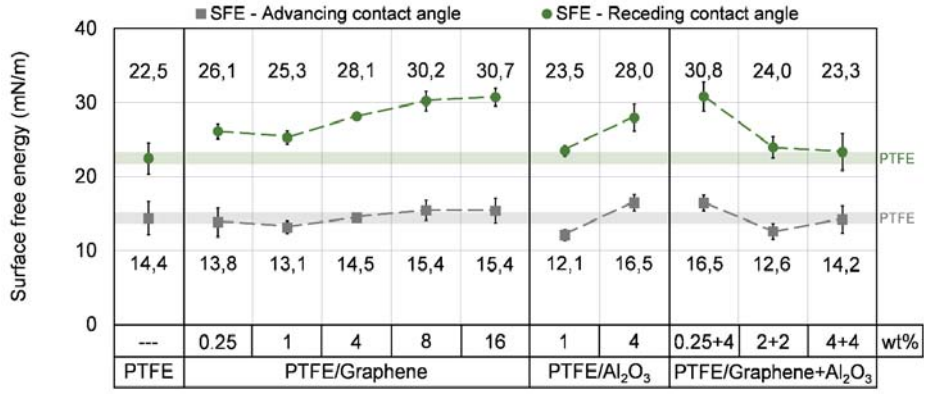

Figure 7.13. Surface free energy (SFE) based on the advancing and receding contact angles of the unfilled and filled PTFE materials. The grey/green transparent lines display the measured SFE (advancing/receding) of the neat PTFE.

7.3.3.4. Filler accumulation in the tested polymers

The aluminium accumulation in the worn hybrid-filled PTFE surfaces was investigated by EDS analysis (Table 7.7 and 7.8). All results confirm the main conclusions of Chapter 6.3.2.6. Significant filler and iron accumulation was observed on the contact surfaces of the worn

polymer samples. PTFE/G/A-0.25/4, PTFE/G/A-2/2 and PTFE/G/A-4/4 polymer samples had ~494%, ~215% and ~303% higher aluminium content than the original unworn surfaces, respectively. Both PTFE/G/A-0.25/4 and PTFE/G/A-4/4 materials had significantly higher iron content on the contact surface compared to PTFE/G/A-2/2, as the lower alumina content caused a reduced abrasive effect on the steel counterface. Due to the less iron and alumina content of the PTFE/G/A-2/2 contact surface, the formed layer is less protective, resulted in the highest wear rate compared to the other hybrid-filled PTFE and PTFE/Al_2O_3-4.

Table 7.7. EDS analysis of unworn samples and contact surfaces (3 MPa contact pressure and 0.1 m/s sliding speed).

Materials	Counterface material	Aluminium content Unworn (%)	Aluminium content Worn surface (%)	Iron (Fe) content Worn surface (%)
PTFE/G/A-0.25/4	42CrMo4	2.18	12.94	14.07
PTFE/G/A-2/2	42CrMo4	1.31	4.13	1.62
PTFE/G/A-4/4	42CrMo4	2.34	9.43	14.33

Table 7.8. Aluminium content increase on the worn surfaces compared to the unworn materials (3 MPa contact pressure and 0.1 m/s sliding speed).

Materials	Counterface material	Aluminium content = worn/unworn (%)
PTFE/G/A-0.25/4	42CrMo4	493.6
PTFE/G/A-2/2	42CrMo4	215.3
PTFE/G/A-4/4	42CrMo4	303.0

7.3.4. Parametrical study of the best performing materials – failure analysis

A parametrical study of the best performing mono- and hybrid-filled PTFE, related to the influence of contact pressure and sliding speed, was also carried out (Phase 4, Chapter 3.3.6.4). The investigated samples are the following: neat PTFE, PTFE/Graphene-4, PTFE/Graphene-8, PTFE/Al_2O_3-4 and PTFE/G/A-4/4. The aim of this research is to analyse the lifetime and the failure of these samples at 1/3/5/7 MPa contact pressure and 0.5/1/1.5/2/3 m/s sliding speed. In Phase 4, the target sliding distance was increased from 1000 m to 3000 m, to compensate for the significantly reduced wear test time, which is a consequence of the increased sliding speed. As the sliding distance increased, more time was available to reach the steady-state conditions.

The criteria of failure are divided into two groups. The first failure criterion is related to the wear depth measured by the displacement sensor. If the wear reached 1 mm depth, the wear test automatically stopped before reaching the stipulated 3000 m sliding distance, so the registered

sliding distance (lifetime) was below 3000 m. The wear depth was measured online by means of a displacement sensor. The colour code of this kind of `failure` method is red (Figure 7.14).

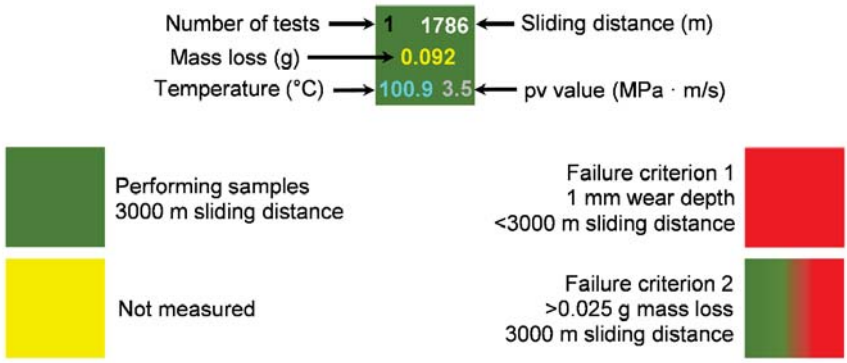

Figure 7.14. The definition of the applied failure criteria, colour codes and indicator numbers.

The second failure criterion is related to those materials which reached the stipulated 3000 m sliding distance. If the measured mass loss was higher than 0.025 g, the samples were classified as failed materials, independently of the contact pressure and sliding speed. This 0.025 g is a good indicator, as most of the samples had considerable lower or higher mass loss. The 0.025 g mass loss can be related to approximately 0.23 mm wear depth. As the wear depth is calculated from the measured mass loss (Equation (7.1) and (7.2)), this value is more accurate compared to the wear depth measured by the displacement sensor, which is also influenced by thermal expansion and creep (Chapter 6.3.1.2, Equation (6.1)). In this criterion, the mass loss / wear depth was chosen as a restriction, because these numbers can indicate the real wear depth, independently of the contact pressure. The introduced wear rate values include the applied normal force as well, which is discussed in Chapter 3.3.2 (Equation (3.16)). The colour code of this kind of failure method is a gradient green-red (Figure 7.14). In the first criterion, the wear depth had to reach the 1 mm value, which is significantly higher than the 0.23 mm wear depth in the second criterion. There are two main reasons for this high difference; the first is to compare as many materials with 3000 m sliding distance as possible, as a wear depth smaller than 1 mm would result in a lower sliding distance. The second is to minimise the uncertainties measured by the displacement sensor. In case of 1 mm wear depth, the ratio of the thermal expansion compared to the total measured wear depth is negligible.

$$m_{d,mass\ loss} = V_{d,mass\ loss} \cdot \rho = (D^2 \cdot \pi\ /\ 4) \cdot W_{d,mass\ loss} \cdot \rho \qquad (7.1)$$

$$W_{d,mass\ loss} = m_{d,mass\ loss}/(\rho \cdot D^2 \cdot \pi/4) = 0.025/(0.002168 \cdot 8^2 \cdot \pi/4) = \sim 0.23mm \qquad (7.2)$$

In Equation (7.1) and (7.2), $m_{d,mass\ loss}$ is the measured mass loss after the wear test (g), $V_{d,mass\ loss}$ is the calculated volume loss after the wear test (mm^3), ρ is the density of the polymer sample (g/mm^3), D is the diameter of the polymer pin (mm), while $W_{d,mass\ loss}$ is the wear depth based on the measured mass loss (mm). Equation (7.2) shows an example, for a neat PTFE sample with a density of 2.168 g/cm^3. All polymer pins had a diameter of 8 mm.
The applicable materials are marked by green, while the not measured ones with yellow (Figure 7.14). If a material failed by the first criterion (reaching 1 mm wear depth), more wear tests with higher contact pressure and/or sliding distance were not carried out. Figure 7.14 also shows an example how the number of tests / mass loss (g) / sliding distance (m) / bulk temperature (°C) indicators are placed and marked in the quadrants. If the materials failed, no more wear tests were carried out with the same test conditions.

7.3.4.1. Neat PTFE

The parametrical study of neat PTFE only focused on the wear-induced crystallisation, as even in case of 3 MPa contact pressure and 0.1 m/s sliding speed, the wear depth of PTFE was ~1.62 mm (Chapter 6.3.1.2 and Table B.16). Two tests series were carried out, the first is with 3 MPa contact pressure, while the second is with 1 m/s sliding speed (Figure 7.15).

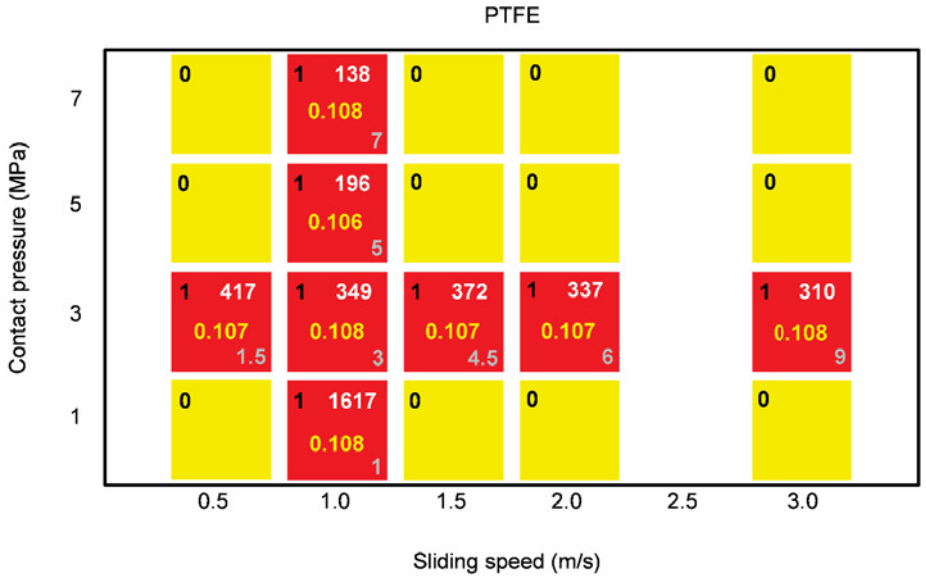

Figure 7.15. Parametrical study of neat PTFE - 1/3/5/7 MPa contact pressure and 0.5/1/1.5/2/3 m/s sliding speed. The number of tests / mass loss (g) / sliding distance (m) / pv values (MPa · m/s) are marked by black / yellow / white / grey, respectively. The colour code of the quadrants are the following: not measured - yellow, failure criterion 1 - red.

None of the samples reached the maximal 3000 m sliding distance; in this way, they failed by the first criterion. All specimens had a mass loss between 0.106-0.108 g, which correlates well with the 1 mm wear depth measured by the displacement sensor. Neat PTFE achieved a maximal sliding distance (1617 m) with the lowest contact pressure and sliding speed (1 MPa, 1 m/s). As it is expected, the sliding distance, or in other words, the lifetime of the samples decreased as the contact pressure or sliding speed increased.

The wear-induced crystallisation of the unfilled/filled PTFE materials was investigated by DSC (Protocol 1, Chapter 3.2.4). Table 7.9 shows the unworn neat PTFE samples, focusing on their initial temperature of melting, melting peak temperature, enthalpy of fusion and degree of crystallinity. In Chapter 5 and 6, all of the tested neat PTFE samples (DSC and wear tests) were cut out from the same PTFE disc (Ø120 mm). In this way, their morphological properties are closely the same. In Chapter 7, another PTFE disc was the base material; in this way, the DSC analysis was carried out again for the unworn (reference) neat PTFE (Table 7.9).

Table 7.9. DSC results of the unworn neat PTFE, applying Protocol 1 for the DSC analysis (Chapter 3.2.4).

Unworn PTFE	First heating			
	Initial temperature of melting (°C)	Melting peak temperature (°C)	Enthalpy of fusion (J/g)	Degree of crystallinity (%)
Tested in Chapter 5 and 6	321.4	326.3	36.82	53.4
Tested in Chapter 7	320.9	325.9	33.97	49.2
	Second heating			
Tested in Chapter 5 and 6	319.5	324.0	29.93	43.4
Tested in Chapter 7	318.7	323.7	28.69	41.6
	First cooling			
	Initial temperature of crystallisation (°C)	Crystallisation peak temperature (°C)	Enthalpy of crystallisation (J/g)	Degree of crystallinity (%)
Tested in Chapter 5 and 6	310.6	308.8	31.25	45.3
Tested in Chapter 7	313.9	307.6	30.56	44.3

Table 7.10 presents the DSC results of the neat PTFE debris tested against 42CrMo4 steel. The first column indicates the contact pressure and sliding speed, respectively. The initial temperature of melting and the melting peak temperature of debris were higher both in the first and second heating cycle compared to the unworn material. The debris also had a higher initial temperature of crystallisation and crystallisation peak temperature compared to the unworn materials. It confirms that the crystallisation process is initiated sooner in case of the debris compared to the unworn samples (Table 7.9 and 7.10).

In the first heating cycle, the degree of crystallinity of the debris increased between 25% and 41% compared to the unworn samples (Table 7.11), which is in agreement with the results of Chapter 6.3.2.5 (Table 6.4). The increase of the degree of crystallinity was also confirmed by the results of the second heating cycle where, after the first melt, all the analysed samples had

the same thermal history. In the second heating cycle, the debris had 17-25% higher degree of crystallinity than the unworn samples (Table 7.11). The degree of crystallinity evaluated from the enthalpy of crystallisation also had an increase between 16% and 31%, compared to the unworn neat PTFE (Table 6.4).

Table 7.10. DSC results of the neat PTFE debris (Phase 4, Chapter 3.3.6.4), applying Protocol 1 for the DSC analysis (Chapter 3.2.4). Here the enthalpy of fusion at the first heating cycle was evaluated between 300°C and 370°C.

PTFE debris (42CrMo4)	First heating			
	Initial temperature of melting (°C)	Melting peak temperature (°C)	Enthalpy of fusion (J/g)	Degree of crystallinity (%)
3 MPa, 0.5 m/s	327.3	335.3	51.58	74.8
3 MPa, 1.0 m/s	327.3	334.9	55.33	80.2
3 MPa, 1.5 m/s	327.0	334.5	57.71	83.6
3 MPa, 2.0 m/s	328.5	335.0	56.56	82.0
3 MPa, 3.0 m/s	328.1	334.8	56.78	82.3
1 MPa, 1.0 m/s	325.8	332.3	62.22	90.2
3 MPa, 1.0 m/s	327.3	334.9	55.33	80.2
5 MPa, 1.0 m/s	327.4	334.3	57.79	83.8
7 MPa, 1.0 m/s	327.1	333.9	57.94	84.0
	Second heating			
3 MPa, 0.5 m/s	324.2	327.3	40.67	58.9
3 MPa, 1.0 m/s	324.8	327.3	41.91	60.7
3 MPa, 1.5 m/s	325.1	327.7	45.47	65.9
3 MPa, 2.0 m/s	324.7	327.6	42.49	61.6
3 MPa, 3.0 m/s	324.6	327.6	42.86	62.1
1 MPa, 1.0 m/s	325.2	327.8	45.94	66.6
3 MPa, 1.0 m/s	324.8	327.3	41.91	60.7
5 MPa, 1.0 m/s	325.1	327.6	45.11	65.4
7 MPa, 1.0 m/s	325.0	327.6	45.78	66.3
	First cooling			
	Initial temperature of crystallisation (°C)	Crystallisation peak temperature (°C)	Enthalpy of crystallisation (J/g)	Degree of crystallinity (%)
3 MPa, 0.5 m/s	314.4	310.7	41.97	60.8
3 MPa, 1.0 m/s	313.3	310.6	43.95	63.7
3 MPa, 1.5 m/s	314.4	311.3	47.97	69.5
3 MPa, 2.0 m/s	315.4	311.5	45.27	65.6
3 MPa, 3.0 m/s	316.0	312.0	46.43	67.3
1 MPa, 1.0 m/s	315.3	312.0	52.08	75.5
3 MPa, 1.0 m/s	313.3	310.6	43.95	63.7
5 MPa, 1.0 m/s	313.9	311.0	47.39	68.7
7 MPa, 1.0 m/s	314.1	311.2	47.66	69.1

These results confirm that PTFE molecular chains undergo mechanical chain scission during the wear tests, which has a remarkable influence on the degree of crystallinity. Due to the shorter molecular chains, the degree of crystallinity can be higher, not only in the first heating cycle but in the second heating cycle as well besides the same thermal history. A more detailed explanation can be found in Chapter 6.3.2.5. Although the increase in the degree of crystallinity is still significant in the second heating cycle, it is remarkably lower compared to the first

heating cycle (Table 7.11). This is in contrast with Chapter 6.3.2.5, Table 6.4, as there this kind of tendency was not registered. A potential explanation for this phenomenon can be the different thermal and mechanical history of the debris, which come from the different wear temperatures caused by the different contact pressure and sliding speeds.

Table 7.11. DSC comparison of unworn neat PTFE with their debris (Protocol 1, Chapter 3.2.4). Polymer samples were tested against 42CrMo4 counterface material (Phase 4, Chapter 3.3.6.4).

Neat PTFE (42CrMo4)	Degree of crystallinity – increase = debris (%) – unworn (%)		
	First heating (%)	First cooling (%)	Second heating (%)
3 MPa, 0.5 m/s	25.5	16.5	17.4
3 MPa, 1.0 m/s	31.0	19.4	19.2
3 MPa, 1.5 m/s	34.4	25.2	24.3
3 MPa, 2.0 m/s	32.7	21.3	20.0
3 MPa, 3.0 m/s	33.1	23.0	20.5
1 MPa, 1.0 m/s	40.9	31.2	25.0
3 MPa, 1.0 m/s	31.0	19.4	19.2
5 MPa, 1.0 m/s	34.5	24.4	23.8
7 MPa, 1.0 m/s	34.7	24.8	24.8

Table 7.12 introduces the calculated molecular weight of the unworn neat PTFE samples and their debris. The molecular weight, and in this way the length of the PTFE molecular chains in the debris, decreased by ~1 order of magnitude compared to the unworn PTFE, which is in agreement with Chapter 6.3.2.5, Table 6.5.

Table 7.12. The calculated molecular weight of unworn neat PTFE samples compared to their debris. Polymer samples were tested against 42CrMo4 counterface material (Phase 4, Chapter 3.3.6.4).

Neat PTFE (42CrMo4)	First cooling		
	Molecular weight - unworn (g/mol)	Molecular weight - debris (g/mol)	Molecular weight = debris/unworn (%)
3 MPa, 0.5 m/s	7.37E+06	1.43E+06	19.5
3 MPa, 1.0 m/s	7.37E+06	1.13E+06	15.3
3 MPa, 1.5 m/s	7.37E+06	7.20E+05	9.8
3 MPa, 2.0 m/s	7.37E+06	9.71E+05	13.2
3 MPa, 3.0 m/s	7.37E+06	8.52E+05	11.6
1 MPa, 1.0 m/s	7.37E+06	4.71E+05	6.4
3 MPa, 1.0 m/s	7.37E+06	1.13E+06	15.3
5 MPa, 1.0 m/s	7.37E+06	7.67E+05	10.4
7 MPa, 1.0 m/s	7.37E+06	7.44E+05	10.1

7.3.4.2. PTFE/Graphene-4

The parametrical study of PTFE/Graphene-4 focused on the wear resistance and the lifetime of the samples. These materials were applicable in only three different conditions: 1 MPa contact pressure with 0.5/1/1.5 m/s sliding speed. At 1 MPa and 2 m/s condition, the mass loss was higher than 0.025 g, while at 1 MPa and 3 m/s condition, the material failed at 2450 m sliding distance. At 3 MPa and higher contact pressures, all of the tested samples failed when the sliding speed was 0.5 m/s (Figure 7.16). In case of 3 MPa contact pressure and 1.0 m/s sliding speed, PTFE/Graphene-4 even could not achieve the stipulated 3000 m sliding distance. This sample reached only 361 m sliding distance, in this way, no more tests were carried out with increased pressure or speed (Figure 7.16, yellow quadrants). Regarding the pv values, above 1.5 MPa·m/s, all of the PTFE/Graphene-4 samples failed, in this way, 1.5 MPa·m/s can be considered as a pv limit of this material. The measured bulk temperature of the steel counterfaces increased as the contact pressure and sliding speed increased. The highest measured bulk temperature was 100.9°C (7 MPa, 0.5 m/s). In 1 MPa – 0.5/1.5 m/s condition, three wear tests were run, to gain information about the reliability of the test results.

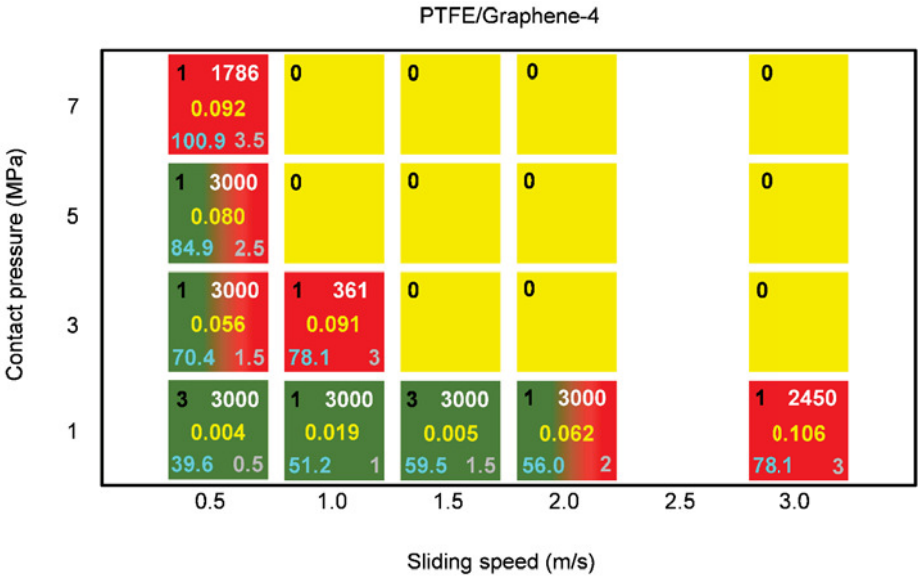

Figure 7.16. Parametrical study of the PTFE/Graphene-4 - 1/3/5/7 MPa contact pressure and 0.5/1/1.5/2/3 m/s sliding speed. The number of tests / mass loss (g) / sliding distance (m) / bulk temperature (°C) / pv values (MPa · m/s) are marked by black / yellow / white / blue / grey, respectively. The colour code of the quadrants are the following: applicable materials – green, not measured - yellow, failure criterion 1 - red, failure criterion 2 - gradient green-red.

Table B.21 introduces the results of the wear rate, mass loss and wear (bulk) temperature with their standard deviation. The wear rate curves of PTFE/Graphene-4 samples tested with 1 MPa contact pressure in comparison with PTFE/Graphene-8 materials are introduced in Chapter 7.3.4.3.

Chapter 6.3.2.6 introduced a remarkable iron-oxide accumulation on the contact surface of PTFE/Al_2O_3-4 polymer samples, which came from the steel disc counterfaces. In this way, the contact surfaces of the worn PTFE/Graphene-4 polymer pins were also investigated by EDS. No Fe content was observed on the worn surfaces, independently of the applied contact pressure or sliding speed.

7.3.4.3. PTFE/Graphene-8

PTFE/Graphene-8 samples performed in a broader spectrum compared to PTFE/Graphene-4 (Figure 7.17). These materials did not fail at 1 MPa contact pressure, independently of the sliding speed. Still, at higher load conditions, none of the tested samples could perform.

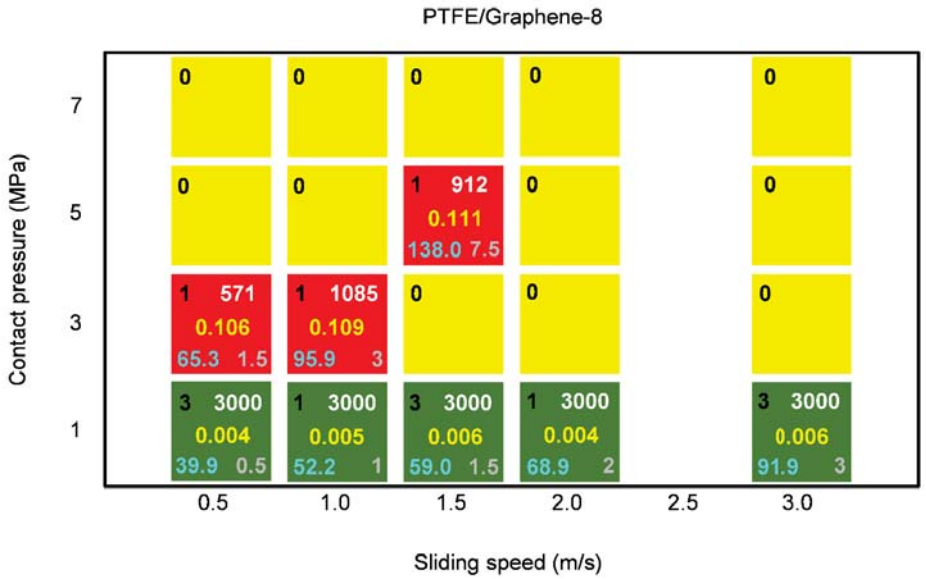

Figure 7.17. Parametrical study of the PTFE/Graphene-8 - 1/3/5/7 MPa contact pressure and 0.5/1/1.5/2/3 m/s sliding speed. The number of tests / mass loss (g) / sliding distance (m) / bulk temperature (°C) / pv values (MPa · m/s) are marked by black / yellow / white / blue / grey, respectively. The colour code of the quadrants are the following: applicable materials – green, not measured - yellow, failure criterion 1 - red.

At 3 MPa contact pressure, samples tested with 0.5/1 m/s sliding speed reached only 571/1085 m sliding distance until 1 mm wear depth, respectively. At 5 MPa – 1.5 m/s condition,

it reached 912 m sliding distance, with 138.0°C bulk temperature (steel counterface). These results indicate that PTFE/Graphene-4 and PTFE/Graphene-8 materials can be used only at low contact pressure (~ 1 MPa) and/or low sliding speed (~0.1 m/s). Above 3 MPa·m/s pv value, all of the PTFE/Graphene-8 samples failed, in this way, 3 MPa·m/s can be considered as a pv limit of this material. Table B.21 introduces the results of the wear rate, mass loss and wear (bulk) temperature with their standard deviation.

Figure 7.18 depicts the wear rate curves of PTFE/Graphene-4 and PTFE/Graphene-8 materials tested with 1 MPa contact pressure. It is clearly shown that PTFE/Graphene-8 is superior in the aspect of wear rate, compared to the PTFE/Graphene-4 material. The green region indicates the applicable materials (<0.025 g mass loss).

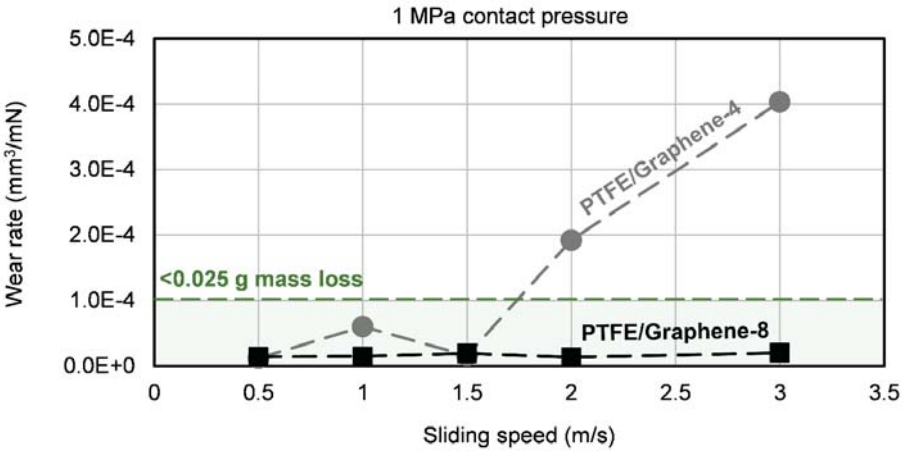

Figure 7.18. The wear rate of PTFE/Graphene-4 and PTFE/Graphene-8 polymer samples at 1 MPa contact pressure as a function of the sliding speed. The green region indicates the applicable materials (<0.025 g mass loss).

PTFE/Graphene-8 polymer pins were also investigated by EDS with the same results as observed in PTFE/Graphene-4 samples. No Fe content was registered on the contact surfaces of the pins, independently of the applied contact pressure or sliding speed.

7.3.4.4. PTFE/Al_2O_3-4

In the aspect of wear rate, PTFE/Al_2O_3-4 samples were superior compared to PTFE/Graphene-4 and PTFE/Graphene-8 (Figure 7.19). Focusing on 0.5 m/s sliding speed, all of the samples were applicable independently of the contact pressure. At 1 MPa pressure, similar good performance was registered, independently of the sliding speed. In case of 3/5/7 MPa contact pressure, the samples were applicable until 2/1/0.5 m/s sliding speed,

respectively. Considering pv values, above 6 MPa·m/s, all of the PTFE/Al_2O_3-4 specimens failed, in this way, 6 MPa·m/s can be used as a pv limit of this material.

All failed samples reached a bulk temperature (steel counterface) higher than 210°C, and this temperature is even higher at the contact surfaces. In this way, the reason for their failure was the softened material, as generally, the service temperature of PTFE is 250°C. This is a huge difference compared to the graphene filled samples. PTFE/Graphene-4 and PTFE/Graphene-8 failed as the contact pressure and, in this way, the shear stress was too high for these materials. In contrast, PTFE/Al_2O_3-4 samples only failed after reaching a high temperature range (>210°C). Table B.22 introduces the results of the wear rate, mass loss and wear (bulk) temperature with their standard deviation.

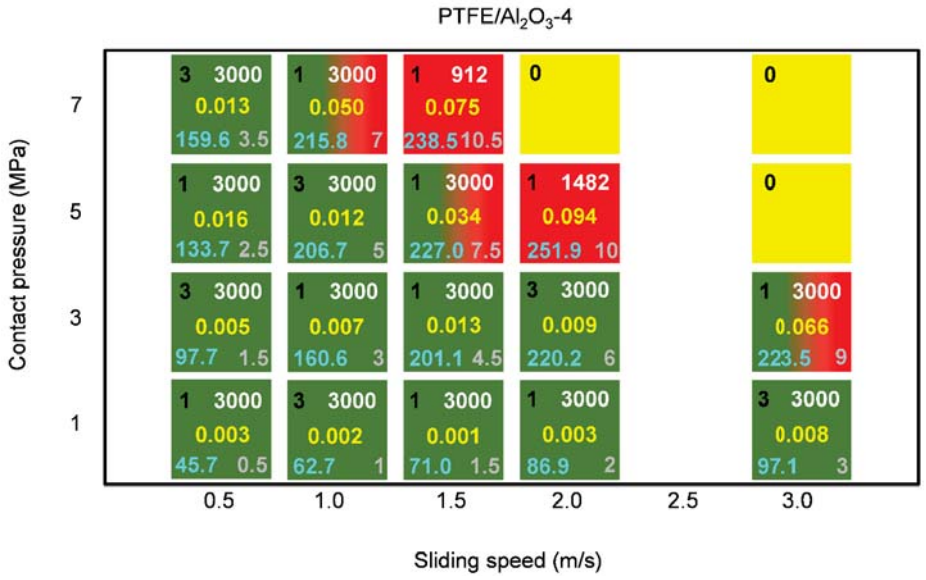

Figure 7.19. Parametrical study of the PTFE/Graphene-8 - 1/3/5/7 MPa contact pressure and 0.5/1/1.5/2/3 m/s sliding speed. The number of tests / mass loss (g) / sliding distance (m) / bulk temperature (°C) / pv values (MPa · m/s) are marked by black / yellow / white / blue / grey, respectively. The colour code of the quadrants are the following: applicable materials – green, not measured - yellow, failure criterion 1 - red, failure criterion 2 - gradient green-red.

Figure 7.20 depicts the wear rate curves of PTFE/Al_2O_3-4 samples at 1/3/5/7 MPa contact pressure and 0.5/1/1.5/2/3 m/s sliding speed. The green region indicates the applicable materials (<0.025 g mass loss).

The aluminium and iron accumulation in the worn polymer surface was investigated by EDS analysis (Table 7.13). All results confirm the main conclusions of Chapter 6.3.2.6 and 7.3.3.4.

Remarkable filler and iron accumulation were registered on the contact surfaces of the worn polymer samples. The worn surfaces, tested against 42CrMo4 steel discs, had 200-600% higher aluminium content than the original unworn surfaces. The Fe content on the polymer contact surfaces, which comes from the steel counterfaces, was also significant.

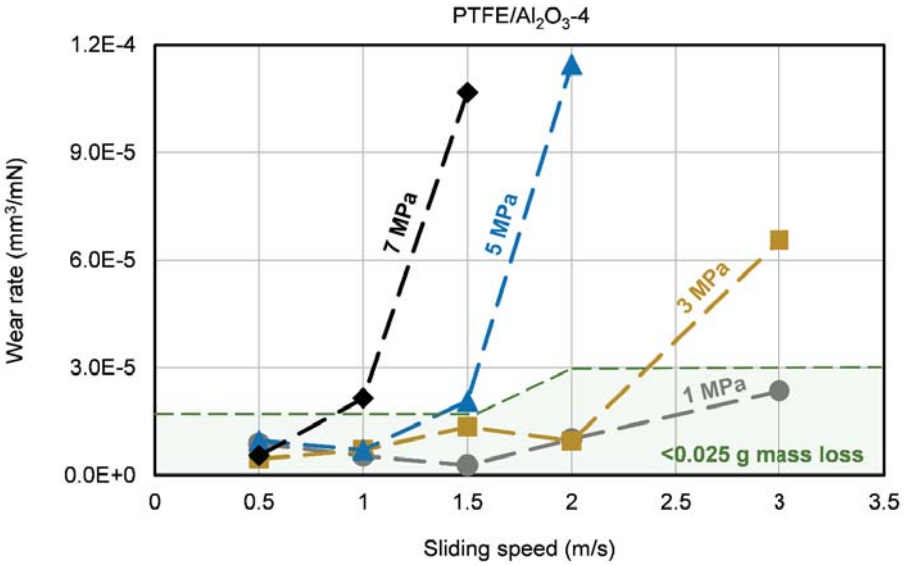

Figure 7.20. The wear rate of PTFE/Al_2O_3-4 polymer samples at 1/3/5/7 MPa contact pressure as a function of the sliding speed. The green region indicates the applicable materials (<0.025 g mass loss).

Table 7.13. The EDS analysis of PTFE/Al_2O_3-4 contact surfaces (Phase 4, Chapter 3.3.6.4).

PTFE/Al_2O_3-4 (42CrMo4)	Aluminium content Unworn (%)	Aluminium content Worn surface (%)	Iron (Fe) content Worn surface (%)	Aluminium content = worn/unworn (%)
3 MPa, 0.5 m/s	2.65	12.66	17.23	477.7
3 MPa, 1.0 m/s	2.65	10.96	16.21	413.6
3 MPa, 1.5 m/s	2.65	17.66	5.39	666.5
3 MPa, 2.0 m/s	2.65	12.77	4.03	481.9
3 MPa, 3.0 m/s	2.65	11.91	2.15	449.4
1 MPa, 1.0 m/s	2.65	8.24	8.45	310.9
3 MPa, 1.0 m/s	2.65	10.96	16.21	413.6
5 MPa, 1.0 m/s	2.65	11.58	2.91	437.0
7 MPa, 1.0 m/s	2.65	12.31	1.46	464.5

7.3.4.5. PTFE/G/A-4/4

Compared to PTFE/Al_2O_3-4 samples, PTFE/G/A-4/4 has some further benefits (Figure 7.21). Both at 1 and 3 MPa pressure, all materials were applicable, independently of the sliding speed. At 0.5 and 1 m/s sliding speed, the same good performance was observed, independently of the contact pressure. Focusing on 5/7 MPa pressure, the samples were applicable until 1 m/s sliding speed. Regarding the pv values, above 9 MPa·m/s, all of the PTFE/G/A-4/4 samples failed, in this way, 9 MPa·m/s can be considered as a pv limit of this material. These positive results indicate that the hybridisation of graphene and alumina fillers is promising as the application range can be further broadened. This positive interaction can come from the modified transfer layer formation and from the increased thermal conductivity (Figure 7.2).

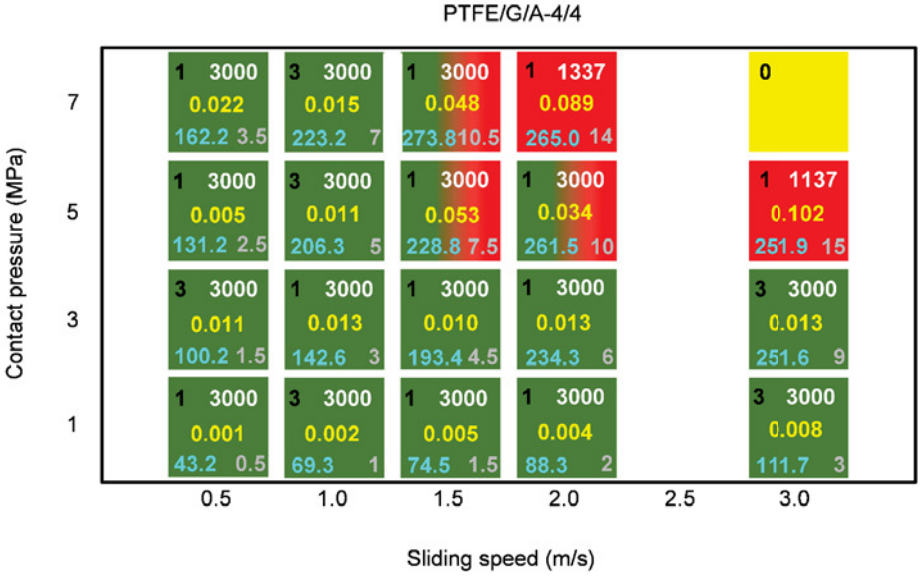

Figure 7.21. Parametrical study of the PTFE/G/A-4/4 - 1/3/5/7 MPa contact pressure and 0.5/1/1.5/2/3 m/s sliding speed. The number of tests / mass loss (g) / sliding distance (m) / bulk temperature (°C) / pv values (MPa · m/s) are marked by black / yellow / white / blue / grey, respectively. The colour code of the quadrants are the following: applicable materials – green, not measured - yellow, failure criterion 1 - red, failure criterion 2 - gradient green-red.

All failed samples reached bulk temperatures above 220°C; therefore, the reason for their failure was the softened material, similarly to PTFE/Al_2O_3-4. Only two samples did not reach the stipulated 3000 m sliding distance with a condition of 7 MPa – 2 m/s and 5 MPa – 3 m/s. Table B.22 introduces the results of the wear rate, mass loss and wear (bulk) temperature with their standard deviation. Figure 7.22 depicts the wear rate curves of PTFE/G/A-4/4 specimens

at 1/3/5/7 MPa contact pressure and 0.5/1/1.5/2/3 m/s sliding speed. The green region indicates the applicable materials (<0.025 g mass loss).

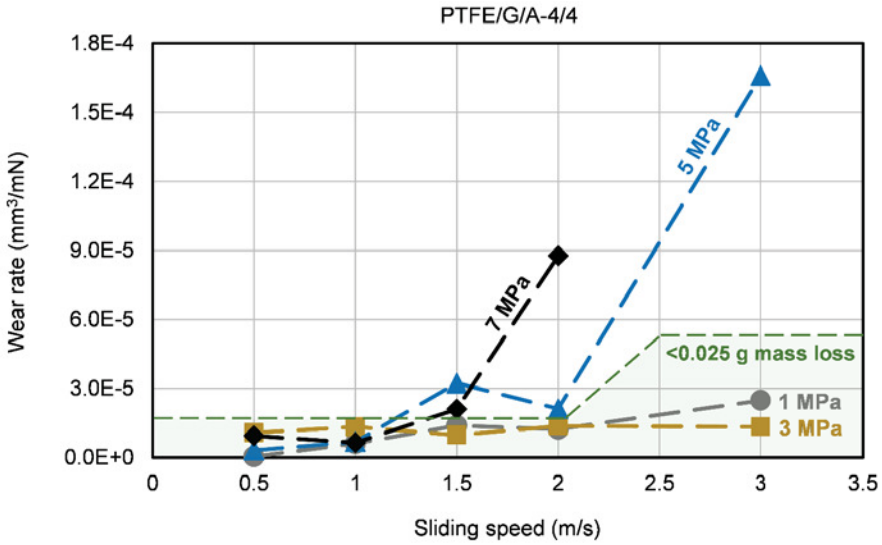

Figure 7.22. The wear rate of PTFE/G/A-4/4 polymer samples at 1/3/5/7 MPa contact pressure as a function of the sliding speed. The green region indicates the applicable materials (<0.025 g mass loss).

Figure 7.23 depicts the wear rate curves of PTFE/G/A-4/4 and PTFE/Al_2O_3-4 polymer samples at 1 MPa, 3 MPa, 5 MPa and 7 MPa contact pressure as a function of the sliding speed. The enhanced wear resistance of PTFE/G/A-4/4 material can be seen compared to the PTFE/Al_2O_3-4 specimens. The most remarkable differences can be found at a higher range of speeds, between 1.5 and 3 m/s sliding speeds. The green region indicates the applicable materials (<0.025 g mass loss).

The aluminium and iron accumulation of PTFE/G/A-4/4 samples are also interesting factors to investigate. The measured values and results are introduced in Table 7.14. All results confirm the main conclusions of Chapter 6.3.2.6, 7.3.3.4 and 7.3.4.4. Here as well, a significant filler and iron accumulation were registered on the top surfaces of the worn polymer specimens. The contact surfaces, tested against 42CrMo4 steel discs, had 170-400% higher aluminium content than the original unworn surfaces. Besides the alumina accumulation, the observed Fe content on the polymer contact surfaces was also significant. These results mean that the graphene filler could not significantly decrease the abrasive effect of the hard alumina particles, resulting in micro-damage on the steel counterfaces, and finally iron-oxide accumulation on the polymer contact surfaces.

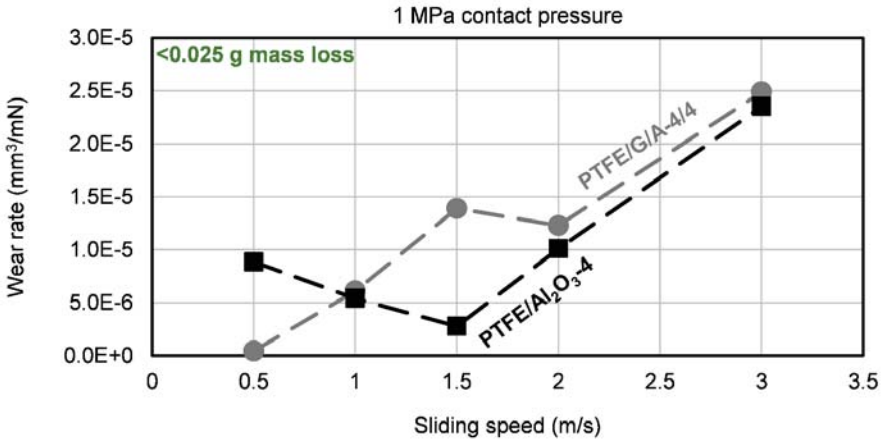
1 MPa contact pressure
<0.025 g mass loss
PTFE/G/A-4/4
PTFE/Al2O3-4
Wear rate (mm3/mN)
Sliding speed (m/s)

(a)

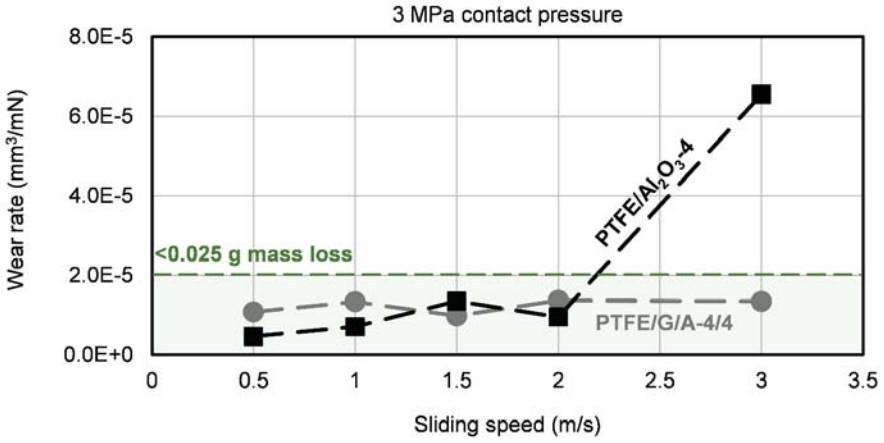
3 MPa contact pressure
PTFE/Al2O3-4
<0.025 g mass loss
PTFE/G/A-4/4
Wear rate (mm3/mN)
Sliding speed (m/s)

(b)

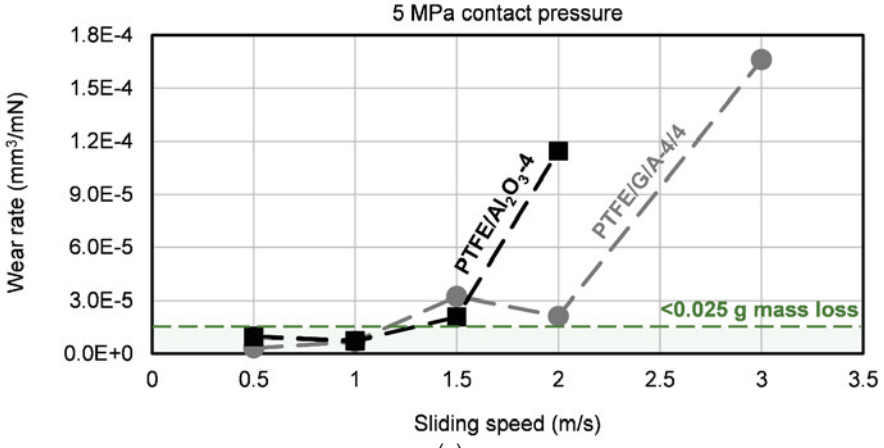
5 MPa contact pressure
PTFE/Al2O3-4
PTFE/G/A-4/4
<0.025 g mass loss
Wear rate (mm3/mN)
Sliding speed (m/s)

(c)

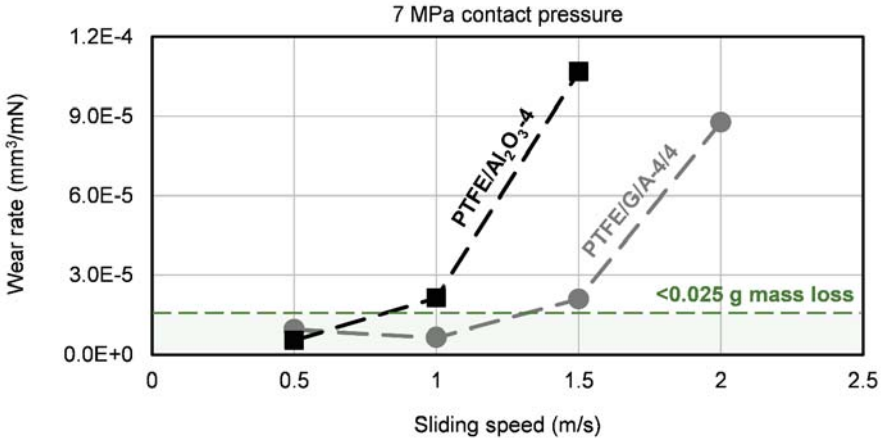

(d)

Figure 7.23. The wear rate of PTFE/G/A-4/4 and PTFE/Al_2O_3-4 polymer samples at 1 MPa (a), 3 MPa (b), 5 MPa (c) and 7 MPa (d) contact pressure as a function of the sliding speed. The green region indicates the applicable materials (<0.025 g mass loss).

Table 7.14. EDS analysis of PTFE/G/A-4/4 contact surfaces (Phase 4, Chapter 3.3.6.4).

PTFE/G/A-4/4 (42CrMo4)	Aluminium content Unworn (%)	Aluminium content Worn surface (%)	Iron (Fe) content Worn surface (%)	Aluminium content = worn/unworn (%)
3 MPa, 0.5 m/s	2.71	13.10	11.21	483.4
3 MPa, 1.0 m/s	2.71	8.67	9.19	319.9
3 MPa, 1.5 m/s	2.71	6.89	1.61	254.2
3 MPa, 2.0 m/s	2.71	11.58	3.44	427.3
3 MPa, 3.0 m/s	2.71	10.41	1.89	384.1
1 MPa, 1.0 m/s	2.71	8.84	9.60	326.2
3 MPa, 1.0 m/s	2.71	8.67	9.19	319.9
5 MPa, 1.0 m/s	2.71	7.35	2.13	271.2
7 MPa, 1.0 m/s	2.71	12.48	3.37	460.5

7.4. Conclusions

This chapter introduced the material and tribological characterisation of hybrid-filled PTFE samples. It is followed by a parametrical study of the best performing materials (Phase 3 and 4, Chapter 3.3.6).

- Low thermal stability was observed in case of all hybrid-filled PTFE materials, confirming the main conclusions of Chapter 4. This low thermal stability was registered during the 10 hours dwelling time as well. It means that these hybrid-filled materials are also sensitive to the applied dwelling time at the maximal sintering temperature (370°C).

- The thermal conductivity of the hybrid-filled PTFE materials enhanced as the graphene filler content increased. PTFE/G/A-4/4 had ~59% higher thermal conductivity compared to reference neat PTFE.
- Compared to neat PTFE, the shear and tensile modulus of the developed hybrid-filled samples were increased, similarly to their mono-filled materials (Chapter 5). The elongation at yield and the measured elongation during shear tests were significantly reduced with decreasing filler content.
- The results of the hybrid-filled samples confirm that the modified compressive/shear/tensile properties and thermal conductivity have a lower influence on the wear mechanism (secondary role) as the tendencies of the wear rate and shear/tensile curves are different.
- The lowest wear rate from the hybrid-filled samples was observed in case of PTFE/G/A-4/4 material with a value of $4.3 \cdot 10^{-6}$ mm^3/Nm. It can be stated that the wear resistance enhancement of Al_2O_3 was moderated by graphene filler.
- The degree of crystallinity of the debris increased by between 25% and 41% compared to the unworn samples. It is in agreement with the conclusions of Chapter 6. This increase comes mainly from mechanical chain scission during the wear process, which shortened the molecular length in the formed debris. In contrast with Chapter 6, the effect of the thermal circumstances and possible molecular chain aligning during the wear process is also remarkable due to the 0.5 m/s or higher sliding speed.
- Similarly to the results of Chapter 6.3.2.6, PTFE/Al_2O_3-4 and PTFE/G/A-4/4 samples had a remarkable filler content and iron-oxide accumulation on their contact surfaces. These accumulations were registered at all of the contact pressures and sliding speeds.

7.5. References

[1] S.K. Sinha, B.J. Briscoe: Polymer tribology. Imperial College Press, London, United Kingdom (2009).

[2] E.F. Finkin: Surface energy and the theory of the friction of solids. Applied Physics Letters 30 (1977) 436.

CHAPTER 8

CONCLUSIONS

This chapter presents the final conclusions of this research work based on the introduced research questions. The conclusions are followed by the potential application areas and further study.
The most relevant research conclusions are available in Dutch and Hungarian language as well.

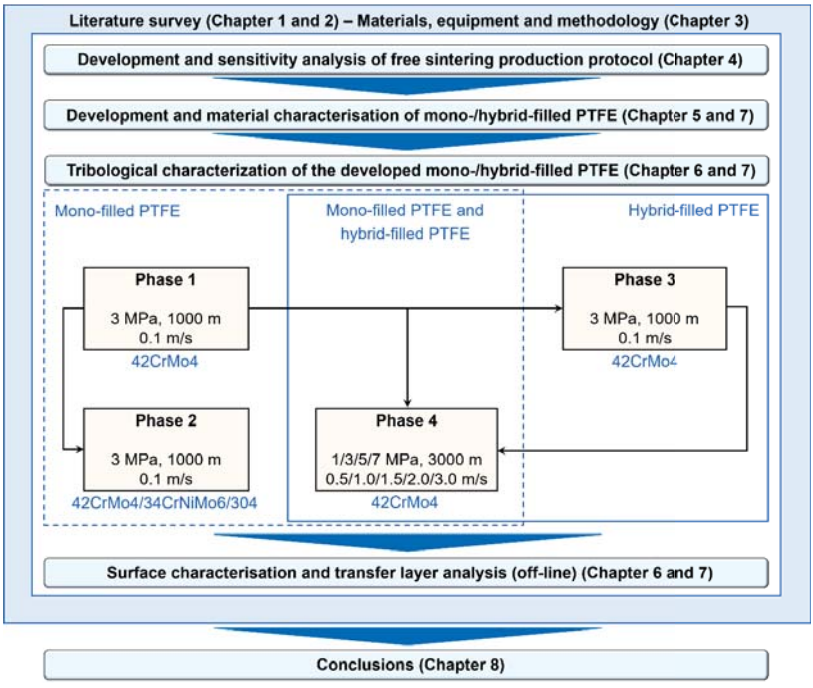

8.1. Research questions

Chapter 4-7 analyse the production protocol and the developed materials in the aspect of the raised research questions in Chapter 1.3 and introduced conclusions of the literature survey in Chapter 2.7. These research questions focus on the following topics:

- The thermal stability of the neat fillers and filled polytetrafluoroethylene (PTFE) during the sintering process (sensitivity analysis). Influence of the fillers on the physical, mechanical and thermal properties of the materials (Chapter 4 and 5).
- Regarding boehmite alumina (aluminium hydroxide oxide - AlO(OH)) and alumina (Al_2O_3), the influence of the functional groups on the wear resistance (Chapter 6).
- The wear-induced crystallisation of the tested materials, considering the thermal and mechanical history of the wear-tested samples and the mechanical chain scission during the wear process (Chapter 6 and 7).
- The ultra-low wear rate of alumina filled PTFE samples, considering the transfer layer and wear mechanism analysis (Chapter 6 and 7).
- The dominant factors of the wear mechanism, focusing on the transfer layer formation and the mechanical/thermal properties of the tested polymer samples (Chapter 5-7).

8.2. Main research conclusions

This section summarises the main research conclusions focusing on the potential use of boehmite alumina in PTFE material; the restrictions related to the sintering of Al_2O_3 filled PTFE; the wear induced crystallinity of unfilled/filled PTFE; the filler content accumulation on the worn polymer surfaces of alumina and boehmite alumina filled PTFE during wear and the dominant wear rate decreasing factors.

8.2.1. Boehmite alumina as a novel filler of PTFE

Boehmite alumina can be used as a filler of PTFE, regarding the low decomposition of boehmite alumina during the sintering process, and the mechanical and thermal properties of these composites. The results of thermogravimetric analysis (TGA) and Fourier-transform infrared spectroscopy (FTIR) validated that ~60-75% of the hydroxyl functional groups of boehmite alumina are still persisting in the developed composites after the applied free-sintering process with 2 and 10 hours heat dwelling time at 370°C maximal temperature. In this way, these hydroxyl functional groups can participate in the friction and wear processes between the PTFE/boehmite composites and the counterfaces. These statements were confirmed by tests of PTFE with 1/4/8/16 wt% filler content [1, 2].

8.2.2. Low thermal stability of alumina filled PTFE

PTFE became thermally unstable during the sintering process due to the added Al_2O_3 filler. Regarding a sintering process with 10 hours dwelling time at 370°C maximal temperature, Al_2O_3 filled PTFE samples had significantly higher mass loss (extra mass loss) compared to neat PTFE and neat Al_2O_3 filler. This extra mass loss was related to the increased decomposition of PTFE caused by the Al_2O_3 filler. The registered mass loss remarkably increased as a function of the applied heat dwelling time and Al_2O_3 filler content. Regarding PTFE with 30 wt% Al_2O_3 content, all of the PTFE is decomposed after 48 hours dwelling time at 370°C maximal temperature. In this way, the sintering process of Al_2O_3 filled PTFE is not suggested with 8 wt% or higher filler content or with heat dwelling time longer than 2-3 hours, as in these circumstances the extra mass loss reaches 1 wt%. These statements were confirmed by TGA and FTIR results, applying a sintering process with a maximal 10 hours heat dwelling time, and testing PTFE samples with 4/8/16/30 wt% Al_2O_3 content [1].

8.2.3. Wear-induced crystallisation

Regarding the wear debris of all developed filled and unfilled PTFE tested against steel counterfaces in dry contact, the degree of crystallinity increased by ~20-40% compared to the unworn polymers. The main reason for this phenomenon was the mechanical chain scission of the PTFE molecular chains during the wear tests, which reduced the molecular weight by 1-2 orders of magnitude. In this way, these shorter molecular chains could more efficiently reach an aligned arrangement. A further conclusion is that focusing on the degree of crystallinity, the effect of the thermal circumstances and possible molecular chain alignment during the wear process was remarkable only at 0.5 m/s or higher sliding speed. The fillers further increased the mechanical chain scission of PTFE molecular chains compared to the unfilled (neat) PTFE. These statements were confirmed by differential scanning calorimetry (DSC), by testing unfilled (neat) PTFE, PTFE samples with 1/4/8/16 wt% boehmite, 0.25/1/4 wt% graphene, 1 wt% alumina and 1/4 wt% hydrotalcite filler content. Filled PTFE samples were tested with 0.1 m/s sliding speed, while neat (unfilled) PTFE was further tested with 0.5/1/1.5/2/3 m/s sliding speeds [3, 4].

8.2.4. Filler accumulation on the worn polymer surface

The alumina and boehmite alumina content of the worn filled PTFE contact surfaces increased significantly after the wear tests. In contrast, the filler content of the polymer wear debris was lower than the filler content of the unworn sample surfaces. The reason is that the softer PTFE particles can be torn easier from the contact surface than the hard filler particles, and thus increasing the PTFE content of the wear debris. Most of the torn unbroken and broken filler particles pressed and stuck again into the softer PTFE during the wear process, increasing the

filler content of the worn surface. In this way, during the wear process, after the running-in period, the wear mechanism is related to a worn surface with a higher filler content compared to the original unworn sample. These statements were confirmed by energy-dispersive X-ray spectroscopy (EDS), testing alumina and boehmite alumina mono-filled PTFE with 4 wt% filler content [3].

8.2.5. Dominant wear rate decreasing factors

Regarding Al_2O_3 filled PTFE, the approximately two orders of magnitude decrease in the wear rate of PTFE/Al_2O_3 samples was caused by the filler accumulation during the wear process, the smaller wear debris and the formed iron-oxide layer on the worn surface of polymer samples. The formed iron-oxide layer from the steel counterfaces on the polymer samples further increased the durability of the transfer layer, increasing the wear resistance. Regarding all of the used fillers, the influence of the modified mechanical and thermal properties (thermal conductivity, hardness and compressive/shear/tensile properties) on the wear rate has only a secondary role: their measure and their tendency can not decrease the wear rate with orders of magnitude. These statements were confirmed by testing PTFE samples with 1/4/8/16 wt% boehmite, 0.25/1/4/8/16 wt% graphene, 1/4 wt% alumina and 1/4 wt% hydrotalcite filler content [2, 3].

8.2.6. Local contact temperature

Regarding the pin-on-disc wear tests between the Al_2O_3 filled PTFE and steel counterface, it is possible to estimate the local contact temperature during the wear process from temperature-induced change in the colour of the PTFE surface. The maximal local contact temperature measured during the wear tests between the PTFE filled with 4 wt% Al_2O_3 and the steel counterfaces can even reach a temperature range between ~375-400°C. This high local contact temperature appeared only locally due to the collision and deformation of surface roughness peaks; the measured bulk temperature of the steel counterfaces was only at the range of 32-36°C. This statement was confirmed by the temperature-induced change in the colour of the iron-oxide, where the initial black colour of the iron-oxide deposits became red. The black iron(II,III) oxide (Fe_3O_4) deposit on the worn surface of the polymer sample went through an oxidation process at the beginning of the running-in period (~100 m) which resulted in the formation of red hematite (α-Fe_2O_3). For this process, at least 375°C temperature is needed according to the literature. These statements were confirmed by EDS using samples wear-tested with 0.1 m/s sliding speed and 3 MPa contact pressure [3].

8.3. Belangrijkste onderzoeksconclusies (Main research conclusions in Dutch)

Conclusie 1

Boehmiet-aluminiumoxide kan worden gebruikt als vulstof van PTFE, omwille van zijn geringe decompositie tijdens het sinterproces en omwille van de gunstige mechanische en thermische eigenschappen van deze composieten. De resultaten van thermogravimetrische analyse (TGA) en Fourier-transform infraroodspectroscopie (FTIR) bevestigen dat ~ 60 à 75% van de hydroxyl functionele groepen van boehmiet-aluminiumoxide nog steeds aanwezig zijn na een sinterproces met 2 tot 10 uren warmte verblijftijd bij een maximale temperatuur van 370 °C. Deze hydroxyl functionele groepen nemen deel aan de wrijvings- en slijtageprocessen van het PTFE-boehmiet-composieten. Dit is hier aangetoond met tribologische testen op PTFE met een vulstofgehalte van 1 / 4 / 8 / 16 gew.% [1, 2].

Conclusie 2

PTFE wordt thermisch onstabiel tijdens het sinterproces vanwege de toegevoegde Al_2O_3. Bij een sinterproces met 10 uur verblijftijd bij een maximale temperatuur van 370 °C, vertonen met Al_2O_3 gevulde PTFE-monsters een significant hoger massaverlies in vergelijking met pure PTFE en puur Al_2O_3-vulmiddel. Dit extra massaverlies houdt verband met de verhoogde afbraak van PTFE, veroorzaakt door het Al_2O_3. Het massaverlies neemt opmerkelijk toe in functie van de toegepaste warmte-verblijftijd en het gehalte aan Al_2O_3. Bij PTFE met 30 gew.% Al_2O_3, wordt alle PTFE afgebroken na 48 uur verblijftijd bij een temperatuur van 370 °C. Een sinterproces van met Al_2O_3 gevulde PTFE wordt dus afgeraden vanaf een Al_2O_3-concentratie van 8 gew.% of meer, of bij een warmteverblijftijd langer dan 2 à 3 uur. In deze omstandigheden bereikt het extra massaverlies immers 1 gew.%. TGA- en FTIR-resultaten na een sinterproces met een warmteverblijftijd van 10 uur voor PTFE-monsters met 4 / 8 / 16 / 30 gew.% Al_2O_3-gehalte bevestigen dit [1].

Conclusie 3

In de slijtage debris van alle geteste gevulde en ongevulde PTFE-monsters (slijtagetesten in droog contact en met stalen tegenloopvlakken) neemt de kristalliniteit toe met ~ 20-40%, in vergelijking met de ongesleten monsters. De belangrijkste reden hiervoor is de mechanische splitsing van de PTFE-molecuulketens tijdens de slijtagetesten, waardoor het moleculair gewicht met 1 à 2 grootteordes afneemt. De kortere ketens die hier het gevolg van zijn, kunnen sneller een gealigneerde oriëntatie bereiken. Verder kan worden besloten dat het effect van de thermische omstandigheden en de mogelijke moleculaire ketenuitlijning tijdens het slijtageproces zich vooral duidelijk manifesteren bij glijsnelheden van 0,5 m/s of hoger. De vulstoffen verhogen ook de mechanische splitsing van PTFE moleculaire ketens in vergelijking

met de ongevulde (zuivere) PTFE, zoals ook kon worden aangetoond aan de hand van differentiële scanning calorimetrie (DSC) op ongevulde (pure) PTFE, met 1 / 4 / 8 / 16 gew.% boehmiet, 0,25 / 1 / 4 gew.% grafeen, 1 gew.% aluminiumoxide en 1 / 4 gew.% hydrotalciet. Gevulde PTFE-monsters werden getest met een glijsnelheid van 0,1 m/s, terwijl ongevulde PTFE verder werd getest met een glijsnelheid van 0,5 / 1 / 1,5 / 2 / 3 m/s [3, 4].

Conclusie 4

Het gehalte aan aluminiumoxide en boehmiet van de gevulde PTFE-contactoppervlakken nam toe aanzienlijk na de slijtagetesten. Daarentegen was het vulstofgehalte van de slijtagedebris lager dan het vulstofgehalte van de monsteroppervlakken vóór slijtage. De reden is dat de zachtere PTFE-deeltjes gemakkelijker van het contactoppervlak afschuiven dan de harde vulstofdeeltjes, waardoor het PTFE-gehalte van de slijtagedeeltjes toeneemt. De meeste van de afgescheurde vulstofdeeltjes worden tijdens het slijtageproces opnieuw in het zachtere PTFE gedrukt, waardoor het vulstofgehalte in het slijtagespoor van het polymeer schijnbaar toeneemt. Op deze manier zal tijdens het slijtageproces, na de inloopperiode, het slijtagemechanisme evolueren naar slijtage van een oppervlak met een hoger vulstofgehalte dan bij de start van het slijtageproces. Dit wordt hier bevestigd door energiedispersieve röntgenspectroscopie (EDS), na slijtagetesten van met aluminiumoxide en met boehmiet-aluminiumoxide mono-gevuld PTFE met een vulstofgehalte van 4 gew.% [3].

Conclusie 5

De afname met twee grootteordes van de slijtagesnelheid van met Al_2O_3 gevulde PTFE wordt veroorzaakt door de opeenhoping van vulstof tijdens het slijtageproces, door de kleinere slijtagedeeltjes en door de gevormde ijzeroxidelaag in het slijtagespoor van de polymeermonsters . De gevormde ijzeroxidelaag op de polymeermonsters verhoogt verder de slijtageweerstand van de transfertlaag en verhoogt aldus de slijtvastheid. Met betrekking tot alle gebruikte vulstoffen spelen de gewijzigde mechanische en thermische eigenschappen (thermische geleidbaarheid, hardheid en compressie-, afschuif-, en trekeigenschappen) slechts een secundaire rol. Ze kunnen de slijtagesnelheid niet significant verminderen, zoals blijkt uit de testen van PTFE-monsters met een vulstofgehalte van 1 / 4 / 8 / 16 gew.% boehmiet, 0,25 / 1 / 4 / 8 / 16 gew.% grafeen, 1/4 gew.% aluminiumoxide en 1/4 gew.% hydrotalciet [2, 3].

Conclusie 6

De flitstemperatuur die optreedt tijdens de pin-on-disc-slijtagetesten op het met Al_2O_3 gevulde PTFE en stalen tegenloopvlak kan worden geschat op basis van de temperatuurgeïnduceerde verandering in de kleur van het PTFE-oppervlak. De flitstemperatuur tijdens de slijtagetesten

van PTFE gevuld met 4 gew.% Al_2O_3 tegenover staal bereikt tussen de 375 en 400 °C . Deze hoge flitstemperatuur treedt echter alleen plaatselijk op, als gevolg van het contact tussen en de vervorming van ruwheidspieken. De gemeten bulktemperatuur van de stalen tegenloopvlakken bedraagt slechts 32 à 36 °C. De kleurverandering van het staaloppervlak (ijzeroxide) van zwart naar bruinrood bevestigt het optreden van de hoge flitstemperaturen. Het origineel zwarte oxide (ijzer (II,III)-oxide, Fe_3O_4) afgezet op het polymeermonster ondergaat een oxidatieproces aan het begin van de inloopperiode (~ 100 m), wat resulteert in de vorming van rood hematiet (α-Fe_2O_3). Voor dit proces is volgens de literatuur een temperatuur van minimaal 375 °C vereist. Dit fenomeen wordt ook aangetoond door EDS na slijtagetesten met een glijsnelheid van 0,1 m / s en een contactdruk van 3 MPa [3].

8.4. Főbb tudományos következtetések (Main research conclusions in Hungarian)

1. Tézis

Bizonyítottam, hogy a böhmit (alumínium-oxid-hidroxid - AlO(OH)) felhasználható politetrafluoretilén (PTFE) adalékanyagaként, a böhmit szintereléskor lejátszódó bomlási folyamatai, és a kompozit mechanikai és termikus anyagjellemzői alapján. Termogravimetriai analízis (TGA) és Fourier-transzformációs infravörös spektroszkópiás (FTIR) vizsgálatokkal igazoltam, hogy a böhmit adalékanyag hidroxil funkciós csoportjainak ~60-75%-a továbbra is jelen van a szinterelt kompozitban a maximális 370°C hőmérsékleten, 2 óra, illetve 10 óra hőntartás mellett végzett, terhelés nélküli szinterelési ciklus befejeztével. Így ezek a hidroxil-csoportok részt tudnak venni a PTFE/böhmit kompozit egy külső ellenfelületen történő súrlódási és kopási folyamatában. Állításaimat 1, 4, 8 és 16 m/m% adalékanyag-tartalom esetében igazoltam [1, 2].

2. Tézis

Bizonyítottam, hogy a politetrafluoretilén (PTFE) alapanyag, az alumínium-oxid (Al_2O_3) hatására termikusan instabillá válik a szinterelés folyamata közben. A 370°C-on történő szintereléskor a PTFE és az Al_2O_3 adalékanyag egymástól szeparáltan vizsgált tömegcsökkenéséhez képest a keverékük nagyobb tömegveszteséget (többlet tömegveszteség) mutatott 10 órás hőntartási idő esetében. Ez a többlet tömegveszteség a PTFE alapanyagnak az Al_2O_3 hatására megnövekedett bomlásának a következménye. Az alkalmazott hőntartási idő, illetve az Al_2O_3 adalékanyag-tartalom növelésével a regisztrált tömegcsökkenés nagymértékben növekszik. Kimutattam, hogy 30 m/m% Al_2O_3 tartalmú PTFE esetében, 48 órás 370°C-on történő hőntartás hatására a teljes PTFE tartalom elbomlik. Ebből következően az Al_2O_3 adalékanyag 8 m/m%-os vagy annál nagyobb koncentrációban, és 2-3 óránál hosszabb hőntartási idő alkalmazásával nem javasolt PTFE alapanyaggal szinterelés útján történő feldolgozásra, mivel ekkor már 1 m/m%-ot elérő többlet tömegveszteség lép fel.

Állításaimat termogravimetriai analízis (TGA) és Fourier-transzformációs infravörös spektroszkópiás (FTIR) vizsgálatokkal igazoltam, 4 / 8 / 16 / 30 m/m% Al_2O_3 adalékanyag-tartalom esetében, 10 óráig terjedő hőntartási idő alkalmazásával [1].

3. Tézis

Megállapítottam, hogy acél ellendarabon történő száraz súrlódásnál, a politetrafluoretilén (PTFE) kompozitok kopadék szemcséinek a kristályossága minden egyes vizsgált minta esetében ~20-40%-kal nagyobb a nem koptatott anyagokhoz képest. Ennek fő oka, hogy a PTFE molekulaláncok koptatás közben lejátszódó tördelődéséből adódóan a kopadék 1-2 nagyságrenddel kisebb átlagos molekulatömeggel rendelkezik, így a PTFE rövidebb molekulaláncai egyszerűbben rendeződnek kristályos szerkezetbe. Továbbá megállapítottam, hogy a koptatás folyamán kialakuló termikus viszonyoknak, illetve a molekulaláncok koptatás irányában történő esetleges orientálódásának a hatása csak 0,5 m/s vagy nagyobb koptatási sebesség esetében jelentős a kristályos részarány változása szempontjából. Az adalékanyagok jelenléte nagyobb fokú PTFE molekulalánc tördelődést okozott a töltetlen PTFE anyaghoz viszonyítva. Állításaimat differenciális pásztázó kalorimetria (DSC) mérésekkel, töltetlen PTFE, illetve 1/4/8/16 m/m% böhmit (alumínium-oxid-hidroxid - AlO(OH)), 0,25/1/4 m/m% grafén, 1 m/m% alumínium-oxid (Al_2O_3) és 1/4 m/m% hidrotalcit (MG70) töltésű mintáknál igazoltam. A töltött mintákat 0.1 m/s sebességgel, míg a töltetlen PTFE mintákat 0.1/0.5/1/1.5/2/3 m/s koptatási sebességgel vizsgáltam [3, 4].

4. Tézis

Megállapítottam, hogy a politetrafluoretilén (PTFE) kompozitok koptatott felületén az alumínium-oxid (Al_2O_3) és böhmit (alumínium-oxid-hidroxid - AlO(OH)) adalékanyag a koptatás következményeként az eredeti, nem koptatott felülethez képest nagymértékben feldúsul, míg ezzel szemben a kopadék adalékanyag-tartalma kisebb, mint a koptatás előtt mért adalékanyag-tartalom a minták felületén. Ennek oka, hogy az adalékanyagnál jelentősen kisebb keménységű PTFE részecskék könnyebben leszakadnak a koptatott felületről, mint a töltőanyag, növelve ezzel a kopadék PTFE tartalmát. A leszakadt töltőanyag-részecskék, illetve törmelékek nagy része a koptatás folyamán benyomódik és újból beágyazódik a puha PTFE alapanyagba, növelve ezzel az adalékanyag koncentrációját a felületen. Ennek következménye, hogy a koptatás folyamán, a bekopási szakasz után, a kopási mechanizmus már az eredeti mintához képest egy nagyobb adalékanyagtartalmú koptatási felületen játszódik le. Az adalékanyag feldúsulására vonatkozó állításomat energiadiszperzív röntgenspektrométer (EDS) vizsgálatokkal, 4 m/m% Al_2O_3 / alumínium-oxid-hidroxid (böhmit) tartalmú PTFE kompozitok esetében igazoltam [3].

5. Tézis

Bizonyítottam, hogy az alumínium-oxiddal (Al_2O_3) töltött politetrafluoretilén (PTFE) minták kopási sebességének körülbelül két nagyságrendbeli csökkenése mögött a kopás közbeni adalékanyag-feldúsulás, a kisebb méretű kopadékok kialakulása és a polimer minta kopási felületén lerakódott vas-oxid réteg áll. Az acél ellendarabból származó, a polimer felületén lerakódott vas-oxid réteg az átmeneti réteg kopással szembeni ellenállóságának további növelését segítette elő. A további adalékanyagokat is vizsgálva, bizonyítottam, hogy a mechanikai és termikus jellemzők (hővezetési tényező, keménység, nyomó/nyíró/húzó mechanikai tulajdonságok) változásának hatása a kopási értékekre csak másodlagos, mértékük és tendenciájuk nem indokolja a kopási sebesség több nagyságrendbeli csökkenését. Állításaimat 1/4/8/16 m/m% böhmit (alumínium-oxid-hidroxid - AlO(OH)), 0,25/1/4/8/16 m/m% grafén, 1/4 m/m% Al_2O_3 és 1/4 m/m% hidrotalcit (MG70) töltésű mintáknál igazoltam [2, 3].

6. Tézis

Bemutattam, hogy a politetrafluoretilén (PTFE) minta felületének az elszíneződéséből következtetni lehet a súrlódási folyamat során fellépő valós kontakt hőmérsékletre alumínium-oxidot (Al_2O_3) tartalmazó PTFE és az acél ellendarab között végzett pin-on-disc koptatási vizsgálatok esetében. Megállapítottam, hogy a 4 m/m% Al_2O_3-ot tartalmazó PTFE és az acél ellendarab között végzett koptatási vizsgálatok folyamán kialakuló maximális hőmérséklet a ~375-400°C hőmérséklettartományt is eléri. Ez a magas hőmérséklet csak a felületérdességi csúcsok ütközése és deformálódása folyamán, lokálisan alakul ki, az acél ellendarab túloldalán mért hőmérséklet mindössze 32-36°C között helyezkedik el. Állításomat a vas-oxid színének a hőmérséklet hatására bekövetkező változásával igazoltam, amelynek során a kezdeti fekete színű lerakódott részecskéket vöröses részecskékből álló réteg váltja fel. A polimer minta koptatási felületére lerakódott fekete vas-oxid (Fe_3O_4) a bekopási szakasz elején (~100 m) oxidáción megy keresztül, amelynek során vörös színű hematit (α-Fe_2O_3) jön létre. Ehhez a folyamathoz szükséges minimális hőmérséklet a szakirodalom alapján 375°C. Állításomat 0.1 m/s koptatási sebességgel és 3 MPa nyomással koptatott mintákon végzett energiadiszperzív röntgenspektrométer (EDS) vizsgálatokkal igazoltam [3].

8.5. Application-oriented comparison of the developed unfilled/filled PTFE materials

1) The developed filled PTFE can be the base material of sliding bearings, guideways and linear slides, as some examples. The wear tests were focusing on dry sliding contact at room temperature.

2) Regarding the pin-on-discs wear tests of the unfilled and mono-filled PTFE pin samples against 42CrMo4 steel disc counterfaces (3 MPa contact pressure, 0.1 m/s sliding speed, 1000 m sliding distance and dry contact at room temperature), the following consequences can be drawn:
    - No significant changes in the coefficient of friction were registered.
    - None of the fillers damaged significantly the surface of the steel counterfaces during the wear process
    - PTFE/Al_2O_3-4 sample reached the lowest wear rate with $2.9 \cdot 10^{-6}$ mm^3/Nm, but low thermal stability was registered during the sintering process. In this way, the potential heat dwelling time during the sintering process is restricted, which is not beneficial in samples with a larger volume, where the necessary sintering time can be even longer than one day.
    - The second lowest wear rate was reached by PTFE/Graphene-16 sample ($8.5 \cdot 10^{-6}$ mm^3/Nm), but this material has even lower thermal stability during the sintering process than PTFE/Al_2O_3-4.
    - PTFE/Graphene-8 and PTFE/Graphene-4 had the third and fourth lowest wear rate ($3.2 \cdot 10^{-5}$ and $4.7 \cdot 10^{-5}$ mm^3/Nm), respectively. Comparing with PTFE/Graphene-16, PTFE/Graphene-8 and PTFE/Al_2O_3-4 materials, PTFE/Graphene-4 was the most reliable regarding the sintering process, as it had the highest thermal stability.

3) The achieved wear rates did not remarkably depend on the steel counterfaces (42CrMo4/304/34CrNiMo6).

4) The following conclusions can be drawn about the hybrid-filled PTFE samples (42CrMo4 steel counterfaces, 3 MPa contact pressure, 0.1 m/s sliding speed, 1000 m sliding distance and dry contact at room temperature):
    - All hybrid samples reached a low wear rate, PTFE/G/A-0.25/4, PTFE/G/A-2/2 and PTFE/G/A-4/4 had $1.2 \cdot 10^{-5}$, $2.8 \cdot 10^{-5}$ and $4.3 \cdot 10^{-6}$ mm^3/Nm wear rate, respectively.
    - PTFE/G/A-4/4 had the lowest thermal stability during the sintering cycle, even less than PTFE/Al_2O_3-4 mono-filled material. Compared to PTFE/Graphene-4, all of the hybrid-filled samples had lower thermal stability at the sintering process.

5) A parametrical study was carried out with PTFE/Graphene-4, PTFE/Graphene-8, PTFE/Al_2O_3-4 and PTFE/G/A-4/4 samples against 42CrMo4 steel counterfaces. The applied parameters and conditions: 1/3/5/7 MPa contact pressure, 0.5/1/1.5/2/3 m/s sliding speed, 3000 m stipulated sliding distance and dry contact at room temperature). The materials were applicable if they reached the stipulated 3000 m sliding distance and if the measured mass loss was lower than 0.025 g. The following conclusions can be drawn:

- PTFE/Graphene-4 and PTFE/Graphene-8 materials could not perform the test requirements when the contact pressure was higher than 1 MPa. PTFE/Graphene-4 was not applicable at 2 and 3 m/s sliding speed, even when the applied contact pressure was only 1 MPa.
- PTFE/Al_2O_3-4 and PTFE/G/A-4/4 can be used in a remarkably wider application range, but their thermal stability was significantly lower during the sintering process compared to PTFE/Graphene-4 and PTFE/Graphene-8 materials. PTFE/G/A-4/4 had the widest application range and the lowest thermal stability.

8.6. Recommendations for further study

For future work, it can be useful to study the effect of coatings on the alumina particles. As there is an interaction between alumina and PTFE during the sintering cycle, which decreases the thermal stability of the composite at the sintering temperature, the use of coatings can compensate it. Regarding the wear mechanism, the use of coated alumina can also indicate the significance of a potential tribo-chemical reaction between the alumina particles and the *in situ* functionalised PTFE chain ends. In other words, the wear performance of the different coatings compared to the reference uncoated alumina can be analysed and related to the significance of the potential tribo-chemical reactions.

Further possibility can be the characterisation of friction and wear behaviour with real scale test equipment. With a large-scale configuration, the applied test conditions, the size and the geometry of the test samples are close to a given real application. These kinds of tests can give further information to customers about the performance of these materials in their application area. Potential test configurations: linear reciprocating sliding flat-on-flat test configuration as a first step, and real scale bearing tests as a second step. The unfilled/filled PTFE bearings can be made with room-temperature pressing – free sintering method, but the applied sintering protocol has to be suitable for the increased size of the product. The required geometry of the sliding bearings can be provided by turning of the sintered base materials. Suggested materials for these wear tests are unfilled PTFE as a reference material, PTFE/Al_2O_3-4 and PTFE/G/A-4/4, as according to the introduced parametrical study (Chapter 7.3.4), they can be used in a wide application range. The sintering protocol of the base material of sliding bearings has to include a relatively long dwelling time at the maximal sintering temperature (~370°C) due to the increased dimension compared to lab-scale samples. In this way, the thermal stability of these materials during the sintering process is an essential factor, which could be provided with the coating of the Al_2O_3 fillers.

8.7. References

[1] L.F. Tóth, P. De Baets, G. Szebényi: Processing Analysis of Nanoparticle Filled PTFE: Restrictions and Limitations of High Temperature Production. Polymers 12 (2020) 2044, 1-14.

[2] L.F. Tóth, P. De Baets, G. Szebényi: Thermal, Viscoelastic, Mechanical and Wear Behaviour of Nanoparticle Filled Polytetrafluoroethylene: A Comparison. Polymers 12 (2020) 1940, 1-17.

[3] L.F. Tóth, G. Szebényi, J. Sukumaran, P. De Baets: Tribological Characterisation of Nanoparticle Filled PTFE: Wear-Induced Crystallinity Increase and Filler Accumulation. Express Polymer Letters, 2021. Accepted.

[4] L.F. Tóth, J. Sukumaran, G. Szebényi, P. De Baets: Tribo-mechanical interpretation for advanced thermoplastics and the effects of wear-induced crystallization. Wear 440-441 (2019) 203083, 1-10.

APPENDIX A – MATLAB CODE

```
Name='A4';
Name2='A4-Diagram.mat';

COF=FrictionCoefficient;
t=Times;
T=ProbeC;
W=Wearm;
SD=Slidingm;
RPM=RPMmin1;
Torque=TorqueNm;
FN=ForceN;
FF=FrictionForceCalculatedN;

AV_COF=mean(COF);
DEV_COF=std(COF);
MAX_COF=max(COF);
MIN_COF=min(COF);
MAX_W=min(W);
MAX_SD=max(SD);
AV_RPM=mean(RPM);
AV_FN=mean(FN);
AV_FF=mean(FF);
MAX_t=max(t);

for i=1:1:length(t)
    ROT(i)=AV_RPM/60*t(i);
end

MAX_ROT=max(ROT);

ONECYCLE=length(t)/MAX_ROT;
ONECYCLE_Round=round(ONECYCLE);

for i=1:1:length(t)
    Floor(i)=floor(i/ONECYCLE_Round);
    Ceil(i)=ceil(i/ONECYCLE_Round);
end

for i=ONECYCLE_Round:ONECYCLE_Round:length(t)
    Floor(i)=floor(i/ONECYCLE_Round)-1;
end

for i=1:1:(length(t)-100)

COFMODC(i)=mean(COF((1+ONECYCLE_Round*Floor(i)):(ONECYCLE_Round*Ceil(i))));
    WMODC(i)=mean(W((1+ONECYCLE_Round*Floor(i)):(ONECYCLE_Round*Ceil(i))));
end

for i=1:1:300
    COFMODC(i)=COFMODC(301);
    WMODC(i)=WMODC(301);
end
```

```
for i=(length(t)-300):1:length(t)
    COFMODC(i)=COFMODC(length(t)-301);
    WMODC(i)=WMODC(length(t)-301);
end

AV_COFMODC=mean(COFMODC);
DEV_COFMODC=std(COFMODC);
MAX_COFMODC=max(COFMODC);
MIN_COFMODC=min(COFMODC);
MAX_WMODC=min(WMODC);

B={'Max_t' 'Av_CoFModC' 'Dev_CoFModC' 'Max_CoFModC' 'Min_CoFModC'
'Max_WModC' 'Max_SD' 'Av_RPM' 'Max_Rot' 'Av_FN'; '[min]' '[-]' '[-]' '[-]'
'[-]' '[um]' '[m]' '[1/min]' '[Rot]' '[N]'; MAX_t/60 AV_COFMODC DEV_COFMODC
MAX_COFMODC MIN_COFMODC MAX_WMODC MAX_SD AV_RPM MAX_ROT AV_FN};

Figure_FrictionModC_Rotation(ROT,COFMODC, Name);
Figure_FrictionModC_Distance(SD,COFMODC, Name);
Figure_WearModC_Rotation(ROT,WMODC, Name);
Figure_WearModC_Distance(SD,WMODC, Name);

save(Name)
save(Name2,'COFMODC','WMODC','SD','ROT')
xlswrite(Name,B)
```

APPENDIX B - TABLES

Table B.1. The density of neat unsintered/sintered PTFE samples pressed with different pressure. Sintered samples: 90 °C/h heating rate, 4 h dwelling time, 30 °C/h cooling rate.

Pressure (MPa)	Before sintering Density (g/cm^3)		After sintering Density (g/cm^3)	
	Average	Deviation	Average	Deviation
5	1.726	0.006	2.162	0.001
12.5	1.979	0.004	2.160	0.002
20	2.068	0.004	2.167	0.002
35	2.165	0.004	2.169	0.001
50	2.193	0.001	2.169	0.002

Table B.2. The compressive stress and modulus of the sintered neat PTFE samples. Sintering: 90 °C/h heating rate, 4 h dwelling time, 30 °C/h cooling rate.

Applied pressure	Compressive stress (MPa)				Compressive modulus (MPa)	
	5% deformation		10% deformation			
(MPa)	Average	Deviation	Average	Deviation	Average	Deviation
5	12.96	0.86	18.75	0.40	362.60	7.88
12.5	13.55	0.48	18.69	0.38	362.61	12.11
20	12.74	0.20	19.07	0.17	359.15	8.28
35	13.46	0.34	19.37	0.31	356.75	15.86
50	13.74	0.33	19.46	0.12	358.23	19.08

Table B.3. The hardness of the sintered neat PTFE samples as a function of applied pressure. Sintering: 90 °C/h heating rate, 4 h dwelling time, 30 °C/h cooling rate.

Applied pressure	Hardness (Shore-D)	
(MPa)	Average	Deviation
5	57.1	1.1
12.5	57.9	0.6
20	56.9	1.0
35	56.4	0.9
50	56.7	0.6

Table B.4. The density of the sintered neat PTFE, samples pressed with 12.5 MPa, 90 °C/h heating rate, 4 h dwelling time.

Cooling rate (°C/h)	Density (g/cm^3)	
	Average	Deviation
60	2.157	0.001
30	2.160	0.002
20	2.158	0.002
15	2.158	0.003

Table B.5. Average density of the sintered neat PTFE, samples pressed with 12.5 MPa, 90 °C/h heating rate, 30 °C/h cooling rate.

Dwelling time (h)	Density (g/cm^3)	
	Average	Deviation
Unsintered	1.979	0.004
0.5	2.170	0.002
1	2.169	0.002
2	2.168	0.001
3	2.169	0.002
4	2.160	0.001
6	2.159	0.001
8	2.158	0.002

Table B.6. The compressive stress and modulus of the sintered neat PTFE samples. Samples pressed with 12.5 MPa at room temperature, sintering: 90 °C/h heating rate, 4 h dwelling time.

Cooling rate	Compressive stress (MPa)				Compressive modulus (MPa)	
	5% deformation		10% deformation			
(°C/h)	Average	Deviation	Average	Deviation	Average	Deviation
60	12.84	0.51	18.81	0.29	344.01	12.27
30	13.55	0.48	18.69	0.38	362.61	12.11
20	13.74	0.37	19.33	0.25	369.87	11.53
15	13.45	0.51	19.26	0.22	374.36	6.19

Table B.7. The compressive stress and modulus of the sintered neat PTFE samples. Pressed with 12.5 MPa at room temperature, sintering: 90 °C/h heating rate, 30 °C/h cooling rate.

Dwelling time	Compressive stress (MPa)				Compressive modulus (MPa)	
	5% deformation		10% deformation			
(h)	Average	Deviation	Average	Deviation	Average	Deviation
Unsintered	5.97	0.26	3.42	0.23	---	---
0.5	14.67	0.30	19.78	0.44	411.97	10.67
1	14.46	0.18	19.47	0.26	397.83	12.45
2	13.92	0.73	18.91	0.57	405.91	11.77
3	13.80	0.52	19.10	0.10	390.94	9.19
4	13.55	0.48	18.69	0.38	362.61	12.11
6	13.79	0.16	18.79	0.18	374.73	11.04
8	13.84	0.28	19.27	0.27	370.23	5.43

Table B.8. The hardness of the sintered neat PTFE samples as a function of cooling rate. Samples pressed with 12.5 MPa at room temperature, sintering: 90 °C/h heating rate, 4 h dwelling time.

Cooling rate	Hardness (Shore-D)	
(°C/h)	Average	Deviation
15	57.6	0.9
20	57.7	0.8
30	57.9	0.6
60	57.2	1.1

Table B.9. The hardness of the sintered neat PTFE samples as a function of dwelling time. Samples pressed with 12.5 MPa at room temperature, sintering: 90 °C/h heating rate, 30 °C/h cooling rate.

Dwelling time	Hardness (Shore-D)	
(h)	Average	Deviation
Unsintered	55.9	1.4
0.5	51.0	1.4
1	53.5	1.5
2	54.3	0.9
3	53.9	0.8
4	57.9	0.6
6	58.3	1.2
8	57.0	0.9

Table B.10. Average density and thermal conductivity of sintered PTFE materials. Samples pressed with 12.5 MPa at room temperature, sintering: 90 °C/h heating rate, 2 h dwelling time, 30 °C/h cooling rate.

Samples	Density (g/cm^3)	Thermal conductivity (W/mK)
PTFE	2.168 ± 0.001	0.243 ± 0.013
PTFE/graphene-0.25	2.169 ± 0.001	0.246 ± 0.007
PTFE/graphene-1	2.166 ± 0.002	0.254 ± 0.023
PTFE/graphene-4	2.137 ± 0.002	0.314 ± 0.013
PTFE/graphene-8	2.074 ± 0.002	0.447 ± 0.022
PTFE/graphene-16	1.946 ± 0.002	0.624 ± 0.033
PTFE/Al_2O_3-1	2.181 ± 0.002	0.249 ± 0.019
PTFE/Al_2O_3-4	2.198 ± 0.001	0.265 ± 0.017
PTFE/BA80-1	2.170 ± 0.002	0.248 ± 0.023
PTFE/BA80-4	2.186 ± 0.002	0.273 ± 0.015
PTFE/BA80-8	2.193 ± 0.001	0.306 ± 0.008
PTFE/BA80-16	2.202 ± 0.001	0.332 ± 0.003
PTFE/MG70-1	2.143 ± 0.002	0.256 ± 0.009
PTFE/MG70-4	2.125 ± 0.002	0.280 ± 0.012
PTFE/G/A-0.25/4	2.199 ± 0.001	0.265 ± 0.007
PTFE/G/A-2/2	2.172 ± 0.001	0.283 ± 0.011
PTFE/G/A-4/4	2.156 ± 0.002	0.386 ± 0.013

Table B.11. Average Shore-D hardness, compressive stress at 5% and 10% deformation and average compressive modulus between 1% and 2% deformation of the sintered materials. Samples pressed with 12.5 MPa at room temperature, sintering: 90 °C/h heating rate, 2 h dwelling time, 30 °C/h cooling rate.

Samples	Hardness (Shore-D)	Compressive stress, MPa (at 5% deformation)	Compressive stress, MPa (at 10% deformation)	Compressive modulus, MPa
PTFE	54.3 ± 0.9	13.92 ± 0.73	18.91 ± 0.57	405.9 ± 11.8
PTFE/graphene-0.25	55.0 ± 0.2	14.14 ± 0.19	19.51 ± 0.15	378.6 ± 9.1
PTFE/graphene-1	55.7 ± 0.9	14.33 ± 0.21	19.36 ± 0.25	435.2 ± 14.8
PTFE/graphene-4	55.6 ± 1.2	14.15 ± 0.48	19.56 ± 0.24	440.2 ± 17.8
PTFE/graphene-8	55.3 ± 0.7	12.27 ± 0.45	18.37 ± 0.13	286.0 ± 10.9
PTFE/graphene-16	53.9 ± 0.9	7.57 ± 0.77	14.35 ± 0.35	172.2 ± 9.9
PTFE/Al_2O_3-1	57.7 ± 1.0	14.52 ± 0.53	19.03 ± 0.64	544.7 ± 11.0
PTFE/Al_2O_3-4	58.8 ± 0.4	14.70 ± 0.26	19.11 ± 0.29	538.2 ± 10.4
PTFE/BA80-1	56.3 ± 0.7	14.44 ± 0.27	18.98 ± 0.32	488.3 ± 10.9
PTFE/BA80-4	58.4 ± 0.5	15.12 ± 0.41	19.55 ± 0.44	540.4 ± 16.1
PTFE/BA80-8	59.1 ± 0.9	13.72 ± 0.93	20.10 ± 0.34	388.9 ± 9.2
PTFE/BA80-16	60.0 ± 1.1	14.27 ± 1.19	21.79 ± 0.26	409.2 ± 9.8
PTFE/MG70-1	53.7 ± 0.9	10.94 ± 1.01	17.16 ± 0.12	362.5 ± 9.3
PTFE/MG70-4	54.5 ± 0.7	10.73 ± 0.48	16.69 ± 0.24	357.4 ± 13.9
PTFE/G/A-0.25/4	56.6 ± 0.8	13.67 ± 0.11	18.85 ± 0.06	345.1 ± 12.7
PTFE/G/A-2/2	56.7 ± 0.5	13.52 ± 0.12	18.86 ± 0.09	327.5 ± 0.1
PTFE/G/A-4/4	58.2 ± 0.3	12.61 ± 0.52	18.18 ± 0.58	315.4 ± 20.3

Table B.12. Shear stress at 2% and 5% strain, elongation at 7 MPa stress and shear modulus of the sintered materials. Samples pressed with 12.5 MPa at room temperature, sintering: 90 °C/h heating rate, 2 h dwelling time, 30 °C/h cooling rate.

Samples	Shear stress at 2% strain (MPa)	Shear stress at 5% strain (MPa)	Elongation at 7 MPa stress (%)	Shear modulus (MPa)
PTFE	3.84 ± 0.08	5.93 ± 0.09	9.28 ± 0.55	223.2 ± 15.1
PTFE/graphene-0.25	3.85 ± 0.64	5.79 ± 0.76	7.55 ± 0.31	226.8 ± 5.3
PTFE/graphene-1	3.94 ± 0.20	6.35 ± 0.31	6.59 ± 0.41	256.6 ± 21.0
PTFE/graphene-4	4.44 ± 0.26	6.89 ± 0.28	5.26 ± 0.60	275.8 ± 25.8
PTFE/graphene-8	6.58 ± 0.22	9.23 ± 0.22	2.29 ± 0.16	507.8 ± 19.6
PTFE/graphene-16	7.11 ± 0.33	9.63 ± 0.47	1.95 ± 0.22	657.4 ± 8.2
PTFE/Al_2O_3-1	4.22 ± 0.02	6.12 ± 0.47	6.82 ± 0.24	272.1 ± 25.9
PTFE/Al_2O_3-4	4.42 ± 0.31	6.83 ± 0.17	5.36 ± 0.39	293.7 ± 11.2
PTFE/BA80-1	3.75 ± 0.38	6.08 ± 0.01	8.16 ± 0.54	225.5 ± 16.0
PTFE/BA80-4	4.19 ± 0.35	6.40 ± 0.42	5.95 ± 0.07	229.6 ± 2.7
PTFE/BA80-8	6.07 ± 0.30	8.63 ± 0.35	2.67 ± 0.32	418.9 ± 28.1
PTFE/BA80-16	7.26 ± 0.34	9.68 ± 0.33	1.86 ± 0.21	611.4 ± 50.3
PTFE/MG70-1	4.35 ± 0.43	6.49 ± 0.22	6.73 ± 0.59	249.9 ± 38.2
PTFE/MG70-4	4.79 ± 0.32	6.99 ± 0.26	5.05 ± 0.68	281.3 ± 30.0
PTFE/G/A-0.25/4	3.77 ± 0.63	6.44 ± 0.84	5.23 ± 0.47	297.9 ± 1.4
PTFE/G/A-2/2	5.01 ± 0.11	7.58 ± 0.28	3.99 ± 0.29	340.5 ± 6.1
PTFE/G/A-4/4	5.84 ± 0.18	8.13 ± 0.22	3.09 ± 0.22	455.0 ± 19.9

Table B.13. Tensile stress at 2% and 5% strain and Young`s modulus of the sintered materials. Samples pressed with 12.5 MPa at room temperature, sintering: 90 °C/h heating rate, 2 h dwelling time, 30 °C/h cooling rate.

Samples	Tensile stress at 2% strain (MPa)	Tensile stress at 5% strain (MPa)	Young`s modulus, (MPa)
PTFE	10.16 ± 0.18	12.18 ± 0.14	511.6 ± 22.3
PTFE/graphene-0.25	10.34 ± 0.13	12.60 ± 0.08	582.6 ± 10.0
PTFE/graphene-1	10.29 ± 0.14	12.19 ± 0.21	551.0 ± 5.5
PTFE/graphene-4	11.23 ± 0.15	13.21 ± 0.18	624.1 ± 53.8
PTFE/graphene-8	12.22 ± 0.82	14.90 ± 0.75	1227.4 ± 60.3
PTFE/graphene-16	13.31 ± 1.32	---	1620.5 ± 153.4
PTFE/Al_2O_3-1	10.33 ± 0.18	12.22 ± 0.24	632.0 ± 12.5
PTFE/Al_2O_3-4	11.51 ± 0.06	12.58 ± 0.11	673.4 ± 23.5
PTFE/BA80-1	10.52 ± 0.43	12.06 ± 0.27	611.2 ± 7.8
PTFE/BA80-4	10.81 ± 0.45	11.95 ± 0.40	661.9 ± 11.2
PTFE/BA80-8	11.87 ± 0.41	13.92 ± 0.55	1013.1 ± 29.2
PTFE/BA80-16	13.27 ± 0.47	14.42 ± 0.63	1336.1 ± 136.1
PTFE/MG70-1	9.58 ± 0.22	11.33 ± 0.26	538.8 ± 13.2
PTFE/MG70-4	10.64 ± 0.32	11.86 ± 0.33	699.8 ± 12.5
PTFE/G/A-0.25/4	11.32 ± 1.01	12.79 ± 1.11	679.5 ± 84.8
PTFE/G/A-2/2	11.09 ± 0.45	13.63 ± 0.54	884.8 ± 24.7
PTFE/G/A-4/4	11.96 ± 0.47	14.16 ± 0.47	1140.1 ± 60.6

Table B.14. The measured coefficient of friction of the tested neat PTFE and PTFE composites (Phase 1 and 3, Chapter 3.3.6.1 and 3.3.6.3). Polymer samples were tested against 42CrMo4 disc counterface at 3 MPa contact pressure, 0.1 m/s sliding speed and 1000 sliding distance.

Materials	Counterface material	Coefficient of friction		
		Average (-)	Deviation (-)	Deviation (%)
PTFE	42CrMo4	0.093	0.009	9.4
PTFE/graphene-0.25	42CrMo4	0.101	0.006	6.2
PTFE/graphene-1	42CrMo4	0.078	0.011	14.0
PTFE/graphene-4	42CrMo4	0.088	0.015	17.2
PTFE/graphene-8	42CrMo4	0.112	0.008	6.9
PTFE/graphene-16	42CrMo4	0.106	0.023	22.0
PTFE/Al_2O_3-1	42CrMo4	0.111	0.011	10.2
PTFE/Al_2O_3-4	42CrMo4	0.099	0.017	17.3
PTFE/BA80-1	42CrMo4	0.089	0.010	10.7
PTFE/BA80-4	42CrMo4	0.105	0.012	11.5
PTFE/BA80-8	42CrMo4	0.117	0.015	12.9
PTFE/BA80-16	42CrMo4	0.115	0.001	1.2
PTFE/MG70-1	42CrMo4	0.102	0.000	0.4
PTFE/MG70-4	42CrMo4	0.106	0.017	15.6
PTFE/G/A-0.25/4	42CrMo4	0.112	0.004	3.9
PTFE/G/A-2/2	42CrMo4	0.128	0.016	12.4
PTFE/G/A-4/4	42CrMo4	0.123	0.006	5.0

Table B.15. The measured coefficient of friction of the tested neat PTFE and PTFE composites (Phase 2, Chapter 3.3.6.2). Polymer samples were tested against 42CrMo4/304/34CrNiMo6 disc counterface at 3 MPa contact pressure, 0.1 m/s sliding speed and 1000 sliding distance.

Materials	Counterface material	Coefficient of friction		
		Average (-)	Deviation (-)	Deviation (%)
PTFE	42CrMo4	0.093	0.009	9.4
PTFE	304	0.096	0.003	3.2
PTFE	34CrNiMo6	0.100	0.003	2.7
PTFE/Graphene-4	42CrMo4	0.088	0.015	17.2
PTFE/Graphene-4	304	0.088	0.013	14.7
PTFE/Graphene-4	34CrNiMo6	0.092	0.005	5.9
PTFE/Al_2O_3-4	42CrMo4	0.099	0.017	17.3
PTFE/Al_2O_3-4	304	0.110	0.007	6.7
PTFE/Al_2O_3-4	34CrNiMo6	0.119	0.008	6.9
PTFE/BA80-4	42CrMo4	0.105	0.012	11.5
PTFE/BA80-4	304	0.112	0.005	4.3
PTFE/BA80-4	34CrNiMo6	0.107	0.010	9.5

Table B.16. The measured wear rate and wear depth of the tested neat PTFE and PTFE composites (Phase 1 and 3, Chapter 3.3.6.1 and 3.3.6.3). Polymer samples were tested against 42CrMo4 disc counterface at 3 MPa contact pressure, 0.1 m/s sliding speed and 1000 sliding distance.

Materials	Counterface material	Wear rate (mm^3/mN)		Wear depth (mm)	
		Average	Deviation (%)	Average	Deviation (%)
PTFE	42CrMo4	$5.16 \cdot 10^{-4}$	8.8	1.550	8.8
PTFE/graphene-0.25	42CrMo4	$5.47 \cdot 10^{-4}$	6.0	1.645	6.0
PTFE/graphene-1	42CrMo4	$5.07 \cdot 10^{-4}$	20.6	1.524	20.6
PTFE/graphene-4	42CrMo4	$4.72 \cdot 10^{-5}$	17.2	0.142	17.2
PTFE/graphene-8	42CrMo4	$3.17 \cdot 10^{-5}$	25.6	0.095	25.6
PTFE/graphene-16	42CrMo4	$8.51 \cdot 10^{-6}$	39.6	0.026	39.6
PTFE/Al_2O_3-1	42CrMo4	$9.26 \cdot 10^{-5}$	12.5	0.278	12.5
PTFE/Al_2O_3-4	42CrMo4	$2.91 \cdot 10^{-6}$	68.4	0.009	68.4
PTFE/BA80-1	42CrMo4	$2.40 \cdot 10^{-4}$	10.9	0.721	10.9
PTFE/BA80-4	42CrMo4	$2.01 \cdot 10^{-4}$	6.7	0.603	6.7
PTFE/BA80-8	42CrMo4	$7.27 \cdot 10^{-5}$	10.3	0.218	10.3
PTFE/BA80-16	42CrMo4	$1.12 \cdot 10^{-4}$	10.9	0.336	10.9
PTFE/MG70-1	42CrMo4	$5.39 \cdot 10^{-4}$	2.2	1.621	2.2
PTFE/MG70-4	42CrMo4	$4.49 \cdot 10^{-4}$	12.7	1.350	12.7
PTFE/G/A-0.25/4	42CrMo4	$1.24 \cdot 10^{-5}$	41.7	0.037	41.7
PTFE/G/A-2/2	42CrMo4	$2.82 \cdot 10^{-5}$	26.2	0.085	26.2
PTFE/G/A-4/4	42CrMo4	$4.34 \cdot 10^{-6}$	22.4	0.013	22.4

Table B.17. The measured wear rate and wear depth of the tested neat PTFE and PTFE composites (Phase 2, Chapter 3.3.6.2). Polymer samples were tested against 42CrMo4/304/34CrNiMo6 disc counterface at 3 MPa contact pressure, 0.1 m/s sliding speed and 1000 sliding distance.

Materials	Counterface material	Wear rate (mm^3/mN)		Wear depth (mm)	
		Average	Deviation (%)	Average	Deviation (%)
PTFE	42CrMo4	$5.16 \cdot 10^{-4}$	8.8	1.550	8.8
PTFE	304	$5.89 \cdot 10^{-4}$	5.6	1.769	5.6
PTFE	34CrNiMo6	$5.10 \cdot 10^{-4}$	0.4	1.533	0.4
PTFE/Graphene-4	42CrMo4	$4.72 \cdot 10^{-5}$	17.2	0.142	17.2
PTFE/Graphene-4	304	$1.88 \cdot 10^{-5}$	37.9	0.056	37.9
PTFE/Graphene-4	34CrNiMo6	$2.19 \cdot 10^{-5}$	21.7	0.066	21.7
PTFE/Al_2O_3-4	42CrMo4	$2.91 \cdot 10^{-6}$	68.4	0.009	68.4
PTFE/Al_2O_3-4	304	$3.17 \cdot 10^{-6}$	61.4	0.010	61.4
PTFE/Al_2O_3-4	34CrNiMo6	$9.83 \cdot 10^{-7}$	19.7	0.003	19.7
PTFE/BA80-4	42CrMo4	$2.01 \cdot 10^{-4}$	6.7	0.603	6.7
PTFE/BA80-4	304	$1.78 \cdot 10^{-4}$	3.1	0.536	3.1
PTFE/BA80-4	34CrNiMo6	$2.11 \cdot 10^{-4}$	4.5	0.636	4.5

Table B.18. Advancing and receding contact angles measured by drop shape analyser and the surface free energy – SFE values (based on the advancing and receding angles, calculated with the equation of state - EoS) of the developed unfilled/filled PTFE and steel counterfaces. The used liquid was distilled water.

Samples	Advancing contact angle (°)	Receding contact angle (°)	SFE based on the advancing contact angle (mN/m)	SFE based on the receding contact angle (mN/m)
PTFE	114.89 ± 4.10	100.97 ± 3.47	14.36 ± 2.26	22.47 ± 2.11
PTFE/graphene-0.25	115.83 ± 3.56	94.97 ± 1.65	13.84 ± 1.97	26.13 ± 1.02
PTFE/graphene-1	117.10 ± 1.60	96.35 ± 1.45	13.12 ± 0.86	25.29 ± 0.89
PTFE/graphene-4	114.65 ± 0.72	91.74 ± 0.91	14.46 ± 0.40	28.14 ± 0.57
PTFE/graphene-8	112.92 ± 2.40	88.39 ± 2.14	15.44 ± 1.35	30.23 ± 1.34
PTFE/graphene-16	112.98 ± 3.00	87.56 ± 1.92	15.40 ± 1.67	30.75 ± 1.20
PTFE/Al_2O_3-1	119.03 ± 1.40	99.26 ± 1.18	12.10 ± 0.74	23.49 ± 0.72
PTFE/Al_2O_3-4	111.07 ± 1.92	92.04 ± 2.92	16.48 ± 1.10	27.96 ± 1.82
PTFE/BA80-1	112.62 ± 2.08	89.06 ± 1.14	15.60 ± 1.17	29.81 ± 0.71
PTFE/BA80-4	116.56 ± 4.63	93.99 ± 2.09	13.46 ± 2.54	26.74 ± 1.29
PTFE/BA80-8	114.87 ± 0.91	92.19 ± 2.24	14.68 ± 1.20	27.86 ± 1.39
PTFE/BA80-16	123.77 ± 2.56	98.22 ± 3.56	9.72 ± 1.21	24.18 ± 2.14
PTFE/MG70-1	114.47 ± 0.51	98.38 ± 0.60	14.56 ± 0.29	24.03 ± 0.37
PTFE/MG70-4	113.53 ± 1.30	95.53 ± 2.41	15.08 ± 0.73	25.79 ± 1.48
PTFE/G/A-0.25/4	111.10 ± 1.88	87.44 ± 3.15	16.46 ± 1.08	30.83 ± 1.96
PTFE/G/A-2/2	118.09 ± 2.01	98.51 ± 2.35	12.60 ± 1.06	23.96 ± 1.43
PTFE/G/A-4/4	115.13 ± 3.41	99.66 ± 4.25	14.22 ± 1.89	23.32 ± 2.48
42CrMo4	70.10 ± 5.71	49.28 ± 6.82	41.64 ± 3.54	54.12 ± 3.93
304	49.33 ± 6.64	29.95 ± 3.86	54.10 ± 3.78	64.46 ± 1.83
34CrNiMo6	71.41 ± 3.65	47.40 ± 2.64	40.83 ± 2.26	55.25 ± 1.51

Table B.19. DSC results of the unworn filled/unfilled PTFE polymers and the formed wear debris against 304 steel (Phase 2, Chapter 3.3.6.2), applying Protocol 1 for the DSC analysis (Chapter 3.2.4). At the first heating cycle, the enthalpy of fusion of the debris was evaluated between 300°C and 370°C.

Unworn polymer (304)	First heating			
	Initial temperature of melting (°C)	Melting peak temperature (°C)	Enthalpy of fusion (J/g)	Degree of crystallinity (%)
PTFE	321.0	325.8	33.95	49.2
PTFE/graphene-4	321.7	326.4	34.49	52.1
PTFE/Al_2O_3-4	321.3	326.4	35.61	53.8
PTFE/BA80-4	320.4	325.3	31.02	46.8
Unworn polymer (304)	Second heating			
PTFE	318.8	323.6	28.21	40.9
PTFE/graphene-4	319.5	324.4	29.51	44.6
PTFE/Al_2O_3-4	319.7	324.7	29.92	45.2
PTFE/BA80-4	318.6	323.5	26.25	39.6
Unworn polymer (304)	First cooling			
	Initial temperature of crystallisation (°C)	Crystallisation peak temperature (°C)	Enthalpy of crystallisation (J/g)	Degree of crystallinity (%)
PTFE	314.3	309.5	27.49	39.8
PTFE/graphene-4	314.6	309.6	28.17	42.5
PTFE/Al_2O_3-4	314.9	308.5	28.43	42.9
PTFE/BA80-4	313.8	309.2	26.12	39.4
Debris (304)	First heating			
	Initial temperature of melting (°C)	Melting peak temperature (°C)	Enthalpy of fusion (J/g)	Degree of crystallinity (%)
PTFE	327.6	334.0	59.55	86.3
PTFE/graphene-4	326.1	332.3	58.69	88.6
PTFE/Al_2O_3-4	---	---	---	---
PTFE/BA80-4	323.7	332.7	58.38	88.1
Debris (304)	Second heating			
PTFE	325.0	327.7	47.59	69.0
PTFE/graphene-4	325.0	328.1	52.39	79.1
PTFE/Al_2O_3-4	---	---	---	---
PTFE/BA80-4	325.8	327.9	58.76	88.7
Debris (304)	First cooling			
	Initial temperature of crystallisation (°C)	Crystallisation peak temperature (°C)	Enthalpy of crystallisation (J/g)	Degree of crystallinity (%)
PTFE	314.6	311.2	47.55	68.9
PTFE/graphene-4	318.0	315.1	52.42	79.1
PTFE/Al_2O_3-4	---	---	---	---
PTFE/BA80-4	316.1	314.1	58.47	88.3

Table B.20. DSC results of the unworn filled/unfilled PTFE polymers and the formed wear debris against 34CrNiMo6 steel (Phase 2, Chapter 3.3.6.2), applying Protocol 1 for the DSC analysis (Chapter 3.2.4). At the first heating cycle, the enthalpy of fusion of the debris was evaluated between 300°C and 370°C.

Unworn polymer (34CrNiMo6)	First heating			
	Initial temperature of melting (°C)	Melting peak temperature (°C)	Enthalpy of fusion (J/g)	Degree of crystallinity (%)
PTFE	321.4	326.3	33.67	48.8
PTFE/graphene-4	320.6	325.6	30.18	45.6
PTFE/Al_2O_3-4	321.5	326.4	33.87	51.1
PTFE/BA80-4	320.4	325.5	33.21	50.1
Unworn polymer (34CrNiMo6)	Second heating			
PTFE	319.6	324.2	28.49	41.3
PTFE/graphene-4	318.8	323.7	25.32	38.2
PTFE/Al_2O_3-4	320.2	324.8	28.50	43.0
PTFE/BA80-4	318.8	323.8	26.75	40.4
Unworn polymer (34CrNiMo6)	First cooling			
	Initial temperature of crystallisation (°C)	Crystallisation peak temperature (°C)	Enthalpy of crystallisation (J/g)	Degree of crystallinity (%)
PTFE	313.7	308.8	29.49	42.7
PTFE/graphene-4	314.5	309.0	25.10	37.9
PTFE/Al_2O_3-4	314.8	308.7	28.14	42.5
PTFE/BA80-4	312.7	308.3	27.91	42.1
Debris (34CrNiMo6)	First heating			
	Initial temperature of melting (°C)	Melting peak temperature (°C)	Enthalpy of fusion (J/g)	Degree of crystallinity (%)
PTFE	327.5	334.0	58.92	85.4
PTFE/graphene-4	---	---	---	---
PTFE/Al_2O_3-4	---	---	---	---
PTFE/BA80-4	323.9	333.3	56.66	85.5
Debris (34CrNiMo6)	Second heating			
PTFE	324.9	327.5	48.66	70.5
PTFE/graphene-4	---	---	---	---
PTFE/Al_2O_3-4	---	---	---	---
PTFE/BA80-4	325.7	328.1	56.37	85.1
Debris (34CrNiMo6)	First cooling			
	Initial temperature of crystallisation (°C)	Crystallisation peak temperature (°C)	Enthalpy of crystallisation (J/g)	Degree of crystallinity (%)
PTFE	314.2	311.1	46.70	67.7
PTFE/graphene-4	---	---	---	---
PTFE/Al_2O_3-4	---	---	---	---
PTFE/BA80-4	316.6	314.2	55.17	83.3

Table B.21. The measured wear rate, mass loss and wear temperature of the tested PTFE/Graphene-4 and PTFE/Graphene-8 samples against 42CrMo4 counterface steels (Phase 4, Chapter 3.3.6.4).

PTFE/Graphene-4	Wear rate (mm^3/mN)		Mass loss (g)		Wear (bulk) temperature (°C)	
	Average	Deviation (%)	Average	Deviation (%)	Average	Deviation (%)
1 MPa - 0.5 m/s	1.19E-05	45.9	0.004	45.9	39.6	3.1
1 MPa - 1.0 m/s	6.02E-05		0.019		51.2	
1 MPa - 1.5 m/s	1.60E-05	48.9	0.005	48.9	59.5	7.4
1 MPa - 2.0 m/s	1.92E-04		0.062		56.0	
1 MPa - 3.0 m/s	4.03E-04		0.106		78.1	
3 MPa - 0.5 m/s	5.75E-05		0.056		70.4	
3 MPa - 1.0 m/s	7.78E-04		0.091		78.1	
5 MPa - 0.5 m/s	4.96E-05		0.080		84.9	
7 MPa - 0.5 m/s	6.86E-05		0.092		100.9	
PTFE/Graphene-8	Wear rate (mm^3/mN)		Mass loss (g)		Wear (bulk) temperature (°C)	
	Average	Deviation (%)	Average	Deviation (%)	Average	Deviation (%)
1 MPa - 0.5 m/s	1.42E-05	44.6	0.004	44.6	39.9	4.8
1 MPa - 1.0 m/s	1.48E-05		0.005		52.2	
1 MPa - 1.5 m/s	1.93E-05	13.7	0.006	13.7	59.0	4.0
1 MPa - 2.0 m/s	1.34E-05		0.004		68.9	
1 MPa - 3.0 m/s	2.02E-05	84.3	0.006	84.3	91.9	3.2
3 MPa - 0.5 m/s	5.93E-04		0.106		65.3	
3 MPa - 1.0 m/s	3.22E-04		0.109		95.9	
5 MPa - 1.5 m/s	2.35E-04		0.111		138.0	

Table B.22. The measured wear rate, mass loss and wear temperature of the tested PTFE/Al_2O_3-4 and PTFE/G/A-4/4 samples against 42CrMo4 counterface steels (Phase 4, Chapter 3.3.6.4).

PTFE/Al_2O_3-4	Wear rate (mm^3/mN)		Mass loss (g)		Wear (bulk) temperature (°C)	
	Average	Deviation (%)	Average	Deviation (%)	Average	Deviation (%)
1 MPa - 0.5 m/s	8.84E-06		0.003		45.7	
1 MPa - 1.0 m/s	5.41E-06	33.6	0.002	33.6	62.7	7.7
1 MPa - 1.5 m/s	2.78E-06		0.001		71.0	
1 MPa - 2.0 m/s	1.01E-05		0.003		86.9	
1 MPa - 3.0 m/s	2.35E-05	43.5	0.008	43.5	97.1	2.9
3 MPa - 0.5 m/s	4.55E-06	59.9	0.005	59.9	97.7	1.1
3 MPa - 1.0 m/s	7.02E-06		0.007		160.6	
3 MPa - 1.5 m/s	1.35E-05		0.013		201.1	
3 MPa - 2.0 m/s	9.50E-06	42.2	0.009	42.2	220.2	0.3
3 MPa - 3.0 m/s	6.56E-05		0.066		223.5	
5 MPa - 0.5 m/s	9.67E-06		0.016		133.7	
5 MPa - 1.0 m/s	7.10E-06	42.3	0.012	42.3	206.7	2.3
5 MPa - 1.5 m/s	2.07E-05		0.034		227.0	
5 MPa - 2.0 m/s	1.15E-04		0.094		251.9	
7 MPa - 0.5 m/s	5.47E-06	37.3	0.013	37.3	159.6	2.4
7 MPa - 1.0 m/s	2.15E-05		0.050		215.8	
7 MPa - 1.5 m/s	1.07E-04		0.075		238.5	
PTFE/G/A-4/4	Wear rate (mm^3/mN)		Mass loss (g)		Wear (bulk) temperature (°C)	
	Average	Deviation (%)	Average	Deviation (%)	Average	Deviation (%)
1 MPa - 0.5 m/s	4.33E-07		0.000		43.2	
1 MPa - 1.0 m/s	6.10E-06	64.3	0.002	64.3	69.3	6.0
1 MPa - 1.5 m/s	1.39E-05		0.005		74.5	
1 MPa - 2.0 m/s	1.23E-05		0.004		88.3	
1 MPa - 3.0 m/s	2.49E-05	36.4	0.008	36.4	111.7	6.8
3 MPa - 0.5 m/s	1.08E-05	13.7	0.011	13.7	100.2	2.2
3 MPa - 1.0 m/s	1.33E-05		0.013		142.6	
3 MPa - 1.5 m/s	9.75E-06		0.010		193.4	
3 MPa - 2.0 m/s	1.37E-05		0.013		234.3	
3 MPa - 3.0 m/s	1.34E-05	31.5	0.013	31.5	251.6	4.6
5 MPa - 0.5 m/s	3.18E-06		0.005		131.2	
5 MPa - 1.0 m/s	6.85E-06	17.6	0.011	17.6	206.3	0.3
5 MPa - 1.5 m/s	3.23E-05		0.053		228.8	
5 MPa - 2.0 m/s	2.12E-05		0.034		261.5	
5 MPa - 3.0 m/s	1.66E-04		0.102		251.9	
7 MPa - 0.5 m/s	9.47E-06		0.022		162.2	
7 MPa - 1.0 m/s	6.47E-06	33.6	0.015	33.6	223.2	3.8
7 MPa - 1.5 m/s	2.10E-05		0.048		273.8	
7 MPa - 2.0 m/s	8.77E-05		0.089		265.0	

CURRICULUM VITAE

Contact and personal information

Name	Levente Ferenc Tóth
Date of birth	30 December 1989
Place of birth	Budapest
Nationality	Hungarian
E-mail	levente.toth@UGent.be
	tothl@pt.bme.hu
	levente8912@gmail.com

Education

2015-2021	PhD student (joint degree programme): Ghent University (UGent), Faculty of Engineering and Architecture, Department of Electromechanical, Systems and Metal Engineering Budapest University of Technology and Economics (BME), Faculty of Mechanical Engineering, Department of Polymer Engineering
2013-2015	MSc in Mechanical Engineering Modelling, Budapest University of Technology and Economics (BME), Faculty of Mechanical Engineering
2009-2013	BSc in Mechanical Engineering, Budapest University of Technology and Economics (BME), Faculty of Mechanical Engineering
2005-2009	Jedlik Ányos Secondary Grammar School, Budapest

Prizes and scholarships

2018	Scholarship in the New National Excellence Program (ÚNKP-17-3-I)
2014	Conference of Scientific Students` Associations, 2nd prize BME, Faculty of Mechanical Engineering
2013	National Conference of Scientific Students` Associations, 1st prize Kecskemét
2012	Conference of Scientific Students` Associations, 2nd prize BME, Faculty of Mechanical Engineering
2011	Conference of Scientific Students` Associations, 3rd prize BME, Faculty of Mechanical Engineering

Teaching experience (2015-2021)

Advanced Machine Design (lab practices, UGent, 2016-2017)

Materials Science and Technology of Polymers - BMEGEPTAG0P (lab practices, BME)

2016	Tensile test of polymers
2016	Joining technologies of polymers
2017	Extrusion of thermoplastic polymers
2018	Thermoforming of thermoplastics
2019	Composites
2019	Injection moulding
2020	Thermoforming of thermoplastics

Polymer Engineering - BMEGEPTAMT0 (lab practices, BME)

2017	Melt flow properties of polymer melts
2018	Injection moulding
2019	Injection moulding

Technology of Polymer Composites - BMEGEPTAGA3 (lab practices, BME)

2016	Manufacturing of thermosetting matrix polymer composites

Supervised BSc/MSc students (2015-2021)

2017	Sam Nowé	UGent, MSc thesis
2017	Luca Belotti	UGent, Summer internship
2017	Magyar Balázs	BME, TDK – Scientific Student Association
2018	Vida Zoltán	BME, BSc thesis
2018	Budai Georgina	BME, BSc thesis
2019	Kozák Gábor	BME, MSc thesis
2021	Briek Vanclooster	UGent, MSc thesis

A1 - Peer-reviewed journal articles included in Science Citation Index

1 **Levente Ferenc Tóth**, Gábor Szebényi, Jacob Sukumaran, Patrick De Baets: Tribological Characterisation of Nanoparticle Filled PTFE: Wear-Induced Crystallinity Increase and Filler Accumulation. Express Polymer Letters, 2021. Accepted.
Impact Factor: 3.083

2 **Levente Ferenc Tóth**, Patrick De Baets, Gábor Szebényi: Processing Analysis of Nanoparticle Filled PTFE: Restrictions and Limitations of High Temperature Production. Polymers, 2020, 12, 2044, 1-14.
Impact Factor: 3.426

3 **Levente Ferenc Tóth**, Patrick De Baets, Gábor Szebényi: Thermal, Viscoelastic, Mechanical and Wear Behaviour of Nanoparticle Filled Polytetrafluoroethylene: A Comparison. Polymers, 2020, 12, 1940, 1-17.
Impact Factor: 3.426

4 **Levente Ferenc Tóth**, Jacob Sukumaran, Gábor Szebényi, Ádám Kalácska, Dieter Fauconnier, Rajini Nagarajan, Patrick De Baets: Large-scale tribological characterisation of eco-friendly basalt and jute fibre reinforced thermoset composites. Wear, 2020, 450-451, 203274, 1-11.
Impact Factor: 4.108

5 **Levente Ferenc Tóth**, Jacob Sukumaran, Gábor Szebényi, Patrick De Baets: Tribo-mechanical interpretation for advanced thermoplastics and the effects of wear-induced crystallization. Wear, 2019, 440-441, 203083, 1-10.
Impact Factor: 4.108

6 Andrea Toldy, Gábor Szebényi, Kolos Molnár, **Levente Ferenc Tóth**, Balázs Magyar, Viktor Hliva, Tibor Czigány, Beáta Szolnoki: The Effect of Multilevel Carbon Reinforcements on the Fire Performance, Conductivity, and Mechanical Properties of Epoxy Composites. Polymers, 2019, 11 (2), 303, 1-13.
Impact Factor: 3.426

7 Jacob Sukumaran, Jan De Pauw, Patric Daniel Neis, **Levente Ferenc Tóth**, Patrick De Baets: Revisiting polymer tribology for heavy duty application. Wear, 2017, 376-377, 1321-1332.
Impact Factor: 2.960

A2 - Peer-reviewed journal articles not included in Science Citation Index

1 **Tóth Levente Ferenc**, Szebényi Gábor, Patrick De Baets: Kísérleti gyártástechnológia fejlesztése PTFE szobahőmérsékletű préselésére és szinterelésére. Polimerek, 2018, 4 (5), 155-160.

2 Gábor Szebényi, **Levente Ferenc Tóth**, József Karger-Kocsis: Effect of an Ionic Liquid on the Flexural and Fracture Mechanical Properties of EP/MWCNT Nanocomposites. Materials Science Forum, 2017, 885, 19-24.

3 **Tóth Levente Ferenc**, Szebényi Gábor, Patrick De Baets: PTFE kopásállóságának növelése részecske adalékanyagokkal – review. Polimerek, 2017, 3 (9), 276-281.

4 Szebényi Gábor, **Tóth Levente Ferenc**: Szénszál/szénnanocső/szénnanoszál erősítésű hibrid kompozitok hő- és elektromos vezetőképességének vizsgálata. Műanyagipari Szemle, 2015, 12 (3), 87-96.

5 Szebényi Gábor, **Tóth Levente Ferenc**: RDP égésgátlóval töltött epoxi hibrid-nanokompozitok éghetőségi vizsgálata. Polimerek, 2015, 1 (4), 120-123.

C1 - Articles in conference proceedings

1 Gábor Szebényi, **Levente Ferenc Tóth**: Szénszál/szén nanocső/szén nanoszál erősítésű hibridkompozitok vizsgálata. XXIII. Nemzetközi Gépészeti Találkozó (OGÉT 2015), Erdélyi Magyar Műszaki Tudományos Társaság (EMT), 346-349, Csíksomlyó, 23-26 April 2015. ISSN 2068-1267.

2 **Levente Ferenc Tóth**: Foszfor alapú égésgátlókkal ellátott, szénszál erősítésű kompozitok éghetőségi és mechanikai vizsgálata. XX. Fiatal Műszakiak Tudományos Ülésszaka (FMTÜ), 3. Műszaki Tudományos Közlemények, Erdélyi Múzeum-Egyesület (EME), 299–302, Kolozsvár, 19-20 March 2015. ISSN 2393-1280.

3 **Levente Ferenc Tóth**: Szénszál/szén nanocső/szén nanoszál erősítésű hibrid kompozitok fejlesztése repüléstechnikai alkalmazásokhoz. XIX. Fiatal Műszakiak Tudományos Ülésszaka (FMTÜ), Erdélyi Múzeum-Egyesület (EME), 413-416, Kolozsvár, 20-21 March 2014. ISSN 2067-6808.

C3 - Conference abstracts

1 **Levente Ferenc Tóth**, Jacob Sukumaran, Gábor Szebényi, Rajini Nagarajan, Winowlin Jappes Thanggiah, Patrick De Baets: Friction and wear properties of jute/polyester composite systems at high load. 2nd International Conference on Polymer Tribology (PolyTrib 2016), Ljubljana (Slovenia), 15-16 September 2016.

2 Jacob Sukumaran, **Levente Ferenc Tóth**, Gábor Szebényi, Patrick De Baets: Tribology of amorphous polymers in heavy-duty applications. 17th Nordic Symposium on Tribology (NordTrib 2016), Hämeenlinna (Finland), 14-17 June 2016.

3 Szebényi Gábor, **Tóth Levente Ferenc**: Nanokompozitok határfelületi adhéziójának módosítása ionos folyadékokkal. X. Országos Anyagtudományi Konferencia (X. OATK), Balatonalmádi (Hungary), 11-13 October 2015.

4 Beáta Szolnoki, **Levente Ferenc Tóth**, Kolos Molnár, Gábor Szebényi, Andrea Toldy, György Marosi: Flame retardancy of CNT-loaded carbon nanofibre-reinforced epoxy resin composites. 7th Asia-Europe Symposium on Processing and Properties of Reinforced Polymers (AESP7), Madrid (Spain), 4-6 February 2015.

5 Beáta Szolnoki, **Levente Ferenc Tóth**, Kolos Molnár, Gábor Szebényi, Andrea Toldy, György Marosi: Flame retardancy of epoxy resin composites reinforced with CNT-loaded carbon nanofibre. 14th European Meeting on Fire Retardancy and Protection of Materials (FRPM 13), Lille (France), 30 June - 4 July 2013.

Polytetrafluoroethylene (PTFE) wear debris on a steel counter surface.